5. DEEP BLAKE-BAHAMA OUTER RIDGE, SITES 1060, 1061, AND 1062[1]

Shipboard Scientific Party[2]

HOLE 1060A

Position: 30°45.597′N, 74°27.990′W (Blake Outer Ridge)

Start hole: 2253 hr, 5 March 1997

End hole: 2200 hr, 6 March 1997

Time on hole: 23.12 hr (0.96 days)

Seafloor (drill-pipe measurement from rig floor, mbrf): 3492.5

Distance between rig floor and sea level (m): 11.3

Water depth (drill-pipe measurement from sea level, m): 3481.2

Total depth (from rig floor, mbrf): 3662.60

Penetration (mbsf): 170.10

Coring totals:

Type: APC; Number: 18; Length: 170.10 m; Recovered: 177.74 m (104.49%)

Oldest formation cored: lower Pleistocene clay with silt

HOLE 1060B

Position: 30°45.585′N, 74°27.989′W (Blake Outer Ridge)

Start hole: 2200 hr, 6 March 1997

End hole: 0925 hr, 7 March 1997

Time on hole: 11.42 hr (0.48 days)

Seafloor (drill-pipe measurement from rig floor, mbrf): 3492.1

Distance between rig floor and sea level (m): 11.3

Water depth (drill-pipe measurement from sea level, m): 3480.8

Total depth (from rig floor, mbrf): 3622.00

Penetration (mbsf): 129.90

Coring totals:

Type: APC; Number: 14; Length: 129.90 m; Recovered: 134.23 m (103.33%)

Oldest formation cored: middle Pleistocene clay with nannofossils

HOLE 1060C

Position: 30°45.568′N, 74°27.990′W (Blake Outer Ridge)

Start hole: 0925 hr, 7 March 1997

End hole: 0400 hr, 8 March 1997

Time on hole: 18.58 hr (0.77 days)

Seafloor (drill-pipe measurement from rig floor, mbrf): 3492.5

Distance between rig floor and sea level (m): 11.3

Water depth (drill-pipe measurement from sea level, m): 3481.2

Total depth (from rig floor, mbrf): 3619.00

Penetration (mbsf): 126.50

Coring totals:

Type: APC; Number: 14; Length: 126.50 m; Recovered: 130.78 m (103.38%)

Oldest formation cored: middle Pleistocene clay with nannofossils

HOLE 1061A

Position: 29°58.498′N, 73°35.993′W (Blake Outer Ridge)

Start hole: 1325 hr, 8 March 1997

End hole: 1325 hr, 11 March 1997

Time on hole: 72.00 hr (3.00 days)

Seafloor (drill-pipe measurement from rig floor, mbrf): 4058.0

Distance between rig floor and sea level (m): 11.4

Water depth (drill-pipe measurement from sea level, m): 4046.6

Total depth (from rig floor, mbrf): 4408.30

Penetration (mbsf): 350.30

Coring totals:

Type: APC; Number: 16; Cored: 152.00 m; Recovered: 157.99 m (103.94%)
Type: XCB; Number: 21; Cored: 198.30 m; Recovered: 140.21 m (70.71%)
Total: Number: 37; Cored: 350.30 m; Recovered: 298.20 m (85.13%)

Oldest formation cored: middle Pliocene clay with nannofossils

HOLE 1061B

Position: 29°58.517′N, 73°35.991′W (Blake Outer Ridge)

Start hole: 1325 hr, 11 March 1997

End hole: 1606 hr, 11 March 1997

Time on hole: 2.68 hr (0.11 days)

Seafloor (drill-pipe measurement from rig floor, mbrf): 4055.0

Distance between rig floor and sea level (m): 11.4

Water depth (drill-pipe measurement from sea level, m): 4043.6

Total depth (from rig floor, mbrf): 4064.50

Penetration (mbsf): 9.50

Coring totals:

Type: APC; Number: 1; Length: 9.50 m; Recovered: 9.82 m (103.37%)

Oldest formation cored: late Pleistocene clay with nannofossils

[1]Keigwin, L.D., Rio, D., Acton, G.D., et al., 1998. *Proc. ODP, Init. Repts.*, 172: College Station, TX (Ocean Drilling Program).

[2]Shipboard Scientific Party is given in the list preceding the Table of Contents.

Prior Chapter Contents Next Chapter

HOLE 1061C

Position: 29°58.515′N, 73°35.992′W (Blake Outer Ridge)

Start hole: 1606 hr, 11 March 1997

End hole: 1048 hr, 12 March 1997

Time on hole: 18.70 hr (0.78 days)

Seafloor (drill-pipe measurement from rig floor, mbrf): 4048.2

Distance between rig floor and sea level (m): 11.4

Water depth (drill-pipe measurement from sea level, m): 4036.8

Total depth (from rig floor, mbrf): 4215.00

Penetration (mbsf): 166.80

Coring totals:

Type: APC; Number: 18; Length: 166.80 m; Recovered: 174.61 m (104.68%)

Oldest formation cored: lower Pleistocene clay with nannofossils

HOLE 1061D

Position: 29°58.533′N, 73°35.990′W (Blake Outer Ridge)

Start hole: 1048 hr, 12 March 1997

End hole: 0837 hr, 13 March 1997

Time on hole: 21.82 hr (0.91 days)

Seafloor (drill-pipe measurement from rig floor, mbrf): 4049.8

Distance between rig floor and sea level (m): 11.4

Water depth (drill-pipe measurement from sea level, m): 4038.4

Total depth (from rig floor, mbrf): 4229.80

Penetration (mbsf): 180.00

Coring totals:

Type: APC; Number: 18; Cored: 162.70 m; Recovered: 169.46 m (104.15%)
Type: XCB; Number: 4; Cored: 17.30 m; Recovered: 25.49 m (147.34%)
Total: Number: 22; Cored: 180.00 m; Recovered: 194.95 m (108.31%)

Oldest formation cored: lower Pleistocene clay with nannofossils and silt

HOLE 1061E

Position: 29°58.556′N, 73°35.993′W (Blake Outer Ridge)

Start hole: 0837 hr, 13 March 1997

End hole: 1842 hr, 13 March 1997

Time on hole: 10.08 hr (0.42 days)

Seafloor (drill-pipe measurement from rig floor, mbrf): 4047.1

Distance between rig floor and sea level (m): 11.4

Water depth (drill-pipe measurement from sea level, m): 4035.7

Total depth (from rig floor, mbrf): 4066.00

Penetration (mbsf): 18.90

Coring totals:

Type: APC; Number: 2; Length: 18.90 m; Recovered: 19.53 m (103.33%)

Oldest formation cored: upper Pleistocene clay with nannofossils

HOLE 1062A

Position: 28°14.782′N, 74°24.419′W (Bahama Outer Ridge)

Start hole: 1045 hr, 14 March 1997

End hole: 2345 hr, 15 March 1997

Time on hole: 37 hr (1.54 days)

Seafloor (drill-pipe measurement from rig floor, mbrf): 4774.8

Distance between rig floor and sea level (m): 11.5

Water depth (drill-pipe measurement from sea level, m): 4763.3

Total depth (from rig floor, mbrf): 4955.5

Penetration (mbsf): 180.7

Coring totals:

Type: APC; Number: 20; Cored: 180.7 m; Recovered: 181.24 m (100.30%)

Oldest formation cored: middle Pliocene clay with nannofossils

HOLE 1062B

Position: 28°14.789′N, 74°24.420′W (Bahama Outer Ridge)

Start hole: 2345 hr, 15 March 1997

End hole: 0625 hr, 17 March 1997

Time on hole: 30.67 hr (1.28 days)

Seafloor (drill-pipe measurement from rig floor, mbrf): 4774.5

Distance between rig floor and sea level (m): 11.5

Water depth (drill-pipe measurement from sea level, m): 4763

Total depth (from rig floor, mbrf): 5023.1

Penetration (mbsf): 248.6

Coring totals:

Type: APC; Number: 17; Cored: 156.7 m; Recovered: 156.20 m (100.08%)
Type: XCB; Number: 9; Cored: 82.3 m; Recovered: 82.26 m (99.96%)
Total: Number: 27; Cored: 239.0 m; Recovered: 239.08 m (100.03%)

Oldest formation cored: lower Pliocene clay with nannofossils

HOLE 1062C

Position: 28°14.795′N, 74°24.416′W (Bahama Outer Ridge)

Start hole: 0625 hr, 17 March 1997

End hole: 2235 hr 17 March 1997

Time on hole: 16.17 hr

Seafloor (drill-pipe measurement from rig floor, mbrf): 4772.1

Distance between rig floor and sea level (m): 11.5

Water depth (drill-pipe measurement from sea level, m): 4760.6

Total depth (from rig floor, mbrf): 4905

Penetration (mbsf): 132.9

Coring totals:

Type: APC; Number: 14; Cored: 132.9 m; Recovered: 134.56 m (101.25%)

Oldest formation cored: lower Pleistocene clay with nannofossils

HOLE 1062D

Position: 28°14.800′N, 74°24.416′W (Bahama Outer Ridge)

Start hole: 2235 hr, 17 March 1997

End hole: 1010 hr, 18 March 1997

Time on hole: 11.58 hr

Seafloor (drill-pipe measurement from rig floor, mbrf): 4771.7

Distance between rig floor and sea level (m): 11.5

Water depth (drill-pipe measurement from sea level, m): 4760.2

Total depth (from rig floor, mbrf): 4853.5

Penetration (mbsf): 81.8

Coring totals: 9

Type: APC; Number: 9; Cored: 81.8 m; Recovered: 82.66 m (101.05%)

Oldest formation cored: middle Pleistocene clay with nannofossils

HOLE 1062E

Position: 28°14.765′N, 74°25.055′W (Bahama Outer Ridge)

Start hole: 1010 hr, 18 March 1997

End hole: 1713 hr, 19 March 1997

Time on hole: 31.05 hr (1.29 days)

Seafloor (drill-pipe measurement from rig floor, mbrf): 4785.7

Distance between rig floor and sea level (m): 11.7

Water depth (drill-pipe measurement from sea level, m): 4774

Total depth (from rig floor, mbrf): 4994.5

Penetration (mbsf): 208.8

Coring totals:

Type: APC; Number: 16; Cored: 145.1 m; Recovered: 147.89 m (101.92%)
Type: XCB; Number: 7; Cored: 63.7 m; Recovered: 55.83 m (87.65%)
Total: Number: 23; Cored: 208.8 m; Recovered: 203.72 m (97.57%)

Oldest formation cored: middle Pliocene clay with nannofossils

HOLE 1062F

Position: 28°14.771′N, 74°25.065′W (Bahama Outer Ridge)

Start hole: 1713 hr, 19 March 1997

End hole: 0300 hr, 20 March 1997

Time on hole: 9.78 hr (0.41 days)

Seafloor (drill-pipe measurement from rig floor, mbrf): 4785.4

Distance between rig floor and sea level (m): 11.7

Water depth (drill-pipe measurement from sea level, m): 4773.7

Total depth (from rig floor, mbrf): 4868.5

Penetration (mbsf): 83.1

Coring totals:

Type: APC; Number: 9; Cored: 83.1 m; Recovered: 83.77 m (100.81%)

Oldest formation cored: lower Pleistocene clay with nannofossils

HOLE 1062G

Position: 28°14.755′N, 74°24.622′W (Bahama Outer Ridge)

Start hole: 0300 hr, 20 March 1997

End hole: 0748 hr, 20 March 1997

Time on hole: 4.80 hr

Seafloor (drill-pipe measurement from rig floor, mbrf): 4759.2

Distance between rig floor and sea level (m): 11.7

Water depth (drill-pipe measurement from sea level, m): 4747.5

Total depth (from rig floor, mbrf): 4768.5

Penetration (mbsf): 9.3

Coring totals:

Type: APC; Number: 1; Cored: 9.3 m; Recovered: 9.27 m (99.68%)

Oldest formation cored: upper Pleistocene nannofossil clay

HOLE 1062H

Position: 28°14.754′N, 74°24.620′W (Bahama Outer Ridge)

Start hole: 0748 hr, 20 March 1997

End hole: 0145 hr, 21 March 1997

Time on hole: 17.95 hr

Seafloor (drill-pipe measurement from rig floor, mbrf): 4757

Distance between rig floor and sea level (m): 11.7

Water depth (drill-pipe measurement from sea level, m): 4745.3

Total depth (from rig floor, mbrf): 4820.5

Penetration (mbsf): 63.5

Coring totals:

Type: APC; Number: 7; Cored: 63.5 m; Recovered: 65.29 m (102.82%)

Oldest formation cored: upper Pleistocene clay with nannofossils

Principal results: Sites 1060, 1061, and 1062 are the deepest water sites along the Blake-Bahama Outer Ridge (BBOR) transect of Leg 172. These sites have similar lithologies, which we grouped into two units. Unit I is defined by its cyclically alternating light-gray nannofossil ooze and dark greenish gray clay containing reddish brown layers. Because of its shallow penetration, Site 1060 is exclusively Unit I. At the deeper sites, Unit II is recognized by its reduced abundance of pelagic carbonates and dominance of clays and silts. At Site 1061, Unit II appears more homogeneous than Unit I, whereas on the mud wave (Site 1062) the lithology is more heterogeneous because of the presence of shallow-water carbonate turbidites. Because the mud-wave field is in the Bahama Basin, a depression adjacent to the Bahama Banks and Blake Escarpment, it is more subject to turbidites than Sites 1060 and 1061. Unit III at these sites is composed of clayey mixed sediments.

All three sites contain excellent paleomagnetic records, especially for the Brunhes Chron. There are no other long, well-dated paleomagnetic records of directional field variability older than about 0.2 Ma available anywhere in the world for the Brunhes time interval. Preliminary analysis of the paleomagnetic secular variation at each Hole of Sites 1060, 1061, and 1062 indicates convincingly that eight excursions may be present in the Brunhes Chron. These sites provide the material necessary for detailed paleoclimatic and sedimentological studies.

Site 1060 consists of various combinations of Holocene and Pleistocene nannofossil ooze, clay, and silt, with clay and clay with nannofossils dominant. Bedding generally ranges from 0.2 to 2 m in thickness. Most lithological changes are gradual, although pronounced transitions can take place within a decimeter. One characteristic of this site is the degree of variability in the lithology, which is evident in the records of color reflectance and carbonate content of the sediment. Sediment color usually ranges from dark greenish gray in the clay to light greenish gray in the sediments with more biogenic carbonate. In some intervals, the clay and clay with nannofossil lithologies have a brownish gray to pale brown color or a reddish tinge. Calcite dominates the carbonate mineralogy and appears primarily in the form of calcareous nannofossils, which can make up a significant proportion of the clay size fraction in carbonate-rich sediments. Carbonate values range from 7 to 44 wt%. Three calcareous nannofossil and planktonic foraminifer events suggest sedimentation rates of 240 m/m.y., with the oldest sediments recovered of early–middle Pleistocene age (between 0.96 and 0.46 Ma). Magnetic susceptibility and magnetic inten-

sities show cyclic variations that appear to correlate with carbonate fluctuations and marine isotope stages (MIS). Paleomagnetic studies indicate that the site is almost all Brunhes normal polarity with the Brunhes/Matuyama boundary occurring near the base of Hole 1060A. Reproducible records of magnetic field secular variation are present in the Brunhes Chron of Site 1060 cores.

Pore-water chemistry shows a very thin (13 m) sulfate reduction zone. Both calcium and magnesium decrease sharply with depth in the zone of sulfate reduction. In the zone of methanogenesis, alkalinity and magnesium decrease downhole, whereas calcium and strontium increase, suggesting dolomitization of carbonates. Methane is biogenic, based on methane/ethane ratios. No gas hydrate was directly observed, but chloride profiles freshen slightly with depth, indicating that gas hydrate may underlie Site 1060.

At Site 1061, the interval from 0 to 183 meters below seafloor (mbsf) was multiply cored and appears to have provided a complete composite sequence down to the latest early Pleistocene. Extended core barrel (XCB) coring at Hole 1061A from 152 to 350 mbsf recovered a sedimentary interval that spans 0.8–3.2 Ma. In addition to high-resolution Pleistocene objectives, Site 1061 was intended to provide a high-resolution record of climate and ocean changes associated with the onset of Northern Hemisphere glaciation (~2.8 Ma) for comparison with other Atlantic records from ODP Legs 154 and 162. Although we XCB cored through the interval, sediment biscuiting, incomplete core recovery, and decreasing rates of sedimentation in the Pliocene lowered the value of Site 1061 as a middle Pliocene reference section.

Sediments at this location are predominantly composed of carbonate-rich and carbonate-poor units that alternate on a scale ranging from ~20 cm to ~10 m. The sediments range from nannofossil ooze in the most calcareous units (carbonate contents of 20 to 55 wt%) to clay in the least calcareous units (carbonate contents of 2 to 15 wt%). A few thin laminations were noted, presumably deposited by currents. Colors range from dark greenish gray to shades of orange and reddish brown. Three sedimentary units have been distinguished on the basis of the bed thicknesses, carbonate content, and color. Additional information for distinguishing sedimentary units comes from downhole logs.

Unit I (0–170 mbsf; Holocene–middle Pleistocene) is defined by cyclically alternating carbonate-rich (20 to 55 wt% $CaCO_3$) and carbonate-poor intervals (4 to 15 wt% $CaCO_3$). Sediments in carbonate-rich intervals range from nannofossil ooze to nannofossil clay. In carbonate-poor intervals, sediments are clay, clay with silt, or clay with nannofossils. Colors range from light greenish gray to dark greenish gray alternating with reddish brown and reddish green intervals. This unit is well resolved on the downhole logs, with clear cyclic variations in gamma ray, bulk density, velocity, and resistivity.

Unit II (170 to 260 mbsf; early Pleistocene) consists of alternating carbonate-rich and carbonate-poor intervals and is defined, in part, by the diminished carbonate contents (range 5 to 20 wt%), which are distinctly lower than in Unit I. Unit II sediments are nannofossil clay and clay with silt. Colors show limited variations from light to dark greenish gray. On downhole logs, the unit has more constant gamma-ray counts and lower bulk density, resistivity, and uranium contents with respect to Unit I. A 40-cm-thick, multicolored, lithified interval occurs at the top of Core 172-1061A-23X (215 mbsf) and marks the top of a gradual downhole increase in carbonate from 10 to 20 wt%.

Unit III (260–360 mbsf; early Pleistocene–middle Pliocene) is defined by alternating intervals of higher and lower carbonate with a somewhat higher carbonate content (2–35 wt%) than Unit II. The sediments are predominantly composed of nannofossil clay, clay with nannofossils, clay with silt, and clay. Colors include greenish gray (light and dark) reddish brown, and numerous purple and green (diagenetic?) layers. Cores 172-1061A-35X and 36X have distinctly less pyrite and perhaps lower carbonate (2–20 wt%) than the overlying sediments, and may represent a distinct subunit. Logs of this unit show increasing gamma ray counts with a further increase below ~315 mbsf and higher resistivity, which decreases abruptly below 325 mbsf.

Eighteen calcareous plankton biohorizons suggest that sedimentation rates have been ~228 m/m.y. in the past 0.5 m.y., 144 m/m.y. between 0.5 and 1.6 Ma, 87 m/m.y. between 1.6 and 2.0 Ma, 52 m/m.y. between 2.0 and 2.5 Ma, and 31 m/m.y. between 2.5 Ma and the bottom of the succession (at 3.2–3.3 Ma). Magnetic susceptibility and magnetic intensities show cyclic variations that evidently correlate with carbonate percentage fluctuations and MISs. Site 1061 has mixed magnetic polarity, and Hole 1061A ended in the Gauss Normal Chron. The Brunhes/Matuyama reversal is found at 149 mbsf in Holes 1061A, 1061C, and 1061D, and appears to be a promising candidate for a high-resolution record of a polarity transition. Several excursions within the Brunhes Chron are reproducible among the holes.

As in previous Blake Ridge sites, pore-water chemistry shows a very thin sulfate reduction zone of about 13 m. Calcium and magnesium distribution suggests carbonate precipitation near the sulfate/methane interface and within the methanogenic zone. Methane is biogenic based on methane/ethane values. No gas hydrate was directly observed, but chloride profiles freshen with depth, indicating that gas hydrate may underlie Site 1061.

Downhole logging measurements were made from 350 to 77 mbsf in Hole 1061A, using two tool strings: the triple-combination (resistivity, density, porosity, and natural gamma tools) and Formation MicroScanner (FMS)-Sonic (resistivity imager and sonic velocity tools). The logs are generally of good quality. The borehole diameter was mostly ~12–13 in, with thin but numerous washouts to 16 in. Resistivity, total natural gamma, and bulk density all show marked cyclicity down to 160 mbsf (i.e., in the past 0.8 m.y). This cyclicity is not evident between 160 and 260 mbsf, and variations are more modest. Below 260 mbsf (2.5 Ma), bulk densities, resistivities, and natural gamma all step up to higher values. The FMS resistivity images show a curious decimeter-scale banding in this lower section.

At Site 1062, we drilled eight holes on either flank and into the crest of the mud wave at the base of the Bahama Outer Ridge. Holes 1062A, 1062B, 1062C, and 1062D are on the east side of the mud wave, Holes 1062E and 1062F are on the west side, and Holes 1062G and 1062H are near the crest. Hole 1062B was cored by XCB from 2.6 to 4.0 Ma, and Hole 1062E was cored by XCB from 2.7 to 3.0 Ma. The far west and far east holes are 1050 m apart. A total of 1000 m of sediment was cored, with a total recovery in excess of 100%.

Unit I (0–79 mbsf on the east flank, 0–61 mbsf on the west flank; Holocene–middle Pleistocene) is composed of cyclically alternating dark gray to reddish brown clay layers (typically 5–10 m thick) and light olive-gray nannofossil–clay mixed sediment layers (typically only 1.5 m thick). The transitions from carbonate-rich to clay layers are abrupt, whereas those from clay-rich to carbonate-rich sediment are gradual. An entire sedimentary cycle typically occupies 10–20 m, and more than five of these cycles are included in Unit I. Four distinctly reddish layers are also present, which can be correlated with the red lutite layers observed at other, shallower Leg 172 sites. Unit II (77.0–167 mbsf on the east flank, 61–117 mbsf on the west flank; middle Pleistocene–late Pliocene) is predominantly composed of interbedded clay and clay with nannofossils. Contacts are gradual and moderately to heavily bioturbated. The average thicknesses of clay layers and nannofossil-rich layers are 2 and 1 m, respectively. Unit II also contains well-sorted foraminifer or carbonate-silt and sand layers, generally 7–12 cm thick, which are interpreted as carbonate turbidites, the source area of which was most probably the Bahama Banks. Unit III (167–239 mbsf on the east flank; 117–209 mbsf on the west flank; middle–early Pliocene) is predominantly dark greenish gray clay with nannofossils interbedded with clay, clay with silt, and nannofossil clay. Thin carbonate-rich layers are present. There is an increase of silt-sized lithologies with respect to the overlying units.

Calcareous nannofossils are the dominant microfossils at Site 1062. However, their abundance and preservation state vary with depth and between holes. Samples with abundant and well-preserved nannoflora assemblages alternate with samples with a few partially dissolved specimens and those barren of nannofossils. Reworking is often strong, making the recognition of horizons around the Pliocene/Pleistocene boundary at Site 1062 difficult. At Hole 1062E the interval between 100 and 120 mbsf is apparently disturbed, as all the biostratigraphic markers appear displaced uphole relative to the ages suggested by magnetostratig-

raphy. Planktonic foraminifer abundance and preservation are highly variable; however, they are better than at Site 1061, although the latter site is 725 m shallower. Benthic foraminifers are rare to very rare, and moderately to poorly preserved.

Magnetic susceptibility and magnetic intensity show cyclic variations that correlate with MISs 1 to 22 in all holes of Site 1062. Magnetic polarity stratigraphy is well defined down to the base of the Jaramillo Subchron. In the underlying interval, the presence of the turbidite layers makes the paleomagnetic record more difficult to interpret. The base of the Brunhes Chron is at 92–95 mbsf at Holes 1062A, 1062B, and 1062C in the eastern flank, whereas it is at 71.5 mbsf at Hole 1062E in the western flank. The Jaramillo Chron is between 108.4 and 112.4 mbsf at Hole 1062B (eastern flank of the mud wave), whereas it is between 79 and 86 mbsf at Hole 1062E (western flank). Paleomagnetic directional changes, which likely reflect paleomagnetic secular variation, are observed within the Brunhes Chron on a variety of length scales from 10 cm to 10 m in all holes. When checked carefully in selected intervals, these correlate between holes and with directional changes observed at Sites 1060 and 1061.

Age control provided by calcareous plankton biostratigraphy and magnetostratigraphy suggests that the sedimentation rates at Site 1062 were generally very high and that the recovered succession is well suited for paleoceanographic reconstruction on orbital and millennial time scales. In addition it suggests, in accordance with the evidence from the seismic images of the investigated mud wave, varying sedimentation rates in the east and west flanks. Specifically, in the east flank (Hole 1062A and 1062B) sedimentation rates were 110 m/m.y. in the past 1 m.y., 32 m/m.y. between 1.0 and 2.5 Ma and 73 m/m.y. between 2.5 and 2.86 Ma. In the west flank (Hole 1062E), sedimentation rates were 82 m/my in the past 1 m.y., 27 m/m.y. between 1.0 and 2.5 Ma, and 109 m/m.y. between 2.5 and 2.86 Ma.

The interface between the sulfate and methanogenic zone is at 70 mbsf, significantly deeper (50 m) than at the Blake Outer Ridge Sites. The sulfate profile displays a distinct concave down profile suggesting that sulfate is predominantly consumed by microbially mediated reactions with sedimentary organic matter. This, however, contrasts with the high methane levels in the lower part of the sulfate reduction zone and with the possible presence of a bottom simulating reflector (BSR) in the area. Although gas hydrate was not directly observed, the chlorinity decreases with depth, suggesting its presence below the recovered interval.

BACKGROUND AND OBJECTIVES

The three deepest sites on the BBOR depth transect (Sites 1060–1062) were occupied to recover a continuous sequence of sediments from near the interface (~4000 m water depth) between present-day North Atlantic Deep Water (NADW) and Antarctic Bottom Water (AABW; Fig. 3, "Introduction" chapter, this volume). Sites 1060 (3481 m) and 1061 (4037 m) are on the crest of the Blake Outer Ridge (Site 1060 is near the position of Deep Sea Drilling Program [DSDP] Site 102). Both sites were cored with the goal of obtaining a history of circulation changes near the boundary between AABW and NADW.

Site 1062 (4763 m) is located on a 37-m-high mud wave situated about 400 m downslope and west of the crest of the Bahama Outer Ridge. This location is near the position of Core KN31-GPC-9, which has provided an important climate and deep-circulation record (Keigwin and Jones, 1994). At present, Site 1062 is under the influence of the Western Boundary Undercurrent (WBUC), which is composed of 15% AABW at this depth. Waters of the WBUC follow a convoluted path along the topographic contours of the eastern and western flanks of the BBOR and flow northward at Site 1062. This deep-current activity has generated a mud-wave field from 26° to 30°N in the area surrounding the location of Site 1062. Previous studies and the site survey data indicate lateral and vertical stratigraphic variability in the architecture of the mud wave, resulting from higher depositional rate on the east flank than on the west flank and from migration of the mud wave with time. This variability may be a response to changing climate and ocean circulation patterns on both orbital and millennial time scales. At Site 1062 a transect of holes across the mud wave should document changes in paleocirculation.

Other objectives at these sites were to (1) provide high-resolution sections for paleomagnetic study and (2) monitor the extent of gas hydrate along the BBOR.

OPERATIONS

Site 1060

The 68-nmi transit from Site 1059 to the survey area of Site 1060 (prospectus site BBOR-5) was accomplished at a very rapid average speed of 13.3 kt. At 2000 hr, the *JOIDES Resolution* slowed to deploy seismic equipment. The ensuing seismic survey consisted of a north-to-south line over Site 1060 and a crossing west-to-east line (see "Site Geophysics" section, this chapter). During this survey, the seismic record from the chart recorder displayed several bright patches (areas with no reflectors) and horizontal reflectors that were slightly upturned on either side of the bright patches. One of these patches occurred at the intended drill site. Because the bright patches could be produced by hydrate accumulations, the presence of which would adversely affect core recovery, permission was requested and obtained to move the site 1.7 nmi north of BBOR-5. For pre-drilling purposes, this new site was designated BBOR-5B.

Drilling operations at Site 1060 began at 2253 hr on 5 March. All holes were cored with the advanced hydraulic piston corer (APC), with recovery ranging from 84% to 108% and with a site average of 104% (Table 1). The Tensor tool was used to orient Cores 172-1060A-3H through 11H, but sustained water damage and no data were retrieved. Thus, no cores were oriented at this site.

The seafloor depth was established at 3481.2 mbsl for Hole 1060A, which was 8.4 m shallower than the Precision Depth Recorder (PDR) depth. APC coring advanced without incident to a total depth of 170.0 mbsf. Hole 1060B is ~22 m southwest of Hole 1060A, and Hole 1060C is ~32 m southwest of Hole 1060B. The starting drill-string position was 3 m lower for Hole 1060B than Hole 1060A and then another 3 m lower for Hole 1060C. By 0400 hr on 8 March, drilling operations were completed at Site 1060 and the vessel was under way to Site 1061.

Site 1061

The 63-nmi transit to the survey area of Site 1061 was accomplished at an average speed of 11.6 kt. At 0930 hr on 8 March, the vessel slowed to deploy the seismic equipment. The ensuing seismic survey consisted of a north-to-south line over Site 1061 and a crossing west-to-east line (see "Site Geophysics" section, this chapter).

At 1325 hr on 8 March, a beacon was deployed on the new site, and at 1153 hr on 9 March, a second beacon was dropped as a backup. Five holes were drilled at Site 1061, with core recovery exceeding 100% at all holes except 1061A (Table 1).

From the first APC core at Hole 1061A, the seafloor depth was estimated as 4046.6 mbsl, which was 8.9 m shallower than the PDR (3.5 kHz) depth. Later, after examining the upper cores from other holes at this site and the downhole logging measurements, we confirmed that Core 172-1061A-1H did not capture the mudline. Instead, the top of the core was ~11 m below the mudline (see "Stratigraphic Correlation" section, this chapter), thus indicating the PDR depth was probably off by ~20 m.

APC coring advanced in Hole 1061A without incident to 152.0 mbsf, which was considered APC refusal. Cores 172-1061A-3H through 8H and 10H through 16H were oriented, whereas no other cores were oriented at this site because there was only one operational Tensor tool. Coring resumed with the XCB and advanced to a total depth of 350.3 mbsf by 1630 hr on 10 March.

In preparation for logging, the hole was flushed with a 30-bbl sepiolite (drill mud) sweep and the drill string was pulled back to 308

Table 1. Coring summary for Sites 1060, 1061, and 1062.

Core, section	Date (March 1997)	Time (UTC)	Interval (mbsf)	Length cored (m)	Length recovered (m)	Recovery (%)
172-1060A-						
1H	6	0610	0-9	9	9.06	100.7
2H	6	0705	9-18.5	9.5	9.97	104.9
3H	6	0755	18.5-28	9.5	9.85	103.7
4H	6	0845	28-37.5	9.5	10.14	106.7
5H	6	0935	37.5-47	9.5	10.11	106.4
6H	6	1025	47-56.5	9.5	10.17	107.1
7H	6	1115	56.5-66	9.5	10.04	105.7
8H	6	1210	66-75.5	9.5	9.34	98.3
9H	6	1310	75.5-85	9.5	10.22	107.6
10H	6	1400	85-94.5	9.5	10.21	107.5
11H	6	1455	94.5-104	9.5	10.19	107.3
12H	6	1550	104-113.5	9.5	10.19	107.3
13H	6	1640	113.5-123	9.5	9.85	103.7
14H	6	1735	123-132.5	9.5	10.14	106.7
15H	6	1815	132.5-142	9.5	10.13	106.6
16H	6	1900	142-151.5	9.5	9.92	104.4
17H	6	1950	151.5-161	9.5	9.07	95.5
18H	6	2035	161-170.1	9.1	9.14	100.4
Coring totals:				170.1	177.74	104.5
172-1060B-						
1H	6	2300	0-6.4	6.4	6.37	99.5
2H	6	2345	6.4-15.9	9.5	9.88	104.0
3H	7	0030	15.9-25.4	9.5	9.83	103.5
4H	7	0115	25.4-34.9	9.5	9.83	103.5
5H	7	0155	34.9-44.4	9.5	10.04	105.7
6H	7	0235	44.4-53.9	9.5	9.96	104.8
7H	7	0320	53.9-63.4	9.5	10.13	106.6
8H	7	0405	63.4-72.9	9.5	9.98	105.1
9H	7	0450	72.9-82.4	9.5	10.07	106.0
10H	7	0535	82.4-91.9	9.5	10.1	106.3
11H	7	0620	91.9-101.4	9.5	10.11	106.4
12H	7	0705	101.4-110.9	9.5	7.96	83.8
13H	7	0745	110.9-120.4	9.5	9.93	104.5
14H	7	0835	120.4-129.9	9.5	10.04	105.7
Coring totals:				129.9	134.23	103.3
172-1060C-						
1H	7	1035	0.0-3.0	3.0	2.94	98.0
2H	7	1135	3.0-12.5	9.5	9.08	95.6
3H	7	1220	12.5-22.0	9.5	9.62	101.3
4H	7	1305	22.0-31.5	9.5	9.72	102.3
5H	7	1350	31.5-41.0	9.5	9.75	102.6
6H	7	1435	41.0-50.5	9.5	9.90	104.2
7H	7	1520	50.5-60.0	9.5	10.12	106.5
8H	7	1610	60.0-69.5	9.5	9.88	104.0
9H	7	1705	69.5-79.0	9.5	10.00	105.3
10H	7	1755	79.0-88.5	9.5	10.02	105.5
11H	7	1840	88.5-98.0	9.5	10.07	106.0
12H	7	1930	98.0-107.5	9.5	10.00	105.3
13H	7	2020	107.5-117.0	9.5	9.74	102.5
14H	7	2110	117.0-126.5	9.5	9.94	104.6
Coring totals:				126.5	130.78	103.4
172-1061A-						
1H	8	2155	0.0-9.5	9.5	9.70	102.1
2H	8	2310	9.5-19.0	9.5	9.87	103.9
3H	9	0010	19.0-28.5	9.5	9.97	104.9
4H	9	0105	28.5-38.0	9.5	9.67	101.8
5H	9	0205	38.0-47.5	9.5	9.97	104.9
6H	9	0300	47.5-57.0	9.5	9.65	101.6
7H	9	0355	57.0-66.5	9.5	10.08	106.1
8H	9	0445	66.5-76.0	9.5	9.81	103.3
9H	9	0540	76.0-85.5	9.5	10.16	106.9
10H	9	0645	85.5-95.0	9.5	10.02	105.5
11H	9	0740	95.0-104.5	9.5	10.09	106.2
12H	9	0840	104.5-114.0	9.5	9.94	104.6
13H	9	0940	114.0-123.5	9.5	10.27	108.1
14H	9	1035	123.5-133.0	9.5	9.49	99.9
15H	9	1125	133.0-142.5	9.5	10.12	106.5
16H	9	1225	142.5-152.0	9.5	9.18	96.6
17X	9	1410	152.0-157.4	5.4	5.24	97.0
18X	9	1520	157.4-167.0	9.6	7.65	79.7
19X	9	1625	167.0-176.6	9.6	8.53	88.9
20X	9	1735	176.6-186.2	9.6	7.34	76.5
21X	9	1840	186.2-195.8	9.6	8.06	84.0
22X	9	1950	195.8-205.4	9.6	7.76	80.8
23X	9	2105	205.4-215.1	9.7	6.75	69.6
24X	9	2215	215.1-224.8	9.7	7.47	77.0
25X	9	2330	224.8-234.5	9.7	6.80	70.1
26X	10	0050	234.5-244.2	9.7	6.96	71.8
27X	10	0155	244.2-253.9	9.7	7.53	77.6
28X	10	0310	253.9-263.5	9.6	7.25	75.5
29X	10	0425	263.5-273.2	9.7	8.15	84.0
30X	10	0535	273.2-282.8	9.6	8.51	88.6
31X	10	0650	282.8-292.4	9.6	6.48	67.5
32X	10	0815	292.4-302.0	9.6	0.22	2.3
33X	10	0940	302.0-311.7	9.7	6.40	66.0
34X	10	1100	311.7-321.3	9.6	3.85	40.1
35X	10	1225	321.3-330.9	9.6	5.32	55.4
36X	10	1430	330.9-340.5	9.6	7.95	82.8
37X	10	1630	340.5-350.3	9.8	5.99	61.1
Coring totals:				350.3	298.20	85.1
172-1061B-						
1H	11	1635	0-9.5	9.5	9.82	103.4
Coring totals:				9.5	9.82	103.4
172-1061C-						
1H	11	1735	0.0-5.8	5.8	5.83	100.5
2H	11	1845	5.8-15.3	9.5	9.61	101.2
3H	11	1935	15.3-24.8	9.5	9.63	101.4
4H	11	2030	24.8-34.3	9.5	9.83	103.5
5H	11	2125	34.3-43.8	9.5	9.98	105.1
6H	11	2220	43.8-53.3	9.5	9.96	104.8
7H	11	2320	53.3-62.8	9.5	9.91	104.3
8H	12	0010	62.8-72.3	9.5	10.17	107.1
9H	12	0105	72.3-81.8	9.5	10.14	106.7
10H	12	0155	81.8-91.3	9.5	10.11	106.4
11H	12	0250	91.3-100.8	9.5	9.86	103.8
12H	12	0350	100.8-110.3	9.5	10.08	106.1
13H	12	0445	110.3-119.8	9.5	10.05	105.8
14H	12	0540	119.8-129.3	9.5	10.10	106.3
15H	12	0640	129.3-138.8	9.5	10.33	108.7
16H	12	0735	138.8-148.3	9.5	9.81	103.3
17H	12	0830	148.3-157.8	9.5	10.01	105.4
18H	12	0930	157.8-166.8	9.0	9.20	102.2
Coring totals:				166.8	174.61	104.7
172-1061D-						
1H	12	1145	0.0-1.2	1.2	1.12	93.3
2H	12	1240	1.2-10.7	9.5	9.24	97.3
3H	12	1335	10.7-20.2	9.5	9.41	99.1
4H	12	1425	20.2-29.7	9.5	9.81	103.3
5H	12	1520	29.7-39.2	9.5	9.92	104.4
6H	12	1605	39.2-48.7	9.5	10.04	105.7
7H	12	1700	48.7-58.2	9.5	9.88	104.0
8H	12	1750	58.2-67.7	9.5	10.15	106.8
9H	12	1835	67.7-77.2	9.5	10.10	106.3
10H	12	1955	77.2-86.7	9.5	10.16	106.9
11H	12	2050	86.7-96.2	9.5	9.83	103.5
12H	12	2150	96.2-105.7	9.5	10.17	107.1
13H	12	2250	105.7-115.2	9.5	10.11	106.4
14H	12	2350	115.2-124.7	9.5	10.03	105.6
15H	13	0050	124.7-134.2	9.5	9.83	103.5
16H	13	0140	134.2-143.7	9.5	10.06	105.9
17H	13	0240	143.7-153.2	9.5	9.54	100.4
18H	13	0335	153.2-162.7	9.5	10.06	105.9
19X	13	0450	162.7-165.7	3.0	5.11	170.3
20X	13	0545	165.7-170.7	5.0	6.58	131.6
21X	13	0640	170.7-175.2	4.5	5.59	124.2
22X	13	0730	175.2-180.0	4.8	8.21	171.0
Coring totals:				180.0	194.95	108.3
172-1061E-						
1H	13	0950	0.0-9.4	9.4	9.40	100.0
2H	13	1045	9.4-18.9	9.5	10.13	106.6
Coring totals:				18.9	19.53	103.3
172-1062A-						
1H	14	2310	0.0-2.2	2.2	2.15	97.7
2H	15	0025	2.2-11.7	9.5	9.48	99.8
3H	15	0120	11.7-21.2	9.5	9.78	102.9
4H	15	0250	21.2-30.7	9.5	9.75	102.6
5H	15	0350	30.7-40.2	9.5	9.92	104.4
6H	15	0455	40.2-49.7	9.5	9.88	104.0
7H	15	0615	49.7-59.2	9.5	10.05	105.8
8H	15	0720	59.2-68.7	9.5	9.51	100.1
9H	15	0825	68.7-78.2	9.5	9.72	102.3
10H	15	0945	78.2-87.7	9.5	9.95	104.7
11H	15	1055	87.7-97.2	9.5	9.94	104.6
12H	15	1240	97.2-106.7	9.5	9.59	100.9
13H	15	1400	106.7-116.2	9.5	9.08	95.6
14H	15	1515	116.2-125.7	9.5	8.11	85.4
15H	15	1625	125.7-135.2	9.5	9.62	101.3
16H	15	1745	135.2-144.7	9.5	9.50	100.0
17H	15	1850	144.7-154.2	9.5	9.31	98.0
18H	15	1955	154.2-163.7	9.5	9.25	97.4
19H	15	2105	163.7-173.2	9.5	9.11	95.9
20H	15	2210	173.2-180.7	7.5	7.54	100.5
Coring totals:				180.7	181.24	100.3
172-1062B-						
1H	16	0100	0.0-5.0	5.0	5.00	100.0
2H	16	0200	5.0-14.5	9.5	9.74	102.5
3H	16	0250	14.5-24.0	9.5	8.50	89.5
4H	16	0345	24.0-33.5	9.5	9.78	102.9

Table 1 (continued).

Core, section	Date (March 1997)	Time (UTC)	Interval (mbsf)	Length cored (m)	Length recovered (m)	Recovery (%)
5H	16	0440	33.5-43.0	9.5	9.94	104.6
6H	16	0535	43.0-52.5	9.5	9.87	103.9
7H	16	0630	52.5-62.0	9.5	9.92	104.4
8H	16	0730	62.0-71.5	9.5	9.68	101.9
9H	16	0820	71.5-81.0	9.5	7.45	78.4
10H	16	0915	81.0-90.5	9.5	9.76	102.7
11H	16	1010	90.5-100.0	9.5	9.76	102.7
12H	16	1105	100.0-109.5	9.5	9.38	98.7
13H	16	1205	109.5-119.0	9.5	9.54	100.4
14H	16	1305	119.0-128.5	9.5	9.74	102.5
15H	16	1405	128.5-138.0	9.5	9.63	101.4
16H	16	1520	138.0-147.5	9.5	9.93	104.5
17H	16	1625	147.5-156.7	9.2	9.20	100.0
18X	16	1740	156.7-162.1	5.4	4.57	84.6
19X	16	1855	162.1-171.7	9.6	9.96	103.8
20X	16	2005	171.7-181.3	9.6	9.69	100.9
21X	16	2125	181.3-190.9	9.6	9.85	102.6
22X	16	2240	190.9-200.5	9.6	9.68	100.8
23X	16	2350	200.5-210.2	9.7	9.97	102.8
24X	17	0100	210.2-219.8	9.6	9.49	98.9
25X	17	0205	219.8-229.4	9.6	9.32	97.1
26X	17	0315	229.4-239.0	9.6	9.73	101.4
270	17	0510	239.0-248.6	0.0	0.00	N/A
Coring totals:				239.0	239.08	100.0
172-1062C-						
1H	17	0805	0.0-9.4	9.4	9.39	99.9
2H	17	0905	9.4-18.9	9.5	9.91	104.3
3H	17	1000	18.9-28.4	9.5	9.74	102.5
4H	17	1055	28.4-37.9	9.5	9.83	103.5
5H	17	1150	37.9-47.4	9.5	9.65	101.6
6H	17	1250	47.4-56.9	9.5	9.75	102.6
7H	17	1345	56.9-66.4	9.5	9.73	102.4
8H	17	1455	66.4-75.9	9.5	9.14	96.2
9H	17	1600	75.9-85.4	9.5	9.71	102.2
10H	17	1710	85.4-94.9	9.5	9.64	101.5
11H	17	1815	94.9-104.4	9.5	9.81	103.3
12H	17	1920	104.4-113.9	9.5	9.32	98.1
13H	17	2025	113.9-123.4	9.5	9.30	97.9
14H	17	2135	123.4-132.9	9.5	9.64	101.5
Coring totals:				132.9	134.56	101.2
172-1062D-						
1H	17	2355	0.0-5.8	5.8	5.81	100.2
2H	18	0245	5.8-15.3	9.5	9.28	97.7
3H	18	0340	15.3-24.8	9.5	9.81	103.3
4H	18	0445	24.8-34.3	9.5	9.42	99.2
5H	18	0540	34.3-43.8	9.5	9.78	102.9
6H	18	0635	43.8-53.3	9.5	9.20	96.8
7H	18	0730	53.3-62.8	9.5	9.64	101.5
8H	18	0830	62.8-72.3	9.5	9.76	102.7
9H	18	0930	72.3-81.8	9.5	9.96	104.8
Coring totals:				81.8	82.66	101.0
172-1062E-						
1H	18	1530	0.0-3.8	3.8	3.79	99.7
2H	18	1650	3.8-13.3	9.5	9.49	99.9
3H	18	1750	13.3-22.8	9.5	9.83	103.5
4H	18	1855	22.8-32.3	9.5	9.58	100.8
5H	18	2000	32.3-41.8	9.5	9.70	102.1
6H	18	2105	41.8-51.3	9.5	9.58	100.8
7H	18	2210	51.3-60.8	9.5	9.87	103.9
8H	18	2315	60.8-70.3	9.5	9.61	101.2
9H	19	0020	70.3-79.8	9.5	10.04	105.7
10H	19	0125	79.8-89.3	9.5	9.67	101.8
11H	19	0220	89.3-98.8	9.5	9.95	104.7
12H	19	0330	98.8-108.3	9.5	9.95	104.7
13H	19	0435	108.3-117.8	9.5	9.50	100.0
14H	19	0540	117.8-127.3	9.5	9.12	96.0
15H	19	0645	127.3-136.8	9.5	9.93	104.5
16H	19	0755	136.8-145.1	8.3	8.28	99.8
17X	19	0855	145.1-151.1	6.0	5.58	93.0
18X	19	0955	151.1-160.7	9.6	8.63	89.9
19X	19	1100	160.7-170.4	9.7	5.58	57.5
20X	19	1205	170.4-179.9	9.5	7.42	78.1
21X	19	1315	179.9-189.5	9.6	8.69	90.5
22X	19	1430	189.5-199.2	9.7	10.06	103.7
23X	19	1545	199.2-208.8	9.6	9.87	102.8
Coring totals:				208.8	203.72	97.6
172-1062F-						
1H	19	1830	0.0-7.1	7.1	7.10	100.0
2H	19	1935	7.1-16.6	9.5	9.22	97.1
3H	19	2035	16.6-26.1	9.5	9.56	100.6
4H	19	2130	26.1-35.6	9.5	9.44	99.4
5H	19	2230	35.6-45.1	9.5	9.65	101.6
6H	19	2330	45.1-54.6	9.5	9.70	102.1
7H	20	0025	54.6-64.1	9.5	9.63	101.4
8H	20	0120	64.1-73.6	9.5	9.71	102.2
9H	20	0225	73.6-83.1	9.5	9.76	102.7
Coring totals:				83.1	83.77	100.8
172-1062G-						
1H	20	0815	0-9.3	9.3	9.27	99.7
Coring totals:				9.3	9.27	99.7
172-1062H-						
1H	20	0925	0.0-6.5	6.5	6.53	100.5
2H	20	1015	6.5-16.0	9.5	9.68	101.9
3H	20	1125	16.0-25.5	9.5	9.86	103.8
4H	20	1225	25.5-35.0	9.5	9.91	104.3
5H	20	1335	35.0-44.5	9.5	10.07	106.0
6H	20	1445	44.5-54.0	9.5	9.59	100.9
7H	20	1555	54.0-63.5	9.5	9.65	101.6
Coring totals:				63.5	65.29	102.8

Notes: UTC = Universal Time Coordinated. For each site, an expanded coring summary table for each hole that includes lengths and depths of sections and sampling comments is included on CD-ROM (back pocket, this volume).

mbsf and then up to 68 mbsf, with a maximum drag of 20 kips. When the drill string was run back to the bottom of the hole, it contacted only 2 m of soft fill. The hole was cleaned with 162 bbl of 8.9 lb/gal sepiolite mud. The drill string was pulled up and the bit positioned at the logging depth of 93 mbsf.

By 2330 hr on 10 March, the Schlumberger equipment was prepared and the first logging tool (triple combination suite consisting of the dual induction tool [DIT], hostile environment litho-density tool [HLDT], accelerator porosity sonde [APS], and hostile environment natural gamma-ray sonde [HNGS]) was run into the drill pipe. The logging tool went almost to bottom with no apparent problems, and the hole was successfully logged from 348 to 77 mbsf and then from 350 to 262 mbsf on a second pass. The final log consisted of two passes with the FMS tool, sonic digital tool (SDT), and natural gamma-ray tool (NGT) combination, which was run in the hole from 338 to 73 mbsf. The diameter of the hole was found to vary from 28 to 38 cm (11–15 in) and the angle of the hole was less than 2° from vertical. The quality of the logging data was considered to be very good (see "Downhole Logging" section, this chapter).

At 1606 hr on 11 March, Hole 1061B was spudded 36 m north of Hole 1061A and the drill string was positioned 3 m higher. The first APC core recovered a full barrel, and so the hole was abandoned. The bit was picked up to 4044.5 mbrf and Hole 1061C was spudded ~4 m to the south of Hole 1061B. Based upon the mudline recovery, the seafloor depth was established at 4036.9 mbsl. APC coring advanced to an APC refusal depth of 166.8 mbsf.

Hole 1061D was spudded ~32 m north of Hole 1061C and the bit was positioned 3 m higher than at Hole 1061C. The seafloor depth was estimated at 4038.4 mbsl. APC coring advanced to 162.7 mbsf, which was just below the APC refusal depth of Hole 1061C. The hole was then deepened with the XCB to a total depth of 180.0 mbsf.

Hole 1061E was spudded ~44 m north and 6 m west of Hole 1061D, with the bit positioned at 4047.0 mbrf, about 2.5 m deeper than at Hole 1061C. The hole consisted of only two piston cores, which were cored to ensure that a complete record of the Holocene and upper Pleistocene section had been recovered. The drill string was pulled out of the hole and cleared the seafloor at 1100 hr on 13 March. By 1845 hr on 13 March, drilling operations were completed and the vessel was under way to Site 1062.

Site 1062

The 61-nmi transit to the survey area of Site 1062 (prospectus sites BBOR-1, -1B, and -1C) was accomplished at an average speed

of 11.3 kt. At 0600 hr on 14 March, the vessel slowed as the generator-injector (GI) air gun and seismic streamers were deployed. The vessel then steered a westerly course as a seismic survey was conducted over BBOR-1, BBOR-1C, BBOR-1B, and then BBOR-1A. The vessel came about and performed crossing profiles: first, a southwest-to-northeast seismic profile across BBOR-1A, then a northeast-to-southwest profile over BBOR-1B, and finally a south-southeast to north-northeast profile over BBOR-1 (see "Site Geophysics" section, this chapter).

Site 1062 includes eight holes drilled into a single mud wave. Holes 1062A, 1062B, 1062C, and 1062D are on the east side of the mud wave, Holes 1062E and 1062F are on the west side, and Holes 1062G and 1062H are near the crest. The far west and far east holes are 1050 m apart. To properly position the vessel over the holes on both the east and west sides, two beacons were required. Normal practice would be to identify the holes on either side of the mud wave as two different sites when two different beacons were used. However, because the holes comprise a transect across a single mud wave, we instead requested that they all be considered a single site, which was approved. The total core recovery for the site was greater than 100%, with 1000 m of core recovered (Table 1).

Drilling operations began at Hole 1062A (BBOR-1) at 1045 hr on 14 March. The drill string was run to 4743.0 mbrf, whereas additional stands of 5.5-in drill pipe were measured and rabbited (see "Operations" section, "Intermediate Depth Blake Outer Ridge" chapter, this volume). The bit was lowered to 4758.0 mbrf, which was 20 m shallower than the PDR indicated. The first attempt at an APC mudline recovered only water, although a second attempt from 4767.5 mbrf successfully established the seafloor depth at 4763.3 mbsl (4774.8 mbrf). APC coring advanced to refusal at 180.7 mbsf. During coring at this hole in the early morning of 15 March, ship motion became severe enough (2 to 3 m of heave and 2° to 3° rolls combined with 520 kips of string weight) that knobby joints (heavy-wall drilling joints) were used rather than drill-pipe joints after recovering Cores 172-1062A-8H through 10H. The weather calmed by mid-morning and the knobby joints were removed and replaced with drill-pipe joints. Adara heat-flow measurements were conducted at 30.7 (Core 172-1062A-4H), 59.2 (7H), 87.7 (10H), 116.2 (13H), and 144.7 (16H) mbsf. Cores 172-1062A-4H through 9H and 10H through 16H were oriented.

Hole 1062B was spudded 13 m north of Hole 1062A and with an initial bit position 9.5 m deeper. APC coring advanced to APC refusal depth (156.7 mbsf), after which coring continued with the XCB. No cores were oriented in this hole.

While attempting to retrieve the core barrel after cutting Core 172-1062B-27X (239.0 to 248.6 mbsf), it was discovered that the XCB shaft, the core barrel, the core, and miscellaneous hardware were missing. Because this hardware was left at the bottom of the hole, further progress to the depth objective of 250 mbsf was not possible.

Hole 1062C was spudded 12 m north and 7 m east of Hole 1062B at 0740 hr with the bit positioned at 4772.0 mbrf. The seafloor depth was estimated at 4772.1 mbrf based upon recovery of 9.39 m. APC coring advanced to a total depth of 132.9 mbsf by 2145 hr on 17 March. Cores 172-1062C-8H through 14H were oriented.

Hole 1062D was spudded 6 m north of Hole 1062C and the bit was positioned at 4768.0 mbrf. The recovery of 5.81 m established the seafloor depth at 4771.7 mbrf. After the core barrel was recovered, a water-sampler, temperature, and pressure (WSTP) probe was run down the pipe to a level just above the seafloor and a water sample was obtained. APC coring resumed and advanced to a total depth of 81.8 mbsf. No cores were oriented in this hole.

To prepare for the offset for Hole 1062E (BBOR-1B), the end of the drill pipe was placed at 4656 mbrf. The beacon was remotely commanded into standby mode to preserve battery life, and then the vessel was slowly offset west. At 1109 hr on 18 March, a second beacon was deployed on the global positioning system (GPS) coordinates of BBOR-1B. The bit was positioned at 4772.0 mbrf, ~10 m shallower than the new PDR depth of 4782.4 mbrf. The first attempt at a mudline resulted in a water core and so the bit was lowered to 4780.0 mbrf, where Hole 1062E was spudded. Hole 1062E is 1044 m west and 62 m south of Hole 1062D. APC coring advanced to the refusal depth of 136.8 mbsf (Core 172-1062E-16H). Coring resumed with the XCB and advanced to the target depth of 208.8 mbsf by 1600 hr on 19 March. APC Cores 172-1062E-4H through 10H and 12H through 16H were oriented.

Hole 1062F was spudded 11 m north and 16 m west of Hole 1062E, and the bit was positioned at 4783.0 mbrf. APC coring advanced to a total depth of 83.1 mbsf by 0230 hr on 20 March. No cores were oriented in this hole.

The end of the drill pipe was positioned at 4670.0 mbrf and the vessel was offset 725 m to Hole 1062G (BBOR-1C). As the drill pipe was being picked up, the second beacon deployed on this site was recovered. The first beacon was commanded out of standby mode as the vessel settled over the coordinates of BBOR-1C. Hole 1062G is 724 m east and 30 m south of Hole 1062F and is 330 m west and 50 m south of Hole 1062A. Hole 1062G was spudded with the APC bit at 4759.0 mbrf, which was 8.4 m shallower than the new PDR reading of 4767.4 m. This time, however, a full core barrel was obtained, and so the hole was abandoned.

The bit was picked up to 4754.0 mbrf where Hole 1062H was spudded 3 m southeast of Hole 1062G at 0902 hr on 20 March. The recovery of 6.5 m of core established the seafloor depth at 4745.3 mbsl (4757.0 mbrf). APC coring advanced to a total depth of 63.5 m (Core 172-1062H-7H) by 1615 hr on 20 March. Cores 172-1062H-3H through 7H were oriented. By 0145 hr on 21 March, all drilling equipment had been secured and the vessel got under way to the Bermuda Rise.

LITHOSTRATIGRAPHY

Sites 1060, 1061, and 1062 were occupied to recover a continuous sequence of sediments near the depth of present-day NADW and a deeper water mass formed from the mixing of NADW with AABW. Site 1062 is located on a mud wave, and holes were located on different wave flanks and on the mud-wave crest to study mud-wave evolution over time. Site 1062 is also located in the Bahama Basin, a depression adjacent to the Bahama Banks and Blake Escarpment, and thus is a local source of carbonate turbidites.

Description of Lithostratigraphic Units

Site 1060

Three holes were continuously cored at Site 1060, with the deepest hole, Hole 1060A, penetrating to 170.10 mbsf. Only one unit is defined at this site based on lithological, magnetic susceptibility, carbonate content, and color reflectance characteristics (data on CD-ROM, back pocket, this volume). This unit exhibits variability characteristics similar to those seen in the uppermost unit at neighboring Leg 172 Sites. The lithologic descriptions for Site 1060 are mostly based on Hole 1060A.

Unit I

Intervals: 172-1060A-1H-1, 0 cm, through 18H-CC, 18 cm (0–170.10 mbsf; bottom of hole); 172-1060B-1H-1, 0 cm, through 18H-CC, 26 cm (0–129.90 mbsf; bottom of hole); 172-1060C-1H-1, 0 cm, through 14H-CC, 19 cm (0–126.50 mbsf; bottom of hole)
Age: Holocene to middle Pleistocene

Unit I consists of Holocene and late to middle Pleistocene nannofossil ooze, clayey nannofossil ooze, nannofossil clay mixed sediment, nannofossil clay, nannofossil clay with silt, clay with nannofossils and silt, clay with silt, clay with nannofossils, and clay,

with the latter two lithologies being dominant. Bedding generally ranges from 0.2 to 2 m in thickness. Most lithological changes are gradual, although pronounced transitions sometimes occur within a decimeter. One characteristic of this unit is the degree of variability in the lithology, which is evident in the records of color reflectance and carbonate content of the sediment (Fig. 1). Sediment color usually ranges from dark greenish gray (5GY 4/1) in the clay to light greenish gray (5GY 8/1) in the sediments, with more biogenic carbonate. In some intervals the clay and clay with nannofossil lithologies have a brownish gray to pale brown (5YR 5/2 to 5YR 5/2) color (e.g., interval 172-1060A-1H-1, 128 cm, to 2H-1, 150 cm) or a reddish tinge (e.g., interval 172-1060A-12H-3, 30–60 cm). In the uppermost 4 cm of Hole 1060A, this is probably due to the sediment being above the redox boundary, whereas below this depth the coloration results from trace quantities of ferruginous minerals or iron-stained grains.

Very distinctive zones of intense black mottling are common in the intervals between 172-1060A-1H-4, 30 cm, and 1H-6, 120 cm, 172-1060A-3H-2, 140 cm, and 3H-5, 110 cm, and 172-1060A-5H-7, 0 cm, and 6H-4, 60 cm, although they are also present in other parts of the hole to a lesser extent. The mottling is also found at similar depths in the other holes, and is caused by the presence of iron sulfide minerals, possibly hydrotroilite. Although not exclusively, it may to some extent account for the low reflectance of these intervals (Fig. 1). A sample of the black material thought to be hydrotroilite was submitted for XRD analysis (Samples 172-1060A-5H-CC, 1 and 2, first as a glass slide and second as a powder mount). The diffractogram showed peaks diagnostic for the iron sulfide troilite. Disseminated black sulfide staining on a much smaller scale is present in most of the sediments below the uppermost section in the hole. Other zones ~1 cm thick with distinct green coloration, coarse texture, and uncertain mineralogy are also distributed throughout the core.

Sequences containing silt laminae are not very common, with only three occurrences noted at this site. Silt laminae at interval 172-1060A-9H-4, 45–55 cm (Fig. 2) are correlative with interval 172-1060B-9H-7, 10–15 cm, and probably also interval 172-1060C-10H-2, 5–10 cm. Although silt layers were not mentioned in the description for this event in Hole 1060C, the whole-core photograph shows a clay layer with similar features and stratigraphic position. Another layer in interval 172-1060B-14H-2, 74–98 cm, can be correlated with interval 172-1060C-14H-5, 2–16 cm (Fig. 3). This bed was not documented in Hole 1060A, but stratigraphic correlation suggests it may have been present just at the base of Section 172-1060A-14H-7 or in the Core 172-1060A-14H-CC paleontology sample. A third layer is found only in interval 172-1060A-16H-3, 50–57 cm, which is below the depth cored in the other holes. In general, the structures consist of darker sediment having sharp basal contacts with the underlying lighter sediment. The bottom few centimeters contain several silty discontinuous laminae, and are overlain by dark green clay. The upper contacts are more gradual than the base but may still be distinct enough for bioturbation to be highlighted by the contrast in sediment colors. In the case of the sequence at interval 172-1060A-16H-3, 50–57 cm, the clay layer has a slight reddish (2.5 YR 6/4) tinge.

Bioturbation is most obvious where there is a rapid change in lithology presenting contrasting colors, and in the lighter beds where diagenetic colors may be more noticeable. However, the presence of faint mottling in most of the sections suggests that bioturbation is pervasive throughout the sediment record. *Chondrites* (Fig. 4) and *Zoophycos* were recognized among the bioturbation forms.

Smear slides show most of the sediment to be in the clay size range, with some silt represented by quartz and mica (see Section 5 for smear-slide tables). Feldspars are probably under-represented because bulk sediment X-ray diffraction indicates their presence in the sediment (Table 2), although in lesser quantities than quartz. This could be the result of misidentification of some of the silt particles or their presence in the clay-sized fraction (Shipboard Scientific Party, 1996).

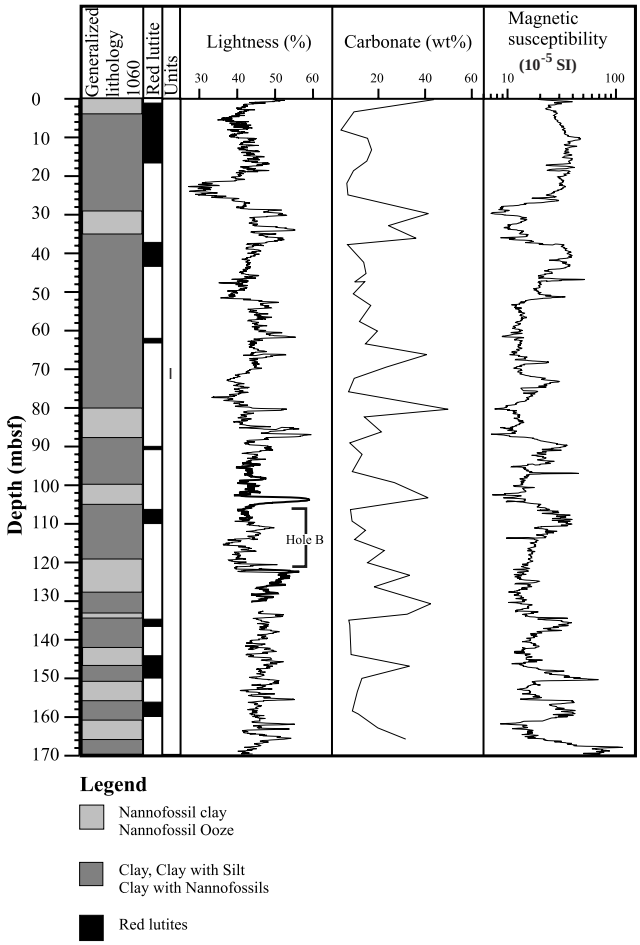

Figure 1. Generalized lithology, occurrence of red lutite beds, sediment units, color reflectance as lightness (L*), weight percent carbonate, and magnetic susceptibility (log scale) for Hole 1060A. Color reflectance is shown for Hole 1060B in the gaps in the Hole 1060A record. Note the degree and nature of the covariance between carbonate and reflectance and the negative covariance between carbonate and magnetic susceptibility, underlining the role carbonate variability plays in the lithology at this site.

Carbonate values range from 7 to 44 wt% (see "Organic Geochemistry" section, this chapter). Calcite dominates the carbonate mineralogy and is present primarily in the form of calcareous nannofossils which can make up a significant proportion of the clay-sized fraction in carbonate-rich sediments. Foraminifers may also contribute a minor amount of calcite—smear slides indicate less than 1%. X-ray diffraction suggests the presence of small quantities of aragonite in Sample 172-1060A-1H-1, 50 cm. Carbonate rhombs 5–25 µm in size and anhedral grains with similar optical characteristics were observed at <1% abundance in many of the smear slides, including those from the top (Sample 172-1060A-1H-1, 15 cm) and bottom cores (Sample 172-1060A-18H-1, 30 cm). Dolomite is present in the diffractograms from each section, and peak heights in low carbonate sediments almost match those of calcite. The persistent dolomite peak and the greater relative abundance of carbonate rhombs in sediments with low carbonate suggest that the rhombs may be dolomite.

Biogenic silica in the sediment is represented by sponge spicules, diatoms, silicoflagellates, and radiolarians. Generally biogenic silica levels are <1% of the sediment. In some cases, however, total biogenic silica levels may comprise almost 10% of the sediment, although no single group dominates. Biosiliceous content is generally higher in the clay and clay with nannofossil lithologies of greenish gray coloration. Sponge spicules occur in nearly all lithologies.

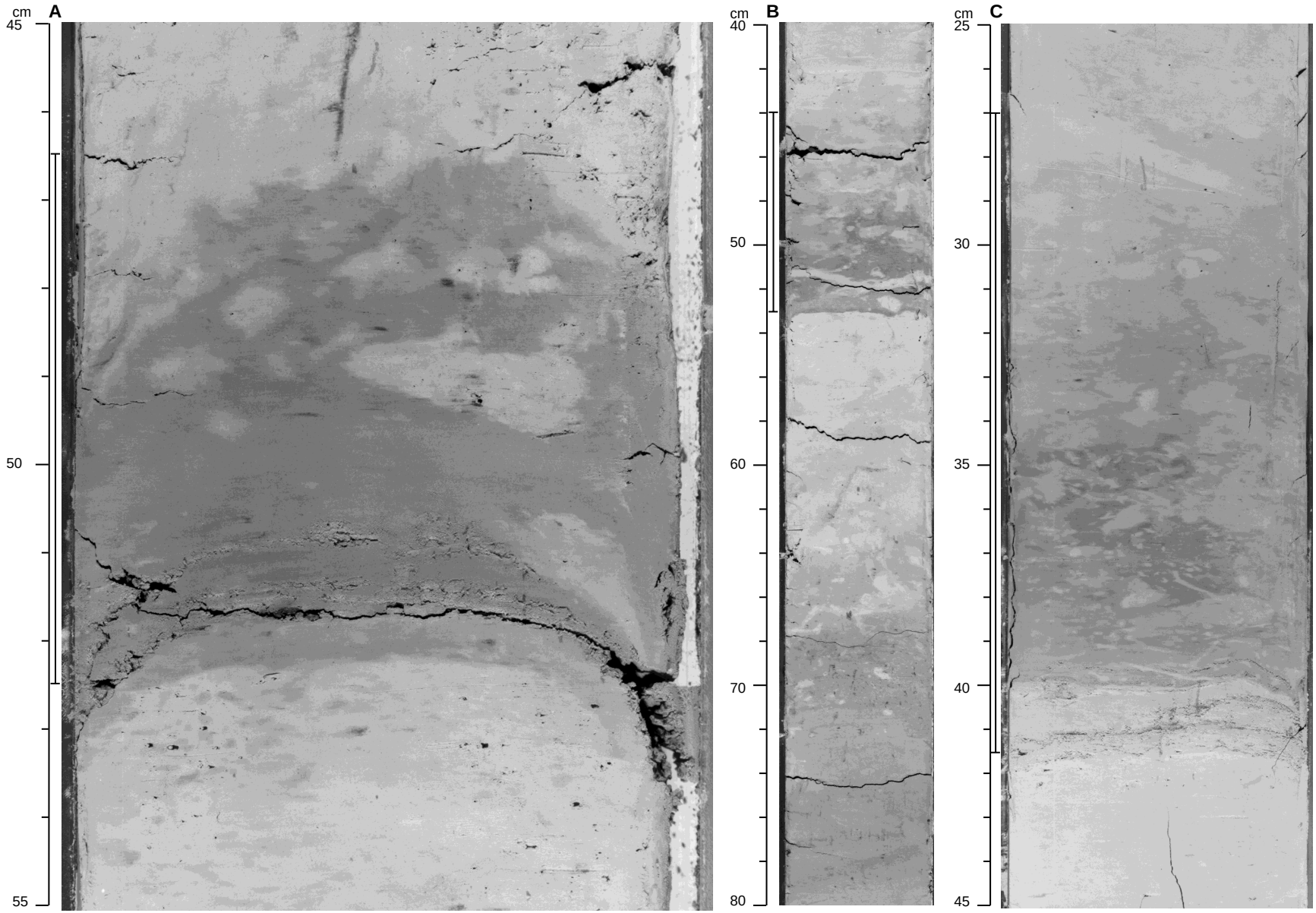

Figure 2. Correlated depositional events at Sites 1060, 1061, and 1062 (upper event) marked by bars next to photos. **A.** Event at interval 172-1060A-9H-4, 46.5–52.5 cm (80.45 mbsf). Silt laminae in a dark clay with a sharp basal contact, and a well-bioturbated upper contact to carbonate units. **B.** Event at interval 172-1061D-9H-4, 44–53 cm (72.75 mbsf). The darker clay layer has a sharp, basal contact, and a clay-rich layer ~0.4 cm thick (52.5–53 cm) lies a short distance above the top of the carbonate layer. The upper contact to a carbonate layer is bioturbated. The bioturbated lower contact of the next deeper carbonate interval is observed at about 65 cm. **C.** Event at interval 172-1062B-6H-4, 27–41.5 cm (47.8 mbsf). Silt laminae are at the base of a darker clay layer (showing burrowing from the above carbonate unit). In this case, the silt laminations are clearly separated from the darker sediment layer by a slightly lighter interval, perhaps suggesting a complex erosional/depositional cycle.

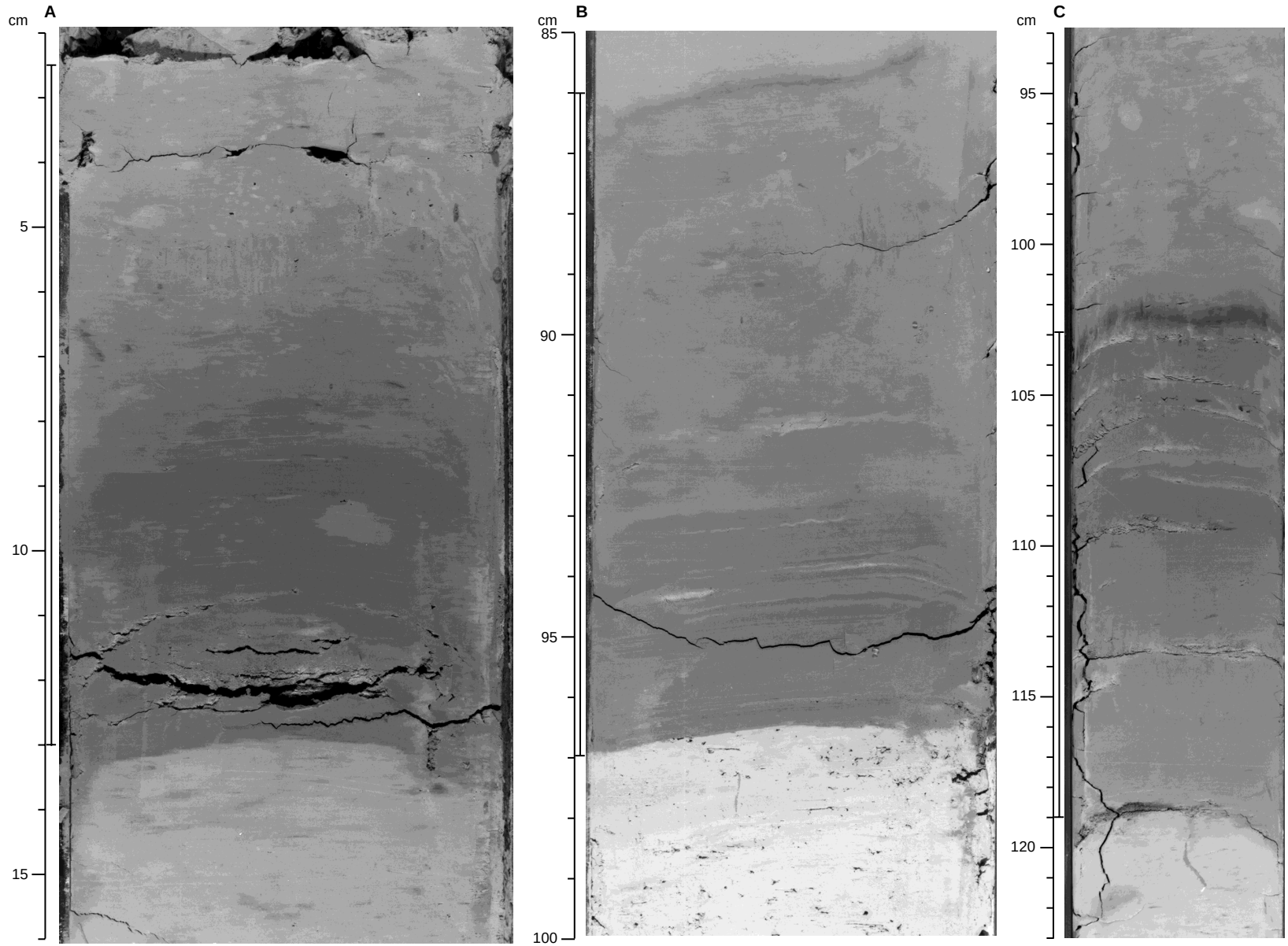

Figure 3. Correlated depositional events at Sites 1060, 1061, and 1062 (lower event) marked by bars next to photos. **A.** Event at interval 172-1060C-14H-5, 2.5–13 cm (122.10 mbsf). This thick clay unit has a sharp contact to an underlying carbonate layer with silt laminations near the base. **B.** Event at interval 172-1061C-13H-4, 86–97 cm (115.77 mbsf). A 10.6-cm thick, clay-rich, weakly bioturbated unit with silt laminations near the base that has a sharp contact with an underlying carbonate layer. Although the contact between the carbonate and clay layers is sharp, a burrow in the carbonate has apparently been filled by darker clay sediment, suggesting that little carbonate sediment was eroded. The faint, darker layer at 86 cm is a purple diagenetic layer below the overlying carbonate interval. **C.** Event at interval 172-1062B-8H-5, 103–119 cm (69.03 mbsf). A 16-cm-thick layer with silt laminations throughout. These yellowish silt layers are interbedded with olive green (5Y 5/1) clay. The lowermost silt layer truncates the underlying yellowish gray carbonate-rich layer, and the overlying contact is bioturbated. The diffuse dark band at 103 cm is a purple diagenetic layer below the overlying carbonate interval.

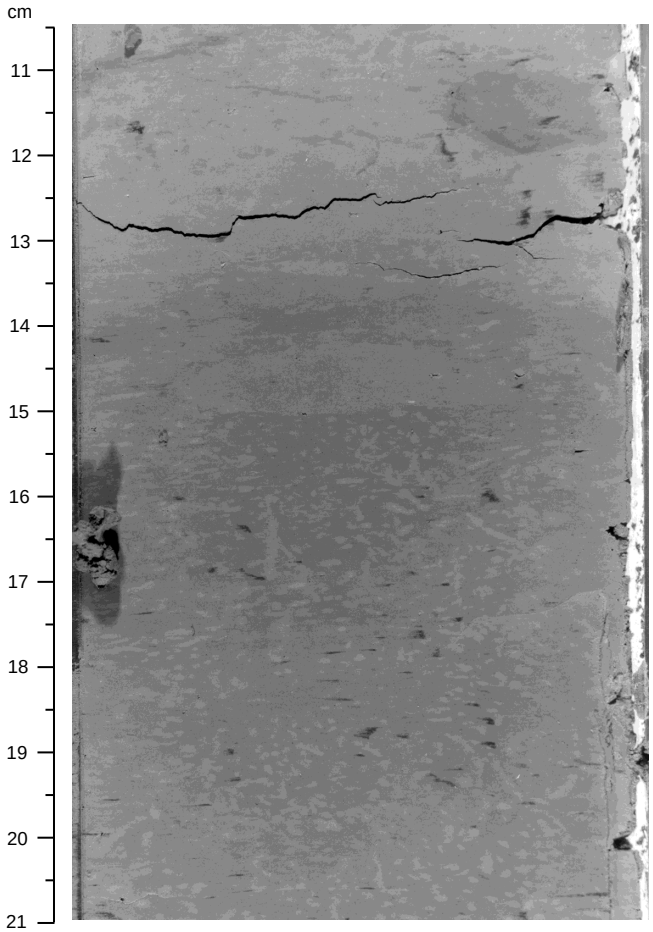

Figure 4. *Chondrites* bioturbation at interval 172-1060C-7H-3, 10-21 cm, highlighted by the contrasting sediment colors.

Site 1061

Five holes were continuously cored at Site 1061, with the deepest hole, Hole 1061A, penetrating to 346.5 mbsf (adjusted depth, 357.5 mbsf; see "Stratigraphic Correlation" section, this chapter). The recovered sediments provide a high-quality sediment record for the past 3.1 m.y. suitable for detailed paleoclimatic study, especially in the region of multiple APC coring (to ~1.0 Ma). The sediments at Site 1061 consist of carbonate-rich and carbonate-poor units that alternate on scales ranging from ~20 cm to ~10 m. Sediment types range from nannofossil ooze (the carbonate-rich units) to clay (the carbonate-poor units). A few distinctive beds and silt laminations were also noted, presumably of bottom current origin. Colors range from light and dark greenish gray to shades of orange and reddish brown. Three lithologic units are distinguished on the basis of bed thicknesses, carbonate content, and lightness (L*) variability (Fig. 5; see data on CD-ROM, back pocket, this volume). Additional information for distinguishing sedimentary units comes from downhole logs (see "Downhole Logging" section, this chapter). Lithology is described primarily from Holes 1061D (Units I and II) and 1061A (Units II and III).

Comparisons between cores recovered at Holes 1061A through 1061E (see "Composite Depths and Stratigraphic Correlation" section, this chapter), and log profiles at Hole 1061A (see "Downhole Logging" section, this chapter) suggest that the first core at Hole 1061A missed the mud line, but started about 11 mbsf. The single core at Hole 1061B also did not recover a mud line, but that hole is not included in the lithologic description. In order to facilitate comparisons between holes and with downhole logs, the depths cited in Unit I are the curated mbsf for Hole 1061D, the hole described in detail. Where depths are based on Hole 1061A, estimated corrected depths (reported mbsf + 11 m or as adjusted depth) are used in preference to the reported mbsf depths.

Unit I

Intervals: 172-1061A-1H-1, 0 cm, through 17X-2, 5 cm (11–164.55 mbsf + 11 m); 172-1061B-1H-1, 0 cm, through 1H-CC, 67 cm (0–9.82 mbsf; bottom of hole); 172-1061C-1H-1, 0 cm, through 17H-CC, 28 cm (0–158.31 mbsf); 172-1061D-1H-1, 0 cm, through 18H-CC, 24 cm (0–163.26 mbsf); 172-1061E-1H-1, 0 cm, through 2H-CC, 26 cm (0–19.53 mbsf; bottom of hole)
Age: Holocene to middle Pleistocene

Unit I is characterized by alternating beds of lighter, bioturbated, and carbonate-rich (nannofossil ooze, nannofossil clay, clay with nannofossils) and darker, more weakly bioturbated, carbonate-poor sediments (clay with silt and nannofossils, clay with biosilica, clay with silt, clay). The upper 70 cm is moderate yellowish brown nannofossil clay (10YR 5/4) of Holocene age underlain by a layer of grayish brown (2Y 5/2) color that appears to have a diagenetic origin. Sediments above ~10 mbsf are stained black by iron sulfides (probably hydrotroilite), and show numerous black layers of weakly cohesive material. Similar layering is also seen in Core 172-1061D-6H (39–44 mbsf). Detailed samples were taken across several layers at 5–8 mbsf to better characterize their nature. Carbonate analyses (see "Organic Geochemistry" section, this chapter) suggest that these layers have systematically lower carbonate values (3–6 wt% carbonate) than adjacent sediments (6–8 wt% carbonate).

The carbonate-rich units, which are intensely bioturbated, are classified as nannofossil ooze to nannofossil clay lithologies. Carbonate-poor units, which are weakly to moderately bioturbated with pyritized worm burrows, are classified as clay, clay with silt, and clay with nannofossils lithology. Carbonate contents in the lighter layers range from 10 to 54 wt% (see "Organic Geochemistry" section, this chapter), whereas carbonate contents in the darker layers are lower, ranging from 4 to 17 wt%. The overlap in carbonate content between the two layers suggests that carbonate content is not the only control on sediment lightness. Sediment colors range from light greenish gray to greenish gray to dark greenish gray, alternating with reddish brown and reddish green sediment. In some cases, the reddish layers appear as distinctive horizons (2.5 YR 5/6; 2.5 YR 5/4) up to about 10 cm thick in the upper part of Unit I and up to about 2 m thick deeper in Unit I, or as a reddish color intermixed with light or dark greenish gray sometimes leading to a brown color. Reddish intervals (groupings of red layers or reddish sediments as thick as 3 to 4 m) occur centered at ~3, 25, 36, 60, 75, 82, 109, 129, 138, and 149 mbsf. The redox state of the sediment plays some role in the variation between red and green sediment. On several occasions, we noted that reddish sediments had become green in the vicinity of a preserved burrow (Fig. 6), suggesting that oxidation of organic matter concentrated in the burrow altered the color of the sediment adjacent to the burrow from red to green. Red and green coloring was also observed to be intermixed where there were no obvious sediment structures, also suggesting a chemical control on color. Thus green sediment now may once have been red. Some of these greenish sediments may change color with time now that they have been exposed to air.

The carbonate-rich beds are numerous but generally thin, ranging from ~20 to 150 cm thick. They are often present in groups up to ~10 m thick, and the groups are rarely spaced more than 5 m apart. The lower contact between light greenish gray carbonate-rich beds and dark greenish gray clay beds often shows a distinctive color pattern, apparently produced by diagenesis. This pattern usually consists of one dark green layer (1–2 cm thick) overlain by one purple layer (0.5–1 cm thick). The purple layer may actually be separated from the dark green layer by as much as 10 cm, and it sometimes occurs nearly in the center of the carbonate-rich layer. The exact diagenetic

Table 2. XRD data for Sites 1060, 1061, and 1062.

Core, section, interval (cm)	Quartz	K-spar	Plagioclase	Clay	Calcite	Dolomite	Aragonite	Pyrite	Mica group	Hematite	Unit
172-1060A-											
1H-1, 50	25.3	0	8.7	6.2	42.2	3.7	1.3	4.4	8.4	0	
2H-4, 121	36.8	2.5	13.6	7.1	20.4	6.9	1	3.3	8.5	0	
3H-3, 20	43.9	0	12.9	5.6	21.1	5.1	1.7	2.5	7.1	0	
3H-4, 53	39.5	2.8	18.1	8.4	14	3.9	1.1	3.3	9	0	
4H-5, 113	38.2	2.6	11.4	7.1	25.4	4.3	1	4.2	5.5	0.1	
5H-5, 86	41.6	1.7	11.3	7.3	16.1	9.3	0.9	3.3	8.6	0	
5H-CC, 1	36.6	0	13.2	4.4	21.0	7.4	1.2	3.9	11.8	0.4	
5H-CC, 2	39.9	2	12.1	5.6	12.3	6.3	1.2	1.8	18.3	0.3	
6H-3, 136	36.2	3	19.7	9	12	7	1	1.6	10.5	0	
6H-5, 89	33.1	1.8	14.3	4.8	31.7	1.9	0.9	3.9	7.6	0	
7H-3, 17	38.1	2.3	13	6.9	20.7	5.7	1	4.3	7.9	0	I
8H-5, 50	37.6	2.4	12.5	8	10.5	5.8	1.2	5.2	16.6	0	
9H-3, 50	32.7	2.7	16.8	7.5	24.7	3.7	0.9	3.6	7.3	0	
10H-4, 75	36.6	2.2	9.8	7.2	26.5	5.5	0.7	2.3	9.1	0	
11H-4, 80	40.1	2.1	13.8	6.8	21.8	3.5	1	3.4	7.6	0	
12H-5, 57	39.7	2.3	11.8	8.6	19.8	6.4	1	2.1	8.2	0.1	
13H-2, 22	41	3	22	7	9.8	2.9	1.3	2.8	10.2	0	
14H-2, 33	37.1	3	20.6	5.4	17.8	4.3	1.3	2.1	8.2	0	
15H-5, 94	43.8	1.8	14	7.6	17.9	4	0.7	2.8	7.3	0	
16H-4, 52	26.2	1.5	11.4	6.1	29.5	3.5	1.3	3.3	17.1	0	
17H-5, 99	38.8	1.7	11.2	9	13.6	6	0.9	2.1	16.7	0	
18H-5, 32	42.1	0	7.3	8.7	14.5	11.2	0.8	3	11.9	0.6	
172-1061A-											
1H-2, 45	26.4	2	11.2	6.3	35.2	4.7	0.8	4.2	8.8	0.5	
2H-2, 65	38.6	2.7	17.5	7.3	13.6	4	1.2	3.5	11.7	0	
3H-5, 99	35.8	2.5	12.7	11.2	18.8	2.1	1.3	3.6	11.6	0.2	
4H-2, 32	42.7	0	11.9	7.3	16.8	7.9	0.9	3	9.5	0	
5H-2, 26	37.3	3.3	20.5	7.3	15.5	2.4	1.1	3.1	9.5	0.1	
6H-6, 86	23.8	1.7	9.2	6.3	42.9	4.1	0.7	4.6	6.8	0	
7H-6, 18	13.7	1.3	8.3	7.2	56.3	6.6	0.5	2.9	3.2	0	
8H-3, 43	25.6	1.7	10.7	6.8	38.3	4.4	0.5	1.8	10.2	0	I
9H-1, 46	20.5	1.5	9	6.2	48	4.5	0.6	2.5	7.2	0	
10H-4, 91	47.2	2.1	12.1	9.7	7.4	7.8	1	1.1	11.4	0.2	
11H-4, 59	39.2	2.6	22.7	7.5	7.5	5.6	1.2	1.8	11.9	0	
12H-4, 54	27.2	2.9	16.9	7.5	31.2	3.6	0.9	2.4	7.5	0	
13H-4, 88	36.3	0	10.5	11	17.6	7.5	0.7	3.4	12.9	0.1	
14H-6, 22	33.3	2.7	13.2	8.3	27.5	4.5	0.9	2.3	7.1	0	
15H-4, 54	46.7	4	15.5	6.8	7.4	6.1	1.1	0.7	11.7	0	
16H-7, 26	43.8	0	7.4	10.4	13.6	10.3	1.1	1.6	11.5	0.3	
17X-1, 59	47.5	0	10.1	11.9	11.3	2.2	1	1.2	14.5	0.3	
18X-3, 103	45.2	3.2	19.6	11	5.2	3.2	1.3	1.9	9.4	0	
19X-4, 15	49.4	2.3	14.1	9	8.2	7.1	1.5	0.9	7.5	0	
20X-2, 55	43.3	2.7	14.9	7.3	14.2	5	1.4	2.1	9	0	
21X-5, 49	43.4	3.4	19.4	9.4	8.4	3.5	1.5	1.8	9.3	0	
22X-3, 50	38.8	4.4	11.9	8.5	23.1	4.3	0.9	1.8	6.3	0	
23X-3, 58	45.1	2.1	11.1	9	16.1	3.4	0.7	1.1	11.1	0.4	II
24X-4, 60	24.3	4.7	22.6	11.1	7.1	13.8	2.8	3.7	9.9	0	
25X-2, 80	47.1	2	12	8.2	14.1	4.7	0.9	1.5	9.6	0	
26X-3, 54	17.8	2.2	9.6	6.3	48.3	5.9	0.6	2.2	7.2	0	
27X-2, 11	41	2.7	14.1	7.6	18.2	4.1	0.8	2.3	9.1	0	
28X-3, 24	38.2	2.5	12.3	6.6	22.7	5.7	1.2	2.3	8.4	0	
29X-4, 45	41.6	1.9	10.2	8	23	2.4	1	2.9	9	0.1	
30X-6, 53	45	2.2	10.8	8.1	13.1	7.7	1.1	4.2	7.7	0.2	
31X-2, 19	28	1.7	8.5	7.2	39.1	3	0.4	3.3	8.8	0	
33X-3, 56	51	2.1	10.3	10.3	5.7	5.9	0.7	3.3	10.6	0	III
34X-2, 7	45.7	2	10.1	9.4	15.4	6.5	0.8	1.5	8.4	0.4	
35X-3, 52	48.8	0	9.7	10.4	12.6	5.1	1.1	2.2	10	0.2	
36X-2, 48	40	0	10.7	10.9	11.7	6.3	0.8	8.1	11.7	0	
37X-3, 59	34.2	1.9	10.1	8.8	33.7	3.5	0.7	1.3	5.9	0	
172-1062A-											
1H-1, 35	22.3	2.0	8.7	6.7	45.3	2.7	0.8	4.2	7.4	0.0	
1H-1, 102	28.7	1.7	9.6	7.2	33.9	4.4	0.8	2.9	10.8	0.1	
2H-2, 55	35.8	2.0	12.3	9.4	22.7	5.2	0.8	2.9	8.9	0.0	
3H-4, 92	17.4	1.7	8.3	5.7	51.1	2.2	0.5	3.9	9.2	0.0	
4H-1, 85	38.2	1.9	9.5	9.5	18.4	7.3	1.1	2.5	10.6	1.0	I
4H-5, 63	27.6	2.2	14.2	6.3	35.7	2.0	0.6	5.0	6.5	0.0	
5H-3, 93	14.1	2.7	6.0	10.1	46.1	5.1	0.4	6.1	9.0	0.5	
6H-3, 10	42.4	4.4	22.7	10.6	2.9	3.8	1.8	3.0	8.4	0.0	
7H-2, 59	28.1	1.8	9.9	7.0	36.1	4.4	0.7	2.1	9.8	0.1	
8H-1, 41	44.4	0.0	11.8	10.0	11.0	8.4	1.3	1.8	11.3	0.0	
9H-4, 123	19.6	1.4	9.1	5.3	46.9	4.2	0.1	3.4	9.5	0.4	
9H-6, 120	32.0	0.0	8.7	7.8	28.8	7.3	0.6	3.0	10.1	1.6	
10H-2, 32	34.5	2.0	13.4	8.0	18.9	9.5	1.2	3.2	9.4	0.0	
10H-6, 93	44.3	0.0	15.6	11.4	3.5	9.3	1.2	2.0	12.6	0.2	
11H-2, 46	42.7	0.0	13.8	7.0	16.7	6.2	0.7	1.7	11.1	0.0	
11H-5, 45	39.8	2.9	14.8	8.5	4.2	9.1	0.6	2.7	15.3	2.0	
12H-1, 119	41.2	3.8	6.3	7.6	18.7	5.9	0.6	1.4	13.5	1.0	
12H-3, 24	27.0	0.0	13.4	6.8	35.2	2.3	0.6	5.2	9.5	0.1	
12H-4, 78	40.3	3.1	13.4	4.9	14.9	6.2	0.2	1.4	14.6	0.9	
13H-6, 18	39.3	3.1	16.8	7.9	18.5	2.9	1.0	1.3	9.2	0.0	
14H-2, 19	27.7	2.5	15.5	9.3	31.7	2.5	0.8	1.8	8.4	0.0	II
15H-3, 56	39.7	3.5	11.7	6.7	19.6	8.3	1.0	2.1	7.3	0.3	
16H-6, 73	4.6	12.8	0.7	1.1	49.4	3.3	18.0	4.4	4.8	1.0	
17H-3, 109	42.6	1.9	8.3	9.2	15.1	8.3	1.2	2.7	10.6	0.1	
18H-4, 53	46.6	1.7	7.2	6.7	21.5	5.7	0.9	3.3	6.2	0.0	
19H-5, 55	35.1	1.7	8.0	9.3	22.6	3.9	1.4	8.7	9.3	0.0	

Table 2 (continued).

Core, section, interval (cm)	Quartz	K-spar	Plagioclase	Clay	Calcite	Dolomite	Aragonite	Pyrite	Mica group	Hematite	Unit
172-1062B-											II
18X-1, 3	3.7	1.3	1.3	2.4	12.8	63.5	2.4	1.6	7.7	3.2	
18X-2, 107	49.9	2.6	10.4	9.8	3.7	7.4	1.0	4.4	10.7	0.0	
19X-4, 53	39.0	1.9	9.2	8.2	24.0	4.7	1.3	4.2	7.5	0.0	
20X-4, 60	24.9	2.8	3.1	6.2	46.5	2.9	3.2	4.8	5.4	0.2	
21X-4, 60	43.5	1.9	9.4	10.8	17.4	2.6	1.0	4.5	8.9	0.0	
22X-3, 110	32.4	0.0	6.9	6.2	30.1	2.5	1.1	5.2	15.6	0.0	
23X-5, 61	50.9	0.0	5.6	10.0	10.9	3.8	0.4	2.9	14.8	0.7	III
24X-2, 88	5.8	6.3	0.6	3.1	58.8	2.0	9.4	5.5	8.2	0.3	
25X-3, 52	50.5	2.4	11.1	6.9	10.4	7.1	0.4	2.5	8.7	0.1	
26X-4, 89	39.1	2.0	6.8	6.4	16.7	12.6	0.5	5.0	10.8	0.1	

Notes: K-spar = potassium feldspar. All data shown are relative percentages. For Sites 1060 and 1061, pyrite and aragonite estimates may be erroneous when reported in low amounts because of interference from other minerals. Relative amounts of different mineral components determined by bulk sediment X-ray diffraction. Note that these percentages are only relative to those minerals analyzed, not the whole sediment. Estimates are calculated from the peak area ratios with no standards. For Site 1062, amounts of aragonite over 9% in samples cause an error in the XRD program, which evaluates the third aragonite peak as the main k-spar peak (d-value = 3.27).

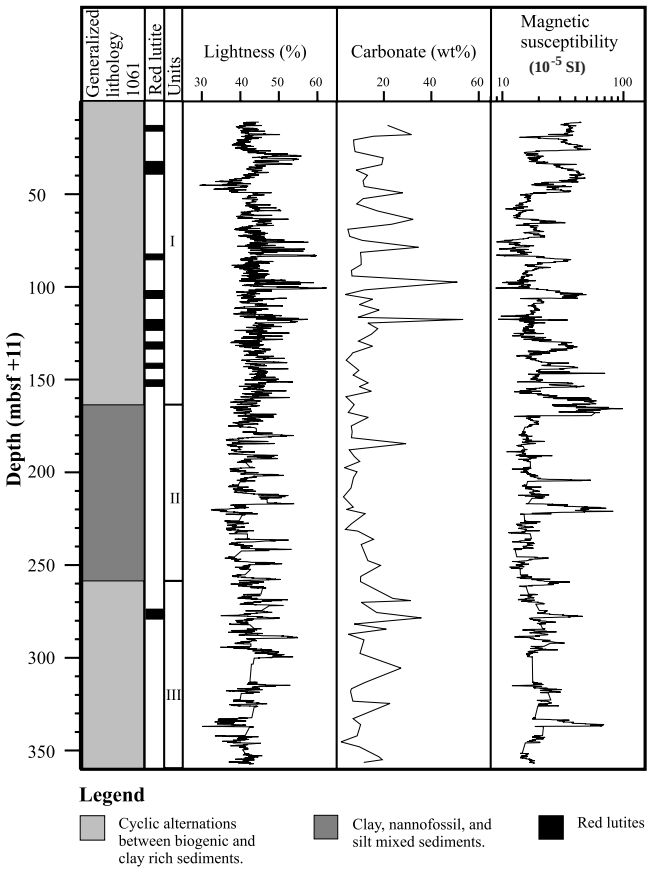

Figure 5. Summary lithologic column for Site 1061 showing generalized lithology, occurrence of red lutite beds, location of sediment units, color reflectance as lightness (L*), weight percent carbonate, and magnetic susceptibility for Site 1061.

conditions that produced this pattern are unknown, but nearly every carbonate layer in this unit (~100) shows this pattern. The upper contact from the carbonate to the clay is generally bioturbated.

Sediment lightness (L*) in Unit I shows a number of larger and smaller peaks that appear to correlate with the carbonate-rich beds superimposed on longer wavelength (10 m) cycles. Also present are some distinctly darker intervals, especially at 5 and 45 mbsf, which correlate to the dark to black sediments with iron sulfide (hydrotroilite) staining. Intervals of overall lightness generally correspond to intervals of reduced magnetic susceptibility. The superposition of the shorter-scale (0.2–1.5 m) variation in carbonate on the longer-scale lightness changes (also presumably related to carbonate) may (1) be related to variations in sediment flux associated with minor climatically-induced sea-level fluctuations; (2) represent increased and decreased transport of sediments to the site by deep currents; or (3) be a result of changes in dissolution.

The most common sedimentary structures relate to bioturbation. Bioturbation is especially visible where light layers lie above dark layers and where the lighter sediments filling individual burrows can be clearly seen (Fig. 2). In several cases, the upper portions of carbonate intervals are abruptly terminated by an apparently unbioturbated clay bed 1–10 cm thick, often with distinct, silt-sized material in laminae (Figs. 2, 3). Rare, distinct silt laminae are also observed within the finer grained intervals, especially deeper in Unit I. These are most likely current deposits (see discussion).

Sediment components determined by smear-slide analysis include clay, quartz, carbonate grains, foraminifers, nannofossils, and siliceous components (diatoms, radiolarians, and sponge spicules). Diatoms appear more common in the upper part of Unit I than in the lower part. Carbonate grains include detrital grains as well as well-formed rhombs, which are presumably dolomite. XRD analysis suggests that dolomite (2%–10%) is present throughout Unit I. Aragonite is often reported at about 1%, but this may represent interference from another mineral. Pyrite is always present between 1% and 5%. Though not quantified, diagnostic peaks for siderite are sometimes observed. Visual and XRD analysis (Table 2) suggest that the sediment composition primarily reflects carbonate and terrigenous endmembers.

Unit II

Intervals: 172-1061A-17X-2, 5 cm, through 27X-3, 75 cm (164.55–258.03 mbsf + 11 m); 172-1061C-18H-1, 0 cm, through 18H-CC, 29 cm (158.31–167.00 mbsf; bottom of hole); 172-1061D-19X-1, 0 cm, through 22X-CC, 27 cm (163.26–183.41 mbsf; bottom of hole)

Age: early Pleistocene

Unit II is characterized by a somewhat more uniform lithology than Unit I, although downcore variations in sediment lightness reflecting variations in carbonate content (supported by smear-slide analysis) are also noted. Unit II has a generally lower carbonate content that Unit I, with sediments ranging from nannofossil clay to clay with silt. The contact between Unit I and Unit II is placed at 162.7 mbsf between Cores 172-1061D-18H and 19X, just below a brown carbonate layer. The same transition apparently occurs at the top of Section 172-1061A-17X-2 at 164.5 mbsf (+11 m) and between Cores 172-1061C-17H and 18H at 157.8 mbsf. Analysis of log profiles (see "Downhole Logging" section, this chapter) and sediment physical properties (see "Physical Properties" section, this chapter) suggest that a distinct change in sediment characteristics occurs at ~170 mbsf with the uphole initiation of a pronounced cyclic density and gamma-ray pattern.

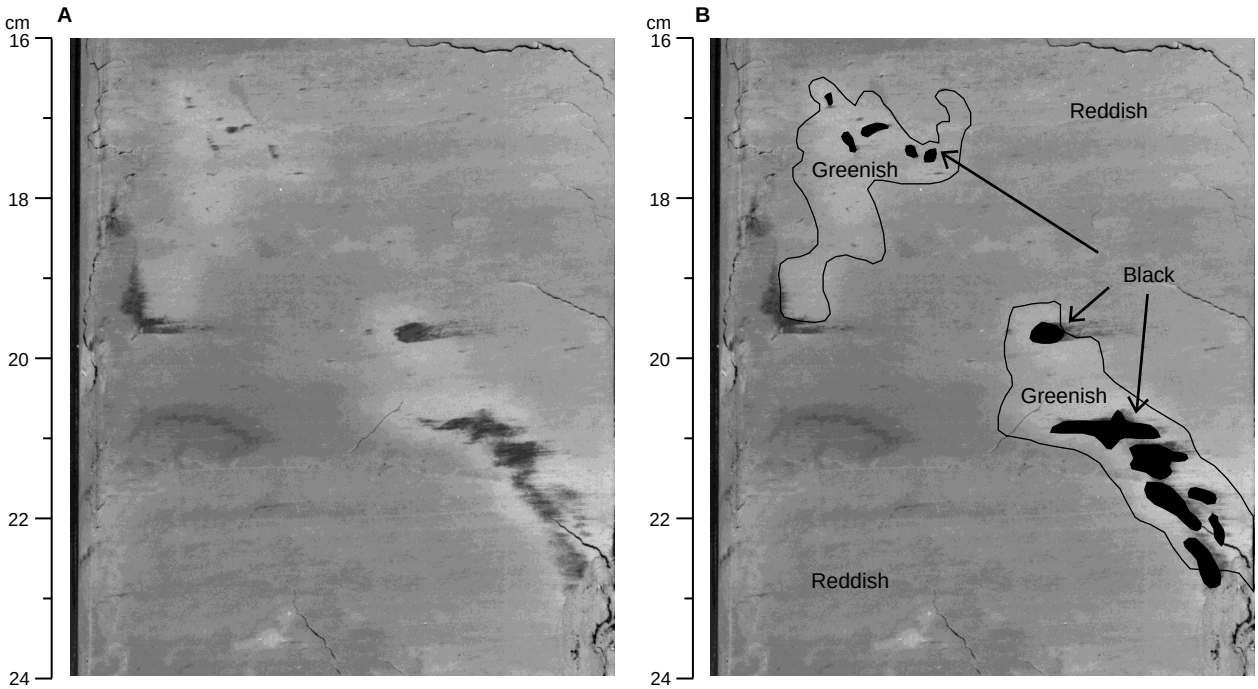

Figure 6. **(A)** Photograph and **(B)** line drawing of an interval that shows the effect of diagenesis on sediment color. The bulk of the sediment is reddish (7.5 YR 4/1 to 4/2) and weakly laminated. Sediments near a prominent, dark burrow from 20.5 to 23 cm (and near several smaller dark burrows) are distinctly lighter, and are greenish in color (5G 5/1). The apparent change of sediment color from red to green near presumably organic-rich burrows suggests a diagenetic origin for the green color here (interval 172-1061D-10H-5, 16–24 cm).

The lighter intervals in Unit II have dimensions and frequencies similar to those described in Unit I, and the overall character of the lightness (L*) record in Unit II is similar to that in Unit I, although the level is lower and most of the carbonate intervals are greenish rather than brown. Carbonate contents in the lighter intervals range from 8 to 29 wt%, whereas carbonate values in the darker intervals range from 3 to 16 wt%. Colors in Unit II are limited to variations of greenish gray (especially light and dark), except for three intervals in Cores 172-1061D-21X and 22X where medium bluish gray and light olive gray are found, and a 40-cm-thick lithified interval recovered at the top of Core 172-1061A-23X (205 mbsf, adjusted depth 216 mbsf). This multicolored unit appears to mark the top of a downhole increase in carbonate from ~10 to 20 wt%. Pyrite is visually noted only in the uppermost (e.g., Core 172-1061A-17X) and lowermost (e.g., Core 172-1061A-25X) parts of Unit II.

Most of this unit was recovered by the XCB corer. The resulting coring disturbance, combined with the generally bioturbated nature of the sediments, results in few preserved sedimentary structures. The most notable structure described is a 7-cm-thick, fine-grained, multicolored bed with an erosional base (interval 172-1061A-21X-4, 70–77 cm; ~191 mbsf). Although no silt laminae were identified, the bed seems similar to a 10-cm clay bed described from Unit I (Fig. 3), which has a probable bottom-current origin. Smear-slide and X-ray diffraction (XRD) studies suggest that the bulk mineralogy of Unit II is in general similar to that of Unit I, although carbonate is less abundant.

Unit III

Interval: 172-1061A-27X-3, 75 cm, through 37X-CC, 52 cm (258.03–357.50 mbsf + 11 m; bottom of hole)
Age: early Pleistocene

Unit III is distinguished by alternating units of lighter (higher carbonate) and darker (lower carbonate) beds, but with overall higher carbonate contents than in Unit II. Sediments are nannofossil clay, clay with nannofossils, clay with silt, and clay. Unit III appears similar to Unit I in carbonate content. Carbonate concentrations in the lighter units range from 17 to 27 wt%, whereas carbonate concentrations in the darker units range from 2 to 19 wt%. The lightness patterns in Unit III are also similar to those in Unit I, although there is a pronounced drop in lightness at the base of Unit III. Colors include greenish gray (light and dark) and reddish brown (especially Cores 172-1061A-29X and 33X), and there are a number of purple and green (diagenetic?) layers similar to those described in Unit I. As in Units I and II, finer grained lithologies tend to be weakly bioturbated, whereas carbonate lithologies are more strongly bioturbated. Some carbonate nodules are noted, and pyrite is common in this unit, often developing as distinct layers of pyrite crystals. Cores 172-1061A-36X and 37X have distinctly less pyrite than the above sediments, and may represent a distinct subunit.

Smear-slide and XRD studies suggest that the bulk mineralogy of Unit III is similar to that of Units I and II, although carbonate contents are intermediate between Units I and II, and discoasters are observed in smear slides.

Site 1062

Eight holes were cored at Site 1062 with a maximum penetration of 239.13 mbsf in Hole 1062B. Bathymetric and seismic evidence indicates that Holes 1062A–1062D are located on the eastern flank of a mud wave, Holes 1062E–1062F on the western flank, and Holes 1062G–1062H on the crest of the mud wave (see "Site Geophysics" section, this chapter). Three lithostratigraphic units, common to all three sets of holes (Fig. 7), are distinguished by lithologic, color reflectance, carbonate content, and magnetic susceptibility characteristics (detailed color reflectance data are on CD-ROM, back pocket, this volume).

Unit I

Intervals: 172-1062A-1H through 9H-5 (0–75.8 mbsf); 172-1062B-1H through 9H-4 (0–77.0 mbsf); 172-1062C-1H through 9H-2 (0–78.8 mbsf); 172-1062D-1H through 9H-5 (0–78.5 mbsf); 172-

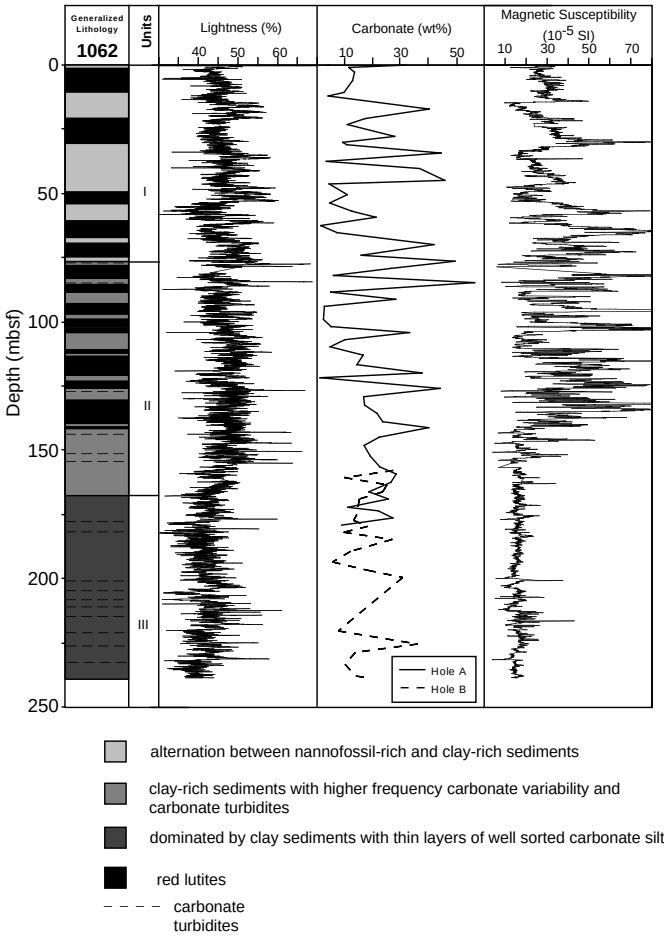

Figure 7. Summary lithologic column for Site 1062 showing generalized lithology, occurrence of red lutite beds, location of sediment units, color reflectance as lightness (L*), weight percent carbonate, and magnetic susceptibility for Holes 1062A and 1062B.

1062E-1H through 7H-CC (0–63.8 mbsf); 172-1062F-1H through 7H-4 (0–60.6 mbsf); 172-1062G-1H through 1H-CC (0–9.3 mbsf; bottom of hole); 172-1062H-1H through 7H-CC (0–63.5 mbsf)
Age: Holocene to middle Pleistocene

Unit I is composed of interbedded clay and nannofossil-clay mixed sediment with gradual transitions between the two lithologies. Clay layers are typically 5–10 m thick, whereas the beds that have the highest nannofossil abundance are typically only 1.5 m thick. The transitions from clay-rich to carbonate-rich sediment are 5–10 m thick and have subtle, repeated carbonate oscillations. The transitions from carbonate end-member to clay end-member sediments are much more abrupt, commonly occurring within decimeters. The contacts of the carbonate oscillations in the transitions to higher nannofossil abundance are always gradational. An entire sedimentary cycle typically spans 10–20 m, and more than five of these are contained in Unit I.

Smear-slide analyses indicate that Unit I sediments are composed mainly of clay and biogenic calcite, with rare coarser grains. Quartz, feldspar, mica, detrital carbonate grains, dolomite, aragonite, pyrite, and hematite are the other sedimentary components, and amorphous red material (iron oxide) is present in the smear slides where the sediment has a reddish hue. Nannofossils comprise the majority of the calcareous microfossils, and foraminifers occur only in minor amounts (<10%). Siliceous microfossils are present as diatoms and sponge spicules, but are almost as scarce as hens' teeth. Contacts between lithologies are typically heavily bioturbated. Trace fossils such as *Planolites*, *Chondrites*, and *Zoophycos* are common.

XRD data show that quartz, calcite, mica, and clay are the major mineral components of Unit I (Table 2; Fig. 8). In general, Unit I is marked by highly variable quartz and calcite content. High-amplitude fluctuations are also observed in carbonate data, which show that Unit I contains between 2 and 50 wt% carbonate (see "Organic Geochemistry" section, this chapter). Feldspar, dolomite, and pyrite are minor sedimentary components. The plagioclase content varies between 8% and 14%, with up to 22% in a single value (XRD Sample 172-1062A-6H-3, 10 cm). Variability in sedimentary plagioclase content may result from changes in the sediment source. Dolomite content fluctuates from 2% to 8%, and aragonite is present in trace amounts (<2%). The presence of aragonite at this site is consistent with the reports by Flood (1978) of aragonite in the upper Pleistocene sediments of KN31-GPC-9 and other cores in the Bahama Basin. Hematite never comprises more than 1% of the sediment, and the presence of pyrite within the range of 2%–6% is ubiquitous in XRD analyses.

The clay-rich layers tend to be dark (dark olive gray, 5Y 4/1; reddish brown, 5YR 5/4-5/3), whereas nannofossil-rich layers are generally lighter (light gray, 5Y 7/1; light olive gray, 5Y 6/1). Aside from Holocene sediments, which are light yellowish brown, sediment color has a relatively narrow range from brownish gray through olive gray to greenish gray. Five distinctly reddish layers are also present in this unit (Fig. 7). Although the red color is not as strong as at shallower Leg 172 sites, these layers can be correlated regionally.

Sedimentary diagenetic features are common in Site 1062 sediments. Iron-manganese hardgrounds and remnants of these hardgrounds are present at the bases of some carbonate rich-layers. Greenish and purplish diagenetic coloration occurs frequently at the boundaries where there is a large carbonate gradient, but also occurs at the boundaries between more subtle lithological changes. Both the greenish and purplish diagenetic colorations are often found together. Pyrite nodules are also common diagenetic features and typically occur as worm burrow casts that can extend vertically for up to 5 cm.

A small interval of inclined and sometimes partially deformed layering was observed in Sections 172-1062E-5H-1 through 5H-3, whereas other sections of this core have horizontal layering (see whole-core photograph in Section 4, this volume). In the interval of inclined layers, truncation of layers (Fig. 9) and abrupt color changes are more frequent than in the rest of Site 1062. Indeed, this is the only example of inclined bedding recorded for this site. The localized deformation appears to have been caused by the inclined bedding surface, and is consistent with the dipping beds being a primary sedimentary feature. Hole 1062E may have been cored through the wall of a buried furrow. Slopes of modern furrow walls can be up to 45°, and evidence of localized slumping is often observed (Flood, 1994).

A number of intervals with 1-mm-thick silt laminae are present in Unit I (Figs. 2, 3). In some instances, these laminae occur in groups of two to five layers (Fig. 3). Silt laminae are most frequently found in clay, clay with nannofossils, or clay with silt beds. Smear-slide analysis reveals that these silt layers are composed almost entirely of quartz grains. The significance of these silt layers is discussed more fully later in this section.

Unit II

Intervals: 172-1062A-9H-5 through 18H-CC (75.8–164.0 mbsf); 172-1062B-9H-4 through 18X-CC (77.0–167.0 mbsf); 172-1062C-9H-2 through 14H-CC (78.8–132.9 mbsf; bottom of hole); 172-1062D-9H-5 through 9H-CC (78.5–81.8 mbsf; bottom of hole); 172-1062E-8H through 13H-CC (63.8–139.5 mbsf); 172-1062F-7H-4 through 9H-CC (60.6–83.1 mbsf; bottom of hole)
Age: middle Pleistocene to late Pliocene

Unit II is composed of interbedded clay, clay with silt, nannofossil clay, nannofossil-clay mixed sediment, clayey nannofossil ooze, and layers of well-sorted and occasionally normally graded foramin-

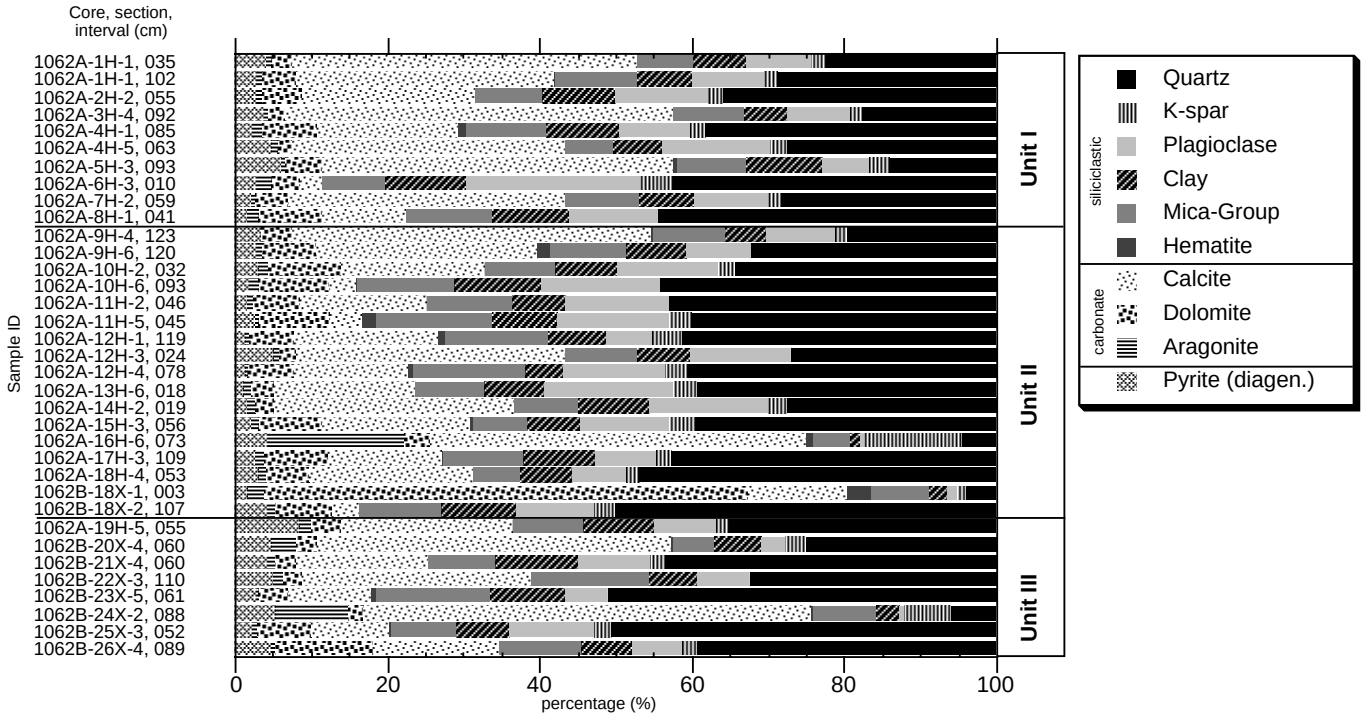

Figure 8. Diagram of XRD results for Holes 1062A and 1062B.

iferal or carbonate silt. The most prevalent lithologies are clay and clay with nannofossils. The transitions between lithologies are about half the thickness of the transitions in Unit I, and the clay layers are typically narrower than in Unit I, with an average thickness of 2 m. Nannofossil-rich layers are also thinner, with an average thickness of about 1 m. The carbonate cycles tend to decrease in length and amplitude downcore such that, in the lowest part of the unit, entire cycles occupy only 3 m and the lithologic end-members are clay and nannofossil clay.

Visual grain-size analyses of the sediments of Unit II show a dominance of clay-sized material; in contrast to Unit I, however, Unit II contains increased proportions of silt-sized material. In Unit I and Unit II, smear-slide analysis results are similar, except that in Unit II more detrital carbonate and quartz grains were observed. The abundance of calcareous microfossils is highly variable and siliceous microfossils are nearly absent. XRD analyses of sediments from Unit II show a major and minor mineral composition that is similar to Unit I, but the content of both quartz and other siliciclastics is generally higher, with quartz content varying between 35% and 50% (Table 2; Fig. 8). Calcite contents of up to 50% are only found in layers that are linked to carbonate redeposition, apparently from the Bahama Banks. Aragonite contents as high as 18% also seem to be connected with these events. Outside of redeposited carbonate layers, the calcite content determined by XRD analysis never comprises more than 20% of the sediment, and aragonite is rare. The dolomite content is mostly less than 10%; however, a single cemented and cross-bedded interval of Unit II (XRD Sample 172-1062B-18X-1, 3 cm) is 63% dolomite. The sediments of Unit II contain between 1 and 57 wt% carbonate (see "Organic Geochemistry" section, this chapter). Pyrite varies between 1% and 9%. Hematite is relatively rare (<1%), but brownish sediments may contain as much as 2%.

Unit II is distinguished from Unit I on the basis of increased sedimentary heterogeneity, including magnetic susceptibility (Fig. 7), which shows erratic fluctuations and overall higher magnetic mineral content. Natural gamma values are also higher in Unit II than in either of the other two units. In addition, the wide fluctuations in sediment color that are observed in Unit II are useful for discriminating between units. Colors in Unit II range from dark to light in hues of reddish brown, brownish, bluish, and greenish gray. Horizons just above the bases of carbonate silt layers are nearly white. However, the wide variety of colors may reflect diagenesis as well as sedimentary heterogeneity. Yet another distinctive characteristic of Unit II is the presence of layers of well-sorted, graded carbonate silt, which we suggest are carbonate turbidites that were deposited by downslope transport. (Fig. 10). The high frequency and amplitude of carbonate variability in this unit is due mainly to deposition of these carbonate turbidites, and not to primary carbonate productivity in the overlying surface ocean. Figure 10 shows an example of a typical turbidite. Note the scoured lower contact of the silt layer, and the layering and flow structure just above the base of the silt. Darker areas near the top of the layer are the result of bioturbation. An example of the type of turbidite that is most common at Site 1062 is shown in Figure 10. These layers are as much as 29 cm thick, but more commonly 7–12 cm thick (Table 3) and consist of well-preserved sand-sized foraminifers (Fig. 10). Four of the turbidite layers have been correlated across all the holes, except Holes 1062G and 1062H, which do not penetrate deep enough to have recovered these intervals. Correlated layers have been marked with an asterisk on Table 3. With more study, it may be possible to correlate many of the turbidite layers between all holes.

Several features found in Unit I are also present in Unit II. One of these features is the millimeter-scale silt laminae that sometimes occur in groups of 2–5 layers. The greenish and purplish diagenetic coloration present in Unit I also occurs in Unit II, and pyritization of worm burrows and the presence of trace fossils is pervasive in both units.

Unit III

Intervals: 172-1062A-19H-1 through 20H-CC (164.0–180.7 mbsf; bottom of hole); 172-1062B-9X-1 through 26X-CC (167.0–239.0 mbsf; bottom of hole); 172-1062E-14H-1 through 23X-CC (135.5–208.8 mbsf; bottom of hole)
Age: middle to early Pliocene

Unit III is predominantly clay with nannofossils, which is interbedded with clay, clay with silt, and nannofossil clay. Unit III also

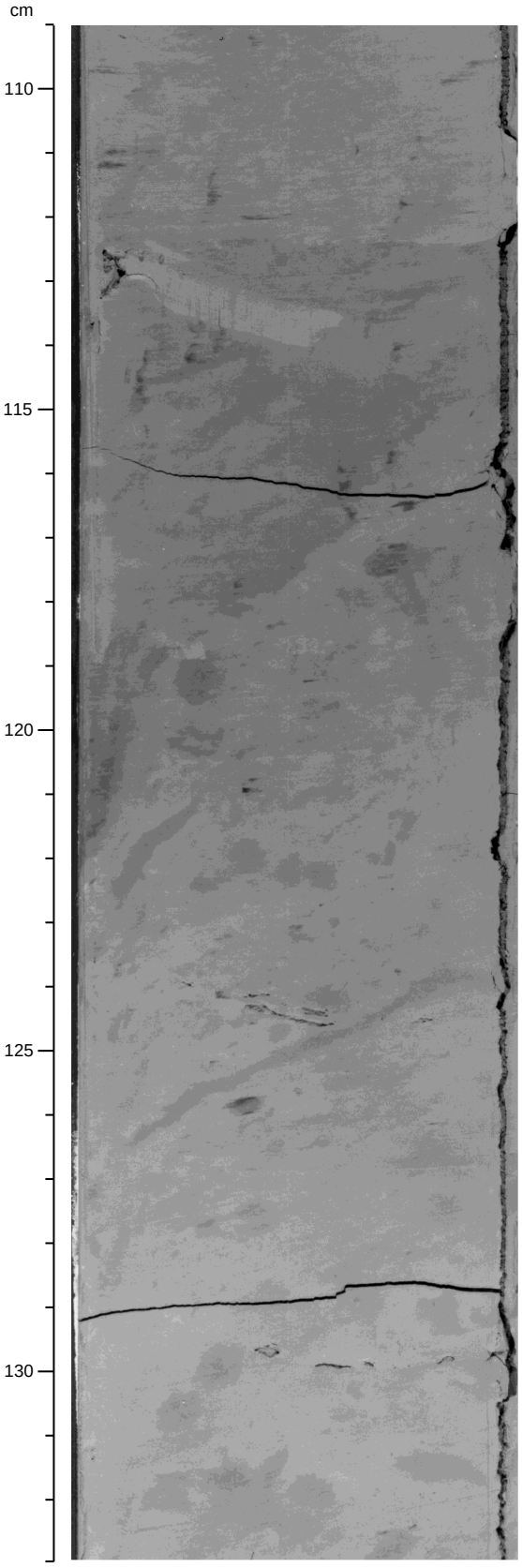

Figure 9. Close-up of the inclined stratification in interval 172-1062E-5H-3, 109–133 cm. See text for discussion.

contains thin carbonate-rich layers that are similar to the turbidite layers of Unit II, but have a much finer texture. In Unit III, the carbonate cycles typical of Units I and II are almost nonexistent. Clay with silt beds are generally 4–10 m thick and alternate with 1- to 9-m-thick beds of clay with nannofossils. Occasionally, thinner beds of silty clay with nannofossils are interbedded with the main lithologies.

As with Units I and II, the sediment of Unit III is composed mainly of clay-sized grains, but Unit III shows consistently higher abundances of silt-sized sediments. Smear-slide results are similar to Unit II, but the abundance of calcareous microfossils is distinctly lower, and siliceous microfossils are absent.

XRD data of Unit III (Table 2; Fig. 8) indicate that the major and minor mineral components are similar to the first two units of this site. Quartz contents as high as 50% are observed. High calcite content (30%–60%) and relatively high aragonite content (10%) may also be the result of carbonate sediment supply from the Bahama Banks, as in Unit II. Generally, the dolomite content fluctuates from 2% to 8%, but locally values increase to 13%. In general, the sediments of Unit III contain between 5 and 36 wt% carbonate (see "Organic Geochemistry" section, this chapter).

The carbonate content of the bulk sediment of Unit III is lower than in the other units of Site 1062, and overall lithological variability is reduced in comparison with Unit II. The color is generally dark greenish gray (5GY 4/1). Extremes of sedimentary composition are rare. Carbonate turbidites occasionally break the uniformity of sedimentation, but the turbidites tend to be thinner than in Unit II, ranging in thickness from 1 to 10 cm. Lithologic transitions are more gradual than in other units and contacts are typically moderately to heavily bioturbated. As in the other units at this site, trace fossils such as *Planolites* and *Chondrites* are common; however, pyrite nodules and crystals are more abundant in this unit.

Colors in this unit are darker with lower amplitude lightness (L*) fluctuations. Calcium carbonate, magnetic susceptibility, and natural gamma-ray data also show lower average values and less variability (see "Organic Geochemistry" and "Physical Properties" sections, this chapter). These patterns suggest reduced clay mineral content and little compositional variability (see "Physical Properties" section, this chapter).

Discussion

The sediment sections recovered at Sites 1060 and 1061 at 3481 and 4047 m, respectively, on the crest of the Blake Outer Ridge, are quite similar to one another, whereas the sediment section at Site 1062 on a mud wave at 4745–4774 m on the western flank of the Bahama Outer Ridge has some distinct differences (Fig. 11). Differences between Sites 1060/1061 and 1062 appear mostly related to the proximity of Site 1062 to the Bahama Banks and the Blake Escarpment, which are potential sources of detrital carbonate for Site 1062. Site 633 (Leg 101, Exuma Sound on the Bahama Banks; Droxler et al., 1988) establishes a record of turbidite sedimentation more proximal to a turbidite source. Similarities among the three Leg 172 sites include the composition of the siliciclastic component (primarily clay and quartz with feldspar) and the overall variations in sediment lightness, especially in Unit I, which is above the interval of carbonate turbidite sedimentation at Site 1062. The similarity in the depositional pattern of Unit I at all sites is remarkable, and individual carbonate peaks within interglacial periods can be correlated between sites. However, contrary to expectation, carbonate contents at Site 1062 are as high as or higher than equivalent age levels at Sites 1060 and 1061, despite the increased water depth. At all sites, secondary minerals include dolomite (often observed as rhombs in smear slides), pyrite (identified visually and by XRD and often present as prominent burrow fillings), siderite (identified by XRD in trace amounts) and hydrotroilite.

Based on preliminary magnetic susceptibility and lightness correlations, overall sedimentation rates appear highest at Site 1060 and

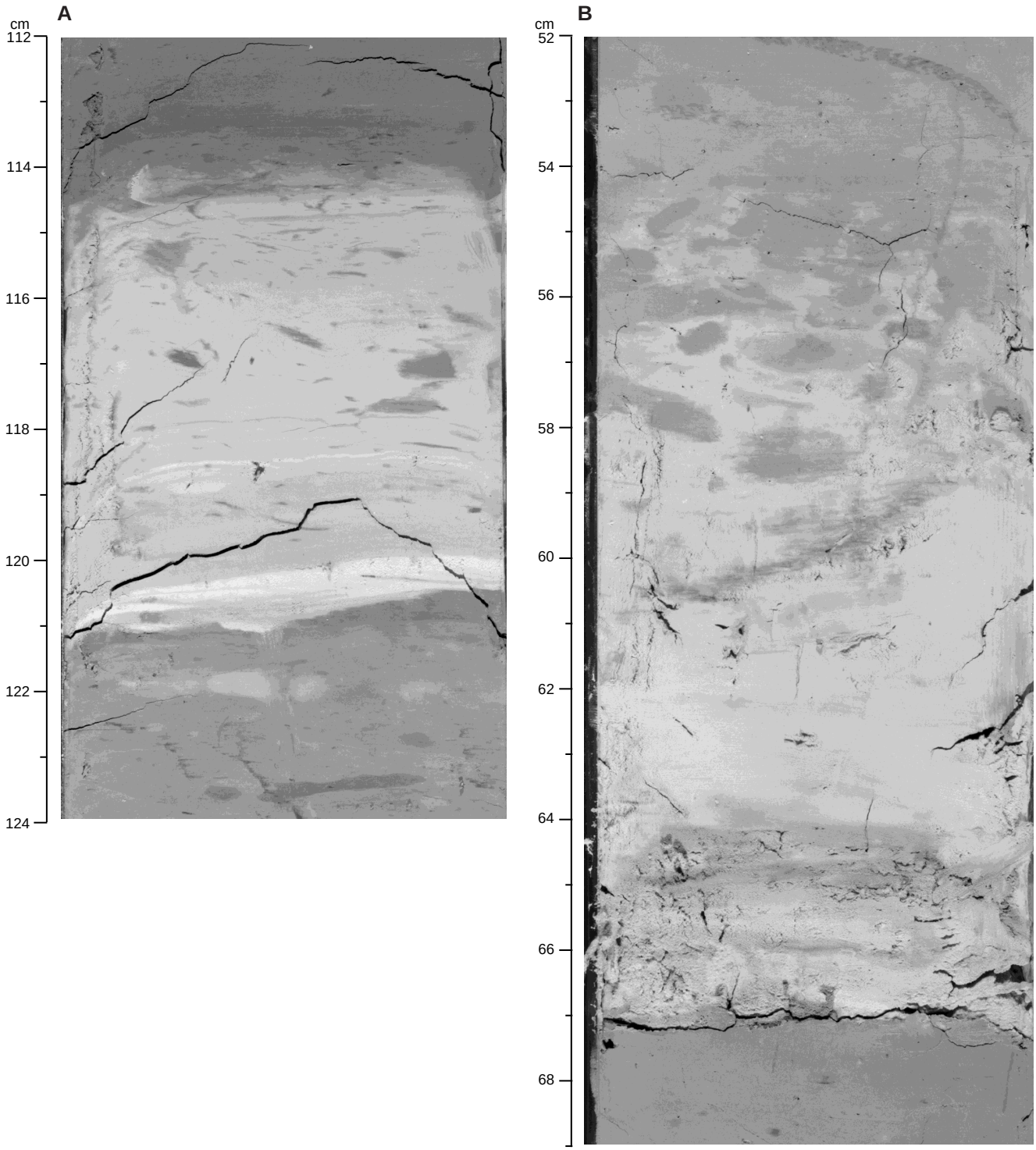

Figure 10. **A.** Photograph of a carbonate turbidite in the interval 172-1062F-9H-6, 114–121 cm. See text for discussion. **B.** An example of the type of carbonate turbidite that is more typical of Unit II at Site 1062 (interval 172-1062A-10H-4, 54–67 cm). The base of the turbidite sharply truncates the underlying light greenish gray clay with nannofossils. The basal section (64–67 cm) is composed of yellowish gray fine sand-sized foraminifers and has a purplish diagenetic band, which is seen in the photograph as a dark region between ~64 and ~66 cm. The basal section is overlain by white to light gray carbonate clay with nannofossils and silt. The upper boundary of the turbidite is heavily bioturbated and underlies light greenish gray clay with nannofossils. In many instances, the green sediments found immediately adjacent to the turbidites appear to have been altered from the red sediments usually found at a greater distance from the turbidites.

Table 3. Position of carbonate turbidites at Holes 1062B and 1062E.

Core, section, interval (cm)	Depth of base (mbsf)	Unit
172-1062B-		
9H-5, 0-14*	77.64	
9H-5, 90-103*	79.00	
10H-3, 40-52	84.52	II
14H-7, 30-38	126.92	
16H-4, 63-75*	143.25	
17H-3, 15-27	150.77	
17H-5, 30-37*	153.87	
20X-4, 75-84	177.04	
20X-7, 5-11	180.81	
22X-7, 0-7	199.97	
23X-3, 0-7	203.57	
23X-5, 32-42	206.92	
23X-7, 43-53	210.03	III
24X-2, 25-32	213.52	
24X-2, 85-90	214.10	
24X-6, 33-38	220.03	
25X-2, 108	222.38	
25X-4, 85-95	225.25	
26X-2, 55-65	231.55	
172-1062E-		
8H-2, 145-149*	63.74	
8H-4, 0-10*	65.40	
10H-2, 72-80	82.10	II
12H-4, 0-15	103.30	
12H-7, 0-12*	107.70	
13H-5, 47-55	114.00	
14H-3, 22-27*	120.60	
20X-4, 125-130	176.20	
21X-2, 80-81	182.20	III

Note: * = correlated layers between Holes 1062B and 1062E.

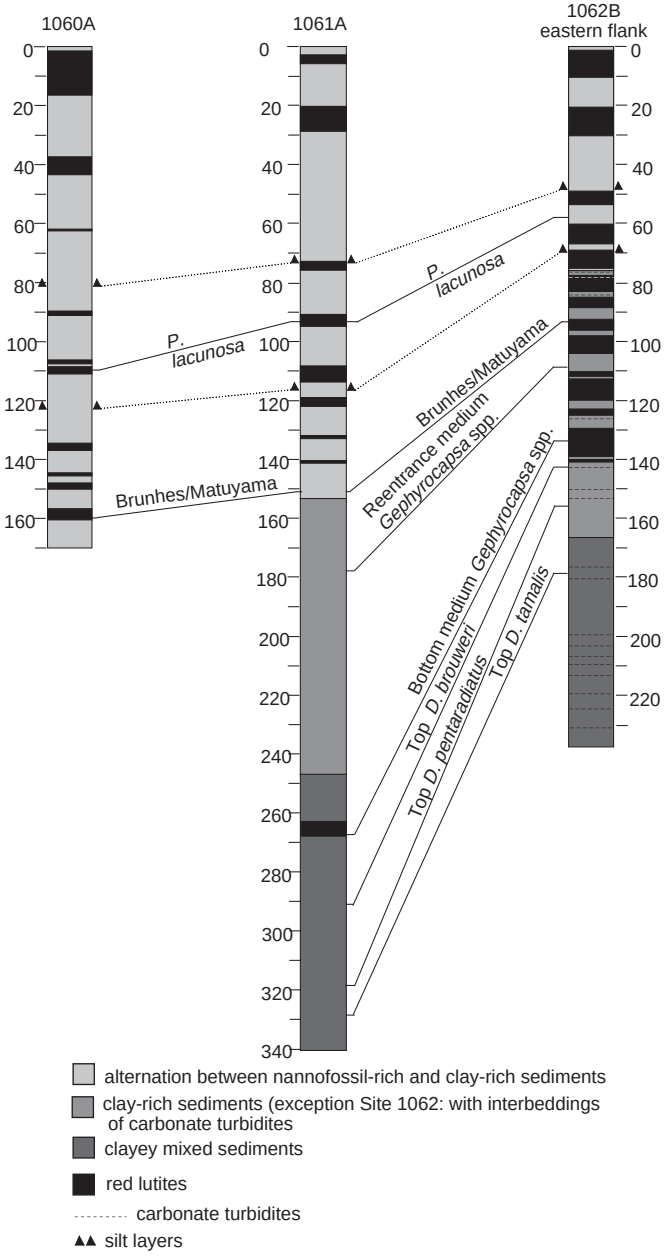

Figure 11. Columnar logs and biostratigraphic correlations among Holes 1060A, 1061A, and 1062B show the overall differences in sedimentation rate and lithologies between sites. Also noted are the positions of the upper and lower silt layers shown in Figures 2 and 3.

lowest at Site 1062 (see "Sedimentation and Mass Accumulation Rates" section, this chapter). These correlations also suggest that Unit I spans a similar time interval at Sites 1060 and 1061, but does not correspond to the same time interval at Site 1062. The Unit I/Unit II contact at Site 1062, which is determined by the presence of carbonate turbidites in Unit II, appears to be somewhat younger than the Unit I/Unit II contact at Site 1061, which is based on a downhole decrease in carbonate content.

Spectral analysis of sediment lightness (L*) provides some insight into the changing nature of carbonate fluctuations at Site 1062. Color reflectance data from Unit I of 1062B (Fig. 7) show that lightness (L*) in this unit displays cyclic oscillations. Using a very simple age model based on the top of the range of the nannofossil *Pseudoemiliania lacunosa*, spectral analysis of L* (Fig. 12) yields strong peaks that most probably correspond to orbital forcing cycles of eccentricity, obliquity, and precession. In contrast, spectral analysis of color reflectance data from Unit II at Site 1062B (Fig. 12) shows that the orbital forcing signature apparent in Unit I is much weaker in these sediments and that additional frequency elements are present. The reduced power in the orbital bands must reflect more than just the presence of carbonate turbidites. Some other fundamental change in sedimentation pattern has also occurred between Unit I and Unit II. That fundamental change could be the increased importance of carbonate sediment flux from the Bahama Banks because adding carbonate uniformly to all sediments of Unit II could alter the character of power spectra and reduce power in the orbital bands. The reduction in orbital power occurs because lightness (and weight percent carbonate) depend on the ratio of carbonate to non-carbonate sediment and not on the carbonate accumulation rate. Thus, doubling the carbonate flux could increase the lightness of low-carbonate intervals many times, but only slightly change the lightness of high-carbonate intervals.

The Unit I/Unit II boundary at Site 1062 is at ~625 ka, indicating a reduction in turbidite sedimentation at Site 1062 at that time. The record of carbonate sedimentation at Site 633 in Exuma Sound or at other Leg 101 sites (Droxler et al., 1988; Shipboard Scientific Party, 1988) does not show a distinct change in sedimentation pattern at this time. This suggests that reduced turbidite sedimentation at Site 1062 may result from changes in turbidity current pathways, perhaps from the evolution of the deep-sea fan at the base of the Bahamas or the growth of the sediment drift between the Bahama Banks and the site. The Unit I/Unit II boundary at Site 1062 occurs somewhat later, after the dominant power in climate changed from a 40-k.y. to a 100-k.y. cycle. In contrast, the Unit I/Unit II boundary at Site 1061 more closely coincides with the change from 40-k.y. to 100-k.y. power. This difference in age may be fortuitous, or it may indicate that some changes in sedimentation patterns in the Bahama Banks/Bahama Basin region lag those in the ocean basin.

Sites 1061 and 1062 both recovered sediments older than the 3.12-Ma *Dentoglobigerina altispira* datum, but the sediment records in this earlier time interval are somewhat different at the two sites because of the proximity of Site 1062 to the Bahama Banks and the

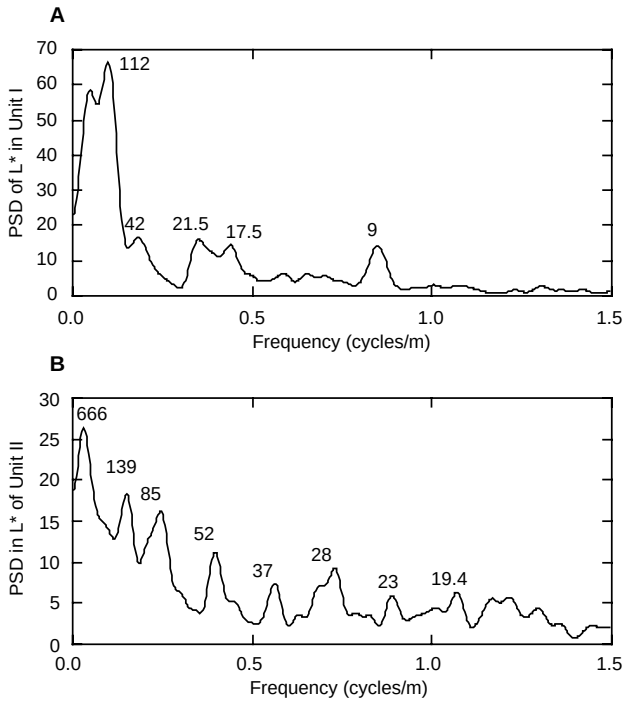

Figure 12. Spectral analysis of lightness (L*) data for Units I and II in Hole 1062B. The spectral analysis is calculated on the basis of distance, resulting in a frequency of cycles/m. Numbers above peaks give periods (in thousands of years) corresponding to the calculated frequencies (cycles/meter) using the age model described in the text. PSD = power spectral density. **A.** Spectral analysis of color reflectance data in Unit I shows strong peaks close to orbital frequencies of ~100, 40, and 20 k.y.). **B.** Spectral analysis of color reflectance data from Unit II shows frequency bands that do not correspond to orbital forcing, and shows a much reduced PSD in general. Only the precessional peaks at ~23 and ~19.5 k.y. are still recognizable.

Blake Escarpment. The Unit II/Unit III contacts, which apparently represent minor changes in sedimentation at the two sites, are also at slightly different ages at Sites 1061 and 1062. However, the unit boundaries are not particularly distinct at either site, so differences in the timing of unit boundaries should not be taken as evidence for lateral sediment variability without further study.

Both large and small variations in lightness can be clearly correlated between Sites 1060 and 1061, and some correlations can also be made to Site 1062, especially in Unit I. The lightness pattern is similar in detail between Sites 1060 and 1061, including the observation that sediment between closely spaced carbonate layer peaks is lighter than sediment between the clusters of carbonate layers. A similar pattern in lightness can also be seen at Site 1062, although the lightness between carbonate peaks is as low as the lightness between clusters of carbonate layers. The high degree of correlation between sites suggests a uniformity of sediment source, distribution, and/or dissolution patterns. Although the relative importance of these factors in controlling carbonate content (lightness) is not yet determined, the accentuated decrease in lightness between closely spaced carbonate layers at Site 1062 probably results from increased dissolution at depth during these times.

Red sediment layers are present at all three sites and appear to be closely correlated. Red sediments at Site 1062, however, appear to comprise a larger fraction of the sediment column, perhaps because of generally lower sedimentation rates and lower diagenetic activity at this site. All sites have clay-rich layers, sometimes with silt laminations that appear to have been formed by bottom current events. Of particular interest are two distinctive clay layers that generally have silt laminations near their bases (Figs. 2, 3). These layers, which occur near the beginning of interglacial intervals and which apparently were associated with flow speeds sufficient to scour the carbonate bed slightly, can be correlated between sites on the basis of their stratigraphic position, supported by magnetic susceptibility and color studies. The presence of these layers over a wide depth range from topographically different settings suggests that these sediment layers were created by unusually strong but short-lived along-slope current events (perhaps augmented by increased sediment flux to the ocean) that transported sediments to the BBOR. Variations in layer structure from site to site may be related to temporal and spatial variability of the circulation event or represent lateral variations caused by small-scale topography. A single turbidity current would not have created similar layers at all of these sites. There may well have been other similar but smaller along-slope current events occurring on a regular basis that have been destroyed by bioturbation.

Mud-Wave Sedimentation Pattern, Site 1062

The depth and geographic location of Site 1062 play pivotal roles in the sedimentology of the site. The site is located about 200 km northeast of the Bahama Banks and east of the Blake escarpment. No bathymetric features protect the site from redeposition of sediment from the Bahama Banks or the Blake Escarpment. Presently, waters of the WBUC follow a complicated path along the topographic contours of the eastern and western flanks of the BBOR and flow northwards at Site 1062. This deep current activity has generated a mud-wave field from 26° to 30°N in the area surrounding the site.

The various holes at Site 1062 sampled differing parts of a mud wave (see "Site Geophysics" section, this chapter), and seismic profiles suggest that holes on differing parts of the mud wave should sample variable thicknesses of similar sequences of beds. Overall, the sedimentary sequence recovered from the two wave flanks is similar, although minor differences in sediment layer thickness have been noted, especially related to carbonate turbidites (see below). Primary evidence for cross-wave changes in sediment accumulation rates comes from biostratigraphic and magnetostratigraphic analysis. The last occurrence of *Discoaster pentaradiatus* (2.52 Ma) is at 157.22 mbsf in Hole 1062B on the present-day eastern flank of the mud wave, and at 124.44 mbsf in 1062E on the present-day western flank of the mud wave. This evidence suggests that between 0 and 2.52 Ma the sedimentation rate was 25% higher at Hole 1062B on the eastern flank of the mud wave than at Hole 1062E on the western flank (Fig. 13). The last occurrence of *D. tamalis* at 179.22 mbsf in Hole 1062B and at 158.5 mbsf in Hole 1062E suggests that from 2.52 to 2.83 Ma the sedimentation rate was 55% higher at Hole 1062E. However, seismic profiles show that the mud wave was at a different position at this time, and that the sediments sampled in Hole 1062E were deposited on the eastern flank of a buried wave (see "Site Geophysics" section, this chapter). Correlation of magnetic susceptibility data among holes supports the conclusions drawn from the calcareous nannofossil biostratigraphy data. Flood (1988) proposed that bedform geometry may exert a localized control on current velocity, causing higher sedimentation rates on the up-current side of mud waves where the current velocity slows while moving uphill. Correlative carbonate turbidites on the eastern mud-wave flank are up to 10 cm thicker (Table 3), suggesting that the sedimentological processes that cause mud-wave migration may also cause marked lateral variability in sedimentation from turbidity currents, and may be responsible for preferential deposition of turbidite materials on upcurrent mud-wave flanks.

Conclusion

The three holes at Site 1060 and the five holes at Site 1061 can generally be correlated to one another on the basis of several different

parameters. This similarity over a distance of 110 km suggests a uniformity of sedimentary processes among these sites on the Blake Outer Ridge. This uniformity in sedimentation is also suggested by the similarity of seismic records at these sites (see "Site Geophysics" section, this chapter). By contrast, at Site 1062 holes only 1 km apart spanning a mud wave and with some turbidite input show a higher degree of lateral variability, especially in intervals where turbidites are present. Preliminary correlations in Unit I at Site 1062 find the same layers on different sides of the mud wave, although layer thicknesses sometimes differ. The correlated patterns of red sediment and the presence of distinctive clay-rich layers among Sites 1060, 1061, and 1062 over 250 km apart horizontally and 1200 m apart vertically suggest that deep currents were active transport agents during at least some portions of glacial periods (Needham et al., 1969) and that strong bottom-current activity may have occurred in a systematic pattern during interglacial periods.

BIOSTRATIGRAPHY

Introduction

Biostratigraphic and biochronologic control at Sites 1060, 1061, and 1062 was provided by shipboard analyses of calcareous nannofossils and planktonic foraminifers. Variable preservation and abundance of calcareous nannofossils were observed throughout the recovered sequences. Assemblages are dissolved to varying degrees; there are intervals that are barren of both foraminifers (planktonic and benthic) and nannofossils. In some intervals the nannofossil and foraminifer (planktonic and benthic) assemblages are strongly diluted by the terrigenous input.

The recovered stratigraphic sequences include the time interval from the Holocene to middle Pleistocene at Site 1060, the Holocene to middle Pliocene at Site 1061 (Hole 1061A), and the Holocene to early Pliocene at Site 1062 (Hole 1062B). The positions of the biohorizons are reported in Table 4 and in Figures 14 through 17.

Calcareous Nannofossils

Site 1060

The nannofossil biohorizons were constrained within 0.3 to 1.5 m in Hole 1060A. Calcareous nannofossils recovered at Site 1060 represent a stratigraphic sequence from the Holocene (corresponding to the interval of *Emiliania huxleyi* dominance) to the upper Pleistocene (~0.8 Ma). We examined smear slides from core-catcher samples and from samples within cores in Hole 1060A to better constrain the biohorizons (Table 4). The presence of abundant terrigenous input and clay minerals throughout the succession can affect the nannofossil assemblages by dispersing the specimens and contributing to a variable preservation state. In some samples, strong dissolution was observed (e.g., Sample 172-1060A-8H-CC). As in the "Carolina Slope" and "Intermediate Depth Blake Outer Ridge" chapters (this volume), we were not able to detect with certainty the beginning of the interval of dominance (0.085 Ma) and the first occurrence (FO) of *E. huxleyi* (0.26 Ma). The extinction of *P. lacunosa,* the only nannofossil biohorizon constrained, was found within Core 172-1060A-12H.

Site 1061

At this site, Hole 1061A was studied in detail to constrain the biohorizons. Calcareous nannofossil abundance and preservation varied throughout the sedimentary section recovered. In some intervals, strong dissolution and/or dilution by terrigenous input was observed in nannofossil assemblages, together with reworked species of various ages (mostly from the late Neogene to Paleogene). Despite the noise produced by poor preservation, dilution, and reworking, the biostratigraphic signal provided by the nannofossil marker species was preserved, and allowed assignment of the recovered section to the time interval Holocene to middle Pliocene. The biohorizons were constrained within 0.4–0.8 m, and are presented in Table 4 and Figure 15.

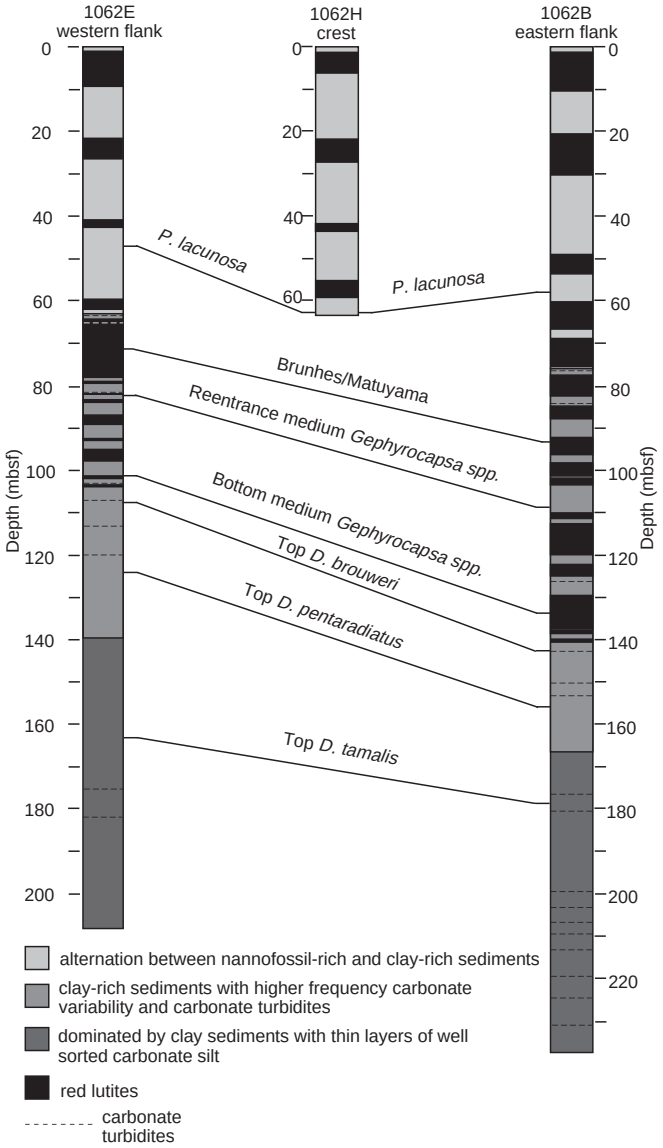

Figure 13. Columnar logs and biostratigraphic correlations among Holes 1062E, 1062H, and 1062B show sedimentation rate differences between holes. The downhole change in higher sedimentation rate from Hole 1062B to Hole 1062E is consistent with wave migration at this site.

Discoasterids are generally abundant to common in the Pliocene interval. The presence of *Discoaster tamalis* and *Discoaster asymmetricus* in the oldest sediments recovered at the base of Hole 1061A (Core 172-1061A-36X) suggests an age for this interval between 2.83 and 3.66 Ma.

Site 1062

Constraints on biohorizons of the calcareous nannofossils recovered at Site 1062 were obtained from samples collected in Holes 1062A, 1062B, and 1062E and core-catcher samples were analyzed in Holes 1062A, 1062B, 1062E, and 1062H. The data are reported in Table 4 and Figures 16 and 17. Preservation and abundance in the nannofossil assemblages were extremely variable throughout the re-

Table 4. Calcareous microfossil datums in Holes 1060A, 1061A, 1062A, 1062B, and 1062E.

Event	ID	Age (Ma)	Core, section, interval (cm) Top	Core, section, interval (cm) Bottom	Depth (mbsf) Top	Depth (mbsf) Bottom	Depth (mbsf) Mean	Depth (mcd) Mean
172-1060A-								
Reent. *G. tumida flexuosa*	F1	0.401	12H-1, 70-72	12H-2, 70-72	104.70	106.20	105.45	121.78
T *P. lacunosa*	N1	0.46	12H-4, 96-97	12H-5, 39-40	109.46	109.79	109.62	125.95
B *G. crassaformis hessi*	F2	0.75	18H-2, 70-75	18H-3, 70-75	163.20	164.70	163.95	184.58
172-1061A-								
T *G. tumida flexuosa*	F1	0.068	2H-CC, 17-20	3H-1, 67-72	19.34	19.27	19.30	33.77
Reent. *G. tumida flexuosa*	F2	0.401	10H-3, 70-75	10H-4, 70-75	89.20	90.70	89.95	115.20
T *P. lacunosa*	N1	0.46	10H-6, 39-40	10H-6, 84-85	93.39	93.84	93.61	118.86
Reent. *G. crassaformis hessi*	F3	0.75	16H-6, 68-73	16H-7, 70-75	148.66	150.18	149.42	184.54
Reent. m. *Gephyrocapsa* spp.	N2	1.00	20X-1, 114-115	20X-2, 39-40	177.74	178.49	178.11	217.38
T large *Gephyrocapsa* spp.	N3	1.24	23X-2, 4-5	23X-2, 40-4	207.10	207.41	207.11	246.38
T *G. obliquus*	F4	1.3	25X-4, 66-73	25X-CC, 38-50	229.96	231.48	230.72	269.99
B large *Gephyrocapsa* spp.	N4	1.58	28X-2, 39-40	28X-2, 60-61	255.05	255.26	255.16	294.43
T *C. macintyrei*	N5	1.67	29X-1, 39-40	29X-1, 86-87	263.89	264.36	264.12	303.39
B m. *Gephyrocapsa* spp.	N6	1.69	29X-3, 66-67	29X-3, 114-115	267.16	267.54	267.35	306.62
T *D. brouweri*	N7	1.95	31X-CC, 48-53	32X-CC. 13-22	289.23	292.53	290.88	330.15
B (common) *G. inflata*	F5	2.16	34X-1, 65-70	34X-2, 65-70	312.35	313.85	313.10	352.37
T *M. exilis*	F6	2.2	34X-CC, 30-36	35X-CC, 28-43	315.49	326.47	326.47	365.74
T *M. miocenica*	F7	2.3	34X-CC, 30-36	35X-CC, 28-43	315.49	326.47	326.47	365.74
T *D. pentaradiatus*	N8	2.52	34X-CC, 30-36	35X-1, 39-40	315.49	321.69	318.59	357.86
T *D. surculus*	N9	2.53	35X-3, 14	35X-3, 22	324.44	324.52	324.48	363.75
T *D. tamalis*	N10	2.83	35X-CC, 28-43	36X-1, 16-17	326.47	331.06	328.77	368.04
T *M. multicamerata*	F8	3.11	36X-4, 64-72	36X-CC, 37-52	335.61	338.70	337.16	376.43
T *D. altispira*	F9	3.12	36X-4, 64-72	36X-CC, 37-52	335.61	338.70	337.16	376.43
172-1062A-								
T *G. tumida flexuosa*	F1	0.068	3H-4, 70-75	3H-5, 70-75	16.90	18.40	17.65	20.57
Reent. *G. tumida flexuosa*	F2	0.401	7H-CC	8H-1, 70-75	59.69	64.40	62.05	69.90
T *P. lacunosa*	N1	0.46	7H-6, 39-40	7H-6, 114-115	57.59	58.34	57.97	66.01
Reent. *G. crassaformis hessi*	F3	0.75	12H-3, 70-75	12H-4, 70-75	100.90	102.40	101.65	109.55
Reent. m. *Gephyrocapsa* spp.	N2	1.00	13H-2, 39-40	13H-2, 114-115	108.56	109.34	108.95	116.71
T large *Gephyrocapsa* spp.	N3	1.24	14H-4, 39-40	14H-5, 39-40	121.09	122.59	121.84	130.20
T *G. obliquus*	F4	1.3	14H-5, 70-75	14H-CC	122.90	124.16	123.53	131.89
B large *Gephyrocapsa* spp.	N4	1.58	15H-3, 130-131	15H-4, 14-15	130.00	130.34	130.17	138.63
T *C. macintyrei*	N5	1.67	15H-5, 39-40	15H-5, 114-115	132.09	132.84	132.47	140.93
B m. *Gephyrocapsa* spp.	N6	1.69	15H-6, 80	15H-6, 115-116	134.00	134.35	134.18	142.64
T *D. brouweri*	N7	1.95	16H-5, 114-115	16H-6, 39-40	142.34	143.09	142.72	151.74
B *T. truncatulinoides*	F5	2.00	17H-1, 70-75	17H-2, 70-75	145.40	146.90	146.15	156.09
B (common) *G. inflata*	F6	2.16	17H-3, 70-75	17H-4, 70-75	148.42	149.90	149.16	159.10
B *D. triradiatus* Acme	N8	2.15	17H-3, 145-146	17H-4, 39-40	149.15	149.59	148.84	158.78
Reent. *Pulleniatina*	F7	2.3	18H-1, 70-75	18H-2, 70-75	154.90	156.40	155.65	167.59
T *M. miocenica*	F8	2.3	18H-6, 61-66	18H-CC, 0-15	162.31	163.40	162.86	174.80
T *D. pentaradiatus*	N9	2.52	18H-2, 114-115	18H-3, 39-40	156.84	157.59	157.22	169.16
T *D. tamalis*	N10	2.83	20H-5, 70-71	20H-5, 100-101	179.90	180.20	180.05	191.99
172-1062B-								
T *M. miocenica*	F8	2.3	19X-1, 70-75	19X-2, 70-75	162.80	164.30	163.55	172.51
T *D. tamalis*	N10	2.83	20X-5, 114	20X-6, 40	178.84	179.60	179.22	188.18
T *D. altispira*	F9	3.12	21X-CC, 24-34	21X-1, 70-75	191.05	191.60	191.33	200.29
T *H. margaritae*	F10	3.58	23X-1, 67-72	23X-2, 67-72	201.17	202.67	201.92	210.88
T *Sphenolithus* spp.	N11	3.66	23X-6, 62	23X-6, 114	208.62	209.67	209.15	218.11
T *R. pseudoumbilicus*	N12	3.82	23X-6, 62	23X-6, 114	208.62	209.67	209.15	218.11
T *G. nepenthes*	F11	4.27	26X-6, 69-74	26X-CC	237.57	238.98	238.28	247.24
172-1062E-								
T *G. tumida flexuosa*	F1	0.068	2H-CC, 0-6	3H-CC, 0-15	13.23	22.98	18.11	19.43
Reent. *G. tumida flexuosa*	F2	0.401	5H-CC, 1-10	6H-CC, 7-17	41.90	51.28	46.59	50.47
T *P. lacunosa*	N1	0.46	5H-CC, 1-10	6H-CC, 7-17	41.90	51.28	46.59	50.47
Reent. m. *Gephyrocapsa* spp.	N2	1.00	10H-2, 125	10H-2, 140	82.55	82.70	82.63	91.49
T large *Gephyrocapsa* spp.	N3	1.24	11H-3, 138	11H-4, 28	93.58	93.93	93.76	102.20
T *G. obliquus*	F3	1.3	9H-CC, 29-44	10H-CC, 0-5	80.19	89.42	84.81	92.57
B large *Gephyrocapsa* spp.	N4	1.58	11H-CC, 22-33	12H-1, 10	99.50	98.90	99.20	107.64
T *C. macintyrei*	N5	1.67	11H-CC, 22-33	12H-1, 10	99.50	98.90	99.20	107.64
B m. *Gephyrocapsa* spp.	N6	1.69	12H-2, 60	12H-2, 90	100.90	101.20	101.05	109.49
T *D. brouweri*	N7	1.95	12H-6, 86	12H-6, 121	106.89	107.24	107.07	115.51
B *T. truncatulinoides*	F4	2.00	12H-CC, 13-23	13H-CC, 1-10	108.90	117.83	113.37	121.81
B (common) *G. inflata*	F5	2.16	12H-CC, 13-23	13H-CC, 1-10	108.90	117.83	113.37	121.81
T *M. miocenica*	F6	2.3	13H-CC, 1-10	14H-CC, 15-25	117.83	127.05	122.44	130.88
Reent. *Pulleniatina*	F7	2.3	13H-CC, 1-10	14H-CC, 15-25	117.83	127.05	122.44	130.88
T *D. pentaradiatus*	N8	2.52	14H-5, 115	14H-6, 24	124.20	124.68	124.44	132.88
T *D. tamalis*	N9	2.83	18X-5, 110	18X-6, 20	158.20	158.80	158.50	166.94

Notes: Event abbreviations: T = top, B = base, Reent. = reentrance, m = medium sized. ID abbreviations: F = planktonic foraminifer datum, N = nannofossil datum. For Hole 1060A, ID numbers correspond to those in Figure 60. For Hole 1061A, ID numbers correspond to those in Figure 63. For Holes 1062A and 1062B, ID numbers correspond to those in Figure 66A. For Hole 1062E, ID numbers correspond to those in Figure 66B.

covered sections, ranging from rich and diversified assemblages with good preservation to samples with a few partially dissolved specimens and those barren of nannofossils. Reworked forms were frequently observed.

In Hole 1062B, only the lower part (from Cores 172-1062B-20X through 26X) was studied in detail. The composite section of Holes 1062A and 1062B (Fig. 17) represents a stratigraphic sequence from the Holocene to the lower Pliocene (~4.3 Ma). In this section, the *P. lacunosa* disappearance corresponds to an interval with strongly dissolved nannofossil assemblages and barren samples, in some cases diluted by abundant terrigenous input. The biohorizon was unusually difficult to pinpoint because of the anomalous distribution pattern of the marker species in its uppermost range, where only very rare and poorly preserved specimens of *P. lacunosa* were observed. The biohorizons in the Pliocene interval were easily recognized, despite the strong reworking of late Miocene and possibly earliest Pliocene dis-

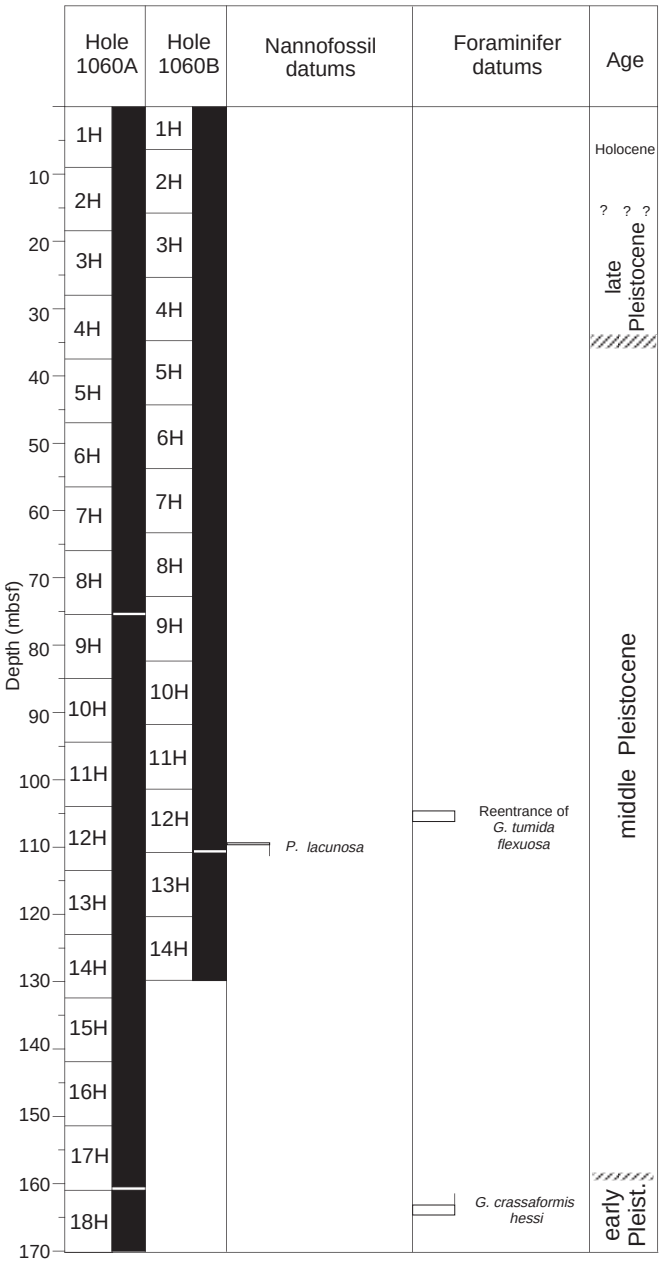

Figure 14. Core recovery and calcareous microfossil datum levels at Site 1060.

coasterids, because of the presence of abundant and well-preserved discoasterids. The lowermost part of Hole 1062B succession is placed within the upper range of *R. pseudoumbilicus.* Representatives of the genus *Sphenolithus* were very rare in their upper range and became extinct with *R. pseudoumbilicus,* although ordinarily their last occurrence (LO) occurs above (~0.2 m.y.) the LO of *R. pseudoumbilicus.*

As observed in the previous holes studied at this site, calcareous nannofossils recovered in Hole 1062E varied in abundance and preservation. In general, the assemblages showed abundant to common well-preserved nannofossils. Terrigenous input and reworking by turbidites affects the nannofossil assemblages in some intervals. This was clearly observed in the interval corresponding to Cores 172-1062E-11H and 12H, where the marker species showed anomalies in their distribution pattern, making some biohorizons difficult to recognize. This is true for the biohorizons corresponding to the Pleistocene/Pliocene boundary: the LO and FO of large *Gephyrocapsa* spp., the LO of *Calcidiscus macintyrei,* and the FO of medium-sized *Gephyrocapsa* spp.

Planktonic Foraminifers

Planktonic foraminifer analyses were confined to Holes 1060A, 1061A, 1062A, 1062B, 1062E, and 1062H, and foraminifer datums were constrained to within 1.5 m, except in Holes 1062E and 1062H, where only core catchers were examined. Preservation of planktonic foraminifers varied from good to poor. Numbers of planktonic foraminifers varied from abundant to barren. At Site 1061 (3975 m water depth), preservation was more consistently poor, but there were no barren samples, whereas at Site 1062 (4700 m water depth) preservation varied cyclically from good to poor. Numbers of foraminifers in the samples were reduced by both dissolution and dilution. Dilution was a significant factor at all sites, making it necessary to process at least 20 cm^3 of sediment to find a minimum number of foraminifer tests.

Site 1060

Preservation of planktonic foraminifers is generally moderate to poor at this site, with intervals of good preservation that appear, by reference to magnetic susceptibility data, to correspond with interglacial stages. Only the reentrance of *Globorotalia tumida flexuosa* (0.401 Ma) and the FO of *Truncorotalia crassaformis hessi* (0.75 Ma) were determined at this site in Hole 1060A (Table 4). The *G. tumida flexuosa* reentrance and the FO of *T. crassaformis hessi* were found, respectively, in the transition between MISs 12 and 11 and in MIS 19 because those stages are represented by the proxy of magnetic susceptibility. The LO of *G. tumida flexuosa* was not determined at this site. Although the samples are not greatly dissolved through this interval, the sand fraction was greatly diluted by terrigenous input.

Site 1061

The section recovered at this site spans the interval between the Holocene and the middle Pliocene (Table 4). Preservation of foraminifers is generally moderate to poor at Site 1061 and the datums were subsequently difficult to constrain (particularly in Cores 172-1061A-35X and 36X). Foraminifer numbers were reduced by clay dilution and carbonate dissolution. The positions of the LO and reentrance of *G. tumida flexuosa* are similar, relative to the magnetic susceptibility record, to those described at previous sites, except that the reentrance of *G. tumida flexuosa* is found at the base of MIS 11, rather than in the transition between MISs 11 and 12. The FO of *T. crassaformis hessi* (0.75 Ma), the LO of *Globigerinoides obliquus* (1.3 Ma), and the FO of *Globoconella inflata* (2.15 Ma) were readily constrained in Hole 1061A with 1.5-m resolution. The occurrence of *Truncorotalia truncatulinoides* is very intermittent in this core and therefore the bottom of the range (2.0 Ma) is difficult to constrain precisely. The first specimen was seen in Sample 172-1061A-32X-CC and it reappears in Core 30X, but the species was not observed in Cores 31X, 29X, 28X, or 27X. This datum was not used to construct the age/depth relation (see Fig. 64, "Sedimentation and Mass Accumulation Rates" section, this chapter). The LOs of *Menardella exilis* (2.2 Ma), *M. miocenica* (2.3 Ma), *M. multicamerata* (3.11 Ma), and *Dentoglobigerina altispira* (3.12 Ma) are found in Cores 172-1061A-35X and 36X, where the dissolution is at a maximum. The resolution for defining these datums is consequently ~3 to 4.5 m. The age model proposed by nannofossil datums through this interval suggests that the tops of the ranges of all these Pliocene foraminifer species are probably truncated by dissolution at this site.

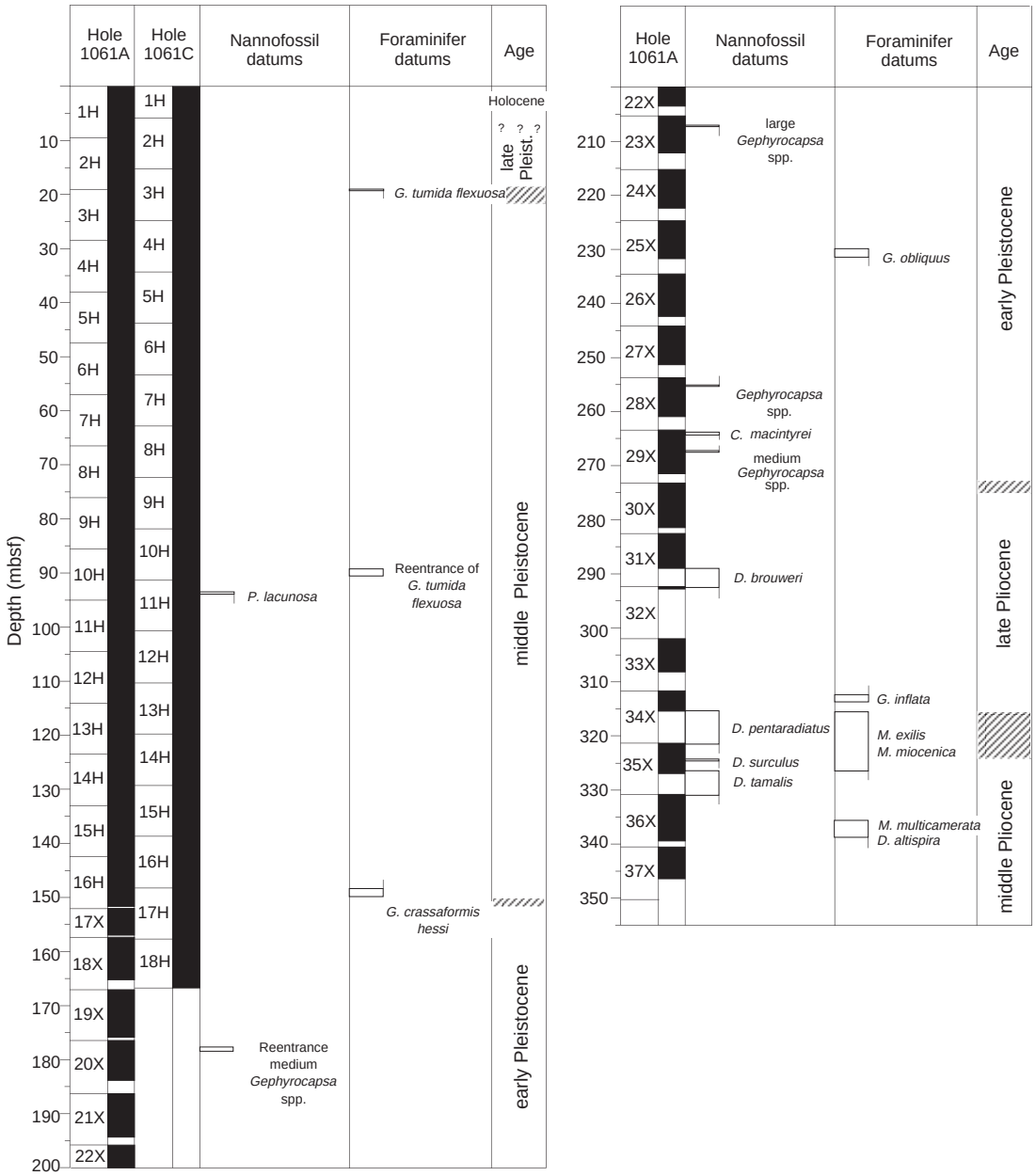

Figure 15. Core recovery and calcareous microfossil datum levels at Site 1061.

Site 1062

At this site, Hole 1062A was studied from 0 to 180 mbsf and Hole 1062B was examined from 163 to 239 mbsf. The past 2.83 m.y. are covered in Hole 1062A and the record is continued to ~4.3 Ma in Hole 1062B (Table 4). The two holes overlap by 0.2 m.y. and the level of the extinction of *M. miocenica* is constrained in both holes. Although the seafloor at this site is 725 m deeper than at Site 1061, the carbonate preservation is generally better. Carbonate eroded from the Bahama Bank may accumulate on the western flank of the mud wave where Holes 1062A and 1062B were cored, locally improving carbonate preservation (see "Site Geophysics" section, this chapter). The marker species in Hole 1062A (Table 4) are the same as at the previous site, except that in Hole 1062A the FO of *T. truncatulinoides* (2.0 Ma) is more precisely defined than it is in Hole 1061A, and this makes it possible to use it as a datum (Table 4). Core catchers from Holes 1062E (on the eastern flank of the mud wave) and 1062H (on the crest of the mud wave) were also studied. Preservation in Hole 1062E is generally poor and only core catchers were examined. Several datums were constrained at this resolution (Table 4). Sediment in Cores 172-1062E-9H through 13H was disturbed and redeposition may have mixed older foraminifers upward in the core. Paleomagnetic events in this hole (see "Paleomagnetism" section, this chapter) suggest that the age horizons are deeper through this interval than indicated by calcareous microfossil data. Foraminifer preservation in Hole 1062H is moderate to good for the first three core catchers, but becomes poor in the bottom four, with an increasing concentration of pyrite-filled burrows. Consequently, no foraminifer datums were found in this hole by examining core catchers.

Benthic Foraminifers

Benthic foraminifers were studied mainly in core-catcher samples from Holes 1060A, 1060B, 1061A, 1061B, 1062A, 1062B, and

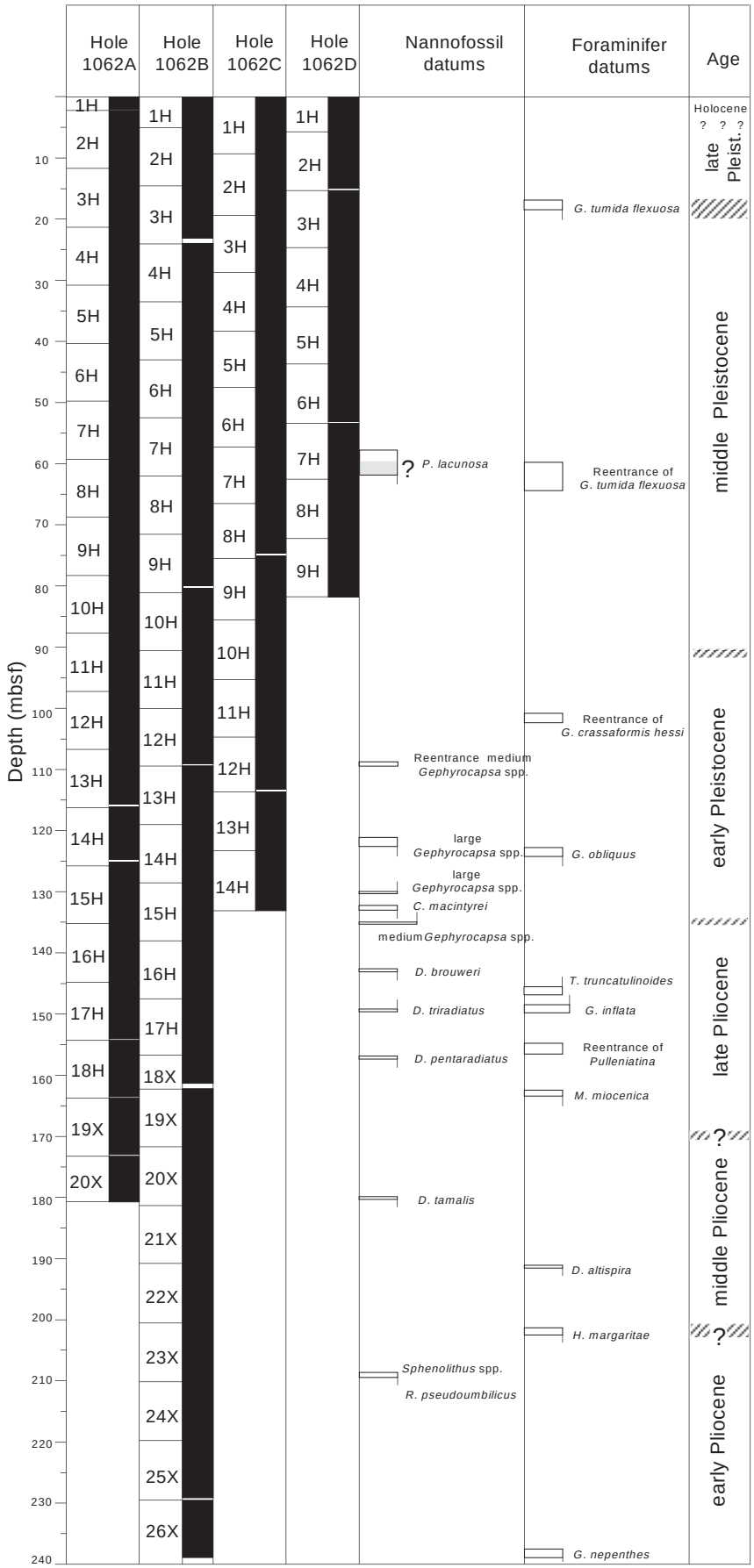

Figure 16. Core recovery and calcareous microfossil datum levels at Holes 1062A–1062D. The shaded area on the *P. lacunosa* LO symbol marks the uncertainty in defining the exact position of the datum in the core.

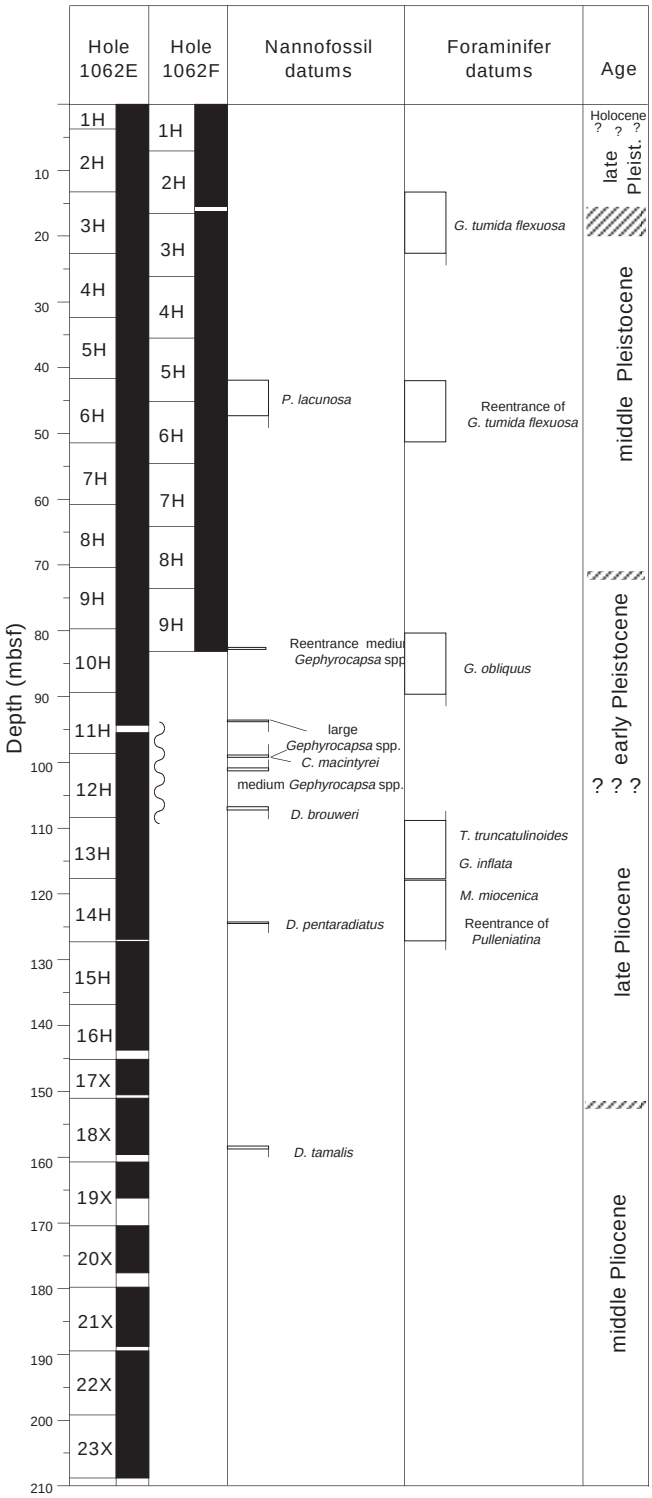

Figure 17. Core recovery and calcareous microfossil datum levels at Holes 1062E and 1062F. Squiggle indicates interval of very disturbed sediment (Cores 172-1062E-11H and 12H).

1062E. At Sites 1060 and 1061 some samples from within cores were also examined. Foraminifer numbers varied from few to rare. Benthic foraminifers, like planktonic ones, are subject to the same problem of dilution, but they are less susceptible to dissolution. The problem of dissolution is worst at Site 1061.

Site 1060

At this site benthic foraminifers are rare to few in abundance and moderately to poorly preserved. Comparison with magnetic susceptibility data indicates that samples with better preservation and a greater number of specimens were collected in interglacial stages. Between Samples 172-1060B-1H-CC and 9H-CC the most common species are *Uvigerina peregrina* and *Globobulimina affinis*, with lower numbers of *Melonis pompilioides* and rare *Chilostomella oolina*. From Sample 172-1060A-9H-CC downward, benthic assemblages are dominated by epifaunal taxa (*Oridorsalis umbonatus*, *Cibicidoides wuellerstorfi*, and *Gyroidinoides* spp.) during the interglacial stages, and by infaunal taxa (*U. peregrina*, *G. affinis*, and *C. oolina*) during the glacials. In Sample 172-1060A-18H-CC the most common species is *Osangularia umbonifera.*

Site 1061

At this site benthic foraminifers are very rare and preservation is poor. The fauna includes small numbers of few species, primarily *U. peregrina* and *O. umbonifera.*

Site 1062

Benthic foraminifers at this site are rare to very rare, and moderately to poorly preserved. The fauna includes small numbers of several species, primarily *M. pompilioides*, *C. wuellerstorfi*, *Globocassidulina subglobosa*, *O. umbonifera*, and *O. umbonatus.*

Diatoms

Diatoms were examined in the core-catcher samples of Holes 1060A, 1061A, 1062A, 1062B, 1062E, and 1062H. Table 5 lists the preservational state and relative abundance of diatoms at each site. Sites 1060 and 1061 have very similar diatom assemblages and they will be discussed together, whereas Site 1062 will be treated separately.

Sites 1060 and 1061

Diatoms are found throughout the entire length of Hole 1060A, with only three barren samples. All samples examined in Hole 1061A through Core 172-1061A-19X contained diatoms. The LO of *Nitzschia reinholdii* was constrained in both Holes 1060A (between Samples 172-1060A-17H-CC and 18H-CC) and 1061A (between Samples 172-1061A-18X-4, 29 cm, and 18X-5, 105 cm). This datum is diachronous across latitude and between oceans. Based on the Leg 172 preliminary age model, the event at these deep-water sites seems closer to the age estimate for the equatorial Pacific (0.65 Ma) than to North Atlantic age estimates (0.44 Ma) (Baldauf, 1984; Barron, 1985; Baldauf, 1987). However, the observed extinction level of *N. reinholdii* could be an artifact of both varying diatom flux and regional transport.

Species normally restricted to coastal environments were found in Samples 1060A-7H-CC and 9H-CC. The relative abundance of the coastal species (listed in the "Intermediate Depth Blake Outer Ridge" chapter, this volume) changes between samples, but they are an important part of the assemblage. In Sample 172-1061A-7H-CC fragments of the species *Ethmodiscus rex* increase in abundance and are the dominant member of the assemblage. Sample 172-1061A-11H-CC contained a relatively large amount of pollen.

Table 5. Distribution of diatoms in Holes 1060A, 1061A, 1062A, 1062B, 1062E, and 1062H.

Core, section	Presence of diatoms
172-1060A-	
1H-CC	C - fragments/R - whole
2H-CC	F - fragments/R - whole
3H-CC	A - fragments and whole
4H-CC	R - fragments
5H-CC	X - fragments
6H-CC	A - fragments/F - whole
7H-CC	A - fragments/C - whole
8H-CC	A - fragments/F - whole
9H-CC	A - fragments/F - whole
10H-CC	F - fragments
11H-CC	Barren
12H-CC	R - fragments
13H-CC	Barren
14H-CC	A - fragments/R - whole
15H-CC	A - fragments and whole
16H-CC	F - fragments
17H-CC	R - fragments
18 H-CC	Barren
172-1061A-	
1H-CC	A - fragments/F - whole
2H-CC	A - fragments/F -whole
3H-CC	C - fragments/R - whole
4H-CC	A - fragments/F- whole
5H-CC	F - fragments
6H-CC	A - fragments/R - whole
7H-CC	A - fragments and whole
8H-CC	Barren
9H-CC	A - fragments and whole
10H-CC	Barren
11H-CC	A - fragments and whole
12H-CC	R- fragments
13H-CC	R - fragments
14H-CC	Barren
15H-CC	Barren
16H-CC	Barren
17X-CC	R - fragments
18X-CC	A - fragments and whole
19X-CC	A - fragments and whole
20X-CC	C - fragments/X - whole
21X-CC	C - fragments/R - whole
22X-CC	Barren
23X-CC	C - fragments/X - whole
24X-CC	C - fragments
25X-CC	R - fragments
26X-CC	F - fragments
27X-CC	R - fragments
28X-CC	Barren
29X-CC	Barren
30X-CC	Barren
31X-CC	Barren
32X-CC	Barren
33X-CC	Barren
34X-CC	Barren
35X-CC	Barren
36X-CC	Barren
37X-CC	Barren
172-1062A-	
1H-CC	Barren
2H-CC	A - fragments and whole
3H-CC	Barren
4H-CC	F - fragments and whole
5H-CC	Barren
6H-CC	Barren
7H-CC	Barren
8H-CC	Barren
9H-CC	Barren
10H-CC	Barren
11H-CC	Barren
12H-CC	Barren
13H-CC	Barren
14H-CC	Barren
15H-CC	Barren
16H-CC	Barren
17H-CC	Barren
18H-CC	Barren
19H-CC	Barren
20H-CC	Barren
172-1062B-	
1H-CC	Barren
2H-CC	A - fragments and whole
3H-CC	Barren
4H-CC	A - fragments and whole
5H-CC	Barren
6H-CC	Barren
7H-CC	Barren
8H-CC	Barren
9H-CC	Barren
10H-CC	Barren
11H-CC	Barren
12H-CC	Barren
13H-CC	Barren
14H-CC	Barren
15H-CC	Barren
16H-CC	Barren
17H-CC	Barren
18 H-CC	Barren
172-1062E-	
1H-CC	Barren
2H-CC	F - fragments
3H-CC	R - fragments
4H-CC	Barren
5H-CC	Barren
6H-CC	Barren
7H-CC	Barren
8H-CC	Barren
9H-CC	Barren
10H-CC	Barren
11H-CC	Barren
12H-CC	Barren
13H-CC	Barren
14H-CC	Barren
15H-CC	Barren
16H-CC	Barren
17X-CC	Barren
18X-CC	Barren
19X-CC	Barren
20X-CC	Barren
21X-CC	Barren
22X-CC	Barren
23X-CC	Barren
172-1062H-	
1H-CC	X - fragments
2H-CC	A - fragments and whole
3H-CC	Barren
4H-CC	X - fragments
5H-CC	X - fragments
6H-CC	Barren
7H-CC	Barren

Note: Quantity abbreviations: X = scarce, R = rare, F = few, C = common, A = abundant.

Site 1062

Good diatom assemblages were found in only four samples: Samples 172-1062A-2H-CC and 4H-CC and Samples 172-1062B-2H-CC and 4H-CC. Samples 172-1062A-2H-CC and 172-1062B-2H-CC were more diverse. The dominant genera in all samples were *Thalassiothrix* and *Thalassionema.* The abundance of open-ocean marker species was very low, but other species that are associated with the open-ocean assemblage were observed (e.g., *Thalassiosira oestrtupii, Nitzschia marina,* and *Cosciniodiscus africanus*). The lower part of Hole 1062B (Cores 172-1062B-18X through 26X) was used to extend the calcareous microfossil biostratigraphy, but the core-catcher samples were barren of diatoms.

PALEOMAGNETISM

Introduction

The natural remanent magnetization (NRM) of the archive-half sections from all holes cored at Sites 1060, 1061, and 1062 (APC and XCB cores) was measured at 5-cm intervals using the pass-through cryogenic magnetometer. After measuring the NRM, most sections were partially demagnetized at 20 mT with the aim of removing overprints to reveal the character of the geomagnetic field changes. More detailed AF demagnetization treatments up to 60 mT were conducted on a few sections to evaluate the demagnetization behavior of the sediments at higher fields. The data for the remanence measurements

are given in Tables 6 through 21 on CD-ROM (back pocket, this volume). Discrete samples were routinely collected from one hole at each site at a sampling interval of one per core section, or approximately every 1.5 m. These samples were progressively demagnetized at 5- to 10-mT increments up to 60 mT using the pass-through cryogenic magnetometer.

As observed at the previous sites drilled on this leg, the NRM inclinations are consistently biased toward high positive inclinations (70° to 90°). The observed NRM directions indicate that a magnetic overprint is present as identified on many previous DSDP and ODP legs. This secondary overprint is characterized by steep inclinations and is probably acquired during drilling. Partial demagnetization in peak fields of 20 mT appears to remove most of the overprint for the upper 100 to 150 m of core at each hole, as evidenced by directional data downcore (Figs. 18–20) and demagnetization behavior of discrete samples (Fig. 21). Below these depths, coring disturbance (particularly in the XCB-cored intervals) and the overprint complicate the assessment of magnetic polarity from long-core measurements alone. Based on combined discrete and long-core measurements, however, we have been able to estimate the polarity stratigraphy at all three sites (Table 22). The intensity of magnetization after treatment at 20 mT at each of these sites covaries proportionally with susceptibility. The intensities vary by as much as three orders of magnitude, ranging from 5×10^{-5} to 5×10^{-2} A/m.

Orientation

The Tensor tool was used to orient some of the APC cores collected from these holes, starting with the third or fourth core at each hole (Table 23 on CD-ROM, back pocket, this volume). Both Tensor tools failed during operations at Sites 1060 and 1061. Unfortunately, none of the Tensor-tool data for Site 1060 could be retrieved. It was,

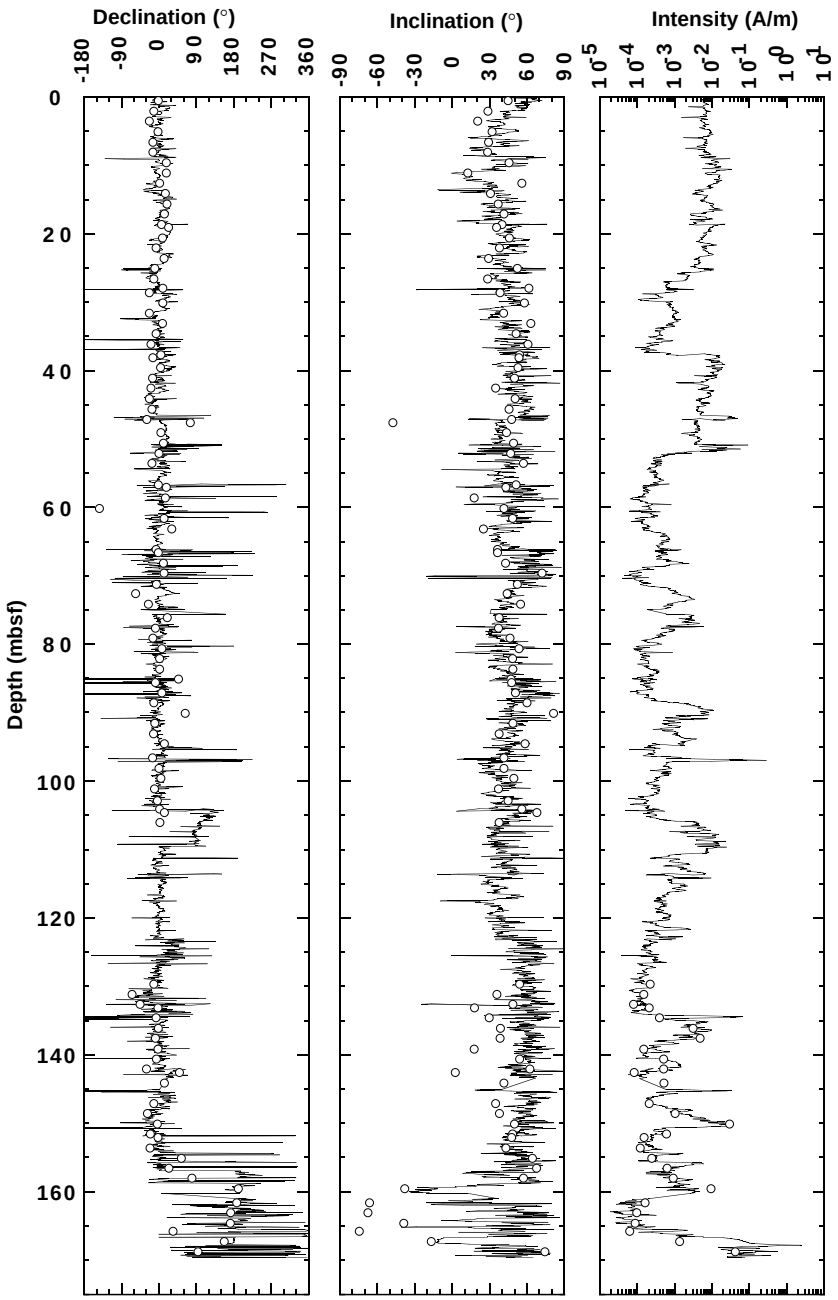

Figure 18. Downhole variation in declination, inclination, and intensity of archive-half cores after partial AF demagnetization at 20 mT (solid lines) and ChRM declinations, inclinations, and intensities of discrete samples (open circles) for Hole 1060A. Declinations were corrected by rotating the mean declination to 0° or 180°.

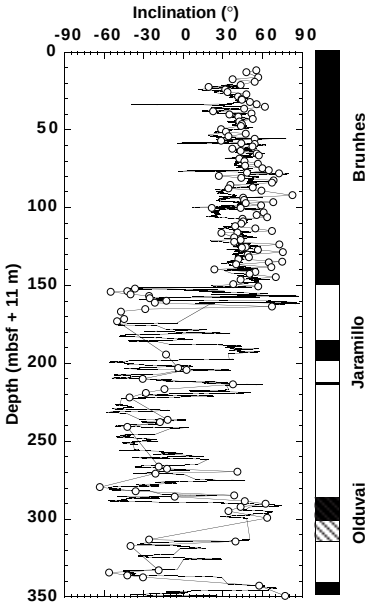

Figure 19. Downhole variation in the inclination of archive-half cores after partial AF demagnetization at 20 mT (solid lines) and ChRM inclinations of discrete samples (open circles) for Hole 1061A. The results are plotted using the +11 m correction for this hole (see "Operations" section, this chapter).

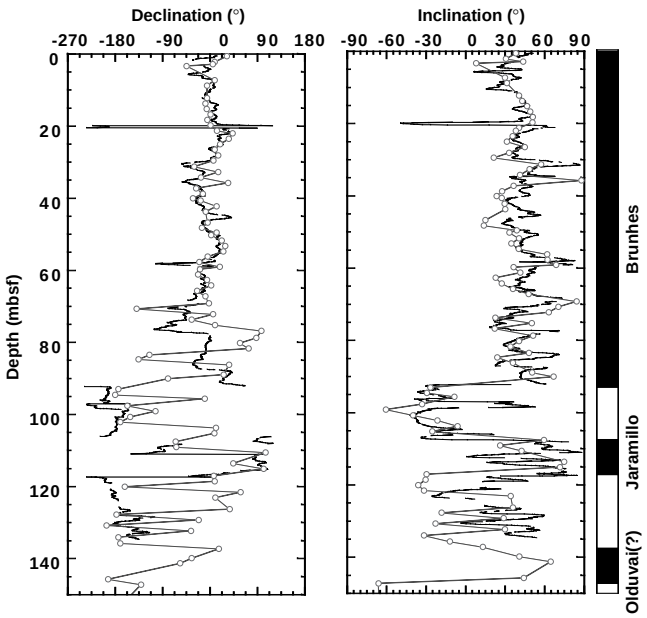

Figure 20. Downhole variation in the declination and inclination of archive-half cores after partial AF demagnetization at 20 mT (solid lines) and ChRM declinations and inclinations of discrete samples (open circles) for Hole 1062B. Declinations were corrected using the Tensor tool orientation data.

however, possible to repair one of the instruments for use at Site 1061 and subsequent sites. We therefore modified our strategy from orienting every core at each hole to attempting to orient all cores from one hole, and to only orient cores thought to contain polarity reversals at the other holes. The orientation data proved to be successful in aligning the declinations between cores in the majority of cases. Sharp offsets between some cores, however, suggest that either the Tensor tool did not function properly or that the core twisted or rotated as it entered the core barrel. In some cases disturbance resulting from gas expansion seriously affected the declination data. Overall, core disturbance caused by gas expansion was much less than at the previous sites drilled on this leg.

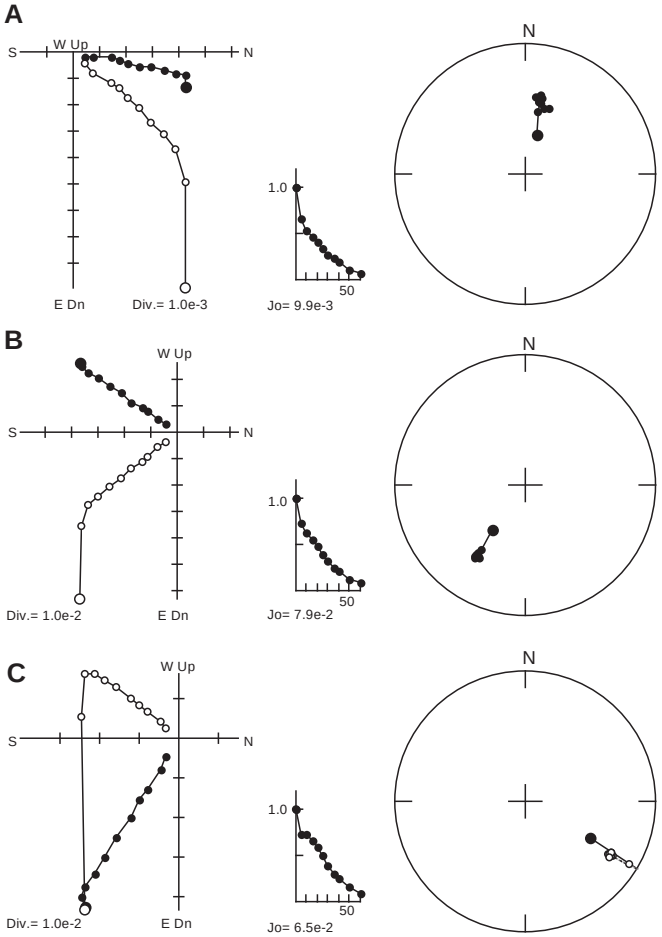

Figure 21. Examples of progressive AF demagnetization of discrete samples taken from the Hole 1062A intervals recording the excursions shown in Figures 22 and 23. **A.** 172-1062A-3H-2, 61 cm (13.81 mbsf). **B.** 172-1062A-10H-3, 60 cm (81.8 mbsf). **C.** 172-1062A-15H-4, 64 cm (130.84 mbsf). A steep downward component is removed by treatment of 5 to 20 mT, isolating well-defined characteristic remanence magnetizations through the excursions.

Discrete Sample Analysis

Excellent agreement is observed between the pass-through measurements of the archive halves and the characteristic remanent magnetization (ChRM) directions obtained from progressive AF demagnetization of the discrete samples at all sites for most of the Brunhes Chron (Figs. 18–20). The intensities measured using discrete samples and pass-through measurements also agree. The overprint is a steep downward magnetization with a 0° average declination in sample coordinates. This is consistent with a radially directed, steep downward overprint direction observed on many previous drilling legs.

Magnetic Polarity Stratigraphy

Polarity assessment proved to be more straightforward at Sites 1060 through 1062 than at the sites cored in shallower water during this leg. This is most likely because there was less core disturbance caused by gas expansion, and reduction diagenesis has been less se-

Table 22. Polarity reversal boundaries observed at Sites 1060, 1061, and 1062.

Core, section, interval (cm)	Age (Ma)	Depth (mbsf)	Reversal
172-1060A-			
17H-6, 80	0.78	159.8	Brunhes/Matuyama
18H-5, 120	0.99	168.0	Jaramillo
172-1061A*			
15H-5, 100	0.78	151.3	Brunhes/Matuyama
20X-1, 25	0.99	176.0	Jaramillo top
21X-2, 5	1.07	186.0	Jaramillo base
30X--4, 85	1.77	276.0	Olduvai top
33X-1, 125	1.95	305.0	Olduvai base
35X-4, 35	2.58	330.0	Gauss (top)?
36X-1, 5			
172-1061C-			
17H-3, 0	0.78	151.3	Brunhes/Matuyama
18H-2, 20	0.99	159.4	Jaramillo top
172-1062A-			
11H-4, 89	0.78	92.2	Brunhes/Matuyama
13H-1, 94	0.99	107.0	Jaramillo top
14H-1, 94	1.07	117.0	Jaramillo base
172-1062B-			
11H-3, 0	0.78	93.5	Brunhes/Matuyama
12H-7, 65	0.99	108.4	Jaramillo top
13H-2, 140	1.07	112.4	Jaramillo base
15H-1, 0-80	1.77	129.0	Olduvai top
17H-1, 0-?	1.95	>147.5	Olduvai base
172-1062C-			
11H-1, 90	0.78	95.8	Brunhes/Matuyama
12H-4, 100	0.99	109.9	Jaramillo top
13H-1, 0	1.07	113.9	Jaramillo base
172-1062E-			
9H-1, 85	0.78	71.1	Brunhes/Matuyama
9H-7, 50	0.99	79.0	Jaramillo top
10H-5, 15	1.07	86.0	Jaramillo base

Note: * = all depths for Hole 1061A include a +11 m correction.

vere at these deeper water sites. Discrete sample results proved useful in defining polarity intervals deeper in the holes where coring disturbance was greater, particularly in intervals cored with the XCB.

Site 1060

Normal polarity directions are observed from the seafloor down to a depth of 159 mbsf in Hole 1060A (Fig. 18; mean direction: declination = 6.4°, inclination = 41.4°, k = 22.6, α_{95} = 2.1°, N = 191, R = 182.6). Reversed polarity directions are observed from 159 mbsf to 168 mbsf in Hole 1060A corresponding to the uppermost part of the Matuyama Chron at this site. The lowermost discrete sample from this hole yields a normal polarity direction, which may be the top of the Jaramillo Subchron. Excellent agreement exists between the discrete sample and long-core directions from the top of the cored interval down to a depth of 124 mbsf. From 124 to 168 mbsf, increased scatter occurs in the long-core results. The Brunhes/Matuyama polarity transition was cored at three holes at this site, with sedimentation rates between 150 and 250 m/m.y. We expect shore-based study of these intervals to yield important polarity transition records across this reversal.

Site 1061

Full normal polarity directions are observed to a depth of 151 mbsf (this and other Hole 1061A depth values include +11 m correction) in Hole 1061A, which we interpret as the base of the Brunhes Chron (Fig. 19; mean direction: declination = –2.6°, inclination = 42.1°, k = 9.3, α_{95} = 1.8, N = 650, R = 579.9). Between 151 and 176 mbsf reversed polarity directions are observed. Between 176 and 186 mbsf normal polarity directions are documented by the pass-through measurements; however, discrete samples were not available from this interval. Normal polarity declinations and inclinations are observed between 276 and 305 mbsf, which we correlate with the Olduvai Subchron. The position of the base of the Olduvai is not clear because of the recovery gap between the base of Core 172-1061A-33X and the top of 34X. Below 330 mbsf, apparent normal polarity magnetizations are observed, which likely represent the top of the Gauss Chronozone.

Site 1062

At Site 1062 the magnetic polarity is well defined down to the base of the Jaramillo Subchron (see Table 22 for reversal positions and depths). Full polarity directions agree with the geocentric axial dipole (GAD) directions expected at this site latitude (mean direction: Declination = 0.9°, Inclination = 48.4°, k = 5.9, α_{95} = 2.12°, N = 712, R = 592.3). Below the base of the Jaramillo Subchron, an increase in turbidite occurrence makes the paleomagnetic record more difficult to interpret. The interval exhibits large swings in magnetization direction, often oscillating between apparent normal and reversed polarity directions. The discrete sample results tend to be less complex, but also exhibit large directional swings. For these reasons it has proven difficult to interpret the polarity zonation below the base of the Jaramillo at the holes cored at Site 1062. The different depths of the Brunhes and Jaramillo reversal boundaries observed on opposite sides of the mud wave cored at this site provide evidence for significant differences in sedimentation rates at these two locations.

Magnetic Field Variability Between Reversals

Paleomagnetic field direction changes that record paleomagnetic secular variation (PSV) are observed within the Brunhes Chron on a variety of length scales from 10 cm to more than 10 m. Careful analysis of PSV within a few short intervals (MISs 5, 7, and 11) indicates that the PSV records can be correlated between holes at each site. These patterns of directional changes can also be correlated between Sites 1060, 1061, and 1062. The PSV during the past 200,000 yr is also correlatable with other previously published directional PSV records (e.g., Lund, 1993). If composite, reproducible PSV records can be derived from each site in general and correlated with the other sites, then these sites could provide a unique opportunity to examine geomagnetic field variability over a wide range of time scales during the past 800 k.y. There are no other long, well-dated paleomagnetic records of directional field variability available anywhere in the world for the Brunhes time interval older than ~200 ka.

Excursions

One aspect of directional PSV that deserves special attention is the presence of reproducible magnetic field excursion records at Sites 1060, 1061, and 1062. The paleomagnetic directions recorded in each hole at these sites exhibit what we term “plausible” excursion records (i.e., the excursion is recorded in at least two sites and two holes at each site). These records are defined as having anomalous paleomagnetic inclinations (negative inclinations in the Brunhes Chron) and/or declinations (declination departures of more than 90° from the local mean value) and a systematic pattern of directional variability defined by coherent, serially correlated directional changes, that fits within the context of the surrounding PSV. In each case, evidence for core distortion, diagenesis, and lithologic variations (e.g., turbidites) was also checked before identifying anomalous directions as “plausible” excursion records. The ages of the excursions were estimated from magnetic susceptibility patterns that clearly identify MISs 1–22 in all holes of all three sites. The excursion records were then named temporarily by the stage within which they occur, with subscripts A and B when multiple excursion records occur in the same stage.

We have identified eight Brunhes-aged excursions at two or more sites (and multiple holes at each site). These are named 3B, 4A, 5B, 7A, 9A, 11A, 15A, and 15B. Excursion 3B fits in age (40 ka) and pat-

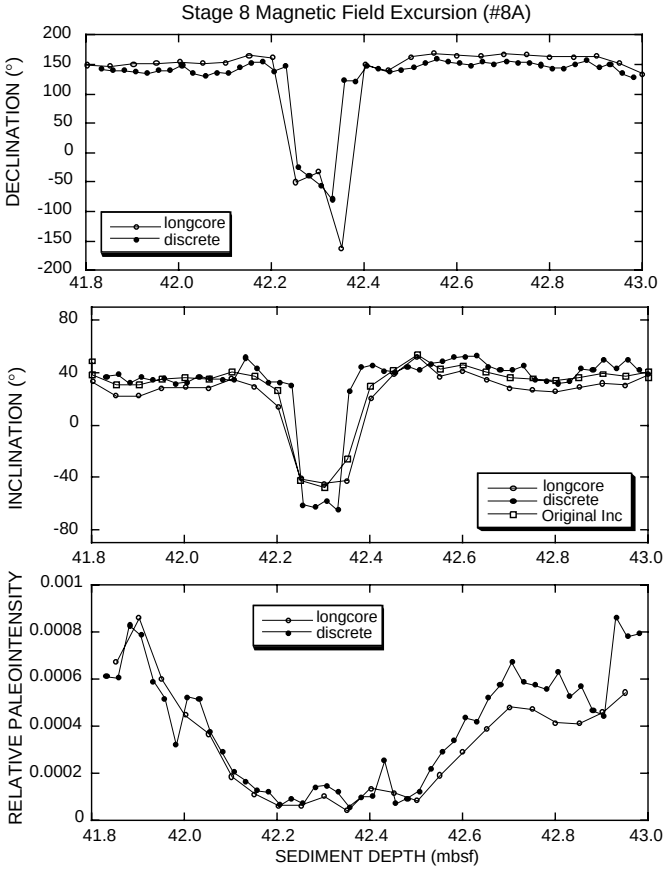

Figure 22. Detailed record of the excursion recorded in Section 172-1062D-5H-6. Relative paleointensity is given by (remanence at 20 mT)/susceptibility.

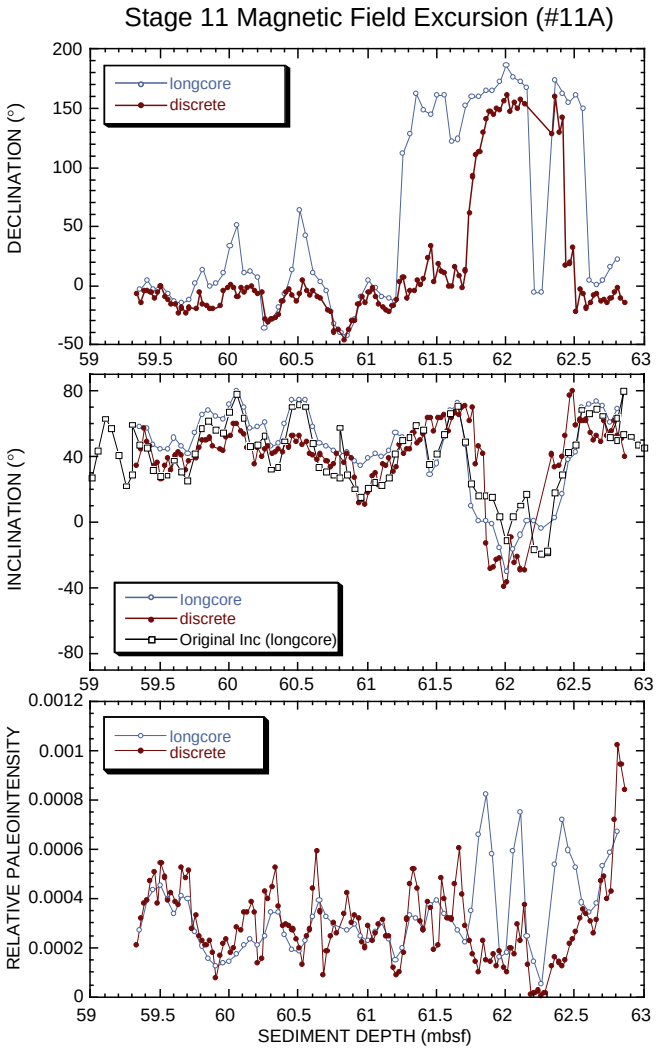

Figure 23. Detailed record of the excursion recorded at Section 172-1062D-7H-5 through 7H-7. Relative paleointensity is given by (remanence at 20 mT)/susceptibility.

tern of secular variation with the Laschamp Excursion (Lund, 1993, unpubl. data; Bonhommet and Babkine, 1967); Excursion 5B tentatively correlates with the Blake Event (Smith and Foster, 1969). There are still questions, however, regarding whether excursion 5B is actually the same age as the Blake Event originally dated by Smith and Foster (1969). At Site 1062 only, we have evidence of a second Stage 5 excursion (termed herein 5A) which may also be a candidate for the Blake Event, if we can verify its reality. We have also identified an additional five excursions at Site 1062 that are all observed in four or more holes. These are termed 5A, 6A, 8A, 13A, and 14A. So far we have identified two excursions at Site 1060, eight at Site 1061, and 13 at Site 1062. If careful analysis and replication with discrete sampling confirms these, there will have to be a major reassessment of the role of excursions within the context of "normal" secular variation and variability in styles of the core dynamo process.

Based on the excellent agreement in secular variation and excursions between holes cored at Site 1062, we decided to sample two of the excursions (8A and 11A) in detail. Standard, 6-cm^3-oriented paleomagnetic sample boxes were used to collect discrete samples continuously (sampling interval: 2.5 cm) through each of these excursions. The discrete samples were subjected to progressive AF demagnetization up to 60 mT, using the long-core magnetometer system, and the characteristic remanence directions were determined using principal component analysis. The results of the two discretely sampled intervals are shown in Figures 22 and 23. In both cases, the discrete measurements verified the existence of the excursions, although the discrete measurements did show a slightly different pattern for each excursion. We can easily attribute this to the broader integration interval of the long-core measuring system and the fact that the long-core measurements include deformed directions along the edges of each core segment (see previous discussion and model by Okada; "Paleomagnetism" section, "Intermediate Depth Blake Outer Ridge" chapter, this volume). To evaluate such deflection on long-core measurements, we calculated an expected "original" inclination, which is a value before the sediments were deformed because of piston coring, by an iteration using the deformation model. The derived "original" inclinations from long-core measurements are also shown in Figures 22 and 23. In the intervals of non-excursional behavior, the expected original inclinations are in better agreement with the discrete data than are the raw inclinations. In the excursional interval, however, the long-core data do not always agree with results from discrete samples. This might be explained by the smearing effect of the long-core measurement system, because the excursional interval is too short relative to the effective sensor length of the magnetometer.

COMPOSITE DEPTHS AND STRATIGRAPHIC CORRELATION

Multisensor track (MST) and color reflectance data collected from all holes at Sites 1060 through 1062 (and smoothed over a 31-cm Gaussian window) were used to correlate between individual holes at each site, to determine depth offsets in the composite section,

and to create spliced records. On the composite depth scale (expressed as meters composite depth [mcd]), features of the plotted MST and reflectance data present in adjacent holes are aligned so that they occur at approximately the same depth. Working from the top of the sedimentary sequence, a constant was added to the depth (mbsf) for each core in each hole to arrive at a composite depth (mcd) for that core. Spliced records were created by combining intervals of the individual composite depth sections to create an overall stratigraphic section. Intervals having significant disturbance or distortion were avoided if possible. This information, along with the offsets suggested for individual core sections, can be used as a sampling guide to recover a single sedimentary sequence and to identify variability in cored records between sites.

The stratigraphic records recovered were quite similar to one another between holes at Sites 1060 and 1061, but there are noticeable differences in accumulation rate and the character of sediment sequences between holes from different parts of the mud wave at Site 1062. As a result, one spliced record was created for each of Sites 1060 and 1061, but three spliced records were created for Site 1062. Holes 1062A through 1062D are located on the eastern wave flank, Holes 1062E and 1062F are located on the western wave flank, and Holes 1062G and 1062H are located on the mud-wave crest. The three spliced records at Site 1062 are referred to as east wave flank (Holes 1062A–1062D), west wave flank (Holes 1062E and 1062F), and wave crest (Holes 1062G and 1062H). The depth offsets used to construct the composite depth and spliced records are given in Tables 24 and 25. Affine and splice data tables appropriate for use in the Splicer program are on CD-ROM (back pocket, this volume). At all sites, a composite sequence could be created for the interval of multiple coring. The integrity of the recovered sedimentary sequence could be documented to ~140 mcd (~120 mbsf) at Site 1060 and to ~214 mcd (~175 mbsf) at Site 1061. At Site 1062, the integrity of the sediment record could be documented to ~166 mcd (~156 mbsf, but based on only two holes that penetrated deeper than ~130 mcd) on the eastern wave flank, to ~79 mcd (~74 mbsf) on the western wave flank, and to ~17 mcd (~16 mbsf) on the wave crest. At all sites there are intervals where precise correlations are difficult to make because of nearly constant values for magnetic susceptibility and sediment color. However, after detailed correlations were re-established deeper in the core, minor variations in susceptibility and/or color within the previously questionable intervals could be correlated between holes.

Magnetic susceptibility and the color indices lightness (L*) and chromaticity (a* and b*) were the primary parameters used for interhole correlation. Gamma-ray attenuation porosity evaluator (GRAPE) density was also examined to provide additional support for composite construction, but it was often noisy because of core expansion. However, the GRAPE data are noticeably more consistent with other parameters at Site 1062, perhaps because of reduced gas expansion at this site compared to shallower sites cored on this leg. Natural gamma-ray measurements and *P*-wave velocity measurements were not systematically made in all holes and were not used for correlation. The GRAPE records were used to identify voids (values less than 1.20 g/cm^3), and GRAPE data from these intervals were not used. No allowance was made, however, for core expansion resulting from large gas voids, decompression, or distributed small gas voids. Within the Splicer computer program, cores can only be shifted as a whole, even where hiatuses are thought to exist within a core. More precise correlation between holes will necessarily be undertaken post cruise based on additional data.

The magnetic susceptibility, GRAPE, and color index (L*, a*, and b*) records used to verify core overlap are shown on a composite depth scale in Figures 24 through 28 for Site 1060, 29 through 33 for Site 1061, and 34 through 48 for the east wave flank, west wave flank, and wave crest holes at Site 1062. The data used for correlation for each hole (with composite depths) and the spliced data at each site are on CD-ROM (back pocket, this volume). Also shown on each figure is a spliced record created by combining selected intervals of the composite cores. The spliced magnetic susceptibility and color reflectance (L*, a*, and b*) for Sites 1060 through 1062 are shown on Figures 49 through 53, and the upper 40 m of the two mud-wave flank magnetic susceptibility and L* splices are shown on Figure 54.

Site 1060

The magnetic susceptibility, lightness (L*), and chromaticity parameters (a* and b*) appear well correlated among Holes 1060A–1060C, and a complete record appears to have been recovered to ~153 mcd (~132 mbsf). However, the records in the different holes differ slightly deeper than ~110 mcd, perhaps because of gas expansion. Unfortunately, no color measurements were made on Cores 172-1060A-11H and 14H, so correlations are more difficult to confirm in these intervals. As a result of core expansion, the composite depth scale (mcd) is consistently 15% larger than the drilled depths (mbsf) to 125 mbsf (Fig. 55). Deeper than 125 mbsf, no additional offset is applied because only one hole was cored. The spliced records from this site utilize data from all three holes.

Site 1061

The magnetic susceptibility, lightness (L*) and the chromaticity parameters (a* and b*) appear well correlated among Holes 1061A through 1061E, and a composite section is constructed to the depth of triple coring (~195 mcd; ~160 mbsf) and appears to exist to the limit of double coring (~210 mcd; ~180 mbsf). As at Site 1060, minor differences between records of different holes are mostly related to gas cracking. In particular, GRAPE bulk density is less well correlated between sites deeper in the cored interval, apparently because of cracks in the sediment, although systematic changes in the upper 80 mcd appear correlated between cores. Interhole correlations suggest that Holes 1061A and 1061B did not recover a mudline. For Core 172-1061A-1H the calculated offset is 11.4 m, whereas for Core 172-1061B-1H the calculated offset is 9.06 m. The offset in Hole 1061A is consistent with the logging results in Hole 1061A. As a result of core expansion, the composite depth scale (mcd) is on average ~15% larger than drilled depths (mbsf) at this site to ~175 mbsf (~215 mcd; Fig. 56). Deeper than ~175 mbsf in Hole 1061A, the offset remains constant at ~40 m. The spliced records from this site were created by combining portions of the composite records from Holes 1061A, 1061C, and 1061D above ~215 mcd (Fig. 56). Deeper than ~215 mcd, the spliced record only contains Hole 1061A. Hole 1061A was logged for its entire depth interval, and postcruise correlations between cored sediment and logs, especially bulk density and natural gamma, and to a lesser extent lithology, should provide additional information about correlating composite depths to absolute depths.

Site 1062

Three separate composite sections were created for Site 1062 because holes which sampled different parts of a mud wave were expected to recover somewhat different sedimentary sequences. Composite and splice sections were created for the east wave flank (Holes 1062A–1062E), the west wave flank (Holes 1062E and 1062F), and the wave crest (Holes 1062G and 1062H). In all three composite sections, the magnetic susceptibility, lightness (L*), and chromaticity parameters (a* and b*) appear well correlated between holes. GRAPE data were also useful in documenting that the same layers were recovered in different holes, especially for the denser carbonate turbidites.

East Wave Flank Composite Record and Splice

A continuous composite section could be constructed to a depth of ~166 mcd (~156 mbsf) on the eastern wave flank. There is an offset toward higher values in L* from ~57 to ~100 mcd in Hole 1062A, although the structure of the L* record is similar to that in other holes.

Table 24. Composite depths and offsets for Sites 1060–1062.

Core, section	Depth (mbsf)	Offset (m)	Depth (mcd)
172-1060A-			
1H-1	0.00	0.00	0.00
2H-1	9.00	1.94	10.94
3H-1	18.50	4.00	22.50
4H-1	28.00	4.62	32.62
5H-1	37.50	5.87	43.37
6H-1	47.00	9.49	56.49
7H-1	56.50	10.39	66.89
8H-1	66.00	12.07	78.07
9H-1	75.50	12.16	87.66
10H-1	85.00	13.18	98.18
11H-1	94.50	15.19	109.69
12H-1	104.00	16.33	120.33
13H-1	113.50	18.83	132.33
14H-1	123.00	20.63	143.63
15H-1	132.50	20.63	153.13
16H-1	142.00	20.63	162.63
17H-1	151.50	20.63	172.13
18H-1	161.00	20.63	181.63
172-1060B-			
1H-1	0.00	0.02	0.02
2H-1	6.40	1.70	8.10
3H-1	15.90	3.08	18.98
4H-1	25.40	3.91	29.31
5H-1	34.90	5.19	40.09
6H-1	44.40	7.59	51.99
7H-1	53.90	8.35	62.25
8H-1	63.40	9.92	73.32
9H-1	72.90	10.60	83.50
10H-1	82.40	11.99	94.39
11H-1	91.90	13.16	105.06
12H-1	101.40	16.43	117.83
13H-1	110.90	18.25	129.15
14H-1	120.40	19.35	139.75
172-1060C-			
1H-1	0.00	0.10	0.10
2H-1	3.00	1.62	4.62
3H-1	12.50	3.40	15.90
4H-1	22.00	4.30	26.30
5H-1	31.50	5.01	36.51
6H-1	41.00	6.81	47.81
7H-1	50.50	8.74	59.24
8H-1	60.00	9.76	69.76
9H-1	69.50	11.07	80.57
10H-1	79.00	12.14	91.14
11H-1	88.50	13.23	101.73
12H-1	98.00	15.51	113.51
13H-1	107.50	17.93	125.43
14H-1	117.00	19.88	136.88
172-1061A-			
1H-1	0.00	11.4	11.40
2H-1	9.50	13.09	22.59
3H-1	19.00	15.83	34.83
4H-1	28.50	16.45	44.95
5H-1	38.00	19.01	57.01
6H-1	47.50	19.35	66.85
7H-1	57.00	22.05	79.05
8H-1	66.50	23.05	89.55
9H-1	76.00	25.05	101.05
10H-1	85.50	25.25	110.75
11H-1	95.00	26.29	121.29
12H-1	104.50	27.8	132.30
13H-1	114.00	29.34	143.34
14H-1	123.50	31.86	155.36
15H-1	133.00	32.72	165.72
16H-1	142.50	35.12	177.62
17X-1	152.00	36.11	188.11
18X-1	157.40	37.52	194.92
19X-1	167.00	39.27	206.27
20X-1	176.60	39.27	215.87
21X-1	186.20	39.27	225.47
22X-1	195.80	39.27	235.07
23X-1	205.40	39.27	244.67
24X-1	215.10	39.27	254.37
25X-1	224.80	39.27	264.07
26X-1	234.50	39.27	273.77
27X-1	244.20	39.27	283.47
28X-1	253.90	39.27	293.17
29X-1	263.50	39.27	302.77
30X-1	273.20	39.27	312.47
31X-1	282.80	39.27	322.07
32X-CC	292.40	39.27	331.67
33X-1	302.00	39.27	341.27
34X-1	311.70	39.27	350.97
35X-1	321.30	39.27	360.57
36X-1	330.90	39.27	370.17
37X-1	340.50	39.27	379.77
172-1061B-			
1H-1	0.00	9.06	9.06
172-1061C-			
1H-1	0.00	0.02	0.02
2H-1	5.80	0.4	6.20
3H-1	15.30	0.08	15.38
4H-1	24.80	2.49	27.29
5H-1	34.30	4.29	38.59
6H-1	43.80	5.27	49.07
7H-1	53.30	7.59	60.89
8H-1	62.80	8.63	71.43
9H-1	72.30	11.75	84.05
10H-1	81.80	13.53	95.33
11H-1	91.30	15.41	106.71
12H-1	100.80	16.59	117.39
13H-1	110.30	18.37	128.67
14H-1	119.80	19.6	139.40
15H-1	129.30	20.9	150.20
16H-1	138.80	21.38	160.18
17H-1	148.30	23.28	171.58
18H-1	157.80	24.28	182.08
172-1061D-			
1H-1	0.00	0	0.00
2H-1	1.20	3.12	4.32
3H-1	10.70	4.06	14.76
4H-1	20.20	4.57	24.77
5H-1	29.70	6.47	36.17
6H-1	39.20	7.25	46.45
7H-1	48.70	10.13	58.83
8H-1	58.20	10.83	69.03
9H-1	67.70	14.27	81.97
10H-1	77.20	14.77	91.97
11H-1	86.70	16.29	102.99
12H-1	96.20	17.17	113.37
13H-1	105.70	18.59	124.29
14H-1	115.20	20.3	135.50
15H-1	124.70	21.22	145.92
16H-1	134.20	23.02	157.22
17H-1	143.70	25.3	169.00
18H-1	153.20	26.12	179.32
19X-1	162.70	27.57	190.27
20X-1	165.70	27.89	193.59
21X-1	170.70	29.41	200.11
22X-1	175.20	28.63	203.83
172-1061E-			
1H-1	0.00	0	0.00
2H-1	9.40	-0.3	9.10
172-1062A-			
2H-1	2.20	2.4	4.60
3H-1	11.70	2.92	14.62
4H-1	21.20	4.44	25.64
5H-1	30.70	4.80	35.50
6H-1	40.20	7.02	47.22
7H-1	49.70	8.04	57.74
8H-1	59.20	7.66	66.86
9H-1	68.70	7.00	75.70
10H-1	78.20	6.86	85.06
11H-1	87.70	7.44	95.14
12H-1	97.20	7.90	105.10
13H-1	106.70	7.76	114.46
14H-1	116.20	8.36	124.56
15H-1	125.70	8.46	134.16
16H-1	135.20	9.02	144.22
17H-1	144.70	9.94	154.64
18H-1	154.20	11.94	166.14
19H-1	163.70	11.94	175.64
20H-1	173.20	11.94	185.14
172-1062B-			
1H-1	0.00	0.00	0.00
2H-1	5.00	1.30	6.30
3H-1	14.50	2.06	16.56
4H-1	24.00	1.84	25.84
5H-1	33.50	3.06	36.56
6H-1	43.00	4.34	47.34
7H-1	52.50	4.80	57.30
8H-1	62.00	5.99	67.99
9H-1	71.50	5.82	77.32
10H-1	81.00	6.06	87.06
11H-1	90.50	6.64	97.14
12H-1	100.00	6.84	106.84
13H-1	109.50	6.74	116.24
14H-1	119.00	7.14	126.14
15H-1	128.50	7.46	135.96
16H-1	138.00	8.98	146.98
17H-1	147.50	8.96	156.46
18X-1	156.70	8.96	165.66
19X-1	162.10	8.96	171.06
20X-1	171.70	8.96	180.66
21X-1	181.30	8.96	190.26
22X-1	190.90	8.96	199.86
23X-1	200.50	8.96	209.46
24X-1	210.20	8.96	219.16
25X-1	219.80	8.96	228.76
26X-1	229.40	8.96	238.36
172-1062C-			
1H-1	0.00	0.36	0.36
2H-1	9.40	0.44	9.84
3H-1	18.90	1.24	20.14
4H-1	28.40	2.08	30.48
5H-1	37.90	3.58	41.48
6H-1	47.40	3.76	51.16
7H-1	56.90	3.76	60.66
8H-1	66.40	5.01	71.41
9H-1	75.90	3.98	79.88
10H-1	85.40	4.53	89.93
11H-1	94.90	4.76	99.66
12H-1	104.40	6.16	110.56
13H-1	113.90	6.24	120.14
14H-1	123.40	5.98	129.38
172-1062D-			
1H-1	0.00	0.02	0.02
2H-1	5.80	-0.42	5.38
3H-1	15.30	0.30	15.60
4H-1	24.80	0.44	25.24
5H-1	34.30	1.48	35.78
6H-1	43.80	2.94	46.74
7H-1	53.30	4.16	57.46
8H-1	62.80	4.69	67.49
9H-1	72.30	4.32	76.62
172-1062E-			
1H-1	0.00	0.84	0.84
2H-1	3.80	1.26	5.06
3H-1	13.30	1.38	14.68
4H-1	22.80	2.56	25.36
5H-1	32.30	3.64	35.94
6H-1	41.80	4.12	45.92
7H-1	51.30	4.98	56.28
8H-1	60.80	6.46	67.26
9H-1	70.30	6.66	76.96
10H-1	79.80	8.86	88.66
11H-1	89.30	8.44	97.74
12H-1	98.80	8.44	107.24
13H-1	108.30	8.44	116.74
14H-1	117.80	8.44	126.24
15H-1	127.30	8.44	135.74
16H-1	136.80	8.44	145.24
17X-1	145.10	8.44	153.54
18X-1	151.10	8.44	159.54
19X-1	160.70	8.44	169.14
20X-1	170.40	8.44	178.84
21X-1	179.90	8.44	188.34
22X-1	189.50	8.44	197.94
23X-1	199.20	8.44	207.64
172-1062F-			
1H-1	0.00	0.00	0.00
2H-1	7.10	1.24	8.34
3H-1	16.60	0.88	17.48
4H-1	26.10	1.94	28.04
5H-1	35.60	3.42	39.02
6H-1	45.10	3.90	49.00
7H-1	54.60	4.60	59.20
8H-1	64.10	4.92	69.02
9H-1	73.60	5.48	79.08
172-1062G-			
1H-1	0.00	2.52	2.52
172-1062H-			
1H-1	0.00	0.00	0.00
2H-1	6.50	1.06	7.56
3H-1	16.00	1.06	17.06
4H-1	25.50	1.06	26.56
5H-1	35.00	1.06	36.06
6H-1	44.50	1.06	45.56
7H-1	54.00	1.06	55.06

Table 25. Splice tie points for Sites 1060–1062.

Core, section, interval (cm)	Depth (mbsf)	Depth (mcd)		Core, section, interval (cm)	Depth (mbsf)	Depth (mcd)
Site 1060						
1060A-1H-5, 86.0	6.86	6.86	Tie	1060C-2H-2, 73.0	5.24	6.86
1060C-2H-5, 92.0	9.92	11.54	Tie	1060A-2H-1, 59.0	9.60	11.54
1060A-2H-6, 74.0	17.24	19.18	Tie	1060B-3H-1, 20.0	16.10	19.18
1060B-3H-6, 134.0	24.74	27.82	Tie	1060A-3H-4, 82.0	23.82	27.82
1060A-3H-6, 46.0	26.46	30.46	Tie	1060B-4H-1, 113.0	26.55	30.46
1060B-4H-6, 59.0	33.49	37.40	Tie	1060C-5H-1, 86.5	32.49	37.50
1060C-5H-7, 39.0	40.89	45.90	Tie	1060B-5H-4, 129.5	40.71	45.90
1060B-5H-7, 14.0	44.04	49.23	Tie	1060C-6H-1, 141.0	42.42	49.23
1060C-6H-6, 140.0	49.90	56.71	Tie	1060A-6H-1, 22.0	47.22	56.71
1060A-6H-7, 44.0	56.53	66.02	Tie	1060B-7H-3, 76.0	57.67	66.02
1060B-7H-7, 24.0	63.14	71.49	Tie	1060A-7H-4, 8.0	61.10	71.49
1060A-7H-7, 24.0	65.74	76.13	Tie	1060B-8H-2, 129.5	66.21	76.13
1060B-8H-7, 29.0	72.69	82.61	Tie	1060C-9H-2, 53.0	71.54	82.61
1060C-9H-7, 20.0	78.70	89.77	Tie	1060A-9H-2, 59.5	77.61	89.77
1060A-9H-6, 84.0	83.84	96.00	Tie	1060B-10H-2, 9.5	84.01	96.00
1060B-10H-7, 19.0	91.59	103.58	Tie	1060C-11H-2, 34.5	90.35	103.58
1060C-11H-6, 139.0	97.39	110.62	Tie	1060B-11H-4, 104.5	97.46	110.62
1060B-11H-6, 129.0	100.69	113.85	Tie	1060C-12H-1, 33.0	98.34	113.85
1060C-12H-6, 100.0	106.50	122.01	Tie	1060B-12H-5, 67.5	105.58	122.01
1060B-12H-7, 114.0	109.04	125.47	Tie	1060A-12H-4, 64.0	109.14	125.47
1060A-12H-6, 88.0	111.88	128.21	Tie	1060C-13H-2, 139.5	110.28	128.21
1060C-13H-6, 40.0	115.27	133.20	Tie	1060A-13H-1, 86.5	114.37	133.20
1060A-13H-6, 128.0	122.28	141.11	Tie	1060B-14H-1, 134.5	121.76	141.11
1060B-14H-6, 109.0	128.99	148.34	Tie	1060A-14H-4, 19.5	127.71	148.34
1060A-14H-7, 60.0	132.60	153.23	Tie	1060A-15H-1, 9.0	132.60	153.23
1060A-15H-7, 76.0	142.26	162.89	Tie	1060A-16H-1, 25.0	142.26	162.89
1060A-16H-7, 64.0	151.64	172.27	Tie	1060A-17H-1, 13.0	151.64	172.27
1060A-17H-6, 128.0	160.28	180.91	Append	1060A-18H-1, 0.0	161.00	181.63
1060A-18H-7, 24.0	169.94	190.57				
Site 1061						
1061C-1H-4, 26.0	4.76	4.78	Tie	1061D-2H-1, 46.0	1.66	4.78
1061D-2H-5, 76.0	7.96	11.08	Tie	1061C-2H-4, 38.0	10.68	11.08
1061C-2H-6, 16.0	13.46	13.86	Tie	1061A-1H-2, 96.0	2.46	13.86
1061A-1H-6, 8.0	7.58	18.98	Tie	1061C-3H-3, 60.0	18.90	18.98
1061C-3H-6, 24.0	23.04	23.12	Tie	1061A-2H-1, 51.5	10.03	23.12
1061A-2H-6, 96.0	17.96	31.05	Tie	1061D-4H-5, 28.0	26.48	31.05
1061D-4H-6, 68.0	28.38	32.95	Tie	1061C-4H-4, 116.0	30.46	32.95
1061C-4H-7, 56.0	34.36	36.85	Tie	1061D-5H-1, 68.0	30.38	36.85
1061D-5H-7, 36.0	39.06	45.53	Tie	1061A-4H-1, 57.0	29.08	45.53
1061A-4H-7, 44.0	37.94	54.39	Tie	1061C-6H-4, 81.0	49.12	54.39
1061C-6H-7, 12.0	52.92	58.19	Tie	1061A-5H-1, 117.0	39.18	58.19
1061A-5H-5, 132.0	45.32	64.33	Tie	1061C-7H-3, 44.0	56.74	64.33
1061C-7H-7, 12.0	62.42	70.01	Tie	1061D-8H-1, 97.0	59.18	70.01
1061D-8H-7, 28.0	67.48	78.31	Tie	1061C-8H-5, 88.0	69.68	78.31
1061C-8H-7, 4.0	71.84	80.47	Tie	1061A-7H-1, 141.0	58.42	80.47
1061A-7H-5, 128.0	64.28	86.33	Tie	1061C-9H-2, 77.0	74.58	86.33
1061C-9H-7, 16.0	81.46	93.21	Tie	1061D-10H-1, 124.0	78.44	93.21
1061D-10H-7, 16.0	86.36	101.13	Tie	1061A-9H-1, 8.0	76.08	101.13
1061A-9H-6, 24.0	83.74	108.79	Tie	1061C-11H-2, 57.0	93.38	108.79
1061C-11H-6, 28.0	99.08	114.49	Tie	1061D-12H-1, 112.0	97.32	114.49
1061D-12H-6, 72.0	104.42	121.59	Tie	1061C-12H-3, 120.0	105.00	121.59
1061C-12H-7, 32.0	110.12	126.71	Tie	1061A-11H-4, 92.0	100.42	126.71
1061A-11H-6, 68.0	103.18	129.47	Tie	1061C-13H-1, 80.0	111.10	129.47
1061C-13H-5, 64.0	116.87	135.24	Tie	1061A-12H-2, 144.0	107.44	135.24
1061A-12H-7, 4.0	113.54	141.34	Tie	1061C-14H-2, 44.0	121.74	141.34
1061C-14H-7, 24.0	129.04	148.64	Tie	1061D-15H-2, 121.0	127.42	148.64
1061D-15H-6, 68.0	132.60	153.82	Tie	1061C-15H-3, 61.0	132.92	153.82
1061C-15H-7, 84.0	139.14	160.04	Tie	1061D-16H-2, 132.0	137.02	160.04
1061D-16H-4, 76.0	139.46	162.48	Tie	1061C-16H-2, 80.0	141.10	162.48
1061C-16H-6, 140.0	147.70	169.08	Tie	1061D-17H-1, 8.0	143.78	169.08
1061D-17H-7, 28.0	152.88	178.18	Tie	1061C-17H-5, 80.0	154.90	178.18
1061C-17H-6, 112.0	156.72	180.00	Tie	1061D-18H-1, 68.0	153.88	180.00
1061D-18H-7, 56.0	162.76	188.88	Tie	1061A-17X-1, 75.5	152.77	188.88
1061A-17X-3, 124.0	156.24	192.35	Tie	1061D-19X-2, 57.0	164.78	192.35
1061D-19X-3, 128.0	166.98	194.55	Tie	1061D-20X-1, 96.0	166.66	194.55
1061D-20X-4, 32.0	170.52	198.41	Tie	1061A-18X-3, 97.0	160.89	198.41
1061A-18X-5, 32.0	163.23	200.75	Tie	1061D-21X-1, 64.0	171.34	200.75
1061D-21X-4, 44.0	175.64	205.05	Tie	1061D-22X-1, 121.0	176.42	205.05
1061D-22X-4, 136.0	181.06	209.69	Tie	1061A-19X-3, 41.0	170.42	209.69
1061A-19X-6, 60.0	175.10	214.37	Append	1061A-20X-1, 0.0	176.60	215.87
1061A-20X-5, 80.0	183.40	222.67	Append	1061A-21X-1, 0.0	186.20	225.47
1061A-21X-6, 120.0	193.95	233.22	Append	1061A-22X-1, 0.0	195.80	235.07
1061A-22X-5, 124.0	203.04	242.31	Append	1061A-23X-1, 0.0	204.31	243.58
1061A-23X-5, 136.0	211.67	250.94	Append	1061A-24X-1, 0.0	215.10	254.37
1061A-24X-5, 112.0	222.22	261.49	Append	1061A-25X-1, 0.0	224.80	264.07
1061A-25X-4, 144.0	230.74	270.01	Append	1061A26X-1, 0.0	234.50	273.77
1061A-26X-5, 52.0	241.02	280.29	Append	1061A-27X-1, 0.0	244.20	283.47
1061A-27X-5, 144.0	250.72	289.99	Append	1061A-28X-1, 0.0	253.16	292.43
1061A-28X-5, 124.0	260.15	299.42	Append	1061A-29X-1, 0.0	263.50	302.77
1061A-29X-5, 140.0	270.90	310.17	Append	1061A-30X-1, 0.0	273.20	312.47
1061A-30X-6, 104.0	281.21	320.48	Append	1061A-31X-1, 0.0	282.80	322.07
1061A-31X-4, 140.0	288.70	327.97	Append	1061A-32X-1, 0.0	292.40	331.67
1061A-32X-CC, 8.0	292.48	331.75	Append	1061A-33X-1, 0.0	302.00	341.27
1061A-33X-CC, 24.0	308.24	347.51	Append	1061A-34X-1, 0.0	311.70	350.97
1061A-34X-CC, 28.0	315.47	354.74	Append	1061A-35X-1, 0.0	321.30	360.57
1061A-35X-CC, 24.0	326.43	365.70	Append	1061A-36X-1, 0.0	330.90	370.17
1061A-36X-CC, 35.0	338.68	377.95	Append	1061A-37X-1, 0.0	340.50	379.77
1061A-37X-CC, 36.0	346.33	385.60				

Table 25 (continued).

Core, section, interval (cm)	Depth (mbsf)	Depth (mcd)		Core, section, interval (cm)	Depth (mbsf)	Depth (mcd)
Site 1062 east wave flank						
1062B-1H-3, 34.0	3.34	3.34	Tie	1062C-1H-2, 148.0	2.98	3.34
1062C-1H-5, 146.0	7.46	7.82	Tie	1062B-2H-2, 1.0	6.52	7.82
1062B-2H-7, 28.0	14.28	15.58	Tie	1062A-3H-1, 96.0	12.66	15.58
1062A-3H-5, 112.0	18.82	21.74	Tie	1062C-3H-2, 10.0	20.50	21.74
1062C-3H-6, 38.0	26.78	28.02	Tie	1062A-4H-2, 88.0	23.58	28.02
1062A-4H-6, 136.0	30.06	34.50	Tie	1062C-4H-3, 102.0	32.42	34.50
1062C-4H-7, 32.0	37.72	39.80	Tie	1062D-5H-3, 102.0	38.32	39.80
1062D-5H-7, 22.0	43.22	44.70	Tie	1062C-5H-3, 22.0	41.12	44.70
1062C-5H-7, 44.0	47.14	50.72	Tie	1062B-6H-3, 38.0	46.38	50.72
1062B-6H-6, 56.0	51.06	55.40	Tie	1062C-6H-3, 124.0	51.64	55.40
1062C-6H-5, 146.0	54.86	58.62	Tie	1062D-7H-1, 116.0	54.46	58.62
1062D-7H-6, 138.0	62.18	66.34	Tie	1062C-7H-4, 118.0	62.58	66.34
1062C-7H-6, 4.0	64.44	68.20	Tie	1062B-8H-1, 21.0	62.21	68.20
1062B-8H-4, 35.0	66.85	72.48	Tie	1062C-8H-1, 106.5	67.47	72.48
1062C-8H-4, 8.0	70.88	75.89	Tie	1062A-9H-1, 18.5	68.89	75.89
1062A-9H-3, 128.0	72.98	79.98	Tie	1062C-9H-1, 9.0	76.00	79.98
1062C-9H-6, 136.0	84.76	88.74	Tie	1062B-10H-2, 17.0	82.68	88.74
1062B-10H-4, 52.0	86.02	92.08	Tie	1062C-10H-2, 68.0	87.55	92.08
1062C-10H-6, 132.0	94.19	98.72	Tie	1062A-11H-3, 57.0	91.28	98.72
1062A-11H-6, 140.0	96.60	104.04	Tie	1062C-11H-3, 137.0	99.28	104.04
1062C-11H-6, 28.0	102.68	107.44	Tie	1062B-12H-1, 60.0	100.60	107.44
1062B-12H-7, 88.0	108.66	115.50	Tie	1062A-13H-1, 104.0	107.74	115.50
1062A-13H-6, 88.0	115.08	122.84	Tie	1062C-13H-2, 120.0	116.60	122.84
1062C-13H-6, 56.0	121.96	128.20	Tie	1062B-14H-2, 56.0	121.06	128.20
1062B-14H-7, 40.0	126.94	134.08	Tie	1062C-14H-4, 20.0	128.10	134.08
1062C-14H-6, 52.0	131.42	137.40	Tie	1062B-15H-1, 144.0	129.94	137.40
1062B-15H-6, 88.0	136.88	144.34	Tie	1062A-16H-1, 12.0	135.32	144.34
1062A-16H-6, 24.0	142.54	151.56	Tie	1062B-16H-4, 8.0	142.58	151.56
1062B-16H-7, 4.0	147.04	156.02	Tie	1062A-17H-1, 137.0	146.08	156.02
1062A-17H-7, 48.0	153.88	163.82	Append	1062B-18X-1, 0.0	156.70	165.66
1062B-18X-3, 136.0	161.06	170.02	Append	1062B-19X-1, 0.0	162.10	171.06
1062B-19X-7, 52.0	171.62	180.58	Append	1062B-20X-1, 0.0	171.70	180.66
1062B-20X-7, 24.0	180.94	189.90	Append	1062B-21X-1, 0.0	181.30	190.26
1062B-21X-7, 60.0	190.78	199.74	Append	1062B-22X-1, 0.0	190.90	199.86
1062B-22X-7, 16.0	200.06	209.02	Append	1062B-23X-1, 0.0	200.50	209.46
1062B-23X-7, 52.0	210.02	218.98	Append	1062B-24X-1, 0.0	210.20	219.16
1062B-24X-6, 132.0	219.02	227.98	Append	1062B-25X-1, 0.0	219.80	228.76
1062B-25X-6, 144.0	228.74	237.70	Append	1062B-26X-1, 0.0	229.40	238.36
1062B-26X-7, 28.0	238.68	247.64				
Site 1062 west wave flank						
1062F-1H-5, 12.0	6.12	6.12	tie	1062E-2H-1, 106.0	4.86	6.12
1062E-2H-5, 120.0	11.00	12.26	tie	1062F-2H-3, 92.0	11.02	12.26
1062F-2H-5, 104.0	14.14	15.38	tie	1062E-3H-1, 69.0	14.00	15.38
1062E-3H-6, 36.0	21.16	22.54	tie	1062F-3H-4, 56.0	21.66	22.54
1062F-3H-7, 4.0	25.64	26.52	tie	1062E-4H-1, 116.0	23.96	26.52
1062E-4H-5, 128.0	30.08	32.64	tie	1062F-4H-4, 9.0	30.70	32.64
1062F-4H-7, 8.0	35.18	37.12	tie	1062E-5H-1, 117.0	33.48	37.12
1062E-5H-7, 4.0	41.34	44.98	tie	1062F-5H-4, 146.0	41.56	44.98
1062F-5H-6, 16.0	43.26	46.68	tie	1062E-6H-1, 76.0	42.56	46.68
1062E-6H-5, 44.0	48.24	52.36	tie	1062F-6H-3, 36.0	48.46	52.36
1062F-6H-6, 144.0	54.04	57.94	tie	1062E-7H-2, 16.0	52.96	57.94
1062E-7H-6, 8.0	58.88	63.86	tie	1062F-7H-4, 16.0	59.26	63.86
1062F-7H-6, 92.0	63.02	67.62	tie	1062E-8H-1, 36.0	61.16	67.62
1062E-8H-5, 116.0	67.96	74.42	tie	1062F-8H-4, 89.0	69.50	74.42
1062F-8H-6, 124.0	72.84	77.76	tie	1062E-9H-1, 80.0	71.10	77.76
1062E-9H-3, 40.0	73.70	80.36	tie	1062F-9H-1, 128.0	74.88	80.36
1062F-9H-7, 44.0	83.04	88.52	append	1062E-10H-1, 0.0	79.80	88.66
1062E-10H-7, 36.0	89.16	98.02	tie	1062E-11H-1, 28.0	89.58	98.02
1062E-11H-8, 84.0	99.20	107.64	tie	1062E-12H-1, 40.0	99.20	107.64
1062E-12H-7, 100.0	108.55	116.99	tie	1062E-13H-1, 23.5	108.55	116.99
1062E-13H-8, 36.0	117.78	126.22	append	1062E-14H-1, 0.0	117.80	126.24
1062E-14H-7, 104.0	126.85	135.29	append	1062E-15H-1, 0.0	127.30	135.74
1062E-15H-8, 40.0	137.29	145.73	tie	1062E-16H-1, 47.5	137.29	145.73
1062E-16H-6, 132.0	144.93	153.37	append	1062E-17X-1, 0.0	145.10	153.54
1062E-17X-4, 84.0	150.44	158.88	append	1062E-18X-1, 0.0	151.10	159.54
1062E-18X-6, 76.0	159.36	167.80	append	1062E-19X-1, 0.0	160.70	169.14
1062E-19X-4, 64.0	165.84	174.28	append	1062E-20X-1, 0.0	170.40	178.84
1062E-20X-5, 96.0	177.36	185.80	append	1062E-21X-1, 0.0	179.90	188.34
1062E-21X-6, 76.0	188.16	196.60	append	1062E-22X-1, 0.0	189.50	197.94
1062E-22X-7, 144.0	199.03	207.47	append	1062E-23X-1, 0.0	199.20	207.64
1062E-23X-7, 44.0	208.64	217.08				
Site 1062 wave crest						
1062H-1H-3, 144.0	4.44	4.44	Tie	1062G-1H-2, 42.0	1.92	4.44
1062G-1H-6, 114.0	8.64	11.16	Tie	1062H-2H-3, 60.0	10.10	11.16
1062H-2H-CC, 10.0	16.08	17.14	Append	1062H-3H-1, 0.0	16.00	17.06
1062H-3H-7, 56.0	25.56	26.62	Tie	1062H-4H-1, 6.0	25.56	26.62
1062H-4H-7, 58.0	35.08	36.14	Tie	1062H-5H-1, 7.0	35.08	36.14
1062H-5H-7, 62.0	44.62	45.68	Tie	1062H-6H-1, 12.0	44.62	45.68
1062H-6H-7, 42.0	53.92	54.98	Append	1062H-7H-1, 0.0	54.00	55.06
1062H-7H-7, 32.0	63.32	64.38				

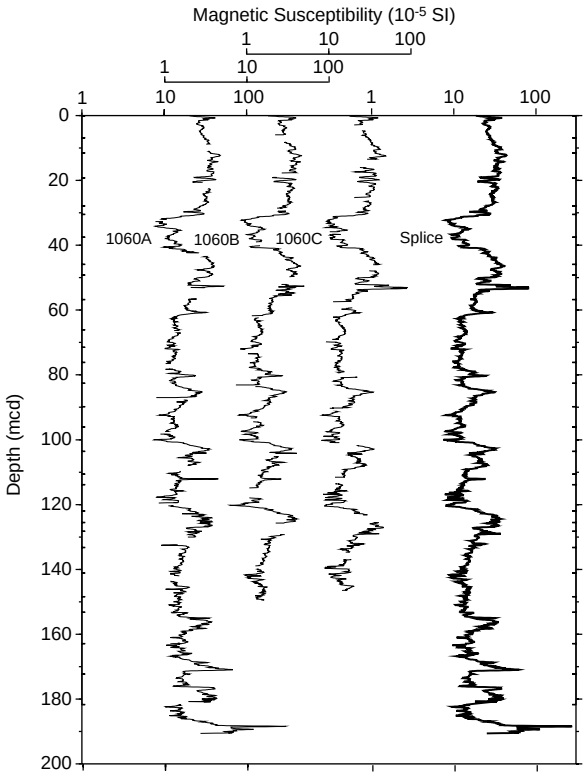

Figure 24. Smoothed magnetic susceptibility data (31-cm Gaussian window; logarithmic scale) from Site 1060 on the mcd scale for Holes 1060A through 1060C and the spliced record.

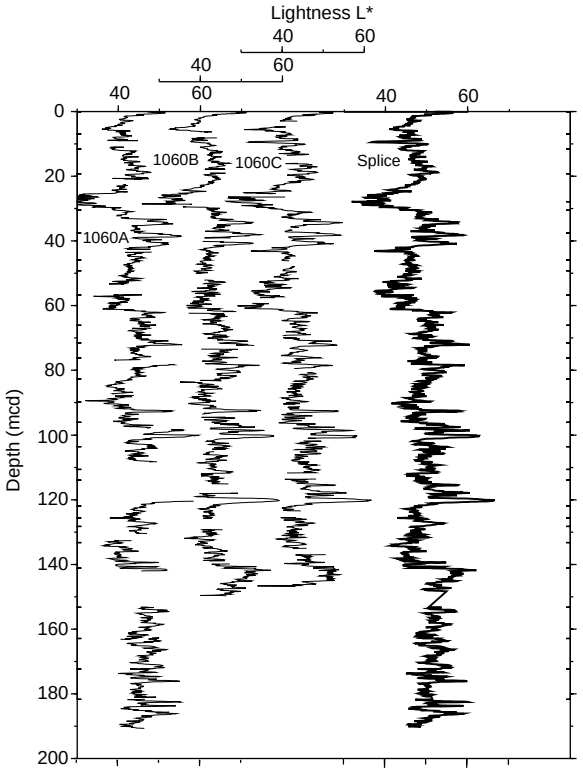

Figure 26. Smoothed lightness (L*) data (31-cm Gaussian window) from Site 1060 on the mcd scale for Holes 1060A through 1060C and the spliced record.

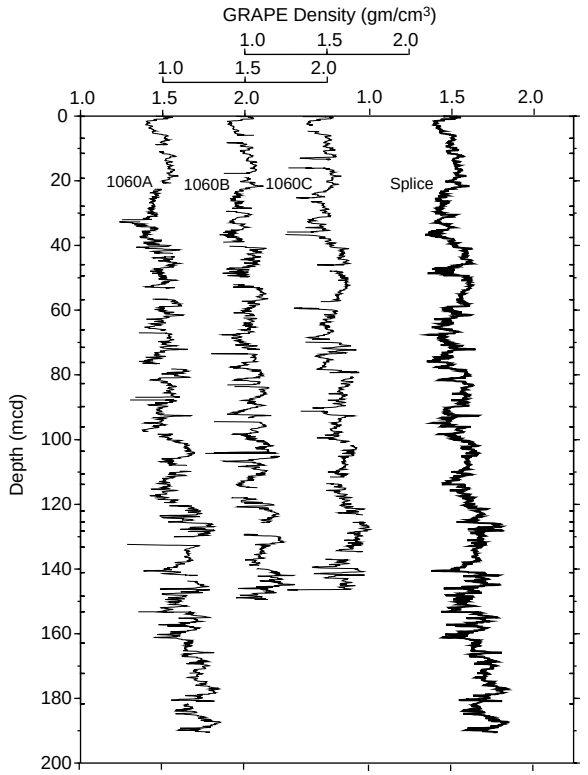

Figure 25. Smoothed GRAPE data (31-cm Gaussian window) from Site 1060 on the mcd scale for Holes 1060A through 1060C and the spliced record.

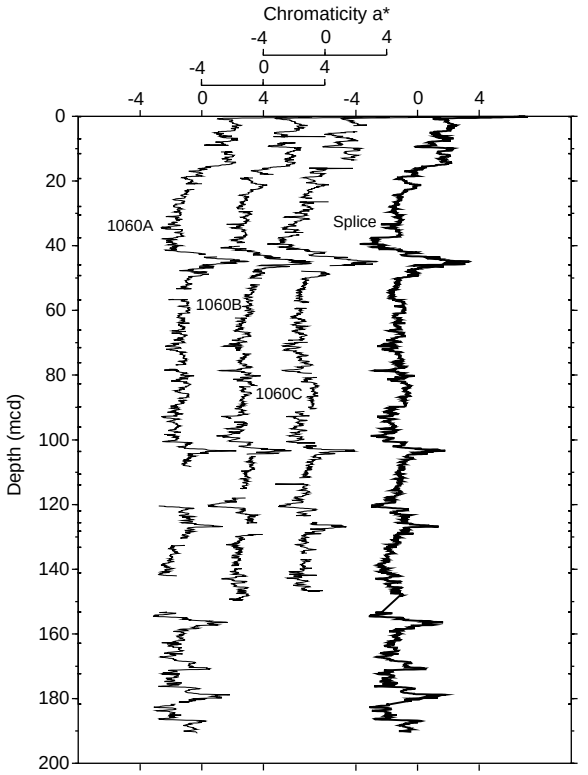

Figure 27. Smoothed chromaticity (a*) data (31-cm Gaussian window) from Site 1060 on the mcd scale for Holes 1060A through 1060C and the spliced record.

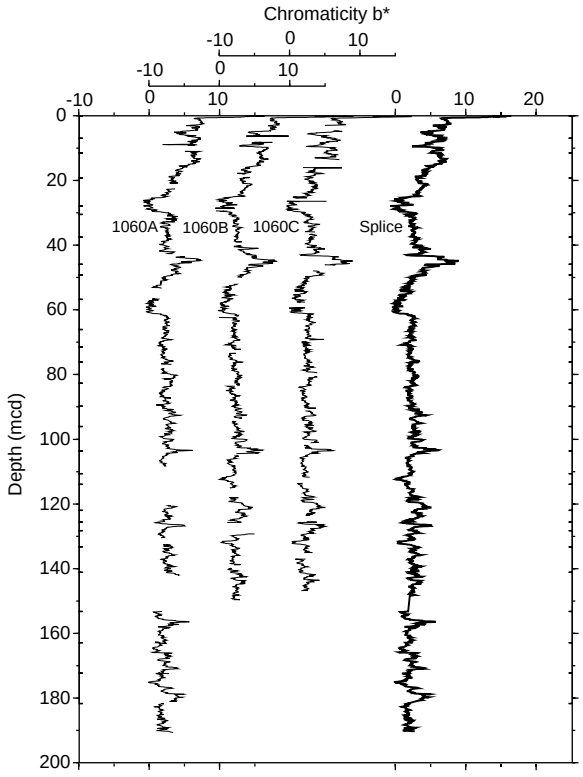

Figure 28. Smoothed magnetic chromaticity (b*) data (31-cm Gaussian window) from Site 1060 on the mcd scale for Holes 1060A through 1060C and the spliced record.

This offset is probably caused by mud being smeared on the reflectometer window. The composite section is based on four APC holes to ~86 mcd, three APC holes to ~130 mcd, and two APC holes to ~165 mcd. There are overlapping XCB cores to ~192 mcd, but not enough distinctive features were identified to allow detailed correlation. As a result of core expansion, the composite depth scale (mcd) is on average 5% longer than the drilled depths (mbsf) at this site, starting ~10% larger to ~50 to 60 mbsf, and then decreasing to ~2% until ~150 mbsf (Fig. 57). Deeper than ~150 mbsf, the offset between mcd and mbsf remains constant at ~10 m. The splice record at this site is formed primarily from Holes 1062A, 1062B, and 1062C.

West Wave Flank Composite Record and Splice

A continuous composite section could be constructed from Holes 1062E and 1062F to a depth of ~79 mcd (~74 mbsf) on the western wave flank, the maximum depth of Hole 1062F. For some cores deeper than ~79 mcd, the reported mbsf depth ranges overlap between adjacent cores; thus, the splice record shows overlap. However, the overlap is not sufficient to document a continuous sequence. As a result of core expansion, the composite depth scale (mcd) is 10% longer than the drilled depths (mbsf) at this site until ~80 mbsf, then the offset remains constant at ~8 m (Fig. 58). The spliced record at this site is formed from Holes 1062E and 1062F above ~79 mcd, and then only from Hole 1062E.

Wave Crest Composite Record and Splice

A continuous composite section could be constructed from Holes 1062G and 1062H only to a depth of ~17 mcd (~16 mbsf). The only core from Hole 1062G did not recover a mudline, so Hole 1062H was initiated. The two holes at this site provide enough overlap to link the upper cores. The drilling plan called for only a single hole at this site, so the limited overlap is an unexpected bonus. As a result of core expansion, the composite depth scale (mcd) is 15% longer than the drilled depths (mbsf) at this site until ~16 mbsf, below which the offset remains constant at ~1 m (Fig. 59). The spliced record at this site is formed from Holes 1062G and 1062H above ~17 mcd, and only from Hole 1062H below.

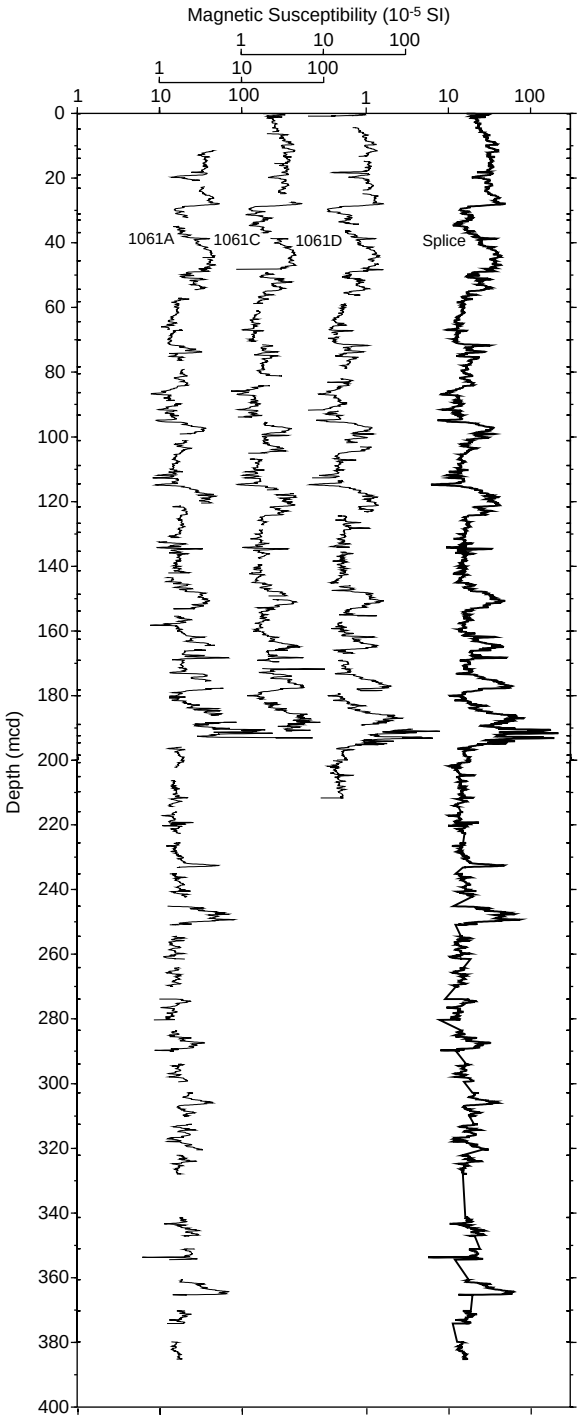

Figure 29. Smoothed magnetic susceptibility data (31-cm Gaussian window, logarithmic scale) from Site 1061 on the mcd scale for Holes 1061A, 1061C, and 1061D and the spliced record.

Correlations Among East Flank, Crest, and West Flank Holes

The depth-averaged spliced records from the east wave flank, wave crest, and west wave flank show remarkable similarity to one

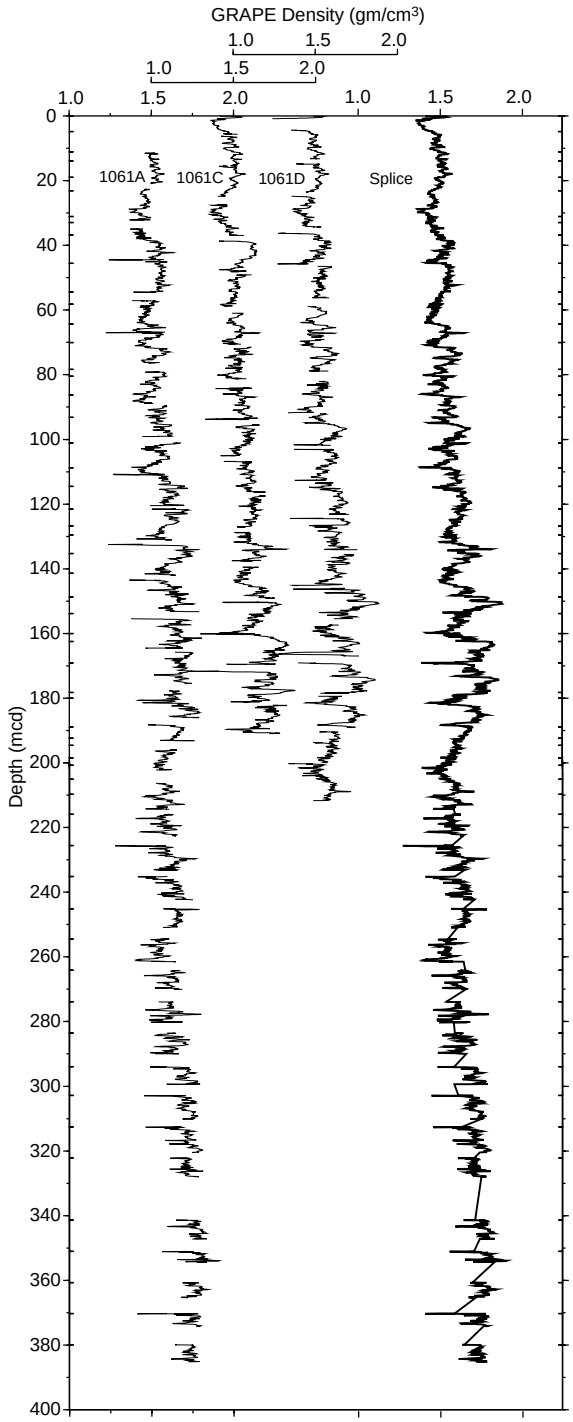

Figure 30. Smoothed GRAPE data (31-cm Gaussian window) from Site 1061 on the mcd scale for Holes 1061A, 1061C, and 1061D and the spliced record.

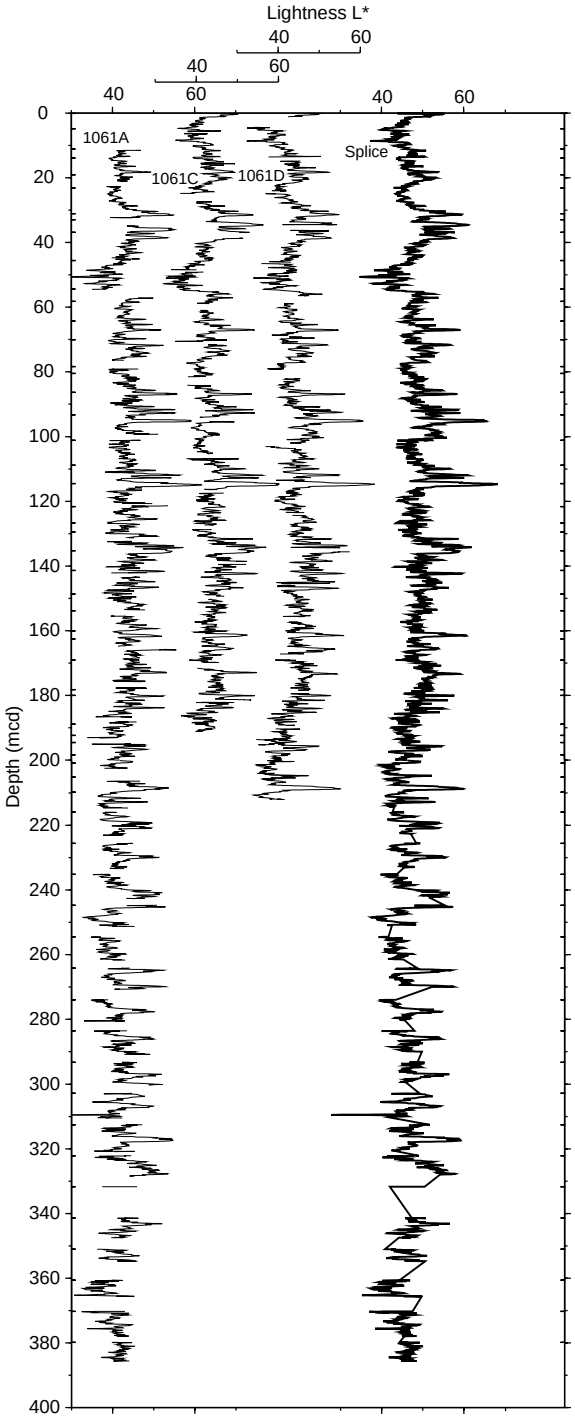

Figure 31. Smoothed lightness (L*) data (31-cm Gaussian window) from Site 1061 on the mcd scale for Holes 1061A, 1061C, and 1061D and the spliced record.

another because individual peaks can in general be correlated across the wave. Overall, the record of the east wave flank is expanded by ~10% with respect to the record of the west wave flank in the upper 60 mcd, with the wave crest record having a thickness intermediate between the eastern and western flanks (especially to ~17 mcd, the limit of two-hole penetration on the crest). The larger sediment thickness on the eastern wave flank is consistent with the mud-wave migration observed on seismic records. In addition to cross-wave differences in the depths to identifiable horizons, there also appear to be cross-wave changes in the thickness of individual sediment layers. For example, correlated peaks in magnetic susceptibility ~16 mcd on the eastern flank and ~14 mcd on the western flank appear to be of different thicknesses, with the east flank peak wider than the west flank peak, suggesting that the wave was more active at this time (Fig. 54). Preliminary cross-wave correlations have not yet been attempted deeper at this site, but initial studies suggest that at least some of the carbonate turbidites present at Site 1062 can be correlated from one wave flank to the other, providing additional corre-

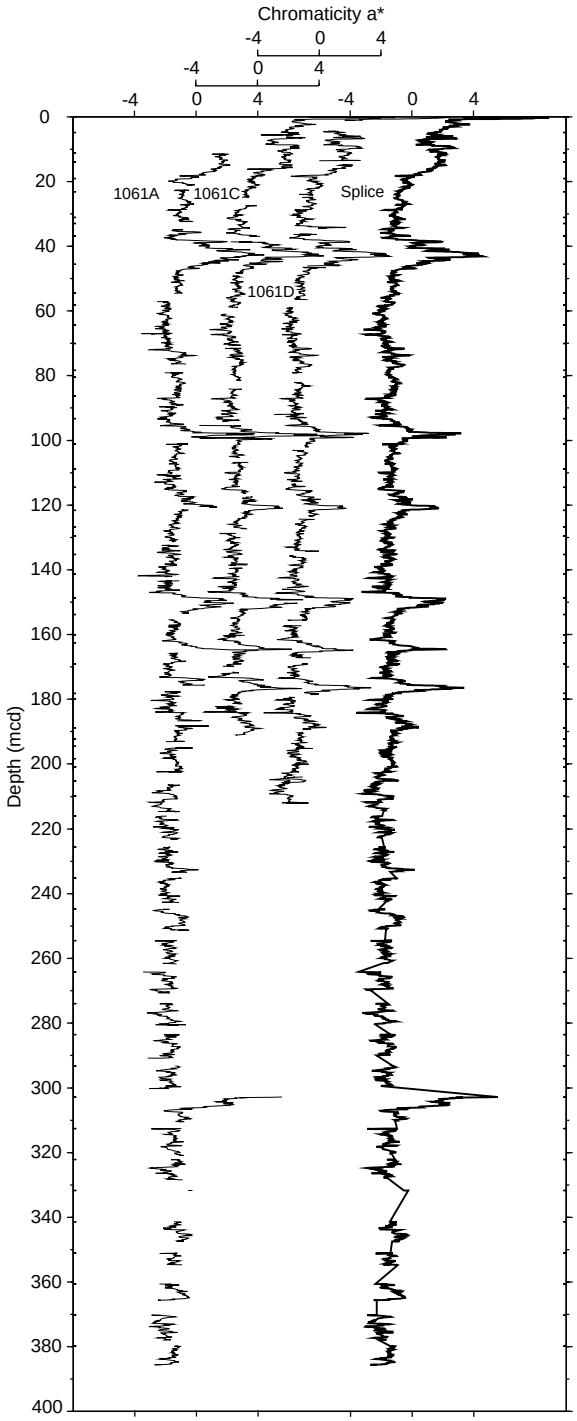

Figure 32. Smoothed chromaticity (a*) data (31-cm Gaussian window) from Site 1061 on the mcd scale for Holes 1061A, 1061C, and 1061D and the spliced record.

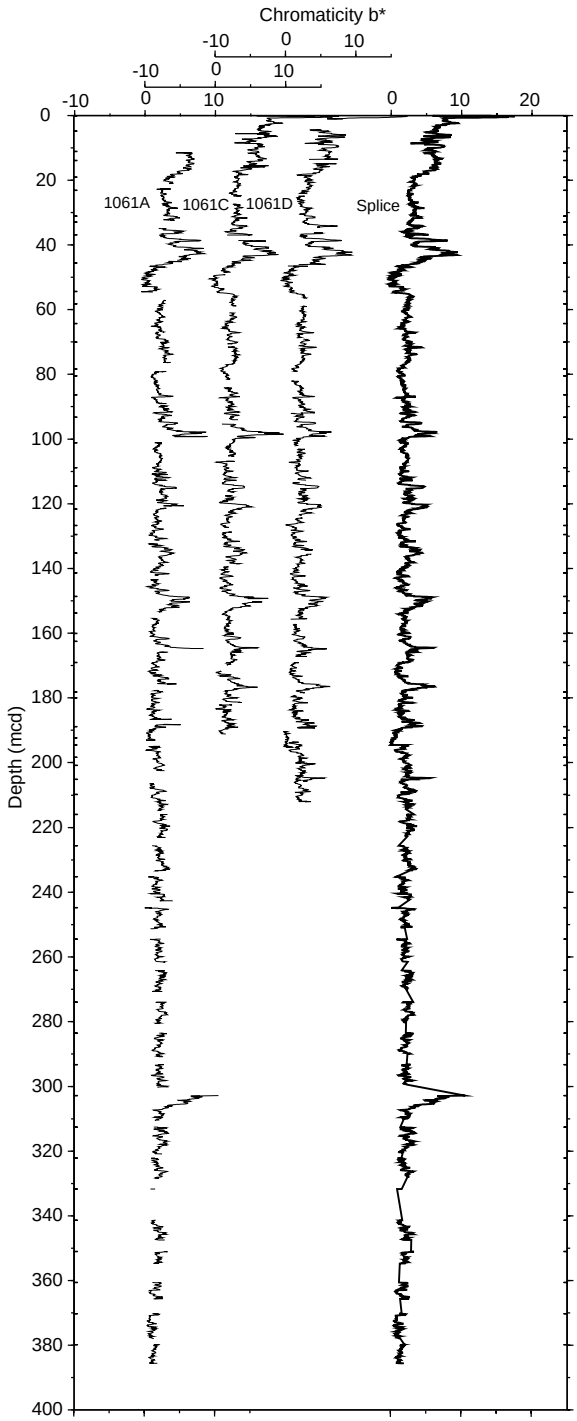

Figure 33. Smoothed magnetic chromaticity (b*) data (31-cm Gaussian window) from Site 1061 on the mcd scale for Holes 1061A, 1061C, and 1061D and the spliced record.

lation horizons (see "Lithostratigraphy" section, this chapter). More extensive shore-based cross-wave correlation will be necessary to understand the detailed sedimentation patterns shown here.

Correlations Among Sites 1060 Through 1062

Spliced records for all sites are plotted on the back-pocket foldout (Fig. 26, "Carolina Slope" chapter, in the back pocket of this volume). High-quality continuous records were recovered for the upper 150 to 200 m at each of these sites, and the records can be correlated to one another providing material suitable for high-resolution climatic and sedimentological studies. There is a high degree of similarity between the sediment records at Sites 1060 and 1061 based on comparison of the spliced records. The color (lightness and chromaticity) variables are more closely correlated between Sites 1060 and 1061 than are the magnetic susceptibility records, perhaps because of

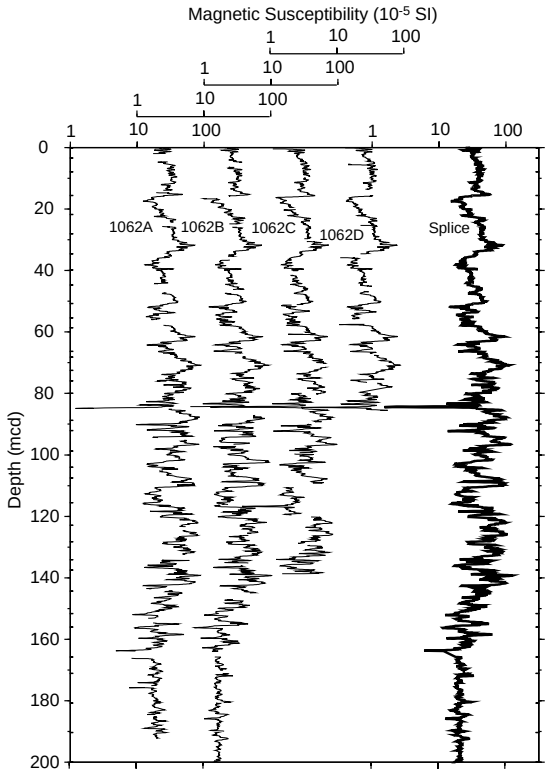

Figure 34. Smoothed magnetic susceptibility data (31-cm Gaussian window, logarithmic scale) from Site 1062 (east wave flank splice) on the mcd scale for Holes 1062A through 1062D and the spliced record.

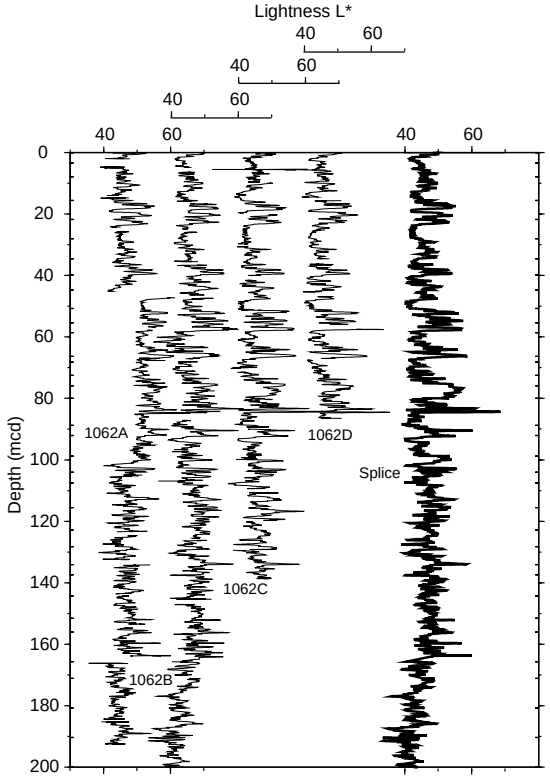

Figure 36. Smoothed lightness (L*) data (31-cm Gaussian window) from Site 1062 (east wave flank splice) on the mcd scale for Holes 1062A through 1062D and the spliced record.

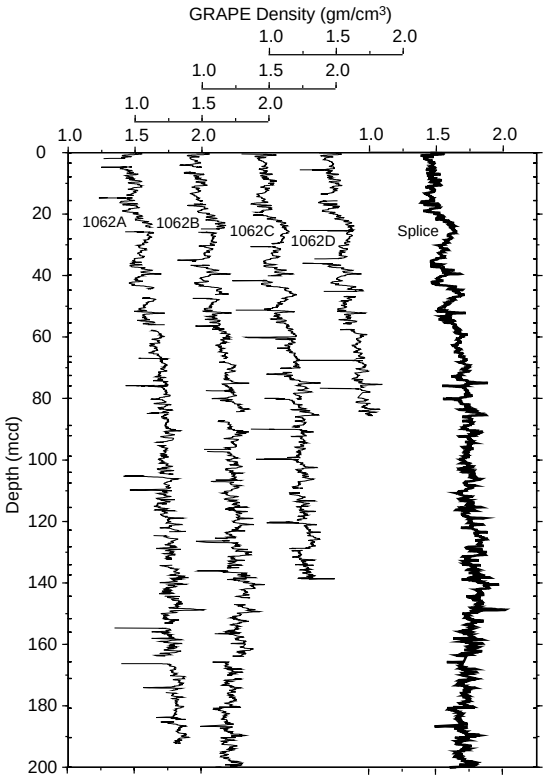

Figure 35. Smoothed GRAPE data (31-cm Gaussian window) from Site 1062 (east wave flank splice) on the mcd scale for Holes 1062A through 1062D and the spliced record.

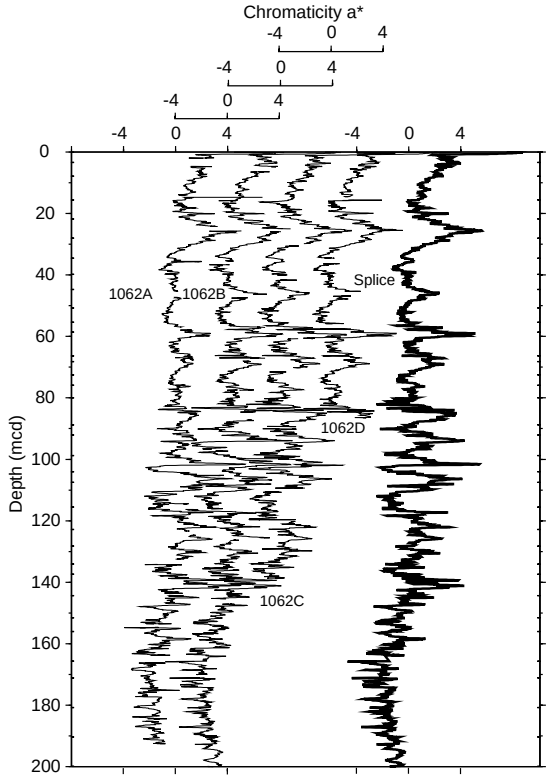

Figure 37. Smoothed chromaticity (a*) data (31-cm Gaussian window) from Site 1062 (east wave flank splice) on the mcd scale for Holes 1062A through 1062D and the spliced record.

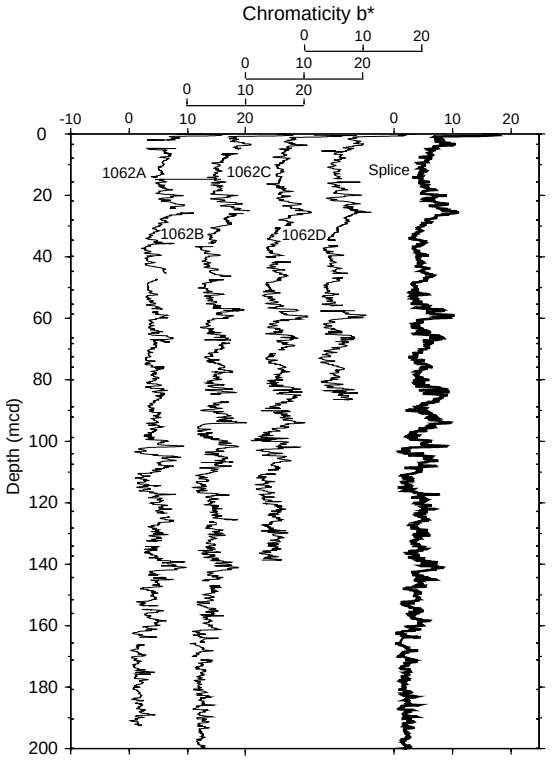

Figure 38. Smoothed magnetic chromaticity (b*) data (31-cm Gaussian window) from Site 1062 (east wave flank splice) on the mcd scale for Holes 1062A through 1062D and the spliced record.

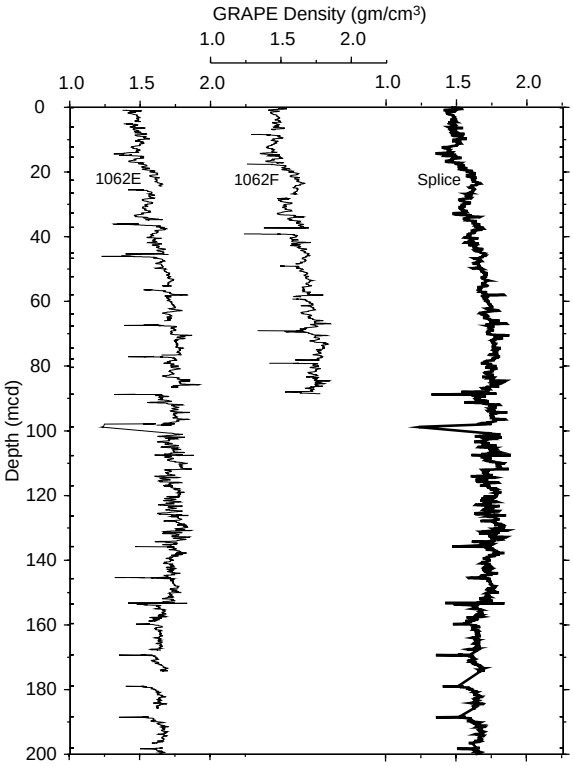

Figure 40. Smoothed GRAPE data (31-cm Gaussian window) from Site 1062 (west wave flank splice) on the mcd scale for Holes 1062E and 1062F and the spliced record.

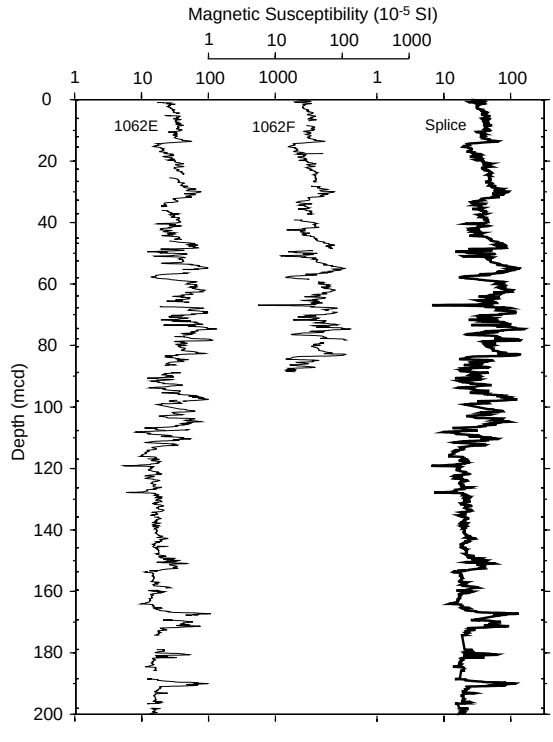

Figure 39. Smoothed magnetic susceptibility data (31-cm Gaussian window, logarithmic scale) from Site 1062 (west wave flank splice) on the mcd scale for Holes 1062E and 1062F and the spliced record.

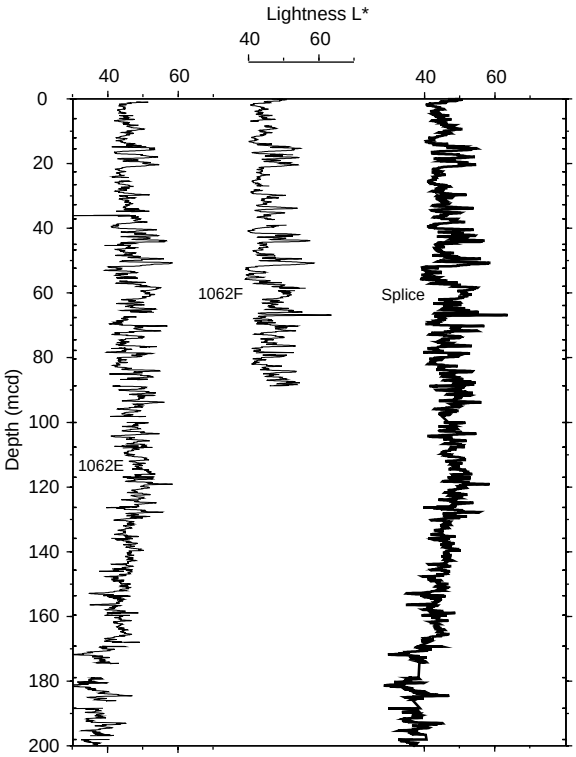

Figure 41. Smoothed lightness (L*) data (31-cm Gaussian window) from Site 1062 (west wave flank splice) on the mcd scale for Holes 1062E and 1062F and the spliced record.

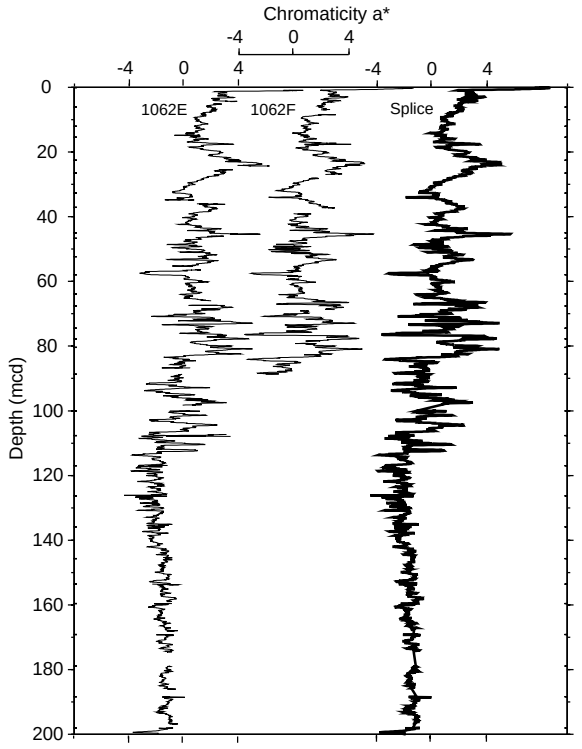

Figure 42. Smoothed chromaticity (a*) data (31-cm Gaussian window) from Site 1062 (west wave flank splice) on the mcd scale for Holes 1062E and 1062F and the spliced record.

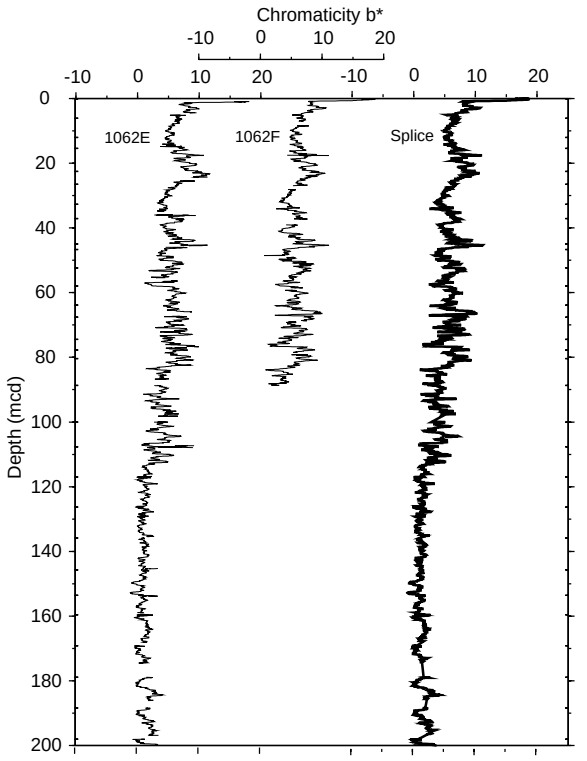

Figure 43. Smoothed magnetic chromaticity (b*) data (31-cm Gaussian window) from Site 1062 (west wave flank splice) on the mcd scale for Holes 1062E and 1062F and the spliced record.

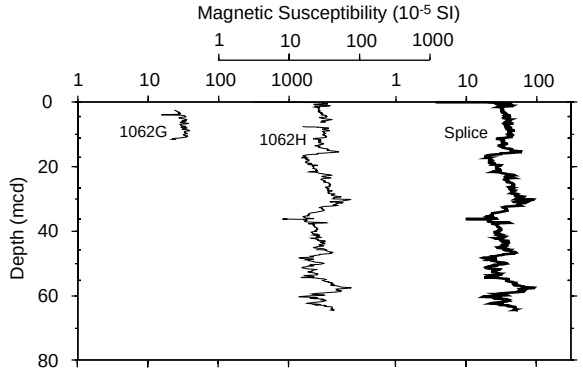

Figure 44. Smoothed magnetic susceptibility data (31-cm Gaussian window, logarithmic scale) from Site 1062 (wave crest splice) on the mcd scale for Holes 1062G and 1062H and the spliced record.

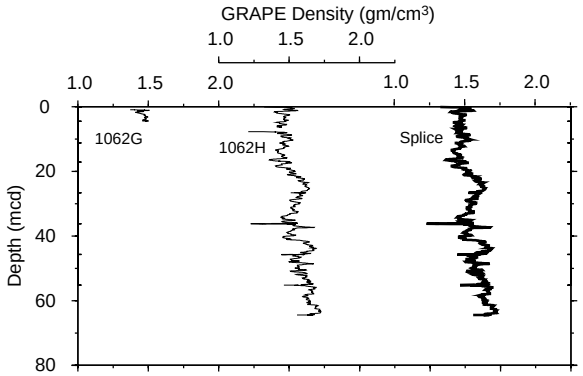

Figure 45. Smoothed GRAPE data (31-cm Gaussian window) from Site 1062 (wave crest splice) on the mcd scale for Holes 1062G and 1062H and the spliced record.

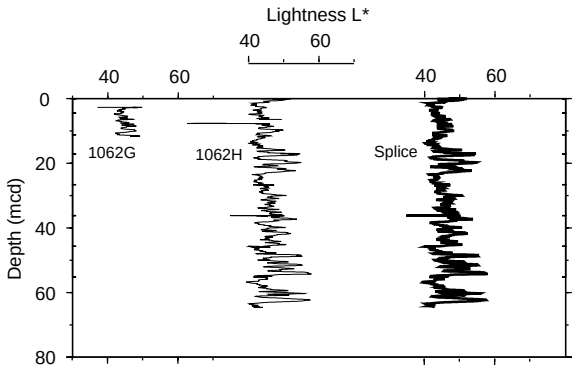

Figure 46. Smoothed lightness (L*) data (31-cm Gaussian window) from Site 1062 (wave crest splice) on the mcd scale for Holes 1062G and 1062H and the spliced record.

the diagenetic formation of magnetic minerals at depth. Indeed, many layers with high L* values (presumably carbonate layers) can be correlated between these two sites, as well as with Sites 1056 through 1059. Color variable correlations yield an overall higher sedimentation rate and longer intervals of black sediment (FeS staining) at Site 1060 than at Site 1061. Site 1062 has broad magnetic susceptibility and lightness patterns that are similar to those at Sites 1060 and 1061, but significant differences are also noted. Overall, sedimentation rate

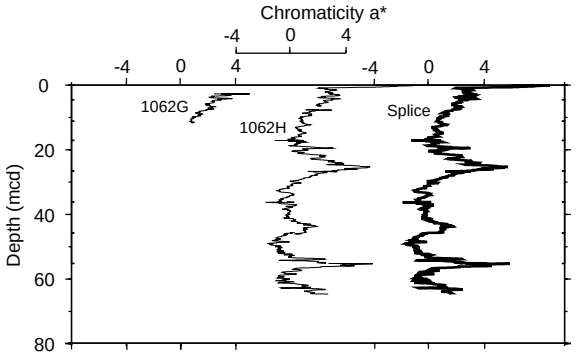

Figure 47. Smoothed chromaticity (a*) data (31-cm Gaussian window) from Site 1062 (wave crest splice) on the mcd scale for Holes 1062G and 1062H and the spliced record.

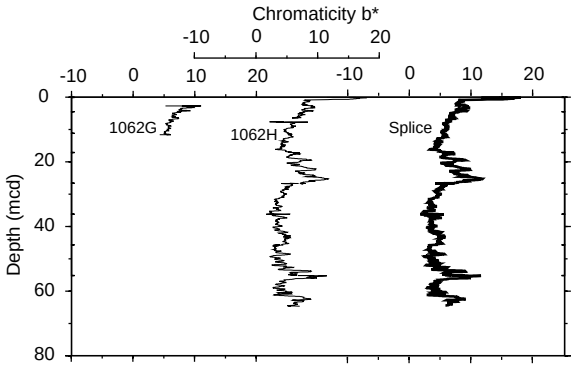

Figure 48. Smoothed magnetic chromaticity (b*) data (31-cm Gaussian window) from Site 1062 (wave crest splice) on the mcd scale for Holes 1062G and 1062H and the spliced record.

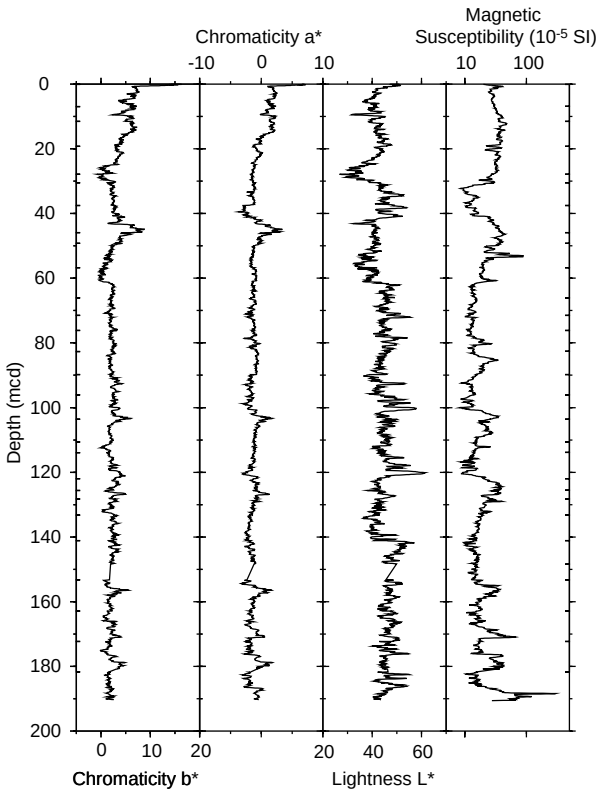

Figure 49. Summary of spliced records for Site 1060.

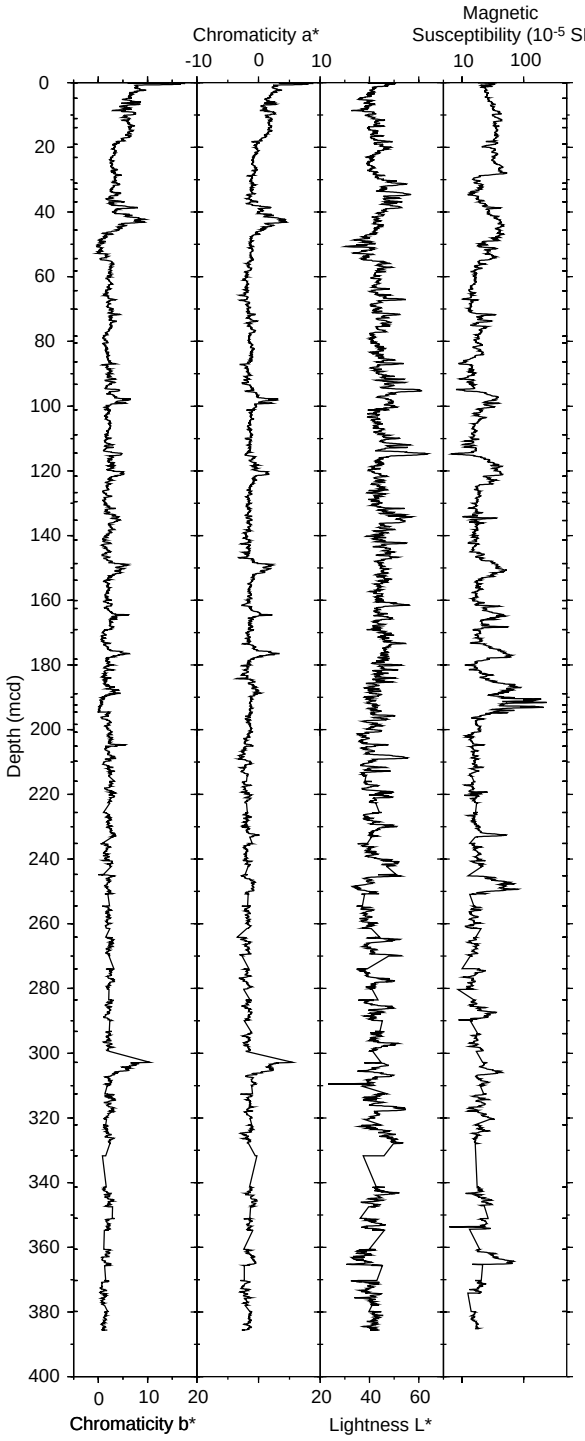

Figure 50. Summary of spliced records for Site 1061.

at Site 1062 is approximately half that observed at Sites 1060 and 1061. Lightness records suggest that for the upper ~50 mcd at Site 1062, the number and thickness of carbonate layers is somewhat similar to those at Sites 1060 and 1061, but that the darker (lower carbonate) intervals are thinner at Site 1062 than at the other sites. This suggests that depth-related changes in accumulation rate are larger during glacial intervals than during interglacial intervals. There may also be some difference in the structure of the magnetic susceptibility record between sites. At Sites 1060 and 1061 (and at shallower sites), magnetic susceptibility maxima tend to be characterized by a gener-

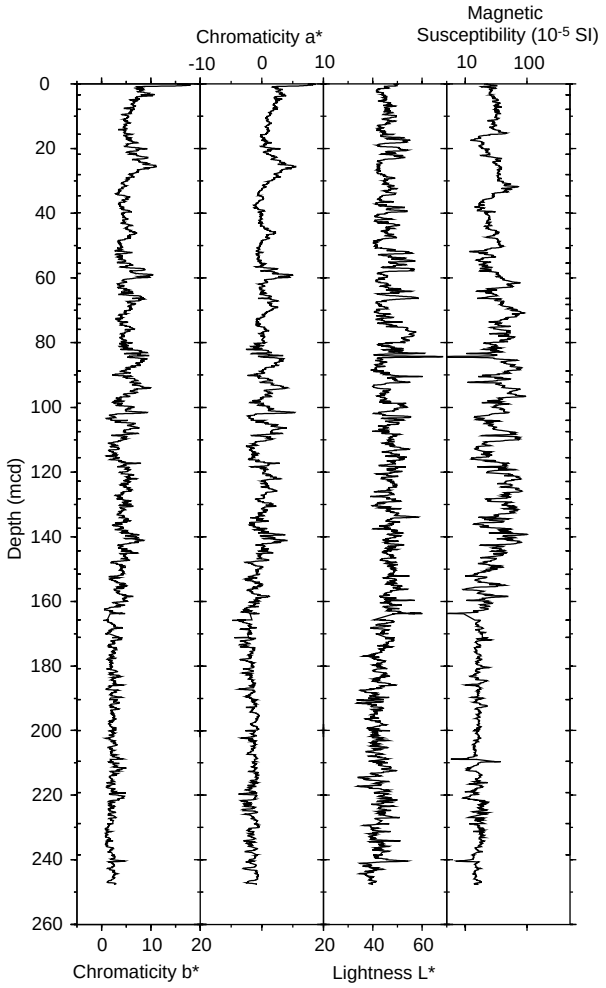

Figure 51. Summary of spliced records for Site 1062, east wave flank.

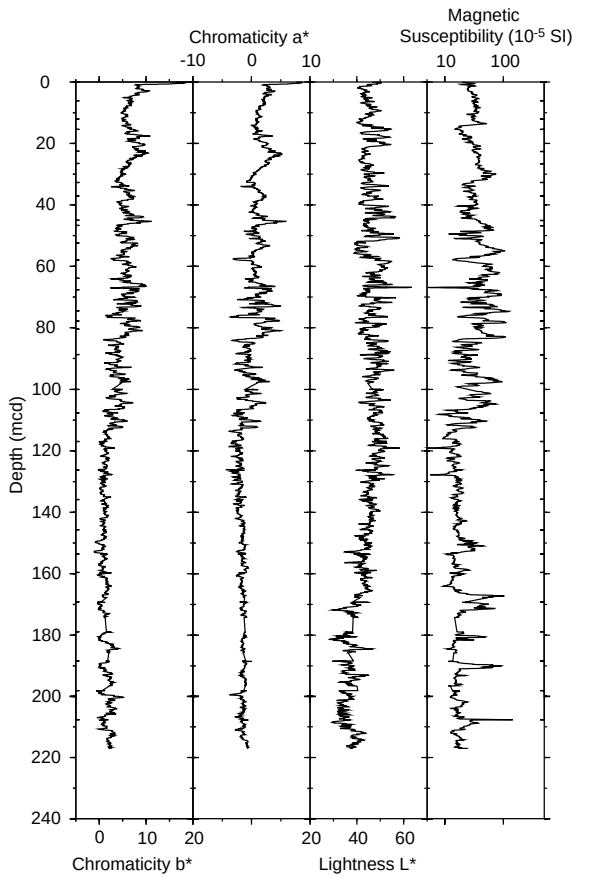

Figure 52. Summary of spliced records for Site 1062, west wave flank.

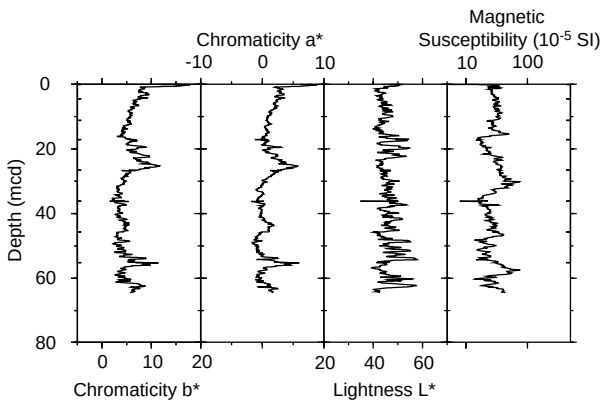

Figure 53. Summary of spliced records for Site 1062, wave crest flank.

ally steeper gradient upcore and a less steep gradient downcore, giving the impression of a saw-tooth record pointing upcore. At Site 1062, however, correlated magnetic susceptibility peaks have a different structure, with steeper downcore gradients than upcore gradients, giving the impression of a saw-toothed record pointing downcore. The different structure may be an indication of systematic changes in bottom-water circulation and/or sediment input with water depth and time.

Detailed correlation between Sites 1060/1061 and 1062 is further complicated by the presence of carbonate turbidites in lithologic Unit II at Site 1062. These carbonate layers have high lightness (L*), low a* and b* values, and low magnetic susceptibility, but they also have high density. The turbidites appear to occur preferentially during interglacial times, characterized by lower magnetic susceptibility.

SEDIMENTATION AND MASS ACCUMULATION RATES

Site 1060

An average sedimentation rate of 23.8 cm/k.y. is calculated for Hole 1060A between the extinction of *P. lacunosa* (0.46 Ma) and the top of the section (Fig. 60). The bottom part of the cored interval at Site 1060 does not reach 1 Ma. On average, sedimentation rates to the Brunhes/Matuyama boundary are 15 cm/k.y.

Within these average intervals, there is likely to be considerable variability. Using the magnetic susceptibility record to calculate sedimentation rates for shorter time intervals (see "Explanatory Notes" chapter, this volume), very high sedimentation rates (30–50 cm/k.y.) are calculated for MISs 9, 7, and 2–4 (Fig. 61; Tables 26, 27). Rates decrease downhole to between 7 and 18 cm/k.y. at 420 ka, and remain within this range in the lower part of the sediment column until 880 ka. The top of the *P. lacunosa* range is calculated to be 452 ka, and the Brunhes/Matuyama boundary to be between 790 and 800 ka. This latter uncertainty may be related to the effects of magnetic overprints displacing the reversal boundary downcore. The sedimentation rates calculated using meters composite depth (mcd) are, on average, inflated 11%–20% (see "Composite Depths and Stratigraphic Correlations" section, this chapter).

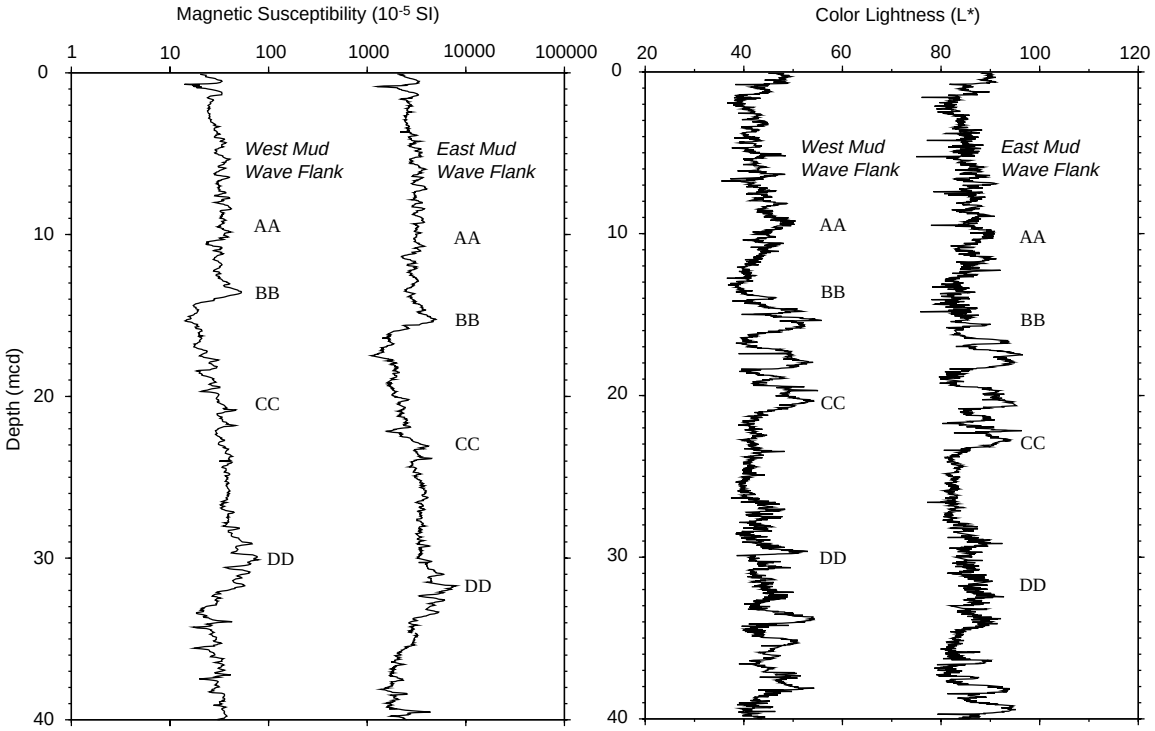

Figure 54. Comparison of unsmoothed spliced records from the east and west wave flanks. AA and CC mark distinctive peaks in lightness, and BB and DD mark distinctive peaks in magnetic susceptibility. Layers on the east wave flank are deeper than on the west wave flank as a result of preferential deposition on the eastern wave flank. This preferential deposition on the east wave flank results in wave migration.

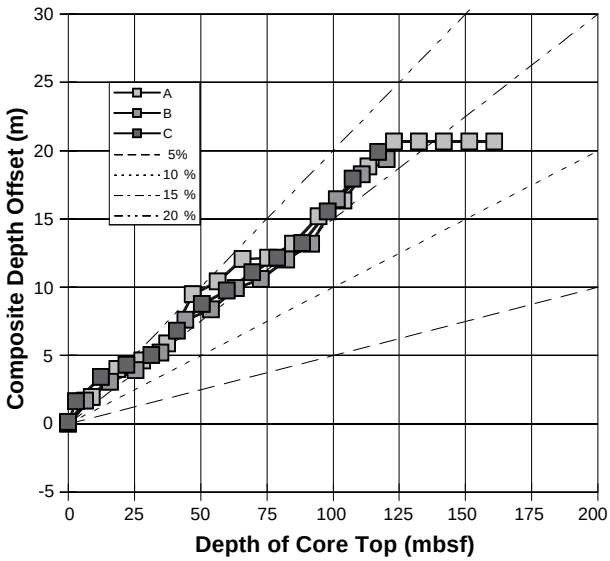

Figure 55. Composite depth offsets vs. core-top depth (mbsf) for Site 1060.

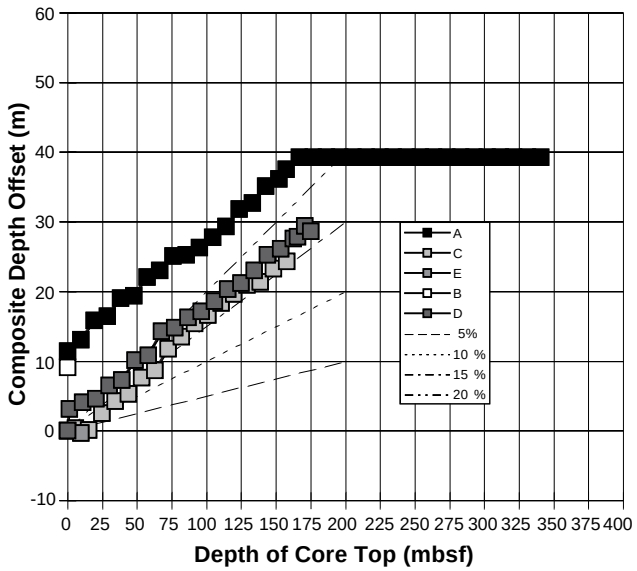

Figure 56. Composite depth offsets vs. core-top depth (mbsf) for Site 1061.

Calcium carbonate accumulation rates average 4.5 g/cm^2/k.y., ranging from 0.6 to 17.1 g/cm^2/k.y. (Fig. 62; Tables 28, 29). Carbonate deposition is higher during the interglacials than during the glacial intervals. The highest values (>13 g/cm^2/k.y.) are calculated for MISs 5, 7, and 9. The very high sedimentation rates and the corresponding relatively low calcium carbonate fluxes observed during MISs 1–4 are probably the result of high detrital supply during this period.

Organic carbon accumulation rates average 0.14 g/cm^2/ k.y., ranging from 0.26 to 0.05 g/cm^2/k.y. High organic carbon accumulation rates (>0.15 g/cm^2/k.y.) are observed during MISs 21, 9, 7, 5, as well as MISs 4–2. The time period represented by MISs 16–11 is characterized by relatively low organic carbon accumulation rates, ranging between 0.6 and 0.11 g/cm^2/k.y. The downhole variations of organic carbon accumulation rate suggest that, with the exception of high organic carbon flux during the glacial MIS 4 and MIS 2, the high organic carbon accumulation took place mainly during the interglacial periods. The high organic carbon accumulation rates during the last glacial are probably caused by a high rate of detrital organic influx and by a very high sedimentation rate, which results in better preser-

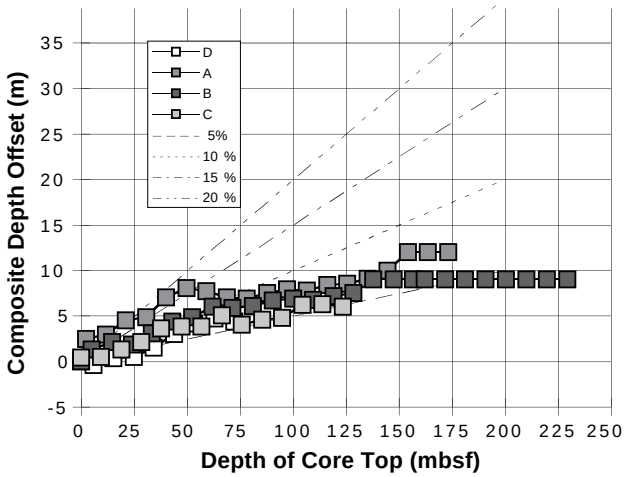

Figure 57. Composite depth offsets vs. core-top depth (mbsf) for Site 1062, east wave flank.

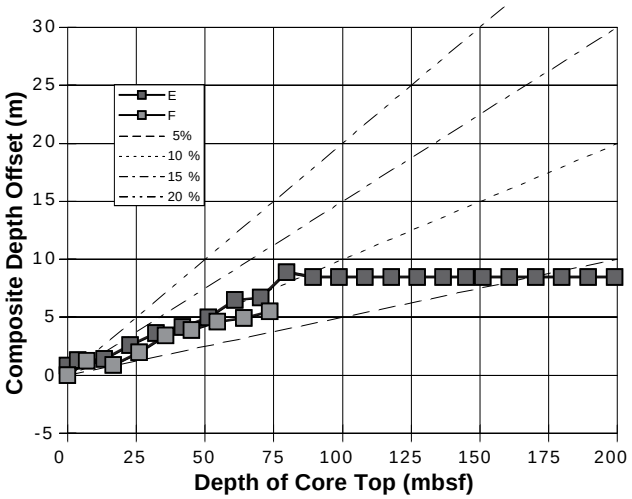

Figure 58. Composite depth offsets vs. core-top depth (mbsf) for Site 1062, west wave flank.

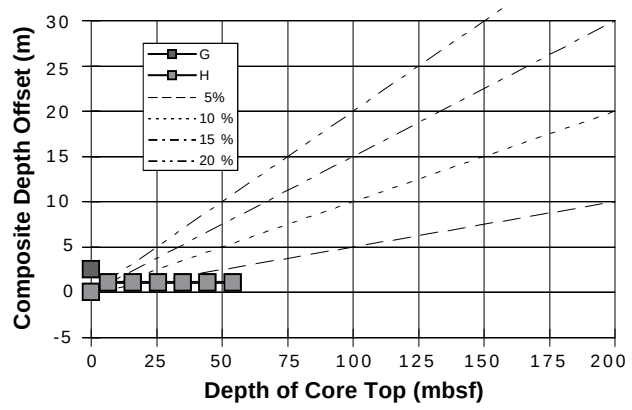

Figure 59. Composite depth offsets vs. core-top depth (mbsf) for Site 1062, wave crest.

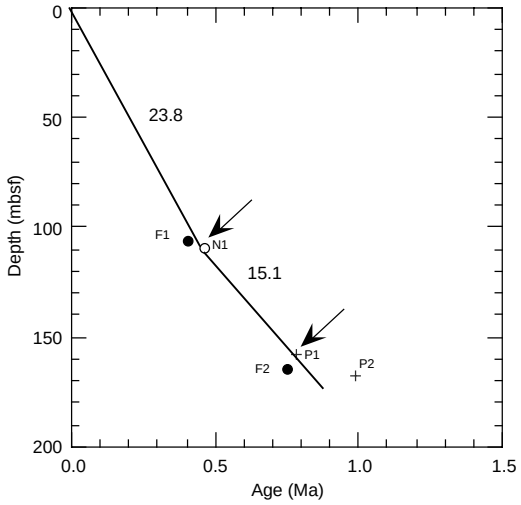

Figure 60. Age/depth plots for Hole 1060A based on biostratigraphic tie points (arrows). Solid circles = planktonic foraminifer markers, open circles = nannoplankton markers, and crosses = magnetostratigraphic markers. See Table 4 in the "Biostratigraphy" section (this chapter) to associate species names with the labels used in this figure. Sedimentation rates are expressed in centimeters per thousand years.

vation of organic matter. Organic carbon accumulation rates generally correlate well with the sedimentation rates at this site, which indicates the importance of the latter factor in organic matter preservation in the sediments.

Site 1061

Between 3.5 Ma (the bottom of the core) and 1 Ma, the sedimentation rates are estimated by using the biostratigraphic markers (see "Biostratigraphy" section, this chapter). Sedimentation rates range from 3 to 13 cm/k.y., increasing uphole, and have an average value of 8 cm/k.y. (Fig. 63).

During the last 900 k.y., the high-resolution sedimentation rate calculated from the magnetic susceptibility record averages approximately 23 cm/k.y., with a maximum of 47 cm/k.y. during the last 70 ka. Using this age model, the top of the *P. lacunosa* range is calculated to be 441 ka, as it is at most of the other sites, and the Brunhes/Matuyama boundary is calculated to be 788 ka, between MISs 19 and 20 (Fig. 64; Table 30).

Calcium carbonate accumulation rates average 2.6 g/cm^2/k.y., ranging from about 0.1 g/cm^2/k.y. to 18.1 g/cm^2/k.y. (Fig. 65; Tables 31, 32). Organic carbon accumulation rates range from 0.01 to 0.4 g/cm^2/k.y., and average 0.1 g/cm^2/k.y.

Since ~1 Ma, and particularly during the past 13 MISs, calcium carbonate and organic carbon accumulation rates show distinct time-variation patterns with reciprocal cyclicity characteristics. Calcium carbonate deposition is higher in the interglacials, whereas organic carbon fluxes generally increase in glacial periods. Deviations from this general pattern observed near the isotopic transitions are probably the result of shifts of data points during composite-depth scale conversion. The time-evolution pattern, also clearly seen in $CaCO_3$ and total organic carbon (TOC) contents, may be explained by terrigenous dilution rather than by oceanic productivity variation (see "Organic Geochemistry" section, this chapter). Between 1.2 Ma and 2.2 Ma, both organic carbon and carbonate deposition rates increase significantly, certainly recording the same event, which might be related to better preservation conditions and/or a general increase in primary productivity. Calcite and organic carbon fluxes do not show the cyclicity observed in the past 1.0 m.y. at previous sites. From about 3.5

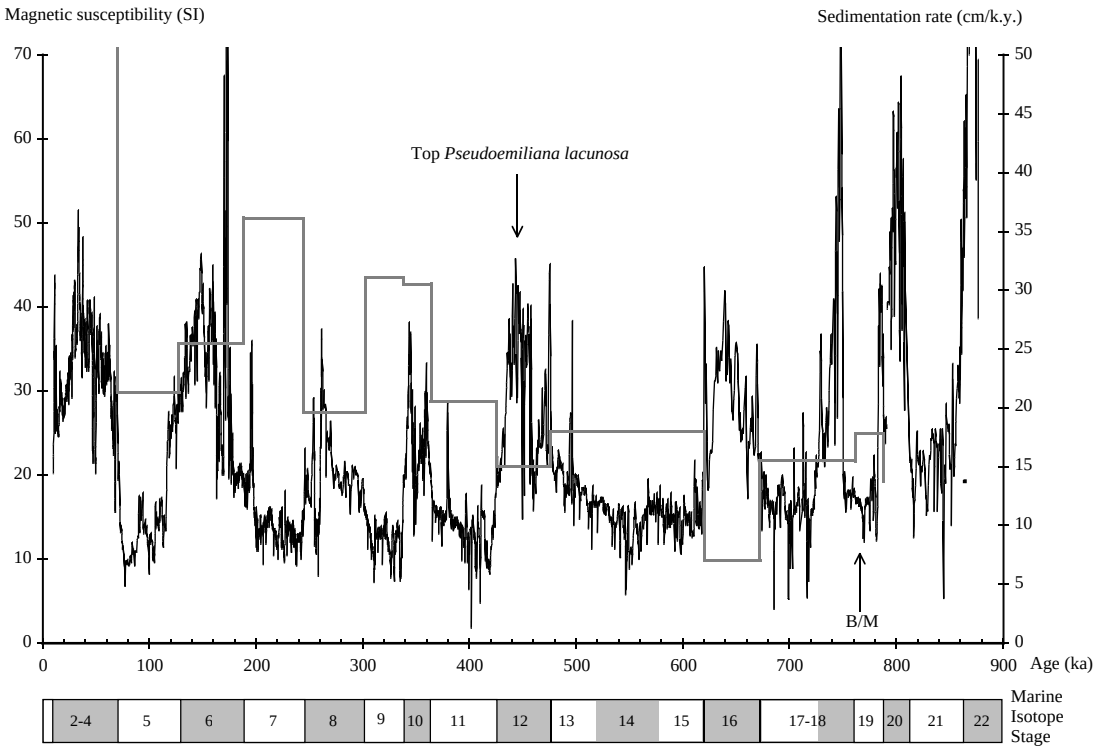

Figure 61. Magnetic susceptibility record (left scale, thin curve) and sedimentation rate (right scale, thick stepwise curve; composite record) of Site 1060 (30°45′N, 74°27′W; 3430 m). The MISs are indicated, with the glacial ones shaded. B/M = Brunhes/Matuyama boundary.

Table 26. Depth-to-depth correlation (mcd) between Sites 1060 and 1061.

Site 1060 depth (mcd)	Site 1061 depth (mcd)	Age (ka)
0.06	0.08	9.96
30.3	27.97	69.15
32.25	29.59	77.06
34.95	32.39	93.27
40.27	35.79	112.95
46.43	44.03	148.66
48.78	46.93	159.28
62.11	58.37	200.17
79.01	71.73	245.75
80.36	73.73	254.53
85.43	75.35	261.64
89.19	84.15	300.25
102.68	97.11	343.56
108.17	100.11	360.59
120.43	114.73	418.95
127.27	121.71	460.17
129.66	124.93	480.80
155.03	148.7	620.00
158.23	152.68	669.51
168.71	161.88	728.61
173.53	169.08	769.92
176.13	173.04	781.89
182.59	179.16	817.34
186.43	184.9	858.42
190.07	188.56	874.61

Note: Correlations based on depth-to-depth relationship between magnetic susceptibility records, using Site 1061 as a reference.

Table 27. Age-depth relationship for Site 1060.

Age (ka)	Depth (mcd)	Average sedimentation rate (cm/k.y.)
10	0.08	50.7
70	30.51	50.7
128	42.87	21.3
188	58.14	25.5
244	78.36	36.1
302	89.74	19.6
338	100.95	31.1
364	108.89	30.5
426	121.60	20.5
476	129.10	15.0
620	155.03	18.0
672	158.67	7.0
762	172.61	15.5
788	177.24	17.8
864	187.69	13.7

to 2 Ma, both carbonate and organic fluxes show little variation with time, which is mainly caused by the low sedimentation rate.

Site 1062

Site 1062 includes several holes cored into different parts of a mud wave. Low-resolution sedimentation rates are estimated in two different locations. Holes 1062A and 1062B are on the eastern flank of the mud wave and their combined records reach the early Pliocene (4.3 Ma). In the Pliocene portion of this record, there are two intervals of more rapid sediment accumulation (between 4.3 and 3.8 Ma and between 2.8 and 2.5 Ma) separating two intervals of slower accumulation (Fig. 66). Average sedimentation rates increase through the Pleistocene. The cored interval in Hole 1062E on the western side of the mud wave reaches 3.1 Ma and is characterized by lower sedimentation rates than those in Holes 1062A and 1062B (Fig. 66).

The high-resolution sedimentation rates obtained from the composite magnetic susceptibility records are presented using "East Site 1062" to refer to the eastern side of the mud wave (Holes 1062A, 1062B, 1062C and 1062D) and "West Site 1062" to refer to the western side of the same mud wave (Holes 1062E and 1062F). At East Site 1062, the sedimentation rate averages 9 cm/k.y. High values of 15 to 25 cm/k.y. are calculated for the past 500 k.y. of the record. The LO of the *P. lacunosa* is calculated to be at 416 ka, almost 50 k.y. younger than expected (within MIS 11 instead of MIS 12). A more precise estimate will be necessary to avoid problems linked to sam-

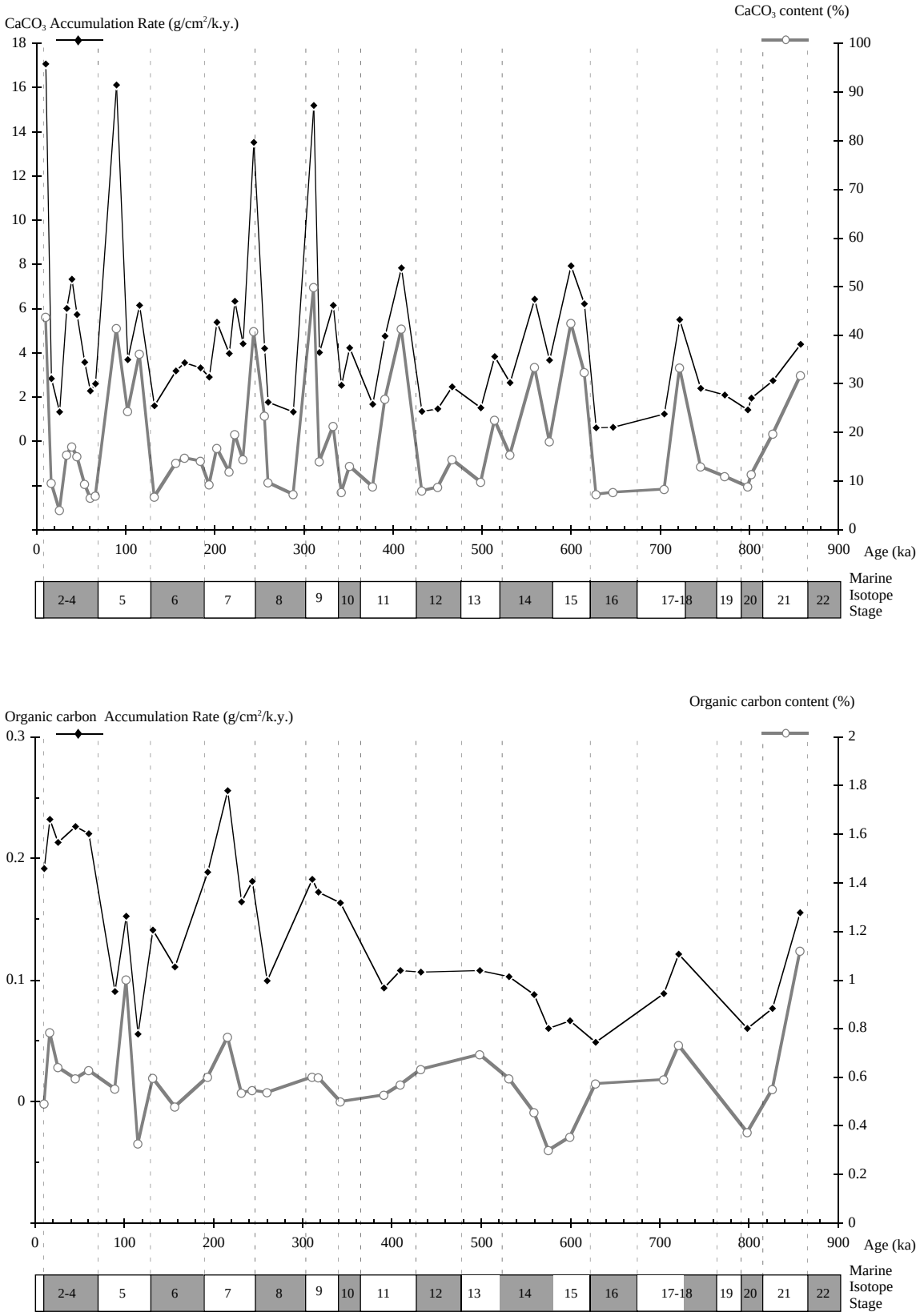

Figure 62. Downhole profiles of calcium carbonate accumulation rates and organic carbon at Site 1060 (composite). MISs are indicated with glacial ones shaded. Dashed lines = magnetic susceptibility-based boundaries. Striped section of MIS scale = stage assignment uncertain.

Table 28. Estimated ages, concentrations, and accumulation rates of calcium carbonate at Site 1060.

Age (ka)	$CaCO_3$ content (wt%)	$CaCO_3$ MAR ($g/cm^2/k.y.$)
10.23	43.78	17.07
16.40	9.57	2.83
25.62	3.98	1.33
33.64	15.36	6.01
39.46	17.08	7.33
45.17	15.05	5.73
54.08	9.33	3.58
60.42	6.48	2.27
66.33	6.97	2.62
89.55	41.38	16.11
102.48	24.31	3.70
115.50	36.18	6.16
132.20	6.78	1.60
156.57	13.70	3.18
166.30	14.70	3.57
183.91	14.15	3.33
193.57	9.25	2.91
202.49	16.73	5.40
216.11	11.89	3.97
222.74	19.58	6.34
231.73	14.44	4.42
243.70	40.77	13.53
256.13	23.35	4.21
260.22	9.65	1.78
288.03	7.23	1.32
310.91	49.86	15.20
317.33	14.00	4.03
333.03	21.26	6.15
342.18	7.73	2.53
351.35	13.02	4.23
377.35	8.81	1.69
390.86	26.88	4.77
409.52	41.33	7.86
432.33	8.03	1.35
450.41	8.73	1.47
466.56	14.48	2.47
498.58	9.81	1.53
514.21	22.52	3.83
531.55	15.34	2.65
559.21	33.44	6.44
575.67	18.18	3.67
599.70	42.44	7.94
614.51	32.32	6.23
628.20	7.31	0.62
646.92	7.74	0.64
704.64	8.30	1.25
721.56	33.30	5.52
745.15	12.94	2.39
772.31	11.00	2.10
798.13	8.85	1.43
802.30	11.39	1.95
826.65	19.75	2.75
857.67	31.71	4.40

Notes: MAR = mass accumulation rate. Estimations based on geochemical measurements at Hole 1060A.

Table 29. Estimated ages, concentrations, and accumulation rates of organic carbon at Site 1060.

Age (ka)	C_{org} content (wt%)	C_{org} MAR ($g/cm^2/k.y.$)
10.23	0.49	0.19
16.40	0.78	0.23
25.62	0.64	0.21
45.17	0.60	0.23
60.42	0.63	0.22
89.55	0.55	0.09
102.48	1.00	0.15
115.50	0.33	0.06
132.20	0.60	0.14
156.57	0.48	0.11
193.57	0.60	0.19
216.11	0.77	0.26
231.73	0.54	0.16
243.70	0.55	0.18
260.22	0.54	0.10
310.91	0.60	0.18
317.33	0.60	0.17
342.18	0.50	0.16
390.86	0.53	0.09
409.52	0.57	0.11
432.33	0.63	0.11
498.58	0.69	0.11
531.55	0.59	0.10
559.21	0.46	0.09
575.67	0.30	0.06
599.70	0.36	0.07
628.20	0.57	0.05
704.64	0.59	0.09
721.56	0.73	0.12
798.13	0.37	0.06
826.65	0.55	0.08
857.67	1.12	0.16

Notes: MAR = mass accumulation rate. Estimations based on geochemical measurements for Hole 1060A.

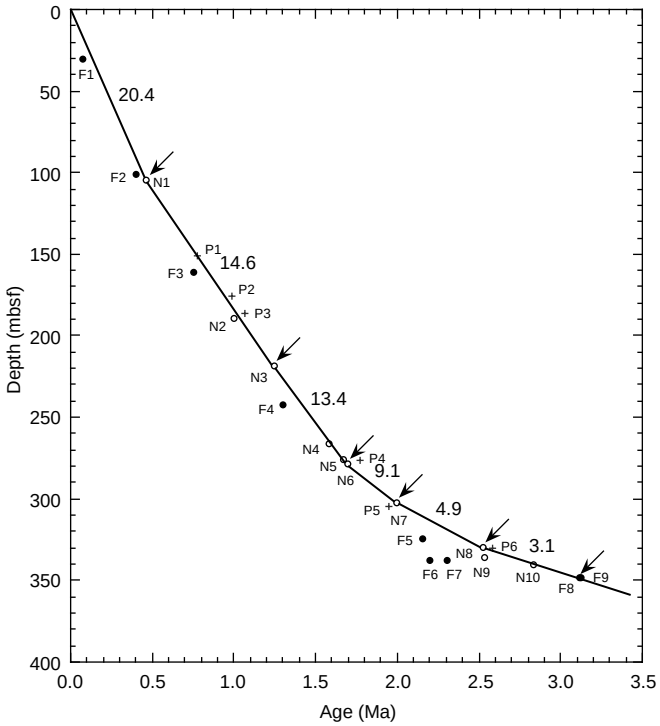

Figure 63. Age/depth plots for Hole 1061A based on biostratigraphic tie points (arrows). Solid circles = planktonic foraminifer markers, open circles = nannoplankton markers, and crosses = magnetostratigraphic markers. See Table 4 in the "Biostratigraphy" section (this chapter) to associate species names with the labels used in this figure. Sedimentation rates are expressed in centimeters per thousand years.

ples barren of nannofossils that confound the identification of the last occurrence (LO) of *P. lacunosa.* At this site, the age of the Brunhes/Matuyama boundary is calculated to be 776 ka (Tables 33, 34; Fig. 67). During the last 900 k.y., the sedimentation rate at West Site 1062 averages 8 cm/k.y., slightly lower than the rate calculated at East Site 1062. A maximum of 22 cm/k.y. is observed during the interval corresponding to the last 70 k.y. of the core, but the values are much lower (1–15 cm/k.y.) in the older part of the record (Tables 35, 36; Fig. 68). The sedimentation rates are higher where the current speed is lower, as it is at the East Site 1062 (see "Site Geophysics" section, this chapter).

Figure 69 compares the sedimentation rates of the East and West Sites 1062 for the past 3.5 Ma. Between 3.5 and 2 Ma, the sedimentation rates are higher on the "present-day" western side than on the "present-day" eastern side of the mud wave, but the trend is reversed during the time period between 2 Ma and the top of the cored interval.

Accumulation rates for calcium carbonate and organic carbon were only calculated for the eastern side of the mud wave cored at Site 1062, based on geochemical analyses of samples from Holes

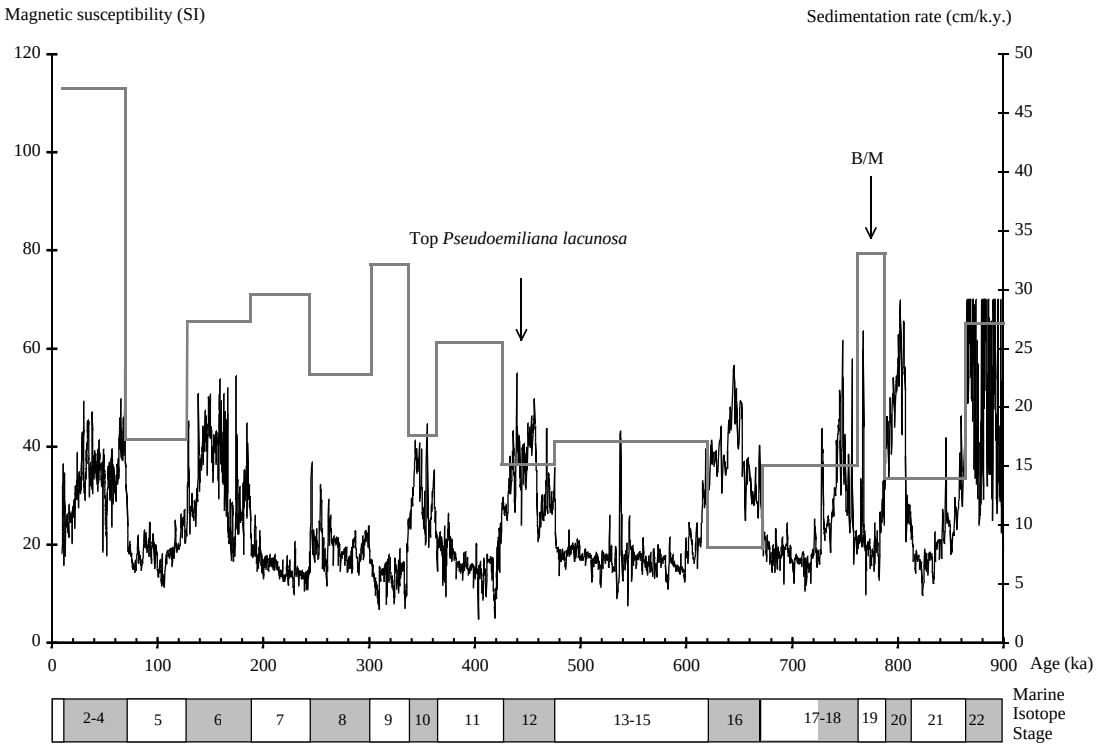

Figure 64. Magnetic susceptibility record (left scale, thin curve) and sedimentation rate (right scale, thick stepwise curve; composite record) of Site 1061 (29°58′N, 73°35′W, 4050 m). The MISs are indicated, with the glacial ones shaded. B/M = Brunhes/Matuyama boundary.

Table 30. Age-depth relationship for Site 1061.

Depth (mcd)	Age (ka)	Average sedimentation rate (cm/k.y.)
0.1	10	47.12
28.37	70	47.12
38.39	128	17.28
54.77	188	27.30
71.33	244	29.57
84.55	302	22.79
96.13	338	32.17
100.71	364	17.62
116.53	426	25.52
124.11	476	15.16
148.7	620	17.08
152.88	672	8.04
166.46	762	15.09
175.06	788	33.08
185.68	864	13.97
195.45	900	27.14

1062A and 1062B. Calcium carbonate accumulation rates show a wide range of variation from less than 0.1 to 10.4 g/cm^2/k.y. (Table 37; Fig. 70). The average value is 1.4 g/cm^2/k.y. Organic carbon fluxes are very low, averaging 0.06 g/cm^2/k.y. (Table 38). From the present data, two depth zones with distinct patterns of biogenic fluxes can be distinguished. From the Holocene to 0.9 Ma, organic carbon and calcium carbonate accumulation rates are high (>3 and 0.05 g/cm^2/k.y., respectively) and highly variable. Moreover, as previously noted at Sites 1060 and 1061, they vary inversely, with high carbonate and low organic carbon fluxes in interglacial periods. The high organic carbon accumulation rates observed during the last glacial are probably the result of a high rate of detrital organic influx. Very high sedimentation rates during this period probably also contributed to high organic carbon accumulation rates through better preservation of the organic matter. Before 900 ka, calcium carbonate and organic carbon fluxes show little fluctuation with depth. Here again, a change of pattern from highly variable to lower, less variable, fluxes is observed near the 900 ka boundary.

ORGANIC GEOCHEMISTRY

Routine monitoring of headspace gases was done for drilling safety in at least every core of Holes 1060A and 1061A, located on the deeper portion of the Blake Outer Ridge in water depths of 3492 and 4040 m, respectively, and in Holes 1062A and 1062B, located on a mud wave near the crest of Bahama Outer Ridge in 4775 m water depth. Whenever gas expansion voids occurred, the gases were sampled using a gas-tight syringe attached to a piercing tool. Calcium carbonate and organic carbon concentrations were also measured on selected samples obtained from all holes. Organic matter atomic C/N values and Rock-Eval analyses were employed to determine the type of sedimentary organic matter.

Volatile Gases

Methane concentrations measured by headspace gas procedures are heavily influenced by coring techniques, the time exposure of cores to atmospheric pressure, the stage of sediment diagenesis (lithification and water content), and analytical procedures (e.g., desorption conditions). Therefore, the measured gas amounts do not represent in situ concentrations (Dickens et al., 1996). However, this standard procedure allows the recognition of comparable methane distribution patterns with depth at Sites 1060, 1061, and 1062 (Fig. 71; Table 39).

Low C_1 concentrations occur in the uppermost sections at each site. In Holes 1060A and 1062A, methane levels are only slightly higher than 100 ppm in the upper 10 m. The uppermost portion of Hole 1061A is more enriched in methane, reaching concentrations as high as 159 ppm in the first section. This is because the first 11 m of

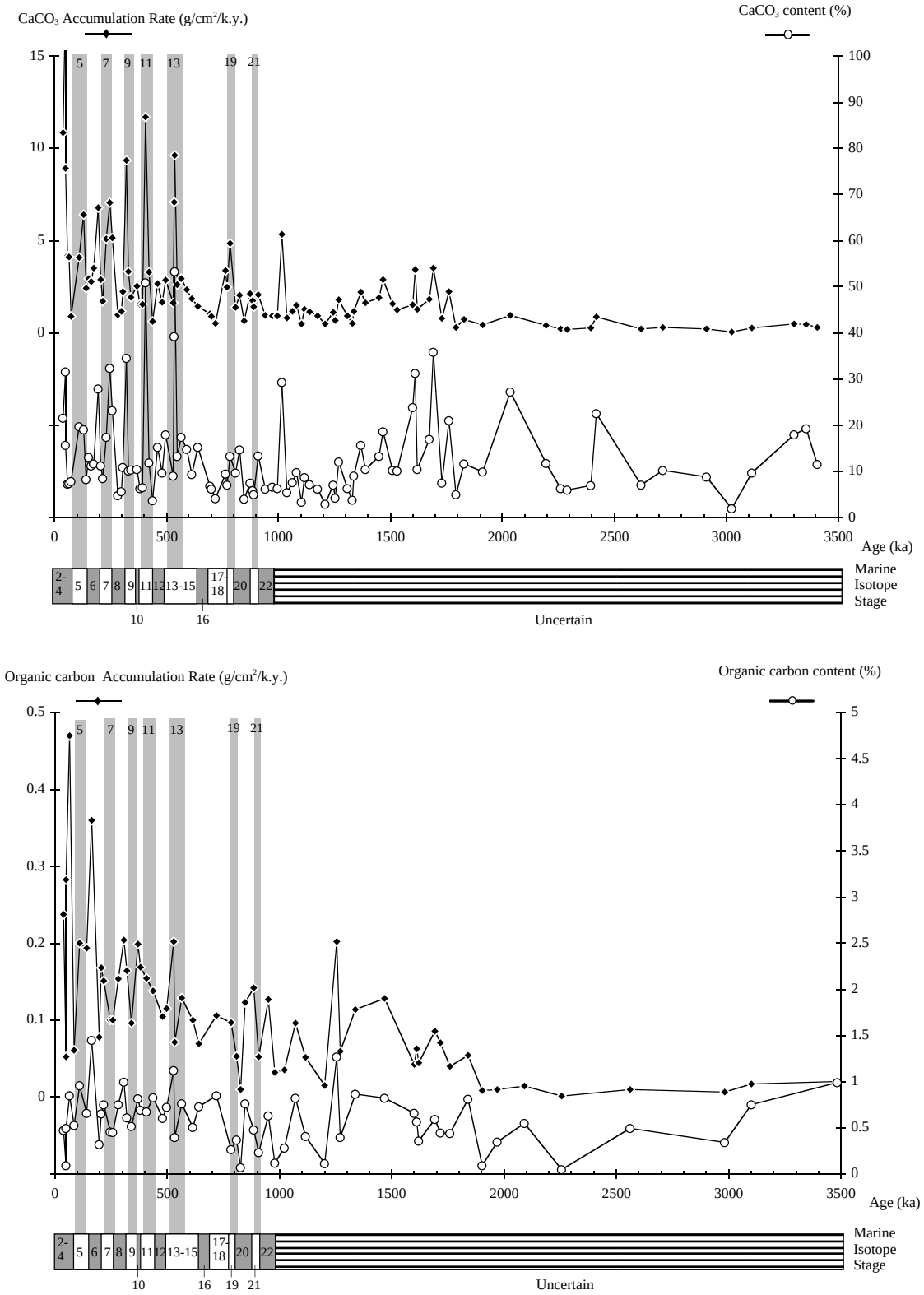

Figure 65. Downhole profiles of organic carbon and calcium carbonate accumulation rates at Site 1061. Shaded columns on the graph indicate interglacial time periods. Striped section of MIS scale = stage assignment uncertain.

Table 31. Estimated ages, concentrations, and accumulation rates of calcium carbonate at Site 1061.

Age (ka)	$CaCO_3$ content (wt%)	$CaCO_3$ MAR ($g/cm^2/k.y.$)
37.95	21.58	10.85
48.50	31.64	18.10
50.41	15.68	8.91
58.28	7.27	4.17
64.84	7.43	4.11
74.46	7.88	0.91
109.88	19.73	4.11
129.65	19.11	6.42
140.42	8.30	2.44
153.20	13.12	2.96
164.12	11.25	2.79
175.25	11.72	3.51
196.45	27.96	6.80
207.17	11.26	2.90
216.78	8.55	1.72
230.68	17.43	5.10
246.46	32.37	7.07
258.21	23.27	5.15
281.99	4.83	0.98
298.58	5.62	1.17
306.38	10.95	2.24
320.99	34.60	9.35
329.54	10.15	3.32
340.55	10.40	1.93
369.17	10.47	2.55
381.36	6.33	1.55
393.08	6.56	1.55
406.91	50.97	11.69
423.26	11.86	3.30
438.01	3.72	0.62
461.22	15.29	2.69
480.16	9.73	1.68
497.37	18.03	2.86
529.29	9.06	1.64
534.33	39.31	7.09
535.91	53.38	9.62
547.33	13.27	2.63
565.07	17.42	2.94
591.42	14.79	2.35
613.32	9.33	1.85
640.03	15.23	1.44
694.39	6.86	1.03
701.94	6.24	0.92
718.99	4.14	0.52
762.73	9.47	3.39
770.34	7.10	2.48
783.19	13.35	4.86
808.75	9.70	1.39
826.36	14.76	2.04
847.40	4.04	0.65
874.80	7.53	2.13
884.93	5.91	1.74
890.42	5.01	1.42
906.69	13.43	3.03
927.91	6.26	1.41
950.23	6.66	1.34
964.89	6.34	1.35
979.65	29.37	7.80
995.05	5.44	1.20
1021.35	7.59	0.94
1042.95	9.85	1.22
1070.94	3.42	0.40
1089.30	8.68	1.03
1114.97	7.22	0.92
1161.66	6.18	0.75
1201.62	2.98	0.39
1246.28	7.13	1.14
1254.89	4.27	0.68
1270.99	12.11	1.81
1309.60	6.34	0.93
1331.19	3.79	0.53
1337.33	9.03	1.19
1368.74	15.67	2.21
1388.51	10.46	1.64
1449.91	13.29	1.91
1468.13	18.62	2.90
1510.19	10.26	1.58
1529.89	10.18	1.26
1599.60	23.85	1.54
1611.40	31.32	3.47
1621.00	10.52	1.29
1673.41	16.98	1.86
1691.40	35.83	5.20
1717.12	7.53	1.19
1738.73	21.07	3.29
1759.72	5.06	0.46
1783.26	11.64	1.08
1840.16	9.93	0.67
1901.63	27.23	2.50
1969.99	11.83	0.33
2053.46	6.36	0.19
2090.85	5.98	0.16
2224.51	6.95	0.22
2256.01	22.62	0.69
2465.73	7.04	0.27
2560.72	10.20	0.20
2835.87	8.80	0.17
2982.71	1.95	0.04
3101.99	9.66	0.22
3348.22	17.98	0.37
3418.70	19.33	0.36
3483.77	11.54	0.24

Notes: MAR = mass accumulation rate. Estimations based on geochemical measurements for Hole 1061A.

the sedimentary section were not cored because of APC overpenetration in Hole 1061A. In Hole 1061E, the uppermost sediments were successfully cored and show the characteristic, extremely low concentrations of methane in the upper 14–15 m (Fig. 71).

A rapid increase in methane concentrations is recorded below these methane-depleted layers. The zone of increasing methane concentrations begins at equivalent depths at Sites 1060 and 1061 (~14 mbsf; see the corrected depths for Site 1061 in Fig. 71) and at ~10 mbsf in Hole 1062A. However, the steepest C_1 gradient appears deeper in Hole 1061A. The highest methane concentrations are similar at Sites 1060 and 1061 (~56,000 ppm); they are much lower in Hole 1062A, reaching ~36,000 ppm at 152.2 mbsf. Below these depths, decreasing amounts of methane occur downhole in Holes 1060A and 1061A. In Hole 1060A, this decrease is sharp and occurs between 60 and 110 mbsf. The same trend is observed in Hole 1061A, but methane decreases over a longer depth interval. Hole 1062A does not show any progressive decrease in methane concentration with depth.

Headspace C_2–C_3 hydrocarbons are present in extremely low amounts. Ethane never reaches concentrations higher than ~10 ppm in Sites 1061 and 1062 and never exceeds 3 ppm in Hole 1061A. Propane occurs at levels of ~4 ppm in Hole 1061A and generally remains below 2 ppm in Holes 1060A and 1062A (Table 39).

The first obvious gas voids are found at 60 mbsf in Holes 1060A and 1061A and only occur at three depths in Hole 1062A (Table 40). These voids, which were sampled before the core liner was split, contain methane, ethane, propane, and low amounts of *iso*-butane. Methane concentrations in the voids are significantly higher than those obtained by the headspace technique (Tables 39, 40). The difference in absolute values between the two methods may result from preferential outgassing of methane, which is then concentrated within the gas expansion voids. Furthermore, the methane measured by the headspace technique may largely be residual methane left behind after outgassing. Headspace methane may also be depleted by exposure of the sediment to air when the core arrives on deck or by leakage of vial septa during heating in the oven (Stein et al., 1995). A general increase with depth in propane and *iso*-butane concentrations is also observed in Hole 1061A (Table 40; Fig. 72), but these levels remain much lower than those of ethane and methane. *Iso*-pentane is never detected in measurable amounts, with the exception of Hole 1061A, where it occurs in trace amounts in two samples below 300 mbsf.

Headspace C_1/C_2 values show a typical decrease with depth, from values as high as 25,000 ppm at shallow depths to 6,000 ppm at 168 mbsf in Hole 1060A. Holes 1061A and 1062A present the same trend, but C_1/C_2 values are generally lower in Hole 1061A (Fig. 73). The same general C_1/C_2 depth pattern is observed in gas void data,

Table 32. Estimated ages, concentrations, and accumulation rates of organic carbon at Site 1061.

Age (ka)	C_{org} content (wt%)	C_{org} MAR ($g/cm^2/k.y.$)
37.95	0.47	0.24
48.50	0.09	0.05
50.41	0.50	0.28
64.84	0.85	0.47
74.46	0.53	0.06
109.88	0.96	0.20
140.42	0.66	0.19
164.12	1.45	0.36
196.45	0.32	0.08
207.17	0.65	0.17
216.78	0.75	0.15
246.46	0.46	0.10
258.21	0.45	0.10
281.99	0.75	0.15
306.38	1.00	0.20
320.99	0.61	0.16
340.55	0.52	0.10
369.17	0.82	0.20
381.36	0.69	0.17
406.91	0.67	0.15
438.01	0.83	0.14
480.16	0.61	0.10
497.37	0.73	0.12
529.29	1.12	0.20
534.33	0.40	0.07
565.07	0.77	0.13
613.32	0.51	0.10
640.03	0.73	0.07
718.99	0.85	0.11
783.19	0.27	0.10
808.75	0.37	0.05
826.36	0.07	0.01
847.40	0.76	0.12
884.93	0.48	0.14
906.69	0.23	0.05
950.23	0.63	0.13
979.65	0.12	0.03
1021.35	0.29	0.04
1070.94	0.82	0.10
1114.97	0.41	0.05
1201.62	0.11	0.02
1254.89	1.27	0.20
1270.99	0.40	0.06
1337.33	0.86	0.11
1468.13	0.83	0.13
1599.60	0.66	0.04
1611.40	0.57	0.06
1621.00	0.36	0.04
1691.40	0.59	0.09
1717.12	0.45	0.07
1759.72	0.44	0.04
1840.16	0.81	0.05
1901.63	0.09	0.01
1969.99	0.35	0.01
2090.85	0.55	0.01
2256.01	0.05	0.00
2560.72	0.50	0.01
2982.71	0.35	0.01
3101.99	0.75	0.02

Note: MAR = mass accumulation rate. Estimations based on geochemical measurements at Hole 1061A.

except in Hole 1060A, which does not display an obvious C_1/C_2 decrease (Table 40). However, the sampling frequency of gas void samples in this hole is not sufficient to obtain a clear concentration pattern. Gas void samples are also too rare in Hole 1062A to see any trend with depth.

Discussion

The subsurface methane enrichment observed at Sites 1060–1062 may have multiple origins. Methane may be biogenically produced, being the metabolic end-product of organic matter oxidation (e.g., CO_2 reduction reactions involving several species of microorganisms; Schoell, 1980; Claypool and Kaplan, 1974). Alternatively, methane may diffuse upward from underlying rocks, where hydrocarbons may be thermally generated through organic-matter cracking

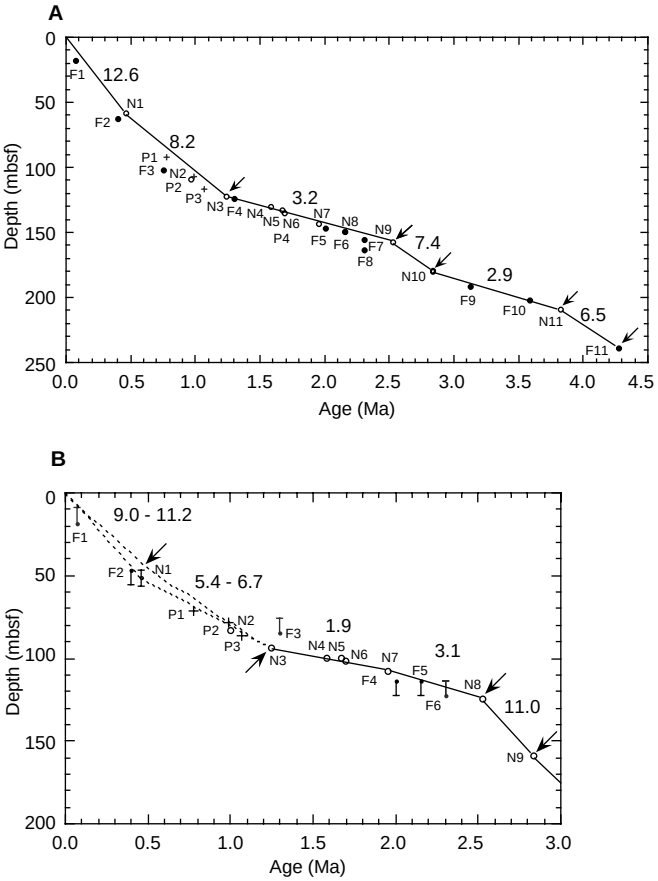

Figure 66. Age/depth plots for (**A**) Holes 1062A and 1062B and (**B**) Hole 1062E based on biostratigraphic tie points (arrows). Solid circles = planktonic foraminifer markers, open circles = nannoplankton markers, and crosses = magnetostratigraphic markers. See Table 4 in the "Biostratigraphy" section (this chapter) to associate species names with the labels used in this figure. Sedimentation rates are expressed in centimeters per thousand years.

processes. In this case, higher molecular-weight gases (C_{2+}) would also be produced to diffuse upward. Thus, high C_1/C_2 values indicate methane formation by microbiological processes, but the occurrence of major amounts of C_2 (and C_3 to C_5) is generally associated with thermogenic hydrocarbons. At Sites 1060, 1061, and 1062, C_1/C_2 values never fall below 1000, although the ratio decreases with depth because early diagenetic processes also generate higher hydrocarbons. Thus, high C_1/C_2 values coupled with generally low levels of higher molecular-weight hydrocarbons (except for Hole 1061A; see below), indicate that the methane is predominantly of microbial origin. A similar interpretation has been inferred from hydrocarbon distribution in sediments elsewhere (see "Organic Geochemistry" sections, "Intermediate Depth Blake Outer Ridge" and "Carolina Slope" chapters, this volume).

Methanogenic bacteria normally become active only beneath the zone of sulfate reduction (Claypool and Kaplan, 1974). This is reflected in the upper sections of Holes 1060A, 1061A, and 1061E, where sulfate declines dramatically to minimal levels at the same depths where methane concentrations begin to increase (see "Inorganic Geochemistry" section, this chapter). Such is not the case, however, in Hole 1062A, where methane concentrations start to increase at 10 mbsf, well above the base of the sulfate reduction zone (65 mbsf; see "Inorganic Geochemistry" section, this chapter).

Depths below the top of the methanogenesis zone are characterized by high methane concentrations, which are higher in Holes

Table 33. Depth-to-depth correlation (mcd) between East Site 1062 and Site 1061.

East Site 1062 depth (mcd)	Site 1061 depth (mcd)	Age (ka)
0.06	0.08	9.96
11.44	19.78	51.77
13.36	23.99	60.70
15.22	27.93	69.07
17.48	30.77	83.89
19.16	34.57	105.89
23.04	38.79	129.47
35.36	54.65	187.56
37.54	65.01	222.63
38.42	67.29	230.34
39.52	71.85	246.28
50.38	84.15	300.25
51.92	86.75	308.84
54.50	91.59	323.89
57.82	94.91	334.21
59.76	95.93	337.38
62.44	100.31	361.73
64.14	105.59	383.13
66.20	114.73	418.95
72.65	124.07	475.74
73.61	125.81	485.96
75.27	130.11	511.14
75.67	131.53	519.45
76.40	132.96	527.83
78.26	134.68	537.90
78.82	136.10	546.21
79.62	138.34	559.33
84.42	146.60	607.70
87.90	150.70	644.88
89.44	152.68	669.51
92.52	160.78	721.69
93.34	161.84	728.36
97.06	166.12	758.54
98.86	168.28	767.50
99.96	173.28	782.62
101.66	177.56	805.89
102.84	180.08	823.92
105.00	183.86	850.98
107.72	186.40	866.65
108.20	187.74	871.59
108.78	189.35	877.52
110.76	196.25	903.67

Note: Estimations based on depth-to-depth relationship between magnetic susceptibility records, using Site 1061 as a reference.

Table 34. Age-depth relationship for East Site 1062.

Age (ka)	East Site 1062 depth (mcd)	Average sedimentation rate (cm/k.y.)
10	0.07	25.48
70	15.36	25.48
128	22.80	12.82
188	35.39	20.98
244	39.36	7.10
302	50.69	19.54
338	59.83	25.37
364	62.62	10.74
426	67.00	7.07
476	72.67	11.35
620	85.57	8.96
672	89.59	7.72
762	97.75	9.08
788	100.35	9.99
864	107.26	9.09
900	110.48	8.95

1060A and 1061A relative to Hole 1062A. Sediments below these intermediate depths exhibit decreasing C_1 concentrations, possibly because of sediment outgassing and concentration of gas within expansion voids. The rare occurrence of gas pockets in Hole 1062A may therefore explain the almost constant trend of methane concentrations below the methanogenesis zone. Similar methane concentration profiles have been observed at other ODP sites associated with gas hydrate (e.g., Peruvian outer continental margin; Kvenvolden and Kastner, 1990). In Hole 1061A, an increase of ethane, propane, and *iso*-butane concentration occurs within sediment voids with increasing depth (Fig. 72). Higher molecular-weight hydrocarbons have been found to accompany biogenically generated methane in other marine sediments (Whelan and Sato, 1980). This explanation is consistent with Rock-Eval analyses, which show no evidence of thermal generation of hydrocarbons (see below).

Inorganic and Organic Carbon

Inorganic carbon analyses were performed on samples from Holes 1060A, 1061A, and 1062A at a frequency of three per core. Elemental analysis and TOC measurements were done at a lower frequency, depending on the inorganic carbon content of the sediments. Results are presented in Table 41 and Figures 74 through 76.

Hole 1060A

Calcium carbonate values in Hole 1060A range from 3 to 50 wt%, and average 18.3 wt%. $CaCO_3$ content shows cyclic variations with depth (Fig. 74). These cycles probably correlate with glacial and interglacial periods recorded in the sediments (see "Organic Geochemistry" section, "Intermediate Depth Blake Outer Ridge" chapter, this volume). High carbonate deposition is observed during interglacial periods, whereas the lowest carbonate values (<5 wt%) are typically seen during glacial intervals. A preliminary stratigraphic correlation based on carbonate concentration depth profiles, biostratigraphy, and magnetic susceptibility data indicates that sediments from this site provide a temporal record extending to late MIS 19 (middle Pleistocene), just above the Brunhes/Matuyama polarity reversal.

TOC values range from 0.3 to 1.12 wt%, averaging 0.6 wt% for the entire hole. This value is about twice the average of 0.3 wt% compiled by McIver (1975) from DSDP Legs 1 through 33. TOC values show little variation with depth.

Hole 1061A

Calcium carbonate values average 13 wt% in Hole 1061A, ranging from ~2 wt% at 337 mbsf to 53 wt% at 106.5 mbsf. Most of the values are distributed between 5 and 15 wt%. TOC values range from ~0.1 wt% at 6.8 mbsf to 1.4 wt% at 31.8 mbsf, and average 0.6% (Fig. 75). Thus, although mean organic carbon contents are comparable at Sites 1060 and 1061, calcium carbonate concentrations are lower in Hole 1061A. Beyond this general trend, Hole 1061A shows three depth zones with distinct carbonate and organic carbon distributions.

From the seafloor to ~130 mbsf, calcium carbonate values average 16 wt% and show abrupt variations similar to those observed for presumed time-equivalent sediments from Hole 1060A (i.e., high carbonate accumulation during interglacials). TOC concentrations there average 0.70 wt%, but reach a markedly high value of 1.45 wt% at 31.8 mbsf. In this depth zone, organic carbon and calcium carbonate concentrations follow opposite trends, with higher TOC values in glacial periods.

Between ~130 and 220 mbsf, Hole 1061A shows a general decrease of calcium carbonate content, with values averaging 8 wt%. With the exception of a single sample with a carbonate value of 29 wt%, just above the depth of reentrance of the medium *Gephyrocapsa* spp.(≈1 Ma), most of the values are distributed within a narrow range of 3–12 wt%, and show low variability. This depth zone is also characterized by highly variable TOC values, but average concentrations (0.5 wt%) are lower than in the overlying zone.

Below 220 mbsf, calcium carbonate values significantly increase and average 13 wt%. They show fluctuations comparable to the ones observed above 130 mbsf, although with lower amplitude. TOC concentrations also increase slightly during this interval, averaging 0.55 wt%. The highest TOC values are measured between 209 and 290 mbsf, which roughly correspond to the interval of increasing calcium

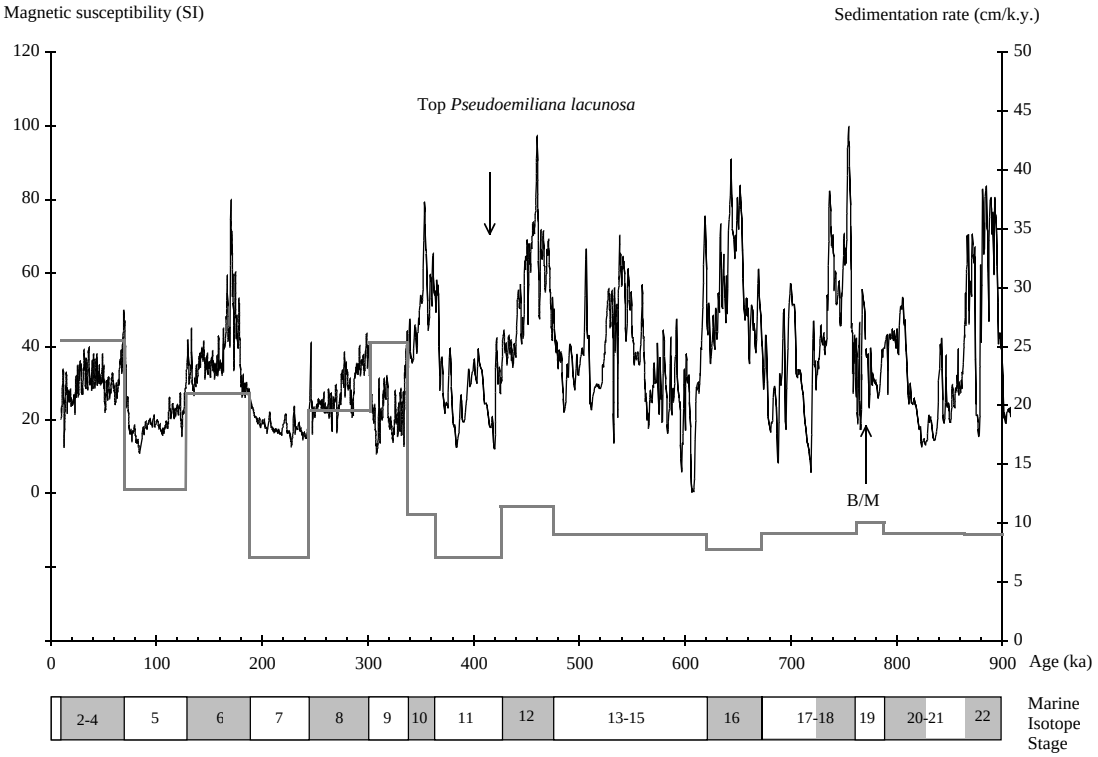

Figure 67. Magnetic susceptibility record (left scale, thin curve) and sedimentation rate (right scale, thick stepwise curve; composite record) of East Site 1062 (28°14′N, 74°24′W, 4775m). The MISs are indicated, with the glacial ones shaded. B/M = Brunhes/Matuyama boundary.

Table 35. Depth-to-depth correlation (mcd) between West Site 1062 and Site 1061.

West Site 1062 depth (mcd)	Site1061 depth (mcd)	Age (ka)
0.08	0.10	10.00
10.60	19.82	51.85
14.20	29.31	75.44
20.84	38.79	129.47
36.26	71.73	245.75
39.86	84.15	300.25
40.34	86.95	309.46
44.28	94.91	334.21
47.36	97.11	343.56
54.74	118.75	440.64
57.78	125.89	486.42
67.58	148.48	618.71
70.08	152.48	667.02
76.38	170.86	775.30
79.62	180.08	823.92

Note: Correlations based on depth-to-depth relationships between magnetic susceptibility records, using Site 1061 as a reference.

Table 36. Age-depth relationship for West Site 1062.

Age (ka)	West Site 1062 depth (mcd)	Average sedimentation rate (cm/k.y.)
10	0.08	22.15
70	13.37	22.15
128	20.66	12.57
188	28.60	13.24
244	36.03	13.26
302	39.95	6.77
338	45.53	15.49
364	48.91	13.02
426	53.63	7.60
476	57.09	6.92
620	67.65	7.33
672	70.37	5.24
762	75.61	5.82
788	77.23	6.23
864	82.20	6.54
900	84.51	6.43

carbonate values. This relationship between $CaCO_3$ and TOC is thus the opposite of that observed above 130 mbsf.

Holes 1062A and 1062B

Holes 1062A and 1062B, extending from the early Pliocene to the Holocene (see "Biostratigraphy" section, this chapter), show a wide range of calcium carbonate and carbon concentrations. Calcium carbonate values range from ~1 wt% at 121.8 mbsf to 57 wt% at 85.0 mbsf, and average 20 wt%, which is surprisingly high for such a great depth (4700 m). This observation is consistent with the abundance of nannofossils in some of the layers of Hole 1062A (see "Biostratigraphy" and "Lithostratigraphy" sections, this chapter). TOC concentrations range from 0.1 wt% at 34.6 mbsf to 1.7 wt% at 1.0 mbsf, and average 0.6 wt%, which is comparable to those measured at Sites 1060 and 1061. Two depth zones with distinct calcium carbonate distributions can be distinguished.

The first zone, 0–95 mbsf, is characterized by highly variable calcium carbonate concentrations. The occurrence of carbonate-rich events of possible turbidite origin (Fig. 76; see also "Lithostratigraphy" section, this chapter) is clearly expressed in magnetic susceptibility and paleontological data. Although some of these events may explain high carbonate values (>50 wt%) measured in the sediments, such as in the intervals interpreted to be MISs 15 and 17, turbidite deposition does not explain all the carbonate content variability. For example, interglacial periods such as MISs 5, 7, and 9 record carbonate levels higher than 40 wt%. Hole 1062A also presents a peculiar carbonate deposition pattern in glacial MISs 6 and 8, where, as opposed to Sites 1060 and 1061, $CaCO_3$ reaches values higher than 25 wt%. These two events have been confirmed by color reflectance and paleontological data (see "Lithostratigraphy" and "Biostratigraphy"

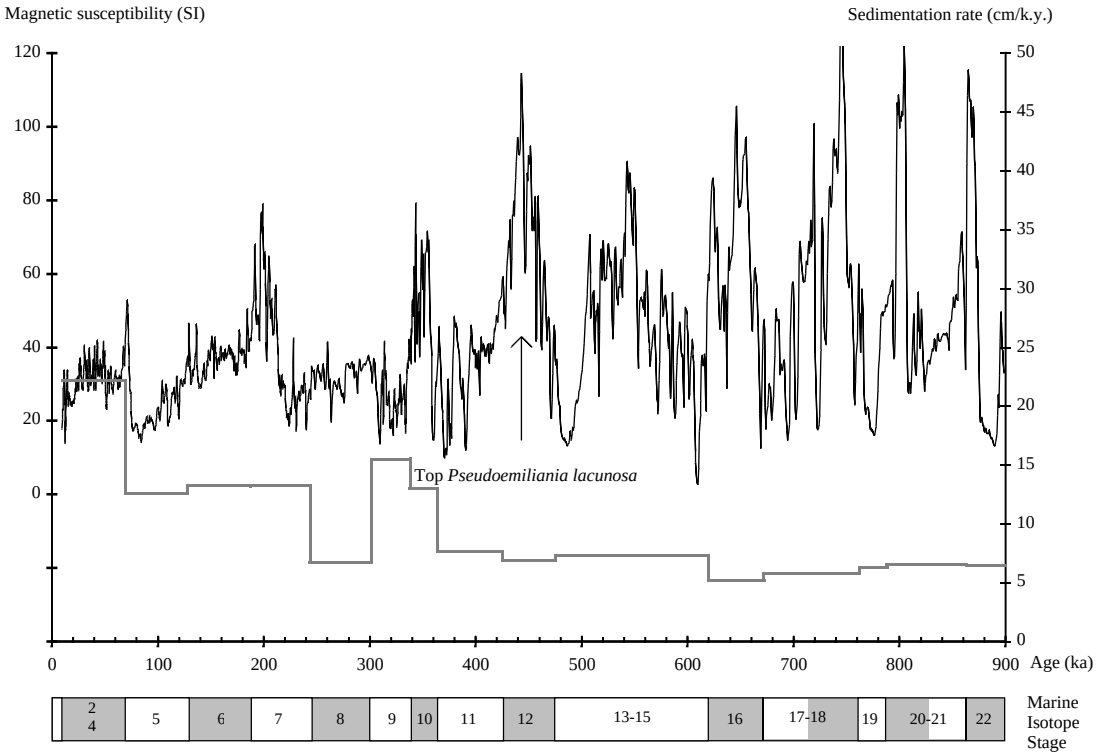

Figure 68. Magnetic susceptibility record (left scale, thin curve) and sedimentation rate (right scale, thick stepwise curve; composite record) of West Site 1062 (28°14′N, 74°25′W, 4775 m). The MISs are indicated, with the glacial ones shaded.

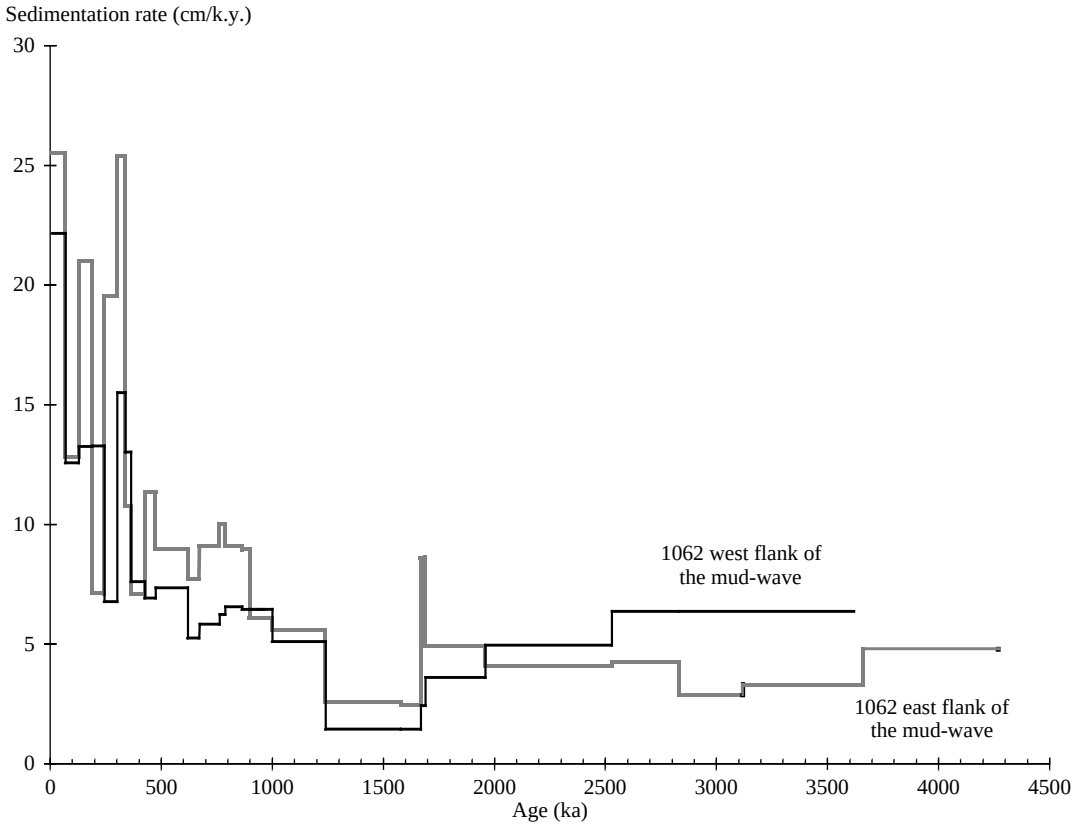

Figure 69. Comparison in the evolution of the sedimentation rates between East Site 1062 and West Site 1062.

Table 37. Estimated ages, concentrations, and accumulation rates of calcium carbonate at Site 1062.

Age (ka)	$CaCO_3$ content (wt%)	$CaCO_3$ MAR ($g/cm^2/k.y.$)
11.10	32.10	5.99
13.34	11.45	1.60
30.02	13.57	2.15
41.74	12.89	1.89
59.82	9.84	1.56
70.05	4.12	0.33
112.88	40.30	3.67
133.14	17.38	3.14
151.02	10.93	1.94
173.65	27.90	4.52
185.11	9.21	1.39
197.37	10.74	0.51
244.98	44.66	8.32
260.44	3.45	0.43
286.08	36.90	5.94
309.48	46.07	10.47
319.22	4.46	0.87
335.89	11.05	2.63
355.64	4.56	0.46
397.73	12.75	0.84
426.61	21.35	2.52
454.60	1.47	0.16
480.53	7.43	0.67
530.59	42.12	4.01
575.46	15.96	1.45
598.73	49.56	4.57
623.73	26.70	2.23
661.35	5.92	0.48
710.17	56.69	5.67
750.35	4.93	1.43
766.76	28.35	3.01
805.89	2.77	0.28
862.68	2.36	0.23
894.16	5.26	0.51
929.94	33.22	2.24
968.61	10.17	0.75
1021.19	4.86	0.32
1075.27	16.64	1.09
1156.57	14.41	0.92
1211.91	37.69	2.35
1242.35	1.19	0.03
1417.56	44.29	1.28
1537.05	16.76	0.45
1671.51	17.14	0.43
1733.87	21.66	1.11
1787.47	23.68	0.89
1826.84	40.18	2.03
1940.38	22.44	1.19
2020.73	17.03	0.64
2120.91	19.30	0.69
2279.35	22.73	1.10
2346.00	28.42	1.40
2420.90	26.66	0.74
2504.27	18.62	0.60
2575.16	25.66	1.31
2650.53	11.11	0.57
2677.38	22.10	0.69
2750.16	27.38	1.34
2815.87	8.99	0.46
2882.57	27.02	0.93
3039.23	12.08	0.41
3185.45	5.66	0.22
3281.82	18.28	0.70
3364.24	30.73	1.15
3895.16	7.69	0.48
3995.05	36.00	2.24
4066.67	13.82	0.85
4157.34	10.10	0.60
4261.00	14.03	0.56
4273.98	17.32	0.90

Note: MAR = mass accumulation rate. Estimations based on geochemical measurements at Holes 1061A and 1062B.

sections, this chapter). Higher TOC concentrations correspond to the lower $CaCO_3$ values during most of the interglacial periods.

The second depth zone of distinct carbonate patterns, extending from 95 mbsf in Hole 1062A to 240 mbsf in Hole 1062B, shows an average increase of carbonate and TOC values, although the amplitude of these $CaCO_3$ excursions is not as high as those occurring in the overlying interval. Some of the larger fluctuations are possibly caused by large turbidite events that transported calcareous material from the nearby Bahamas Banks. Abrupt increases in carbonate values coupled with sharp decreases in organic contents, such as those observed between 149 and 153 mbsf, may be indicative of turbidite deposition.

Discussion

The major factors leading to sharp calcium carbonate variations at Sites 1061 and 1062 above the reentrance of medium *Gephyrocapsa* spp. (~1 Ma), as well as those observed in sediments from Site 1060, are assumed to be identical to those controlling carbonate variability in recent deep-sea sediments, (i.e., the production rate of calcium carbonate, the production ratio of calcium carbonate to organic matter, the saturation state of deep water masses, and input rates of noncarbonate material).

At each site, calcium carbonate concentrations are higher during interglacial periods, which may be related to increased calcium carbonate production by coccoliths and foraminifers at that time. The poor state of preservation of nannofossils and foraminifers at Sites 1060 and 1061 in glacial periods (see "Biostratigraphy" section, this chapter) suggests that dissolution processes also widely controlled the carbonate content in sediments. In Hole 1060A, carbonate dissolution during glacials may have been caused by increased organic carbon accumulation rates from the overlying productive water layers (Emerson and Bender, 1981). At Site 1061 such an explanation is probable because the organic content of the sediments increases during these intervals. Dissolution processes linked to vertical shifts of the lysocline, however, are also possible (see "Lithostratigraphy" section, this chapter). The fluctuations in carbonate concentrations at Site 1062 may partially be explained by these hypotheses, but not the high average calcium carbonate value (≈20 wt% for the entire hole). Sharp increases in calcium carbonate to more than 40 wt% in both glacial and interglacial stages may better be explained by carbonate inputs deposited by turbidites from the nearby Bahamas Banks. The frequency of these events is not clear from the present data.

Below the reentrance of *Gephyrocapsa* spp., the increase of both carbonate and TOC contents at Sites 1061 and 1062 may indicate better preservation conditions, a decrease in marine productivity, and/or an increase in terrigenous inputs. A similar conclusion has already been inferred from preliminary results at Sites 1056–1059. This general trend may be altered by intense (or frequent) turbidite events in Holes 1062A and 1062B.

Organic Matter Source Characterization

Elemental Analyses

Higher terrestrial plants contain significantly more carbon relative to nitrogen than do marine organisms. Nitrogen is usually found within proteinaceous material, but terrestrial plants require carbon-rich compounds such as cellulose and lignin to provide structural rigidity. Thus, C/N can be used as an indicator of organic matter provenance. Average C/N values of marine zooplankton and phytoplankton tend to lie between 5 and 8, whereas land plants have ratios between 20 and 200 (Emerson and Hedges, 1988).

C/N values of most of the samples range from 3 to 12 in Holes 1060A, 1062A, and 1062B. They show much more variation at Site 1061, where C/N values range from 1.13 at 294 mbsf to 21.69 at 267.5 mbsf. Figures 74–76 show that the lower C/N values are generally associated with the lower TOC concentrations (<0.5 wt%). This is certainly an artifact in sediment with low carbon content because clay minerals tend to absorb ammonium ions during diagenesis (Müller, 1977). C/N ratios are thus not perfect or unequivocal indicators of organic matter provenance. As a consequence, only samples containing more than 0.5 wt% TOC were analyzed for C/N. Results are similar for Sites 1060 and 1062, where C/N values average 6 and 8, respectively. Although C/N values may change during diagenesis and maturation, such values reflect a marine organic matter origin

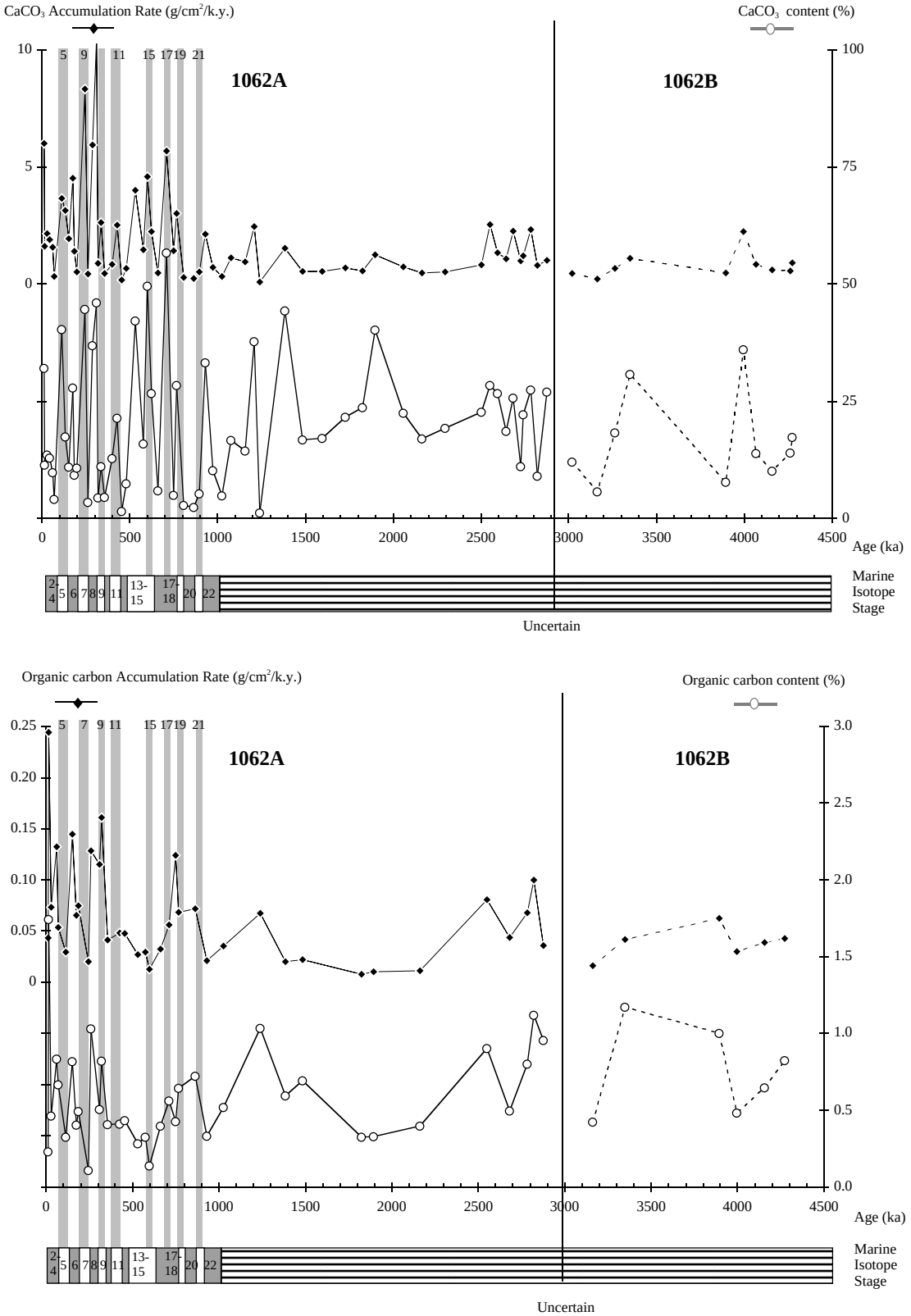

Figure 70. Downhole profiles of organic carbon and calcium carbonate accumulation rates at Site 1062. Shaded columns on the graph indicate interglacial time periods. Striped section of MIS scale = stage assignment uncertain.

(Meyers, 1994). In Hole 1061A, C/N values are slightly higher, averaging 11, which suggests predominant inputs of marine materials with some admixture of terrigenous organics. Also, significant fluctuations in C/N values can be related to variations in organic carbon content. In particular, at Site 1061, where sample frequency is high, higher C/N values correspond to glacial periods. This may indicate the input of high levels of terrigenous material during these time intervals.

Below the reentrance of medium *Gephyrocapsa* spp., C/N values and carbonate and TOC concentrations increase at corresponding depths, which probably indicates an increase in marine and terrigenous input and/or less oxidizing conditions in deep waters. Such patterns are not easily discernible at Site 1062.

Table 38. Estimated ages, concentrations, and accumulation rates of organic carbon at Site 1062.

Age (ka)	C_{org} content (wt%)	C_{org} MAR ($g/cm^2/k.y.$)
11.10	0.23	0.04
13.34	1.74	0.24
30.02	0.46	0.07
59.82	0.83	0.13
70.05	0.67	0.05
112.88	0.33	0.03
151.02	0.82	0.14
173.65	0.41	0.07
185.11	0.49	0.07
244.98	0.11	0.02
260.44	1.03	0.13
309.48	0.51	0.11
319.22	0.82	0.16
355.64	0.41	0.04
426.61	0.41	0.05
454.60	0.43	0.05
530.59	0.28	0.03
575.46	0.32	0.03
598.73	0.14	0.01
661.35	0.40	0.03
710.17	0.56	0.06
750.35	0.43	0.12
766.76	0.64	0.07
862.68	0.72	0.07
929.94	0.33	0.02
1021.19	0.52	0.03
1242.35	1.03	0.03
1417.56	0.59	0.02
1537.05	0.69	0.02
1787.47	0.33	0.01
1826.84	0.33	0.02
2020.73	0.40	0.01
2346.00	0.90	0.04
2575.16	0.50	0.03
2750.16	0.80	0.04
2815.87	1.12	0.06
2882.57	0.95	0.03
3185.45	0.42	0.02
3364.24	1.17	0.04
3895.16	1.00	0.06
3995.05	0.48	0.03
4157.34	0.65	0.04
4273.98	0.82	0.04

Notes: MAR = mass accumulation rate. Estimations based on geochemical measurements at Holes 1061A and 1062B.

Rock-Eval Analyses

T_{max} values (i.e., the temperature values measured when maximum release of hydrocarbons from cracking of kerogen during pyrolysis occurs) of most of the samples are below 435°C, indicating that the organic matter is immature (Table 42). Some shallower samples have T_{max} values >435°C, such as from Hole 1060A at 32.8 mbsf, from Hole 1061A at 12.9 mbsf, and from Hole 1062A at 46.7 mbsf. These anomalous values are probably caused by mineral matrix effects, because organic matter encountered in such shallow sediments cannot have reached temperature and pressure conditions suitable for in situ maturation. Two samples with T_{max} values >435°C and high TOC concentrations are observed in Hole 1061A at 125 and 209 mbsf. However, no relationship between T_{max} and the occurrence of high molecular weight hydrocarbons is evident; deep sediments with significant concentrations of ethane, propane, and *iso*-butane show T_{max} values lower than 400°C. Thus, no thermal maturation of hydrocarbons can be inferred from our data. Van Krevelen–type plots of the Hydrogen Index (HI) and Oxygen Index (OI) values of samples having elevated TOC concentrations (>0.5 wt%) suggest that the sedimentary organic matter of the three holes mostly contains type III land-derived organic matter (Fig. 77). Most of the data plot in a field of low HI (<100 mg HC/g TOC) and high OI (>200 mg CO_2/g TOC). The HI does not vary with depth, and furthermore, no relation seems to exist between HI and TOC concentrations.

This source assignment conflicts with the relatively low C/N values recorded at Sites 1060 and 1062, which indicate a predominance of marine organic material. This is evidence for heavy oxidation of marine organic matter, probably by microbial reworking (Espitalié et al., 1986). In Hole 1061, however, this source assignment better corresponds to high C/N values recorded in samples containing more than 0.5 wt% TOC. This tendency may indicate significant terrigenous inputs and possible calcium carbonate dilution by allochthonous supply of material during glacials. Moreover, terrestrial organic compounds tend to contain complex and refractory compounds that are less prone to degradation than marine organic matter. Strong oxidizing conditions would then alter marine organic matter more than terrestrial organics and would also contribute to higher C/N values during these periods.

Discussion

Sites 1060 and 1062 present the same overall patterns concerning the organic matter characterization, suggesting that high reworking processes and oxidative conditions prevailed near the sediment/water interface. Hole 1061A seems to be affected by terrigenous inputs in

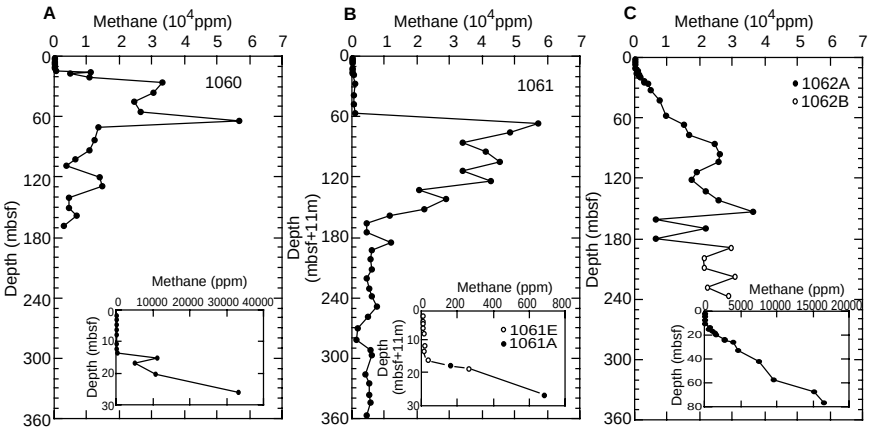

Figure 71. Downhole profile of headspace methane concentrations in (**A**) Hole 1060A, (**B**) Holes 1061A, and 1061E, and (**C**) Holes 1062A and 1062B. Note that in (B) the depth scale is labeled "Depth (mbsf + 11 m)" because mbsf depths had to be corrected for APC overpenetration in Hole 1061A by adding 11 m.

Table 39. Results of headspace gas analyses of sediments from Sites 1060, 1061, and 1062.

Core, section, interval (cm)	Depth (mbsf)	C_1 (ppm)	C_2 (ppm)	C_3 (ppm)	C_1/C_2
172-1060A-					
1H-2, 0-5	1.5	110	ND	ND	—
1H-3, 0-5	3.0	28	ND	ND	—
1H-4, 0-5	4.5	17	ND	ND	—
1H-5, 0-5	6.0	12	ND	ND	—
1H-6, 0-5	7.5	4	ND	ND	—
2H-2, 0-5	10.5	7	ND	ND	—
2H-3, 0-5	12.0	7	ND	ND	—
2H-4, 0-5	13.5	285	ND	ND	—
2H-5, 0-5	15.0	10,974	0.40	ND	27,435
2H-6, 0-5	16.5	4,902	0.20	ND	24,510
3H-2, 0-5	20.0	10,549	0.40	ND	26,373
3H-6, 0-5	26.0	33,062	1.20	0.50	27,552
4H-6, 0-5	35.6	30,334	1.40	0.40	21,667
5H-6, 0-5	45.0	24,189	1.00	ND	24,189
6H-6, 0-5	54.6	26,438	1.20	0.60	22,032
7H-6, 0-5	64.0	56,603	2.72	ND	20,810
8H-4, 0-5	70.6	13,270	0.90	ND	14,744
9H-6, 0-5	83.0	12,002	0.82	ND	14,637
10H-6, 0-5	92.5	10,629	0.89	ND	11,943
11H-6, 0-5	102.0	6,301	0.43	ND	14,653
12H-4, 0-5	108.5	3,704	0.53	ND	6,989
13H-5, 0-5	119.5	13,873	1.16	ND	11,959
14H-5, 0-5	129.0	14,479	1.32	0.43	10,969
15H-6, 0-5	140.0	4,484	0.50	0.30	8,968
16H-6, 0-5	149.5	4,437	0.48	ND	9,244
17H-5, 0-5	157.5	6,781	0.75	ND	9,041
18H-6, 0-5	168.2	2,947	0.43	ND	6,853
172-1061E-					
1H-2, 0-5	1.5	3	ND	ND	—
1H-3, 0-5	3.0	5	ND	ND	—
1H-4, 0-5	3.9	5	ND	ND	—
1H-5, 0-5	5.4	6	ND	ND	—
1H-6, 0-5	6.9	9	ND	ND	—
2H-2, 0-5	10.9	15	ND	ND	—
2H-3, 0-5	12.4	12	ND	ND	—
2H-5, 0-5	15.4	32	ND	ND	—
2H-7, 0-5	18.3	261	ND	ND	—
172-1061A-					
1H-5, 0-5	6.0	159	ND	ND	—
2H-5, 0-5	15.5	683	ND	ND	—
3H-6, 0-5	26.6	495	ND	ND	—
4H-6, 0-5	36.0	238	ND	ND	—
5H-6, 0-5	45.5	838	ND	ND	—
6H-6, 0-5	55.0	57,141	8.00	2.00	7,143
7H-6, 0-5	64.5	48,555	7.00	1.00	6,936
8H-6, 0-5	73.9	33,970	6.00	1.50	5,662
9H-6, 0-5	83.5	41,056	7.00	2.00	5,865
10H-6, 0-5	93.0	45,219	9.00	2.30	5,024
11H-6, 0-5	102.5	33,649	7.00	2.00	4,807
12H-6, 0-5	112.0	42,580	9.00	2.00	4,731
13H-6, 0-5	121.5	20,349	6.00	2.00	3,392
14H-6, 0-5	129.7	28,528	6.00	3.00	4,755
15H-6, 0-5	140.5	22,106	5.40	1.57	4,094
16H-6, 0-5	146.5	11,363	4.00	1.43	2,841
17X-3, 0-5	155.0	4,135	2.25	1.28	1,838
18X-5, 0-5	162.9	4,446	2.50	1.50	1,778
19X-5, 0-5	173.0	11,615	4.50	1.90	2,581
20X-4, 0-5	181.1	6,067	3.80	2.20	1,597
21X-4, 0-5	189.8	5,445	3.00	0.50	1,815
22X-4, 0-5	200.3	5,825	3.45	2.00	1,688
23X-4, 0-5	208.8	4,351	2.90	2.00	1,500
24X-4, 0-5	219.6	5,227	3.20	1.90	1,633
25X-2, 0-5	226.3	5,754	3.30	1.20	1,744
26X-3, 0-5	237.5	7,530	3.70	2.00	2,035
27X-4, 0-5	247.8	4,828	3.00	2.00	1,609
28X-4, 95-100	258.6	1,652	0.70	0.20	2,360
29X-5, 0-5	269.5	1,300	1.00	1.00	1,300
30X-6, 0-5	280.2	5,353	3.00	2.00	1,784
31X-2, 120-125	285.5	5,997	3.00	1.00	1,999
33X-3, 0-5	305.0	4,083	3.00	2.40	1,361
34X-2, 0-5	313.2	5,212	3.11	1.60	1,676
35X-3, 0-5	324.3	5,113	4.96	4.42	1,031
36X-2, 0-5	332.4	5,354	3.20	2.00	1,673
37X-4, 0-5	345.0	4,216	3.48	2.19	1,211
172-1062A-					
1H-2, 0-5	1.5	3	ND	ND	—
2H-2, 0-5	3.7	15	ND	ND	—
2H-4, 0-5	6.7	46	ND	ND	—
2H-6, 0-5	9.7	72	ND	ND	—
3H-2, 0-5	13.2	678	ND	ND	—
3H-3, 0-5	14.7	453	ND	ND	—
3H-4, 0-5	16.2	1,036	ND	ND	—
3H-5, 0-5	17.7	1,275	ND	ND	—
3H-6, 0-5	19.2	1,537	ND	ND	—
4H-2, 0-5	22.7	2,765	ND	ND	—
4H-3, 0-5	24.2	2,649	ND	ND	—
4H-4, 0-5	25.7	3,828	ND	ND	—
5H-2, 0-5	32.2	4,537	ND	ND	—
6H-2, 0-5	41.7	7,380	ND	ND	—
7H-6, 0-5	57.2	9,459	ND	ND	—
8H-6, 0-5	66.7	15,020	1.00	ND	15,020
9H-6, 0-5	76.2	16,509	2.00	ND	8,255
10H-6, 0-5	85.7	24,387	4.00	ND	6,097
11H-6, 0-5	95.2	25,991	5.40	ND	4,813
12H-5, 0-5	103.2	25,611	6.82	ND	3,755
13H-5, 0-5	112.7	18,899	5.41	ND	3,493
14H-4, 0-5	120.7	17,282	5.00	ND	3,456
15H-5, 0-5	131.7	21,632	6.50	0.30	3,328
16H-5, 0-5	140.8	25,738	8.49	ND	3,032
17H-6, 0-5	152.2	36,280	11.50	0.11	3,155
18H-5, 0-5	160.2	6,237	3.00	0.11	2,079
19H-5, 0-5	169.7	21,783	9.43	0.97	2,310
20H-5, 0-5	179.2	6,313	2.93	0.19	2,155
172-1062B-					
21X-6, 0-5	188.7	29,386	22.40	0.51	1,312
22X-6, 0-5	198.4	20,900	9.40	ND	2,223
23X-6, 0-5	208.0	21,218	9.30	ND	2,282
24X-6, 0-5	217.7	30,597	14.00	ND	2,186
25X-6, 0-5	227.3	22,213	12.00	ND	1,851
26X-6, 0-5	236.9	28,191	17.00	0.60	1,658

Notes: ND = not detected. — = not applicable.

glacial periods above the reentrance of *Gephyrocapsa* spp. and during high TOC accumulation periods below this depth.

Summary

Methane concentration data and methane/ethane ratios indicate that gases are produced microbially, despite the significant amounts of higher molecular-weight hydrocarbons that occur in deeper samples of Hole 1061A. The sulfate/methane boundary is significantly deeper in Hole 1062A, indicating a fundamental shift in sulfate reduction processes from the Blake Outer Ridge sites to the Bahama Outer Ridge.

Carbonate fluctuations recognized at each site appear to be correlative with magnetic susceptibility cycles (see "Sedimentation and Mass Accumulation Rates" section, this chapter). Periods with relatively low but uniform values of calcium carbonate occur in Hole 1061A. This general pattern has already been observed at Sites 1056–1059, and the intervals are probably correlative. Below the reentrance of *Gephyrocapsa* spp., both Sites 1061 and 1062 record a significant increase of calcium carbonate, even if turbidite events have altered the lithostratigraphic and temporal record of the latter hole. Dissolution may explain the cyclicity in the uppermost sections of each hole. Low carbonate levels may also be caused by a decrease in calcium carbonate production, increased dissolution, and/or increased terrigenous fluxes. These last two possibilities are consistent with elemental and Rock-Eval analysis data of Site 1061. High carbonate values observed at Site 1062 may be artifacts caused by turbidite events and therefore unrelated to glacial and interglacial cycles.

INORGANIC GEOCHEMISTRY

Interstitial waters were collected and analyzed from 124 whole-round section samples from Sites 1060, 1061, and 1062. Samples were generally collected at a frequency of once per core, but high-resolution samples were also taken with a frequency of once per section in the upper portion of some holes (Table 43). Interstitial water data for the three sites are presented as depth concentration profiles in Figures 78 through 84. The main objectives were to document early diagenetic changes and to locate possible gas hydrate zones.

These three sites possess different interstitial geochemistry because of their different geographical and geological settings. Sites

Table 40. Results of vacutainer gas analyses of sediments from Sites 1060, 1061, and 1062.

Core, section, interval (cm)	Depth (mbsf)	C_1 (ppm)	C_2 (ppm)	C_3 (ppm)	*i*-C_4 (ppm)	*i*-C_5 (ppm)	C_1/C_2
172-1060A-							
8H-2, 6-7	67.6	892,662	184	22.0	ND	ND	4,851
9H-1, 91-92	76.4	906,330	186	22.0	ND	ND	4,873
11H-1, 147-148	96.0	928,390	273	28.0	ND	ND	3,401
12H-4, 24-25	108.7	796,098	167	25.0	ND	ND	4,767
13H-4, 51-52	115.5	846,847	176	29.0	0.1	ND	4,812
14H-3, 81-82	126.8	1,494,492	286	51.3	0.9	ND	5,225
14H-4, 29-30	127.8	880,388	157	26.0	ND	ND	5,608
15H-2, 44-45	134.4	880,388	157	26.0	ND	ND	5,608
16H-3, 57-58	145.6	937,077	168	35.5	0.7	ND	5,578
16H-5, 80-81	148.8	1,289,757	234	52.7	1.6	ND	5,512
17H-6, 117-118	160.2	666,764	107	30.6	ND	ND	6,231
18H-3, 64-65	164.6	932,655	177	44.8	1.3	ND	5,269
18H-4, 114-115	166.3	848,994	151	38.3	0.8	ND	5,622
172-1061A-							
6H-1, 141	48.9	908,858	277	17.0	ND	ND	3,281
7H-1, 104-105	58.0	901,940	308	20.0	ND	ND	2,928
8H-2, 36-37	68.2	924,617	351	25.0	ND	ND	2,634
9H-1, 103-104	77.0	927,310	277	25.0	ND	ND	3,348
10H-4, 54-5	90.5	927,842	399	30.0	ND	ND	2,325
12H-2, 130-131	107.3	942,149	365	30.0	ND	ND	2,581
13H-3, 15-16	117.2	935,915	372	32.0	0.3	ND	2,516
14H-4, 120-121	127.9	942,031	377	37.0	ND	ND	2,499
15H-2, 54-55	135.0	939,222	476	42.0	0.4	ND	1,973
16H-5, 96-97	147.4	864,142	294	42.0	ND	ND	2,939
18X-4, 67-68	162.1	820,652	267	41.0	ND	ND	3,074
19X-5, 37-38	173.4	793,434	270	48.0	1.2	ND	2,939
20X-4, 97-98	182.1	799,275	272	50.0	0.5	ND	2,939
21X-4, 41-42	190.2	849,409	293	56.0	1.0	ND	2,899
22X-4, 33-34	200.6	838,590	148	60.0	1.0	ND	5,666
24X-4, 131-132	220.9	1,140,495	571	125.0	4.0	ND	1,997
25X-3, 110-111	228.9	649,836	325	66.0	1.7	ND	1,999
28X-4, 54-55	258.2	938,288	403	82.0	2.0	ND	2,328
30X-4, 50-51	277.7	929,684	450	86.0	3.0	ND	2,066
31X-3, 50-51	286.3	942,838	393	81.0	1.4	ND	2,399
33X-2, 13-14	303.6	937,125	500	120.0	4.0	3.0	1,874
34X-2, 48-49	313.7	942,760	541	109.2	4.0	ND	1,743
35X-3, 123-124	325.5	815,764	463	137.0	7.3	0.2	1,762
36X-1, 1-2	330.9	868,641	415	115.0	4.0	ND	2,093
37X-1, 57-58	341.1	791,632	414	86.4	2.1	ND	1,914
172-1062A-							
16H-1, 107-108	136.3	750,616	413	13	0.38	ND	1,817
17H-1, 86-87	145.6	624,781	301	11	ND	ND	2,076
18H-3, 6-7	157.3	768,224	370	14	1.5	ND	2,076

Note: ND = not detected.

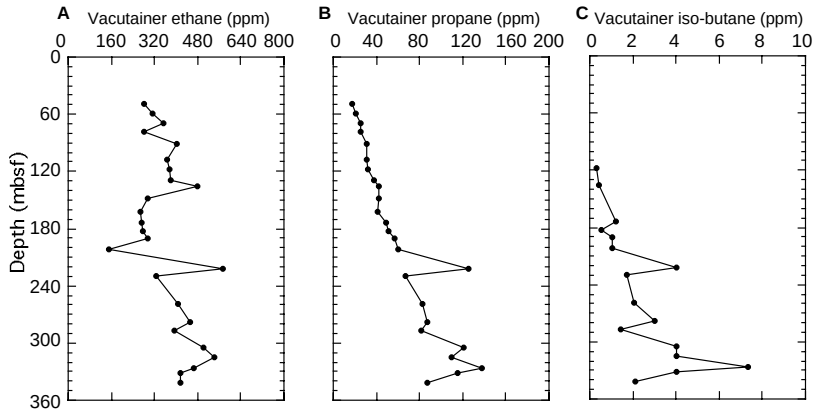

Figure 72. Downhole concentration profiles of (**A**) ethane, (**B**) propane, and (**C**) *iso*-butane of Hole 1061A.

1060 and 1061 are located on the deeper portion of the Blake Outer Ridge in water depths of 3492 and 4040 m, respectively. Site 1062 is situated about 400 m downslope and west of the crest of the Bahama Outer Ridge in water depth of 4775 m.

Early Diagenesis Associated with Organic Matter Decomposition

Interstitial water sulfate, alkalinity, ammonium, and phosphate are related to microbial decomposition of sedimentary organic matter during early diagenesis. The depth to the sulfate/methane interface is 15, 18, and 70 mbsf at Sites 1060, 1061, and 1062, respectively (Figs. 78–80). The sulfate reduction zone thus thickens by ~50 m from the Blake Outer Ridge sites to the Bahama Outer Ridge site. Moreover, the sulfate profiles at the Blake Outer Ridge are approximately linear, whereas at Site 1062 the profile displays a distinct, concave-down shape. Headspace methane profiles at Sites 1060 and 1061 show the characteristic reciprocal relationship with sulfate, with methane concentrations starting to rise below the sulfate/methane boundary (Figs. 78, 79). At Site 1062, however, methane levels are anomalously high within the lower portion of the sulfate reduction zone (Fig. 80).

In the shallower sediments, rapid downhole increases in alkalinity are closely linked to microbial sulfate reduction processes. Alkalinity is lowest at Site 1062, reaching about 75% of the values at the Blake

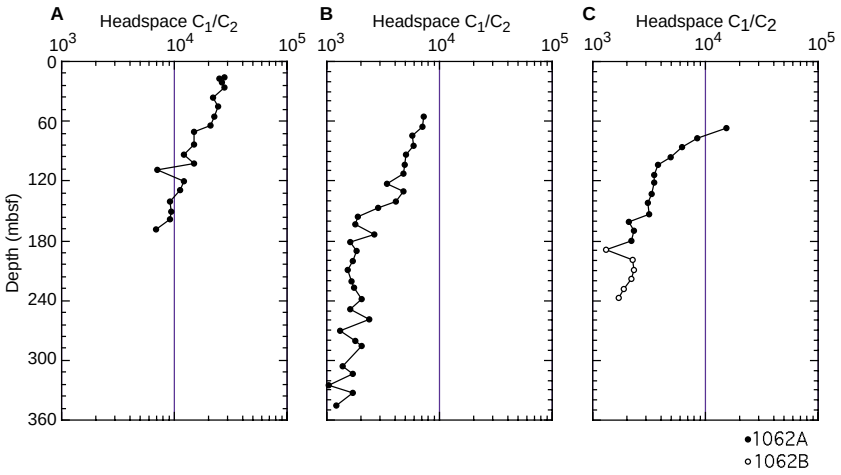

Figure 73. Downhole concentration profiles of headspace methane to ethane (C_1/C_2) ratio of (**A**) Hole 1060A, (**B**) Hole 1061A, and (**C**) Holes 1062A and 1062B.

Table 41. Results of coulometric and elemental analyses from Sites 1060, 1061, and 1062.

Core, section, interval (cm)	Depth (mbsf)	IC (wt%)	$CaCO_3$ (wt%)	TC (wt%)	TOC (wt%)	TN (wt%)	TS (wt%)	C/N
172-1060A-								
1H-1, 20-21	0.2	5.26	43.78	5.75	0.49	0.06	0.48	8.0
1H-3, 35-36	3.4	1.15	9.57	1.93	0.78	0.11	0.67	7.1
1H-6, 56-57	8.1	0.48	3.98	1.12	0.64	0.09	0.78	7.0
2H-1, 122-123	10.2	1.84	15.36					
2H-3, 119-120	13.2	2.05	17.08					
2H-5, 111-112	16.1	1.81	15.05	2.40	0.60	0.08	0.58	7.6
3H-1, 10-12	18.6	1.12	9.33					
3H-3, 34-36	21.8	0.78	6.48	1.41	0.63	0.09	0.63	7.2
3H-5, 36-38	24.9	0.84	6.97					
4H-2, 21-22	29.7	4.97	41.38	5.52	0.55	0.11	0.31	5.0
4H-4, 32-33	32.8	2.92	24.31	3.92	1.00	0.14	0.14	7.2
4H-6, 53-54	36.1	4.34	36.18	4.67	0.33	0.06	0.50	5.2
5H-1, 22-23	37.7	0.81	6.78	1.41	0.60	0.12	0.04	5.0
5H-4, 31-32	42.3	1.65	13.70	2.12	0.48	0.09	0.56	5.4
5H-6, 16-17	45.2	1.77	14.70					
6H-1, 32-33	47.3	1.70	14.15					
6H-3, 47-48	50.5	1.11	9.25	1.71	0.60	0.09	0.63	6.9
6H-5, 48-49	53.5	2.01	16.73					
7H-1, 113-114	57.6	1.43	11.89	2.19	0.77	0.09	0.64	8.9
7H-3, 59-60	60.1	2.35	19.58					
8H-1, 92-93	63.4	1.73	14.44	2.27	0.54	0.16	0.70	3.4
8H-1, 18-19	66.2	4.89	40.77	5.45	0.55	0.10	0.00	5.5
8H-3, 43-44	69.4	2.80	23.35					
8H-5, 35-36	72.4	1.16	9.65	1.70	0.54	0.08	0.60	6.4
9H-1, 34-35	75.8	0.87	7.23					
9H-4, 35-36	80.4	5.99	49.86	6.42	0.44	0.12	0.13	3.6
9H-5, 85-86	82.4	1.68	14.00	2.28	0.60	0.08	0.61	7.3
10H-1, 122-123	86.2	2.55	21.26					
10H-3, 107-108	89.1	0.93	7.73	1.43	0.50	0.10	0.66	5.2
10H-5, 101-102	92.0	1.56	13.02					
11H-2, 50-51	96.5	1.06	8.81					
11H-4, 34-35	99.3	3.23	26.88	3.75	0.53	0.09	0.54	5.7
11H-6, 126-127	103.3	4.96	41.33	5.53	0.57	0.11	0.05	5.2
12H-2, 82-83	106.3	0.96	8.03	1.60	0.63	0.10	0.73	6.3
12H-4, 82-83	109.3	1.05	8.73					
12H-6, 68-69	111.7	1.74	14.48					
13H-1, 57-58	114.1	1.18	9.81	1.87				
15H-2, 93-94	134.9	0.88	7.31	1.45	0.57	0.10	0.66	5.6
15H-3, 64-65	136.1	0.93	7.74					
16H-2, 33-34	143.8	1.00	8.30	1.59	0.59	0.10	0.68	5.7
16H-4, 33-34	146.8	4.00	33.30	4.73	0.73	0.11	0.08	6.7
16H-6, 51-52	150.0	1.55	12.94					
17H-2, 42-43	153.4	1.32	11.00					
17H-5, 96-97	158.5	1.06	8.85	1.43	0.37	0.08	0.62	4.6
17H-6, 22-23	159.2	1.37	11.39					
18H-2, 33-34	162.8	2.37	19.75	2.92	0.55	0.10	0.60	5.8
18H-4, 53-54	165.7	3.81	31.71	6.20	1.12	0.17	1.04	6.6
172-1061A-								
1H-2, 37-38	1.9	2.59	21.58	3.06	0.47	0.05	0.13	9.18
1H-5, 84-85	6.8	3.80	31.64	3.89	0.09	0.05	0.11	1.80
1H-6, 24-25	7.7	1.88	15.68	2.38	0.50	0.07	0.00	7.14
2H-1, 26-27	9.8	0.87	7.27					
2H-3, 35-36	12.9	0.89	7.43	1.74	0.85	0.07	0.00	11.53
2H-5, 55-56	16.1	0.95	7.88	1.48	0.53	0.08	0.13	6.63
3H-1, 43-44	19.4	2.37	19.73	3.33	0.96	0.11	0.00	8.73
3H-3, 101-102	23.0	2.29	19.11					
3H-5, 95-96	26.0	1.00	8.30	1.65	0.66	0.06	0.00	11.51
4H-1, 32-33	28.8	1.58	13.12					
4H-3, 30-31	31.8	1.35	11.25	2.80	1.45	0.09	0.26	16.11
4H-5, 34-35	34.8	1.41	11.72					
5H-1, 26-27	38.3	3.36	27.96	3.68	0.32	0.05	0.00	5.93

Table 41 (continued).

Core, section, interval (cm)	Depth (mbsf)	IC (wt%)	$CaCO_3$ (wt%)	TC (wt%)	TOC (wt%)	TN (wt%)	TS (wt%)	C/N
5H-3, 43-44	41.4	1.35	11.26	2.01	0.65	0.07	0.00	9.29
5H-5, 27-28	44.3	1.03	8.55	1.78	0.75	0.09	0.00	8.33
6H-1, 54-55	48.0	2.09	17.43					
6H-4, 54-55	52.5	3.89	32.37	4.34	0.46	0.05	0.06	9.36
6H-6, 22-23	55.2	2.79	23.27	3.25	0.45	0.06	0.00	7.50
7H-1, 94-95	57.9	0.58	4.83	1.33	0.75	0.09	0.00	8.33
7H-4, 22-23	61.7	0.68	5.62					
7H-5, 91-92	63.9	1.32	10.95	2.31	1.00	0.07	0.12	13.49
8H-1, 111-112	67.6	4.15	34.60	4.76	0.61	0.05	0.00	12.32
8H-3, 100-101	70.4	1.22	10.15					
8H-5, 117-118	73.5	1.25	10.40	1.77	0.52	0.08	0.00	6.50
9H-1, 99-100	77.0	1.26	10.47	2.08	0.82	0.06	0.00	13.08
9H-3, 110-111	80.1	0.76	6.33	1.45	0.69	0.09	0.00	7.67
9H-5, 108-109	83.1	0.79	6.56					
10H-1, 91-92	86.4	6.12	50.97	6.79	0.67	0.03	0.00	20.68
10H-4, 58-59	90.6	1.42	11.86					
10H-6, 11-12	93.1	0.45	3.72	1.28	0.83	0.08	0.00	10.38
11H-1, 58-59	95.6	1.84	15.29					
11H-3, 53-54	98.5	1.17	9.73	1.77	0.61	0.05	0.41	12.83
11H-5, 47-48	101.5	2.16	18.03	2.89	0.73	0.09	0.00	8.11
12H-1, 91-92	105.4	1.09	9.06	2.21	1.12	0.10	0.00	11.20
12H-2, 27-28	106.3	4.72	39.31	5.12	0.40	0.03	0.00	15.81
12H-2, 54-55	106.5	6.41	53.38					
12H-3, 99-100	108.5	1.59	13.27					
12H-5, 102-103	111.5	2.09	17.42	2.86	0.77	0.08	0.00	9.63
13H-1, 48-49	114.5	1.78	14.79					
13H-3, 122-123	118.2	1.12	9.33	1.63	0.51	0.07	0.46	7.66
13H-5, 97-98	121.0	1.83	15.23	2.56	0.73	0.08	0.00	9.13
14H-1, 108-109	124.6	0.82	6.86					
14H-3, 8-9	125.8	0.75	6.24					
14H-5, 25-26	128.5	0.50	4.14	1.35	0.85	0.08	0.11	10.11
15H-1, 98-99	134.0	1.14	9.47					
15H-3, 50-51	136.5	0.85	7.10					
15H-6, 25-26	140.8	1.60	13.35	1.87	0.27	0.07	0.00	3.86
16H-1, 34-35	142.8	1.17	9.70	1.53	0.37	0.05	0.00	7.25
16H-4, 19-20	145.3	1.77	14.76	1.84	0.07	0.06	0.00	1.17
16H-6, 26-27	148.2	0.49	4.04	1.25	0.76	0.09	0.09	8.44
17X-1, 50-51	152.5	0.90	7.53					
17X-3, 25-26	155.3	0.71	5.91	1.19	0.48	0.08	0.03	6.36
17X-4, 24-25	156.7	0.60	5.01					
18X-2, 98-99	159.4	1.61	13.43	1.84	0.23	0.16	0.00	1.44
18X-5, 111-112	164.0	0.75	6.26					
19X-1, 14-15	167.1	0.80	6.66	1.43	0.63	0.08	0.09	7.78
19X-3, 34-35	170.3	0.76	6.34					
19X-5, 56-57	173.6	3.53	29.37	3.65	0.12	0.05	0.00	2.40
20X-1, 32-33	176.9	0.65	5.44					
20X-3, 97-98	180.6	0.91	7.59	1.20	0.29	0.04	0.00	7.21
20X-5, 57-58	183.2	1.18	9.85					
21X-1, 34-35	186.5	0.41	3.42	1.24	0.82	0.08	0.08	10.25
21X-3, 50-51	188.8	1.04	8.68					
21X-5, 59-60	191.8	0.87	7.22	1.28	0.41	0.03	0.00	14.15
22X-2, 16-17	197.5	0.74	6.18					
22X-5, 47-48	202.3	0.36	2.98	0.47	0.11	0.06	0.00	1.83
23X-3, 47-48	207.8	0.86	7.13					
23X-4, 19-20	209.0	0.51	4.27	1.78	1.27	0.07	0.00	18.41
23X-5, 97-98	211.3	1.45	12.11	1.85	0.40	0.10	0.00	4.00
24X-2, 15-16	216.8	0.76	6.34					
24X-4, 21-22	219.8	0.46	3.79					
24X-4, 108-109	220.7	1.08	9.03	1.95	0.86	0.08	0.00	10.96
25X-1, 33-34	225.1	1.88	15.67					
25X-3, 13-14	227.9	1.26	10.46					
26X-2, 63-64	236.6	1.60	13.29					
26X-4, 21-22	239.2	2.24	18.62	3.06	0.83	0.04	0.05	19.60
27X-2, 39-41	245.2	1.23	10.26					
27X-4, 18-20	248.0	1.22	10.18					
28X-3, 86-87	257.0	2.86	23.85	3.53	0.66	0.05	0.10	13.31
28X-4, 54-55	258.2	3.76	31.32	4.33	0.57	0.03	0.00	17.69
28X-5, 25-26	259.2	1.26	10.52	1.62	0.36	0.08	0.15	4.50
29X-1, 112-113	264.6	2.04	16.98					
29X-3, 102-103	267.5	4.30	35.83	4.89	0.59	0.03	0.00	21.69
29X-5, 133-134	270.8	0.90	7.53	1.35	0.45	0.06	0.10	7.30
30X-1, 41-42	273.6	2.53	21.07					
30X-3, 64-65	276.3	0.61	5.06	1.05	0.44	0.08	0.00	5.50
30X-5, 67-68	279.3	1.40	11.64					
31X-1, 50-51	286.7	1.19	27.23	2.00	0.81	0.08	0.42	10.13
31X-3, 86-87	294.6	3.27	9.93	3.36	0.09	0.08	0.00	1.13
33X-1, 47-48	302.5	1.42	11.83	1.77	0.35	0.08	0.00	4.38
33X-3, 73-74	305.7	0.76	6.36					
33X-4, 69-70	307.2	0.72	5.98	1.27	0.55	0.08	0.00	6.55
34X-1, 71-72	312.4	0.83	6.95					
34X-2, 44-45	313.6	2.72	22.62	2.76	0.50	0.06	0.00	8.33
35X-1, 53-54	321.8	0.85	7.04					
35X-3, 72-73	325.0	1.23	10.20	1.72	0.50	0.06	0.00	7.99
36X-1, 21-22	331.1	1.06	8.80					
36X-3, 51-52	334.4	0.23	1.95	0.58	0.35	0.09	0.43	3.89
36X-5, 53-54	337.0	1.16	9.66	1.91	0.75	0.09	0.58	7.91
37X-2, 45-46	342.5	2.16	17.98					
37X-3, 51-52	344.0	2.32	19.33					
37X-4, 45-46	345.5	1.39	11.54	2.38	0.99	0.10	0.63	10.21

Table 41 (continued).

Core, section, interval (cm)	Depth (mbsf)	IC (wt%)	$CaCO_3$ (wt%)	TC (wt%)	TOC (wt%)	TN (wt%)	TS (wt%)	C/N
172-1062A-								
1H-1, 37-38	0.4	3.85	32.10	4.08	0.23	0.06	0.00	3.69
1H-1, 98-99	1.0	1.37	11.45	3.12	1.74	0.12	0.00	14.29
2H-1, 92-93	3.1	1.63	13.57	2.09	0.46	0.08	0.00	6.16
2H-3, 111-112	6.3	1.55	12.89					
2H-6, 107-108	10.8	1.18	9.84	2.01	0.83	0.12	0.08	7.25
3H-1, 75-76	12.5	0.49	4.12	1.16	0.67	0.09	0.05	7.81
3H-4, 119-120	17.4	4.84	40.30	5.16	0.33	0.06	0.00	5.03
3H-7, 20-21	20.9	2.09	17.38					
4H-2, 47-48	23.2	1.31	10.93	2.13	0.82	0.13	0.06	6.18
4H-5, 77-78	28.0	3.35	27.90	3.75	0.41	0.08	0.00	5.11
4H-7, 20-21	30.4	1.11	9.21	1.60	0.49	0.08	0.36	6.10
5H-1, 47-48	31.2	1.29	10.74					
5H-3, 93-94	34.6	5.36	44.66	5.47	0.11	0.06	0.00	1.68
5H-5, 87-88	37.6	0.41	3.45	1.44	1.03	0.12	0.53	8.89
6H-1, 31-32	40.5	4.43	36.90					
6H-4, 31-32	45.0	5.53	46.07	6.04	0.51	0.06	0.00	8.11
6H-5, 48-49	46.7	0.54	4.46	1.35	0.82	0.10	0.00	7.81
7H-1, 111-112	50.8	1.33	11.05					
7H-3, 103-104	53.7	0.55	4.56	0.95	0.41	0.08	0.00	5.09
7H-5, 124-125	56.9	1.53	12.75					
8H-1, 21-22	59.4	2.56	21.35	2.97	0.41	0.08	0.00	5.16
8H-3, 39-41	62.6	0.18	1.47	0.61	0.43	0.08	0.00	5.58
8H-5, 24-26	65.4	0.89	7.43					
9H-1, 121-122	69.9	5.06	42.12	5.34	0.28	0.06	0.00	4.71
9H-4, 102-103	74.2	1.92	15.96	2.24	0.32	0.05	0.00	6.02
9H-6, 33-34	76.5	5.95	49.56	6.09	0.14	0.05	0.00	2.53
10H-1, 86-87	79.1	3.21	26.70					
10H-3, 87-88	82.1	0.71	5.92	1.11	0.40	0.07	0.00	5.75
10H-5, 78-79	85.0	6.81	56.69	7.37	0.56	0.05	0.00	10.46
11H-1, 91-92	88.6	0.59	4.93	1.02	0.43	0.08	0.18	5.70
11H-3, 57-58	91.3	3.40	28.35	4.05	0.64	0.09	0.00	7.38
11H-5, 52-53	94.2	0.33	2.77					
12H-2, 43-44	99.1	0.28	2.36	1.00	0.72	0.10	0.00	7.54
12H-4, 44-45	102.1	0.63	5.26					
12H-5, 125-126	104.5	3.99	33.22					
14H-4, 107-108	121.8	0.14	1.19	1.18	1.03	0.08	0.00	12.67
15H-1, 44-45	126.1	5.32	44.29	5.91	0.59	0.05	0.00	12.49
15H-3, 47-48	129.2	2.01	16.76	2.70	0.69	0.10	0.00	6.92
15H-5, 89-90	132.6	2.06	17.14					
16H-1, 84-85	136.0	2.60	21.66					
16H-3, 78-79	139.0	2.84	23.68	3.17	0.33	0.07	0.19	4.84
16H-5, 34-35	141.1	4.82	40.18	5.15	0.33	0.05	0.00	6.18
17H-1, 48-49	145.2	2.69	22.44					
17H-3, 68-69	148.4	2.05	17.03	2.44	0.40	0.09	0.00	4.41
17H-6, 17-18	152.4	2.32	19.30					
18H-2, 98-99	156.7	2.73	22.73					
18H-4, 77-78	159.5	3.41	28.42	4.32	0.90	0.09	0.25	9.62
18H-6, 95-96	162.7	3.20	26.66					
19H-2, 99-100	166.2	2.24	18.62					
19H-4, 100-101	169.2	3.08	25.66	3.58	0.50	0.09	0.20	5.65
19H-6, 120-121	172.4	1.33	11.11					
20H-1, 34-35	173.5	2.65	22.10					
20H-3, 43-44	176.6	3.29	27.38	4.09	0.80	0.10	0.16	8.41
20H-5, 22-23	179.4	1.08	8.99	2.20	1.12	0.15	0.80	7.71
18X-1, 107-108	157.8	3.29	27.36	4.03	0.75	0.11	0.20	6.77
18X-3, 98-99	160.7	1.19	9.91	1.56	0.37	0.07	0.20	5.62
19X-1, 108-109	163.2	3.03	25.21					
19X-3, 97-98	166.1	2.83	23.55	3.90	1.08	0.11	0.78	9.83
19X-5, 91-92	169.0	1.83	15.25					
20X-3, 36-37	175.1	1.73	14.39					
20X-4, 97-98	177.2	1.58	13.19					
20X-6, 47-48	179.7	2.21	18.38	3.04	0.84	0.15	0.61	5.66
21X-1, 33-34	181.6	1.14	9.48					
21X-3, 33-34	184.5	3.24	27.02	4.20	0.95	0.15	0.22	6.49
21X-6, 33-34	189.0	1.45	12.08					
22X-2, 109-110	193.5	0.68	5.66	1.10	0.42	0.10	0.31	4.06
22X-4, 127-128	196.7	2.20	18.28					
22X-6, 99-100	199.4	3.69	30.73	4.86	1.17	0.14	0.62	8.49
25X-1, 58-59	220.4	0.92	7.69	1.92	1.00	0.15	0.43	6.76
25X-4, 85-86	225.2	4.32	36.00	4.81	0.48	0.09	0.00	5.37
25X-6, 127-128	228.6	1.66	13.82					
26X-3, 50-51	232.9	1.21	10.10	1.86	0.65	0.13	0.92	4.96
26X-6, 95-96	237.9	1.68	14.03					
26X-7, 7-8	238.5	2.08	17.32	2.90	0.82	0.14	0.78	6.05

Note: IC = inorganic carbon, TC = total carbon, TOC = total organic carbon, TN = total nitrogen, TS = total sulfur.

Outer Ridge sites (Table 43). Maximum alkalinity values occur at or near the sulfate/methane interface at Sites 1060 (28.6 mM) and 1061 (28.1 mM), whereas at Site 1062 the alkalinity maximum (21.2 mM) occurs within the sulfate reduction zone (Figs. 78–80). Alkalinity generally decreases with depth in the zone of methanogenesis. At Site 1062, however, alkalinity decreases to values less than 8 mM between 121 and 152 mbsf and then increases below this interval.

Ammonium concentrations generally increase with depth, reaching maximum values within the methanogenesis zone (Figs. 78–80; Table 43). At Site 1061, however, the ammonium values reach a maximum of 5.2 mM (180 mbsf) and then decrease downhole to a low of 3.1 mM (324 mbsf). Ammonium gradients are always steeper within the sulfate reduction zone than within the methanogenesis zone (Figs. 78–80). Phosphate values are highest in the sulfate reduc-

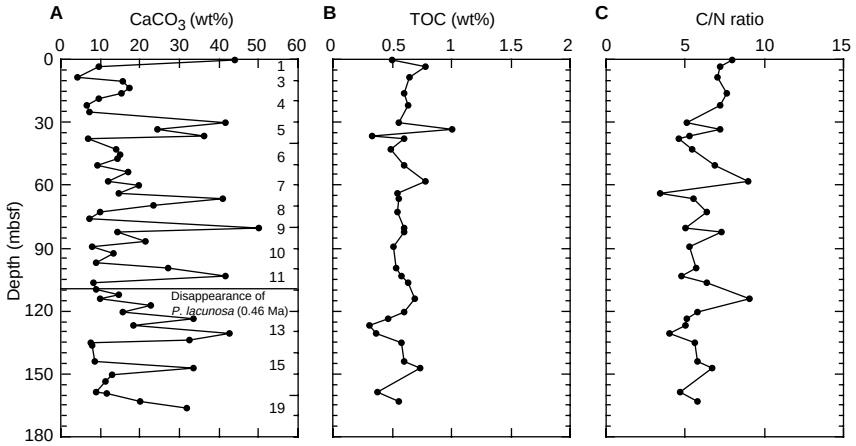

Figure 74. Downhole profile of (**A**) calcium carbonate content, (**B**) total organic carbon content, and (**C**) carbon-to-nitrogen (C/N) ratio of Hole 1060A.

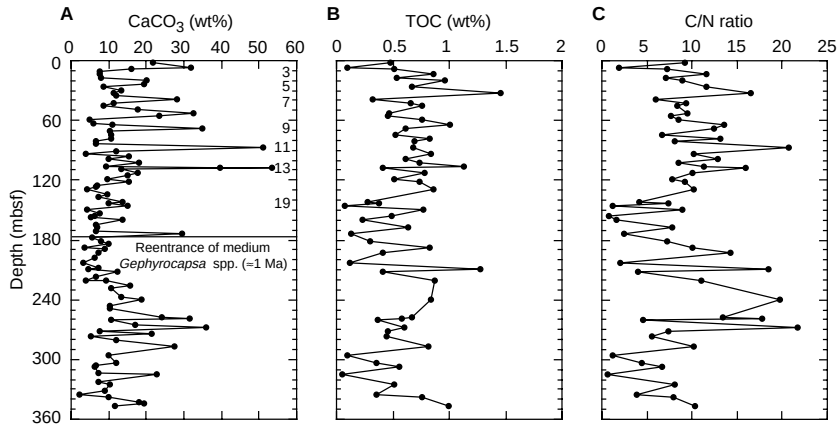

Figure 75. Downhole profile of (**A**) calcium carbonate content, (**B**) total organic carbon content, and (**C**) carbon-to-nitrogen (C/N) ratio of Hole 1061A.

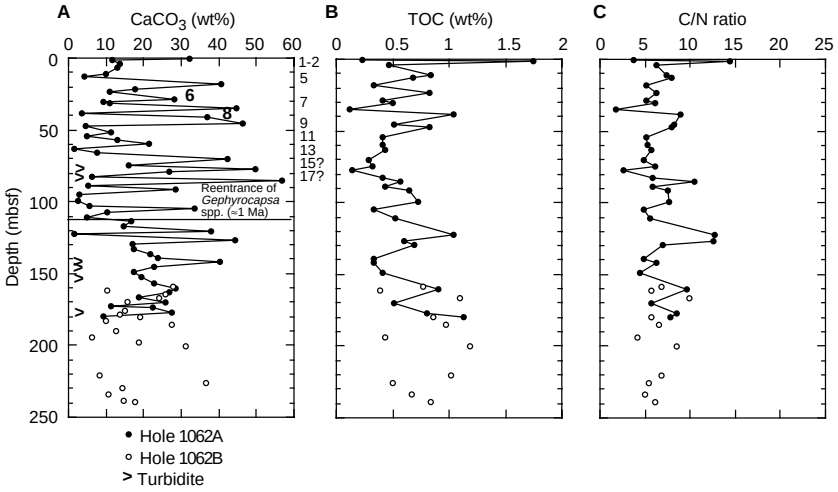

Figure 76. Downhole profile of (**A**) calcium carbonate content, (**B**) total organic carbon content, and (**C**) carbon-to-nitrogen (C/N) ratio of Holes 1062A and 1062B. Numbers along the curve in (A) denote MIS.

tion zone. At Sites 1060 and 1061, maximum phosphate values are found near the sulfate/methane boundary, whereas at Site 1062 the phosphate concentrations peak in the sulfate reduction zone at 32 mbsf (84 µM), about 38 m above the sulfate/methane boundary (Figs. 78–80).

Discussion

The distinct change in the shape of the sulfate profiles indicates a fundamental shift in sulfate reduction processes from the Blake Outer Ridge (Sites 1060 and 1061) to the Bahama Outer Ridge (Site 1062). Borowski et al. (1996) have related linear sulfate profiles, together with shallow sulfate/methane interfaces, to significant upward methane flux. Higher delivery of methane to the sulfate/methane boundary increases the consumption of sulfate by anaerobic methane oxidation ($CH_4 + SO_4^{2-} \rightarrow HCO_3^- + HS^- + H_2O$; Reeburgh, 1976; Hoehler et al., 1994), which in turn induces the diffusion of sulfate from the overlying seawater to the sulfate/methane interface. This diffusion results in linear sulfate concentration profiles and causes a shoaling of the sulfate/methane interface within the sediment. Conversely, when upward methane flux is low, sulfate depletion occurs predominantly by normal sulfate reduction ($SO_4^{2-} + 2CH_2O \rightarrow H_2S + 2HCO_3^-$; e.g., Gieskes, 1981), where interstitial micro-organisms use sulfate to metabolize sedimentary organic matter. In this case, sulfate profiles

Table 42. Results of Rock-Eval analyses from Sites 1060, 1061, and 1062.

Core, section, interval (cm)	Depth (mbsf)	TOC (wt%)	T_{max} (°C)	S_1	S_2	S_3	S_2/S_3	PC	HI	OI	PI
172-1060A-											
1H-3, 35-36	3.4	0.78	375	0.1	0.76	2.04	0.37	0.07	97	261	0.12
3H-3, 34-36	21.8	1.41	417	0.23	1.31	3.30	0.40	0.12	131	330	0.15
4H-4, 32-33	32.9	0.63	438	0.12	0.63	2.01	0.31	0.06	100	319	0.16
7H-1, 113-114	57.6	0.77	394	0.15	0.6	2.48	0.24	0.06	77	322	0.2
12H-2, 82-83	106.3	0.63	392	0.08	0.48	1.87	0.25	0.04	76	296	0.14
13H-1, 57-58	114.1	0.69	383	0.07	0.33	1.66	0.19	0.03	47	240	0.17
18H-4, 53-54	165.7	1.12	375	0.04	0.14	2.32	0.06	0.01	12	207	0.22
172-1061A-											
2H-3, 35-36	12.9	0.85	529	0.11	0.66	2.04	0.32	0.06	77	240	0.14
4H-3, 30-31	31.8	1.45	434	0.06	0.31	1.99	0.16	0.03	21	137	0.17
7H-5, 91-92	63.9	1.00	378	0.14	0.84	2.48	0.34	0.08	84	248	0.14
8H-1, 111-112	67.6	0.61	368	0.07	0.26	2.53	0.10	0.02	42	414	0.22
9H-1, 98-99	77.0	0.82	383	0.09	0.40	1.92	0.21	0.04	48	234	0.19
10H-1, 91-92	86.4	0.67	371	0.05	0.13	2.23	0.06	0.01	19	332	0.28
11H-3, 53-54	98.5	0.61	383	0.06	0.33	1.57	0.21	0.03	54	257	0.16
12H-1, 91-92	104.5	1.12	384	0.11	0.54	2.28	0.24	0.05	48	203	0.17
13H-3, 122-123	118.2	0.51	393	0.05	0.31	1.42	0.22	0.03	60	278	0.14
14H-5, 25-27	125.8	0.85	490	0.12	0.76	1.27	0.60	0.07	89	149	0.14
23X-4, 19-20	209.0	1.27	532	0.06	0.99	1.87	0.53	0.08	77	147	0.06
24X-4, 108-109	220.7	0.86	400	0.13	0.71	2.10	0.34	0.07	82	244	0.15
26X-4, 21-22	239.2	0.83	394	0.09	0.46	1.85	0.25	0.04	55	222	0.17
28X-3, 86-87	257.0	0.66	382	0.08	0.30	1.86	0.16	0.03	45	281	0.21
28X-4, 54-55	258.2	0.57	378	0.04	0.23	1.85	0.12	0.02	40	324	0.15
29X-3, 102-103	267.5	0.59	359	0.06	0.09	2.16	0.04	0.01	15	366	0.43
33X-4, 69-70	307.2	0.55	378	0.05	0.44	1.55	0.28	0.04	80	281	0.10
35X-3, 72-73	325.0	0.50	383	0.06	0.41	1.58	0.26	0.03	82	316	0.13
36X-5, 53-54	337.0	0.75	380	0.10	0.38	1.69	0.22	0.04	50	225	0.21
37X-4, 45-46	345.5	0.99	376	0.18	0.60	2.41	0.25	0.06	60	243	0.23
172-1062A-											
1H-1, 98-99	1.0	1.74	359	0.16	0.28	2.98	0.09	0.03	16	171	0.36
2H-6, 107-108	10.8	0.83	439	0.11	0.34	2.15	0.16	0.03	40	259	0.25
3H-1, 75-76	12.5	0.67	—	0.14	0.87	1.50	0.58	0.08	129	223	0.14
5H-5, 87-88	37.6	1.03	—	0.17	0.93	1.92	0.48	0.09	90	186	0.15
6H-5, 48-49	46.7	0.82	531	0.11	0.58	1.68	0.35	0.05	70	204	0.16
12H-2, 43-44	99.1	0.72	—	0.04	0.72	1.13	0.64	0.06	100	156	0.05
14H-4, 107-108	121.8	1.03	—	0.05	0.93	1.14	0.82	0.08	90	110	0.05
15H-3, 47-48	129.2	0.69	375	0.06	0.24	1.94	0.12	0.02	34	281	0.20
18H-4, 77-78	159.5	0.90	392	0.09	0.44	2.32	0.19	0.04	48	257	0.17
20H-3, 43-44	176.6	0.80	400	0.08	0.49	2.32	0.21	0.04	61	290	0.14
20H-5, 22-23	179.4	1.12	401	0.09	0.60	2.01	0.30	0.05	53	179	0.13
172-1062B-											
19X-3, 97-98	166.1	1.08	402	0.12	0.76	2.33	0.33	0.07	70	215	0.14
20X-6, 47-48	177.2	0.84	405	0.12	0.82	2.24	0.37	0.07	97	266	0.13
25X-4, 58-59	225.2	0.48	409	0.08	0.76	2.00	0.38	0.07	76	200	0.10

Notes: TOC = total organic carbon, PC = petroleum potential, HI = hydrogen index, OI = oxygen index, PI = production index. — = not measured.

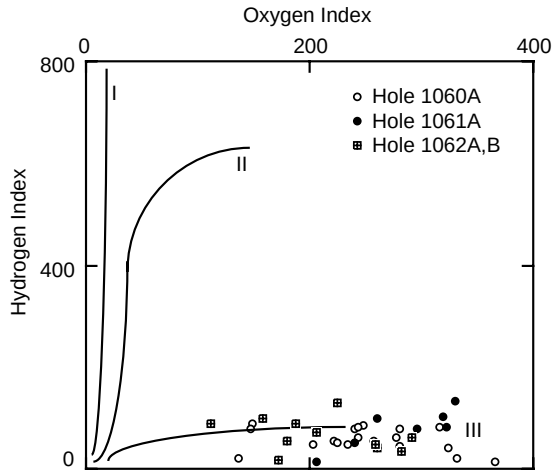

Figure 77. Organic matter properties. Rock-Eval van Krevelen-type diagram of sediment samples from Holes 1060A, 1061A, 1062A, and 1062B. (Hydrogen Index = mg HC/g TOC, Oxygen Index = mg CO_2/g TOC). This plot relates chemical characteristics of organic matter in sediments to origin of organic matter, maturity, and type of hydrocarbon produced. The curves I, II, and III refer to three types of organic matter: type I = algal, oil prone organic matter; type II = marine, oil/gas prone organic matter; and type III = terrestrial, gas prone organic matter.

characteristically display a concave-down, exponential profile (e.g., Berner, 1980).

At Site 1062, the relationship between sulfate and methane is inconsistent with either scenario discussed above. Sulfate reducers and methanogens compete for the same substrates (e.g., Hoehler et al., 1994), so the coexistence of sulfate concentrations above ~1 mM (Martens and Berner, 1974) with significant amounts of methane cannot be explained by in situ microbial production. Nonsteady-state processes may occur here, but other profiles such as calcium, magnesium, and strontium have distinct linearity in the same depth interval where methane displays its anomalously high concentrations, implying diffusive processes and steady-state conditions. Alternatively, upward methane advection may act to deliver increased amounts of methane into the sulfate reduction zone, but other interstitial species show no sign of advective processes. This anomalous occurrence of methane in the sulfate reduction zone at Site 1062 is confounding.

Alkalinity and phosphate all reach their highest values either within the sulfate reduction zone or near the sulfate/methane interface, suggesting that organic matter is remineralized primarily in these zones. At Site 1062, bicarbonate and phosphate production are at their highest entirely within the sulfate reduction zone. The drop in alkalinity within the methanogenesis zone at all three sites is mainly the result of carbonate precipitation (as discussed below under the next heading). The downhole decrease in the phosphate values may be due to its adsorption onto newly crystallizing carbonate mineral surfaces (e.g., Morse and Mackenzie, 1990). In contrast, ammonium continues to increase within the methanogenesis zone, probably as a

Table 43. Interstitial water analyses for Sites 1060, 1061, and 1062.

Core, section, interval (cm)	Depth (mbsf)	pH	Alkalinity (mM)	Salinity	Cl (mM)	SO_4 (mM)	PO_4 (μM)	NH_4 (μM)	Na (mM)	Mg (mM)	Ca (mM)	K (mM)	SiO_2 (μM)	Mn (μM)	Fe (μM)	Sr (μM)
172-1060A-																
1H-1, 145-150	1.45	7.45	6.23	35.0	560	25.3	40	60	482	51.21	9.65	12.55	600	16.5	14.3	76
1H-2, 145-150	2.95	7.63		35.0	560	22.0	43	410	471	50.62	9.22	12.64	742	15.0	13.8	74
1H-3, 145-150	4.45	7.62	12.83	35.0	556	18.6	55	650	476	50.32	8.67	11.67	675	14.0	1.2	72
1H-4, 145-150	5.95	7.69	14.56	34.5	558	15.8	57	920	480	48.53	7.73	11.46	537	12.0	0.8	70
1H-5, 145-150	7.45	7.69	17.49	34.0	553	12.2	53	1260	475	47.16	6.90	11.41	518	10.0	0.5	68
2H-1, 145-150	10.45			33.5	554	3.5	133	2040	450	44.99	5.06	10.75	686	3.5	0.0	61
2H-2, 145-150	11.95	7.82	26.85	33.0	558	1.3	156	2210	481	44.12	4.15	10.01	693	2.0	0.0	60
2H-3, 145-150	13.45	7.89	28.23	33.5	558	0.8	149	2410	481	43.90	3.97	10.72	660	1.5	0.0	60
2H-4, 145-150	14.95	7.69	27.83	33.0	558	0.2	94	2730	483	42.33	3.50	11.75	811	1.5	5.8	58
2H-5, 145-150	16.45	7.33	25.58	33.5	557	0.1	123	2430	478	43.11	3.55	11.06	697	1.5	40.5	60
2H-6, 145-150	17.95	7.38	28.64	33.0	558	0.7	111	2530	485	42.37	3.50	11.06	734	1.5	22.5	59
3H-1, 140-150	19.90	7.70	28.58	33.5	547	0.1	122	2700	473	42.56	3.56	10.69	719	3.0	43.4	59
3H-5, 140-150	25.90	7.82	27.17	33.0	560	0.1	98	2870	489	40.11	3.23	11.80	699	4.0	2.7	58
4H-5, 146-156	35.46	7.36	23.60	32.0	558	0.2	120	2920	488	38.80	2.83	11.10	740		24.9	
5H-5, 144-154	44.94	7.85	23.16	32.5	559	0.2	93	3310	489	38.42	3.12	10.75	701	1.0	15.8	60
6H-5, 149-159	54.49	7.77	23.94	32.5	558	0.2	137	3410	490	37.55	3.28	10.75	775	1.0	9.0	62
7H-5, 140-150	63.90	7.89	24.25	32.5	558	0.0	110	3700	488	38.15	3.38	10.87	794	1.0	16.1	64
8H-3, 150-160	70.50	7.80	23.80	32.5	557	0.3	82	3850	488	37.75	3.46	11.04	783	1.5	7.0	63
9H-5, 140-150	82.90	7.82	21.69	33.5	557	0.0	77	4190	488	36.18	3.19	11.54	792	1.0	4.0	64
10H-5, 140-150	92.40	7.82	20.70	32.5	556	0.0	55	4000	490	34.24	3.50	11.33	669	1.0	2.2	65
11H-5, 140-150	101.90	7.76	19.25	32.0	556	0.0	48	3700	490	33.59	3.19	11.36	731	1.0	2.9	66
12H-5, 140-150	108.4	7.69	18.76	32.0	555	0.2	59	3650	489	33.28	3.76	10.65	595	0.5	1.3	68
13H-5, 140-150	119.4	7.67	19.28	32.0	552	0.0	59	3900	486	33.18	3.90	10.78	846	1.0	18.0	69
14H-5, 140-150	128.90	7.67	18.34	32.0	552	0.1	31	4000	487	31.92	4.02	11.43	760	1.5	2.7	70
15H-5, 140-150	139.90	7.72	16.71	32.0	550	0.2	19	4240	485	31.67	3.96	11.06	658	1.5	0.9	74
16H-5, 140-150	149.40	7.75	16.15	32.0	554	0.0	21	4040	489	30.95	4.15	11.17	677	1.0	0.5	76
17H-4, 140-150	157.40	7.76	14.59	32.0	549	0.2	21	4040	485	29.74	4.19	10.76	563	0.5	2.6	78
18H-5, 140-150	168.10	7.44	15.23	32.0	548	0.3	23	4190	485	30.03	4.67	9.94	550	0.5	1.9	81
172-1061A-																
1H-4, 145-150	5.95	7.59	25.17	33.5	560	0.0	189	2020	481	43.23	3.91	10.29	687	2.0	5.2	63
2H-4, 140-150	15.40	7.42	26.23	33.0	560	0.0	141	2880	484	42.67	3.57	10.25	703	3.0	47.7	62
3H-5, 146-150	26.46	7.50	22.57	32.0	556	0.0	124	3070	482	39.80	3.10	10.62	571	0.5	27.3	62
4H-5, 140-150	35.90	7.56	23.32	32.5	557	0.0	146	3440	485	38.78	3.42	10.57	692	1.0	15.7	63
5H-5, 144-154	45.44	7.55	23.27	32.5	552	0.3	124	4050	480	39.05	3.55	10.75	716	1.0	29.9	64
6H-5, 140-150	54.90	7.52	22.00	32.5	559	0.0	78	3770	488	38.07	3.43	10.41	760	1.0	16.3	65
7H-5, 140-150	64.40	7.72	22.09	32.5	559	0.0	96	4270	489	37.28	3.42	10.66	799	2.5	15.1	66
8H-5, 140-150	73.76	7.65	19.96	32.5	556	0.2	75	4160	488	34.91	3.80	10.71	670	0.5	3.8	68
9H-5, 140-150	83.40	7.78	18.73	32.5	556	0.0	59	3770	487	34.36	3.96	10.61	619	2.0	11.5	70
10H-5, 140-150	92.90	7.73	17.79	32.5	556	0.0	52	3660	489	33.17	4.15	9.75	547	0.5	3.6	71
11H-5, 140-150	102.40	7.55	17.33	32.5	555	0.0	50	3990	488	32.62	4.42	10.42	797	1.5	14.7	71
12H-5, 140-150	111.90	7.77	15.44	32.0	553	0.0	24	4610	486	31.54	4.17	10.82	663	1.5	2.8	70
13H-5, 140-150	121.40	7.65	14.90	32.0	556	0.0	27	4220	490	31.34	4.39	9.61	551	0.5	9.1	73
14H-5, 140-150	129.64	7.75	13.66	32.0	552	0.0	19	4770	485	30.73	4.37	10.13	676	1.0	13.1	71
15H-5, 140-150	140.40	7.65	13.10	32.0	553	0.0	14	3880	488	29.78	4.39	9.97	610	1.0	5.9	74
16H-5, 140-150	147.88	7.71	13.41	32.0	551	0.0	16	4550	485	29.42	5.11	9.95	681	0.5	2.2	77
17X-2, 140-150	154.90	7.75	12.75	32.0	550	0.3	16	4830	486	28.88	5.23	9.40	571	0.5	2.1	79
18X-4, 135-150	162.76	7.60	13.31	32.0	554	0.6	16	4110	490	29.05	5.41	9.75	792	1.0	4.1	80
19X-4, 135-150	172.85	7.55	13.80	32.0	554	0.0	12	4890	487	29.67	6.15	9.46	885	1.0	10.0	82
20X-3, 135-150	180.95	7.52	13.16	32.0	551	0.1	9	5160	485	29.15	5.95	9.54	828	1.5	3.5	82
21X-3, 135-150	189.60	7.60	13.12	32.0	551	0.0	7	4380	486	28.18	6.08	9.20	810	1.0	1.8	84
22X-3, 130-150	200.10	7.61	12.75	32.0	552	0.0	6	4830	486	28.50	6.66	8.70	681	1.0	0.5	84
23X-3, 130-150	208.61	7.65	12.31	32.0	547	0.0	6	3830	480	28.55	7.10	8.02	547	0.5	1.0	87
24X-3,130-150	219.40	7.47	14.36	32.0	552	0.0	6	5050	487	27.93	7.17	8.73	880	1.0	3.0	87
25X-1,125-150	226.05	7.72	10.82	32.0	557	0.0	2	4720	489	27.90	7.12	8.66	795	1.0	1.5	86
26X-2, 125-150	237.25	7.63	10.57	32.0	556	0.0	4	4830	490	27.42	7.16	7.91	749	1.5	4.6	88
27X-3, 125-150	247.53	7.64	9.25	32.0	553	0.0	4	4440	485	27.56	7.10	7.77	652	1.5	1.8	88
28X-4, 100-125	258.66	7.71	6.14	31.5	550	0.0	2	4660	483	26.78	6.45	7.17	413	0.5	1.9	85
29X-4, 125-150	269.25	7.76	5.76	31.5	551	0.0	2	4220	484	27.04	6.43	6.31	238	0.5	0.0	85
30X-5, 125-150	279.92	7.75	5.65	31.0	547	0.0	2	4110	480	26.86	6.67	5.90	288	0.5	6.3	86
31X-2, 125-150	285.55	7.84	4.74	31.0	548	0.0	2	3940	481	26.71	6.30	6.19	257	0.5	0.7	85
33X-2, 120-150	304.70	7.83	6.14	30.5	549	0.0	2	3380	481	27.39	6.76	5.67	255	0.5	0.0	86
34X-1, 120-150	312.90	8.06	6.07	31.5	546	0.0	2	3270	481	26.62	6.56	5.19	205	0.5	0.0	84
35X-2, 130-150	324.10	7.76	6.15	31.0	550	0.0	6	3160	484	26.91	6.25	5.41	268	0.5	0.0	82
36X-1, 130-150	332.20	8.02	5.92	31.0	542	0.0	2	3490	480	26.07	5.43	5.07	216	0.5	0.0	82
37X-3, 120-150	344.70	7.92	6.48	31.5	545	0.1	2	3600	483	26.39	5.40	5.17	231	1.5	0.0	83
172-1061E-																
1H-1, 145-150	1.45			35.0	558	25.2	27	210	608	52.64	10.34	12.75	546	9.5		73
1H-2, 145-150	2.95	7.44	8.14	35.0	558	22.3	64	500	611	52.05	9.90	12.42	712	13.0	45.1	73
1H-3, 85-90	3.85	7.43	9.85	34.0	555	20.5	62	740	606	50.72	9.46	12.32	710	14.5	36.7	71
1H-4, 145-150	5.35	7.85	12.11	34.0	554	18.2	17	910	602	50.13	8.97	12.08	478	14.5	0.3	
1H-5, 145-150	6.85	8.04	15.14	34.0	558	15.3	58	1200	604	48.70	8.52	11.79	516	14.0	4.2	69
1H-6, 145-150	8.35	8.03	17.64	34.0	560	12.2	88	1350	602	47.81	7.80	11.25	620	12.0	0.6	68
2H-1, 145-150	10.85	8.05	21.53	34.0	559	8.2	163	1690	597	46.92	6.37	10.80	747	9.0	0.3	66
2H-2, 145-150	12.35	8.07	23.10	34.0	569	7.0	158	1910	606	46.24	5.80	11.00	755	6.5	0.8	67
2H-3, 145-150	13.85	8.22	25.22	34.0	559	5.0	151	2030	594	45.61	5.59	11.08	710	4.5	0.6	67
2H-4, 145-150	15.35	7.63	23.44	33.5	559	2.7	184	2150	588	44.44	4.89	10.96	813	4.0	6.3	63
2H-5, 132-137	16.72	7.76	26.83	33.5	558	1.1	167	2300	587	43.28	4.06	10.60	751	2.5	4.7	63
2H-6, 145-150	18.22	7.82	28.16	33.5	559	0.5	184	2400	588	43.79	4.14	11.04	744	1.5	4.1	63
172-1062A-																
1H-1, 145-150	1.45	7.48	4.83	35.0	558	27.5	11	12	618	52.13	10.38	12.27	435	9.0	28.9	72
2H-1, 140-150	3.60	7.60	9.13	35.0	559	22.3	55	460	613	50.12	9.03	12.08	691	15.5	54.6	71
2H-2, 140-150	5.10	7.39	10.25	35.0	560	21.8	73	609	614	50.64	8.82	12.00	708	15.0	31.5	71
2H-3, 140-150	6.60	7.56	10.87	35.0	559	20.1	47	729	610	50.00	8.46	12.20	734	13.5	18.8	69
2H-4, 140-150	8.10	7.62	11.85	34.5	560	18.6	46	818	609	49.57	7.86	12.60	699	10.5	10.8	68
2H-5, 140-150	9.60			34.5	560	18.7	64	860		49.55	7.91	12.28	753	12.0		69
2H-6, 140-150	11.10	7.74	13.88	35.0	560	17.2	75	1146	608	48.85	7.69	12.52	794	12.0	4.8	67

Table 43 (continued).

Core, section, interval (cm)	Depth (mbsf)	pH	Alkalinity (mM)	Salinity	Cl (mM)	SO_4 (mM)	PO_4 (µM)	NH_4 (µM)	Na (mM)	Mg (mM)	Ca (mM)	K (mM)	SiO_2 (µM)	Mn (µM)	Fe (µM)	Sr (µM)
3H-1, 140-150	13.10	7.75	13.36	34.5	559	15.5	79		603	48.11	7.11	12.50	779	11.0	4.9	66
3H-2, 140-150	14.60	7.75	14.48	34.5	561	14.6	55	1355	605	48.38	6.44	13.27	805	8.5	15.4	65
3H-3, 140-150	16.10	7.69	15.55	34.0	560	14.0	68	1564	604	47.92	6.89	12.58	833	9.0	22.5	66
3H-4, 140-150	17.60	7.74	15.27	34.0	560	13.5	42	1534	602	47.85	6.05	12.28	740	7.0	13.4	64
3H-5, 140-150	19.10	7.69	16.14	34.0	559	12.3	49	1445	600	47.78	6.35	12.18	678	6.5	34.9	63
3H-6, 140-150	20.60	7.73	16.04	34.0	560	12.2	27	1475	600	47.48	5.86	12.29	596	5.5	13.5	62
4H-1, 140-150	22.60	7.37	17.62	34.0	558	10.5	42	1683	597	46.84	6.01	12.15	628	5.5	18.2	63
4H-2, 140-150	24.10	7.82	17.73	34.0	561	9.6	57	1713	598	46.76	5.93	12.11	639	6.0	26.9	61
4H-3, 140-150	25.60	7.75	18.16	34.0	561	9.1	57	1654	597	46.54	5.76	11.83	682	7.0	12.7	62
4H-4, 140-150	27.10	7.45	18.25	34.0	560	8.8	49	1773	596	45.92	5.62	12.05	742	7.5	4.8	61
4H-5, 140-150	28.60	7.75	19.20	34.0	560	8.6	70	1773	596	45.56	5.72	11.80	824	7.5	10.2	61
4H-6, 140-150	30.10	7.67	19.60	34.0	562	7.5	75	1624	597	45.28	5.73	11.72	878	7.5	9.3	61
5H-1, 140-150	32.10	7.75	20.06	33.5	559	7.6	84	1654	594	45.65	5.64	12.02	863	7.0	2.9	61
5H-2, 140-150	33.60			33.5	559	6.8	55	1922		45.43	5.16	12.18	766	5.0		59
5H-3, 140-150	35.10	7.80	19.37	33.5	558	6.9	59	1743	591	44.94	5.14	11.85	787	4.5	2.2	61
5H-4, 140-150	36.60	7.82	19.99	33.5	558	6.3	59	1982	591	44.01	5.03	11.88	856	4.5	2.4	61
5H-5, 140-150	38.10	7.89	20.11	33.5	557	5.7	70	1982	589	44.99	5.14	11.55	867	4.5	15.1	61
5H-6, 140-150	39.60	7.83	19.65	33.5	556	5.3	47	1743	586	44.30	4.91	11.21	802	4.0	5.4	60
6H-1, 140-150	41.60	7.89	21.19	33.5	565	4.2	60	1743	595	43.44	4.95	11.45	787	4.5	2.3	61
6H-5, 140-150	47.60	7.89	19.61	33.5	561	3.5	51	2042	588	43.36	4.40	11.38	800	3.0	2.5	59
7H-5, 140-150	57.10	7.82	18.81	32.5	559	1.4	33	2131	581	40.97	3.79	10.94	458	2.0	0.3	60
8H-5, 140-150	66.60	7.76	18.53	32.5	559	0.5	36	2071	579	40.06	3.96	9.50	656	3.0	3.9	63
9H-5, 140-150	76.10	7.69	16.19	32.5	557	0.2	18	2131	574	39.98	3.51	8.94	398	1.5	4.0	63
10H-5, 140-150	85.60	7.69	14.88	32.5	558	0.3	14	2191	573	39.47	4.02	8.39	435	2.0	10.9	67
11H-5, 140-150	95.10	7.69	13.15	32.0	558	0.4	12	2191	572	37.97	4.20	7.60	370	1.0	10.5	68
12H-4, 140-150	103.10	7.71	12.63	32.0	555	0.0	11	2071	568	38.28	4.68	6.70	415	2.0	2.3	74
13H-4, 135-150	112.55	7.65	10.88	32.0	555	0.0	7	2250	566	37.61	4.48	6.81	329	1.5	0.4	76
14H-3, 135-150	120.55	7.69	8.70	32.0	556	0.0	5	2370	565	36.66	4.30	7.07	267	0.5	0.5	75
15H-3, 135-150	131.55	7.82	7.73	32.0	553	0.0	5		561	36.01	3.99	7.21	189	0.5	0.2	77
16H-4, 135-150	140.65	7.69	7.57	32.0	556	0.0	1	2698	564	35.20	4.21	7.19	245	0.5	1.7	79
17H-5, 135-150	152.05	7.85	7.75	32.0	553	0.2	1	2668	561	35.63	4.60	7.25	232	0.5	0.5	79
18H-4, 135-150	160.05	7.68	8.32	32.0	552	0.3	3	2907	561	34.43	5.24	7.61	357	1.0	1.4	79
19H-4, 135-150	169.55	7.67	9.18	32.0	551	0.0	3	2638	560	34.82	5.68	7.12	469	1.5	2.1	81
20H-4, 135-150	179.05	7.93	10.58	32.0	551	0.2	3	3235	562	34.38	6.29	8.12	420	1.0	3.7	82
172-1062B-																
20X-4, 120-130	177.40	7.66	8.59	32.5	558	0.1	5	3095	567	34.75	5.85	8.30	420	1.5	2.3	79
21X-5, 130-150	188.48	7.69	9.60	32.0	557	0.4	7	2966	567	35.40	6.54	7.87	445	1.5	2.6	82
22X-5, 130-150	198.20	7.60	8.59	32.0	557	0.9	5	2966	567	35.01	6.18	7.60	404	1.0	1.8	81
23X-5, 140-150	207.90	7.66	10.90	32.0	559	0.0	5	3018	570	35.87	6.89	7.29	301	0.5	3.0	85
24X-5, 130-150	217.50	7.69	9.63	32.0	560	0.2	2	3224	570	34.44	6.79	7.77	284	0.5	1.8	85
25X-5, 125-150	227.05	7.50	10.38	32.0	556	0.4	2	3379	567	34.49	7.13	7.64	344	1.0	1.1	88
26X-5, 125-150	236.65	7.41	12.63	32.0	552	0.2	2	3405	565	35.02	8.67	7.46	437	2.0	1.0	92

Note: Blank values in the table indicate that measurements were not made.

result of microbial fermentation reactions (e.g., Claypool and Kaplan, 1974; Pedersen and Shimmield, 1991). The decrease in ammonium below 280 mbsf at Site 1061 may be caused by reduced levels of organic carbon associated with reduced rates of sedimentation in this interval (see "Organic Geochemistry" and "Biostratigraphy" sections, this chapter) and ammonium adsorption by clay minerals (Rosenfeld, 1979).

Authigenic Precipitation and Dissolution of Minerals

Interstitial calcium, magnesium, and strontium concentrations are sensitive to carbonate formation and dissolution. Rapid downhole decreases in the concentrations of these three elements occur in the sulfate reduction zone at all three sites (Figs. 81–83). Inflection points in the gradients take place at or near the sulfate/methane interface. In the methanogenesis zone, magnesium levels continue to decrease with depth, whereas calcium and strontium concentrations increase. At Site 1061, however, the calcium and strontium values decrease below 247 mbsf (Fig. 82). At Sites 1060 and 1061, similar magnesium concentrations are observed for a given depth, whereas at Site 1062 magnesium levels are ~20% higher within the lower methanogenesis zone.

Iron and manganese are redox-sensitive elements. Therefore, interstitial profiles of these elements are sensitive indicators of redox fronts in a sediment column. Interstitial iron and manganese profiles show enrichments in the upper sulfate reduction zone and, to a lesser extent, in the upper methanogenesis zone (Figs. 81–83). The highest concentration of these elements is found in the top of the sulfate reduction zone at Site 1062. With increasing depth, iron and manganese concentrations decline to low levels in the lower part of the methanogenesis zone.

At all three sites, interstitial potassium concentrations decrease rapidly in the sulfate reduction zone (Figs. 81–83). Potassium concentrations generally decrease with depth in the zone of methanogenesis at Sites 1061 and 1062. At Site 1060, potassium values show high variation in the sulfate reduction zone and near the sulfate/methane boundary, but remain between 10.5 and 11.5 mM in the lower sediment column. In the methanogenesis zone at Site 1061, the potassium profile displays gradually decreasing values below 140 mbsf and a more rapid decline below 240 mbsf. Potassium values at Site 1062 show a sharp downhole decrease below the sulfate/methane boundary to 100 mbsf, and then remain between 7 and 8 mM below this depth.

In general, interstitial silica concentrations display similar profiles to those of potassium at the respective sites (Figs. 81–83). This similarity is especially marked at Site 1062, where silica concentrations are high in the main part of the sulfate reduction zone and decrease to between 200 and 450 µM in the methanogenesis zone. At Site 1061, reduced silica levels (200–300 µM) are observed below 280 m (adjusted depth).

Discussion

Calcium, magnesium, and strontium concentrations decrease with depth in the sulfate reduction zone as a result of diffusion of these ions from overlying seawater into the sediment and their removal by precipitation of carbonate minerals near the sulfate/methane boundary. At all sites, carbonates are probably forming at the sulfate/meth-

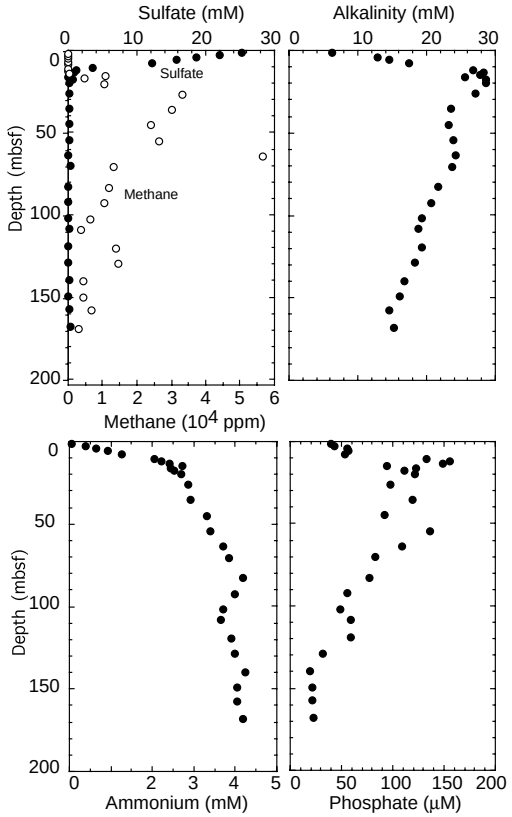

Figure 78. Concentration vs. depth profiles for interstitial waters at Site 1060.

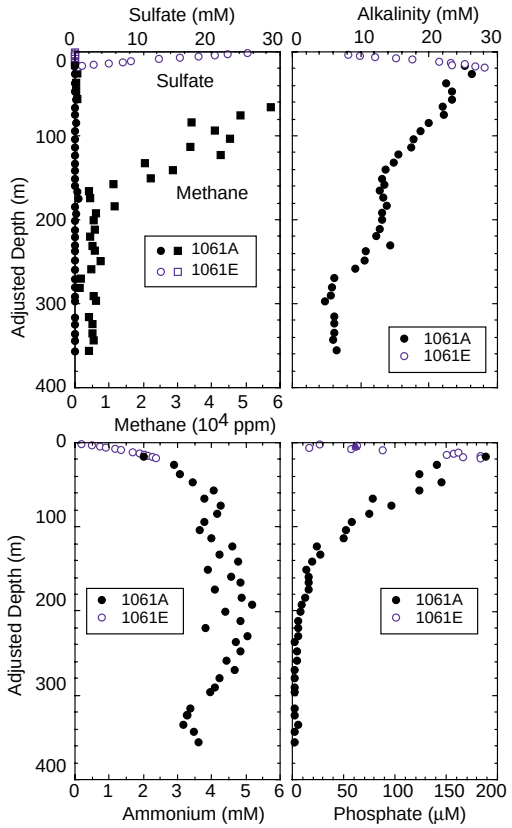

Figure 79. Concentration vs. depth profiles for interstitial waters at Site 1061. Note the depth scale is labeled Adjusted Depth because 11 m was added to mbsf depths of Hole 1061A to correct for overpenetration of the APC.

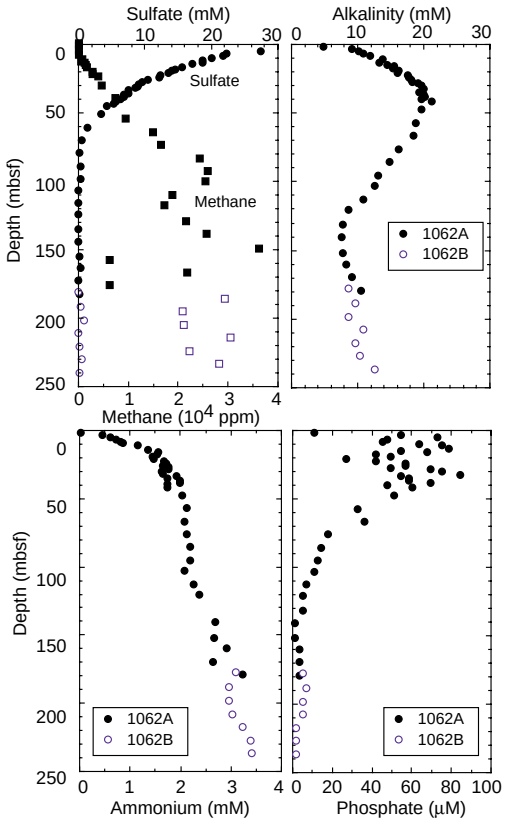

Figure 80. Concentration vs. depth profiles for interstitial waters at Site 1062.

ane interface, where inflection points in the concentration gradients of all three elements occur, and where alkalinity decreases as well. Similar profiles have been observed elsewhere on the Blake Outer Ridge (see "Inorganic Geochemistry" sections, "Carolina Slope" and "Intermediate Depth Blake Outer Ridge" chapters, this volume; Paull, Matsumoto, Wallace, et al., 1996). Downhole increases in interstitial calcium and strontium in the methanogenesis zone indicate recrystallization of carbonate minerals (probably biogenic) and preferred release of calcium and strontium to the pore waters. Depletion of magnesium with depth within the methanogenesis zone suggests dolomite formation.

Reduced iron concentrations in parts of the zone of sulfate reduction at Sites 1060, 1061, and 1062 indicate the authigenic formation of iron sulfides. Low levels of interstitial iron and manganese within the methanogenesis zone are consistent with their incorporation into newly forming carbonate minerals such as ankerite and siderite. These conclusions are supported by the common presence of dolomite (and/or ankerite), pyrite, and low amounts of siderite in these sediments, as determined by the XRD analysis of bulk samples (see "Lithostratigraphy" section, this chapter). Presumably, more magnesium-bearing carbonates are forming at Sites 1060 and 1061 than at Site 1062 because magnesium concentrations at depth are higher at Site 1062.

At the Carolina Slope and intermediate-water depth sites on the Blake Outer Ridge, potassium and silica concentrations increase downhole. Presumably, the increase in interstitial potassium is caused by replacement of potassium ions residing within clay-mineral exchange sites by ammonium ions (e.g., Rosenfeld, 1979; Mackin and Aller, 1984). Increases in silica are probably caused by increased alkalinity (see "Inorganic Geochemistry" sections, "Carolina Slope" and "Intermediate Depth Blake Outer Ridge" chapters, this volume). At the deep-water sites (Sites 1060, 1061, and 1062), however, potassium and silica generally decrease downhole. Ion-exchange reactions involving potassium may not be as important here because of lower ammonium concentrations at the deep-water sites. In addition, alka-

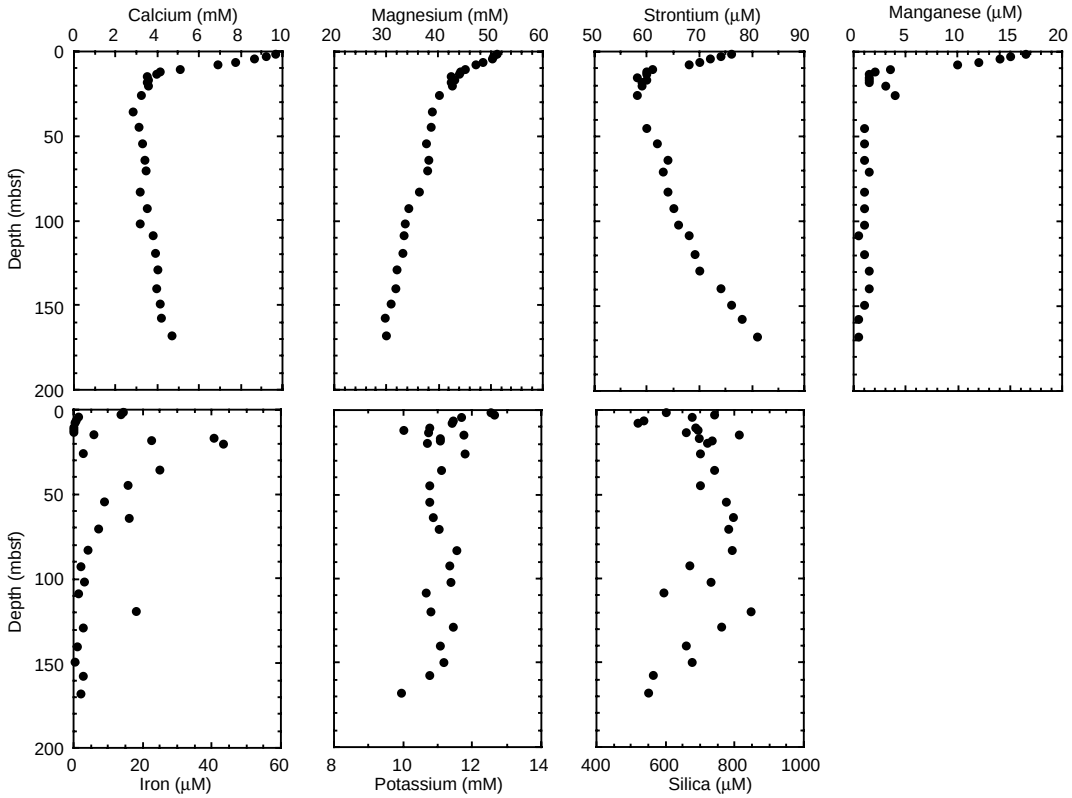

Figure 81. Concentration vs. depth profiles for interstitial waters at Site 1060.

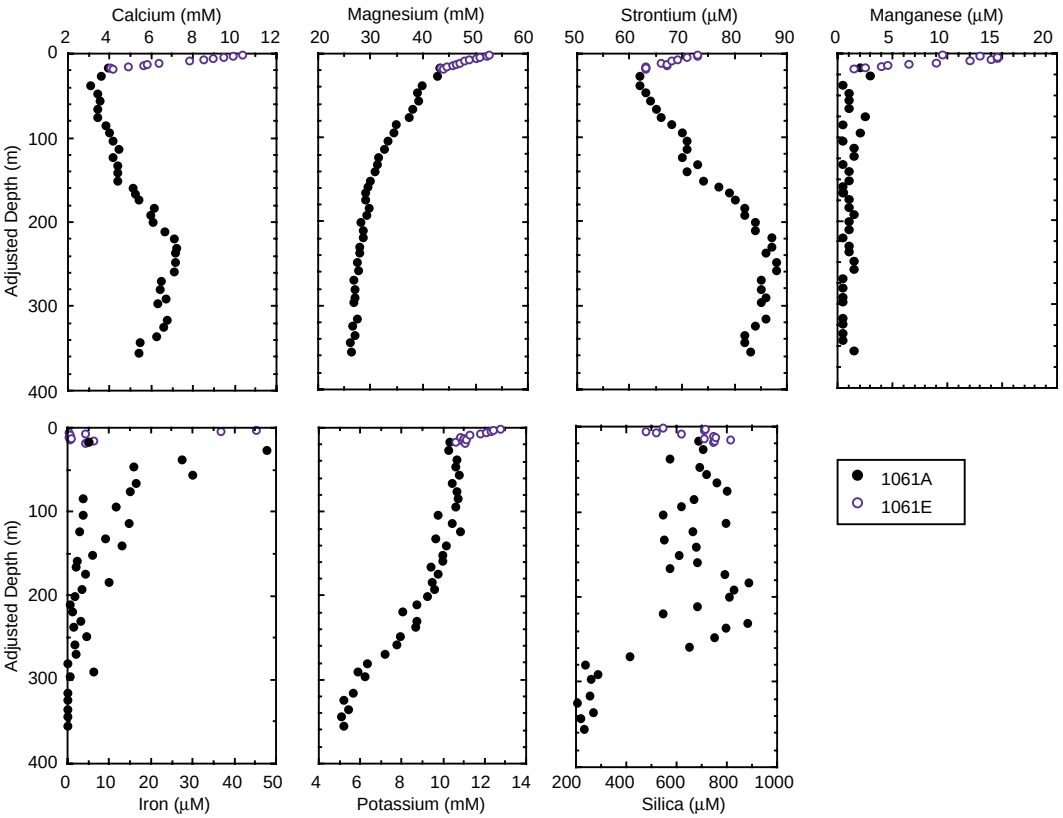

Figure 82. Concentration vs. depth profiles for interstitial waters at Site 1061. Note the depth scale is labeled Adjusted Depth because 11 m was added to mbsf depths of Hole 1061A to correct for overpenetration of the APC.

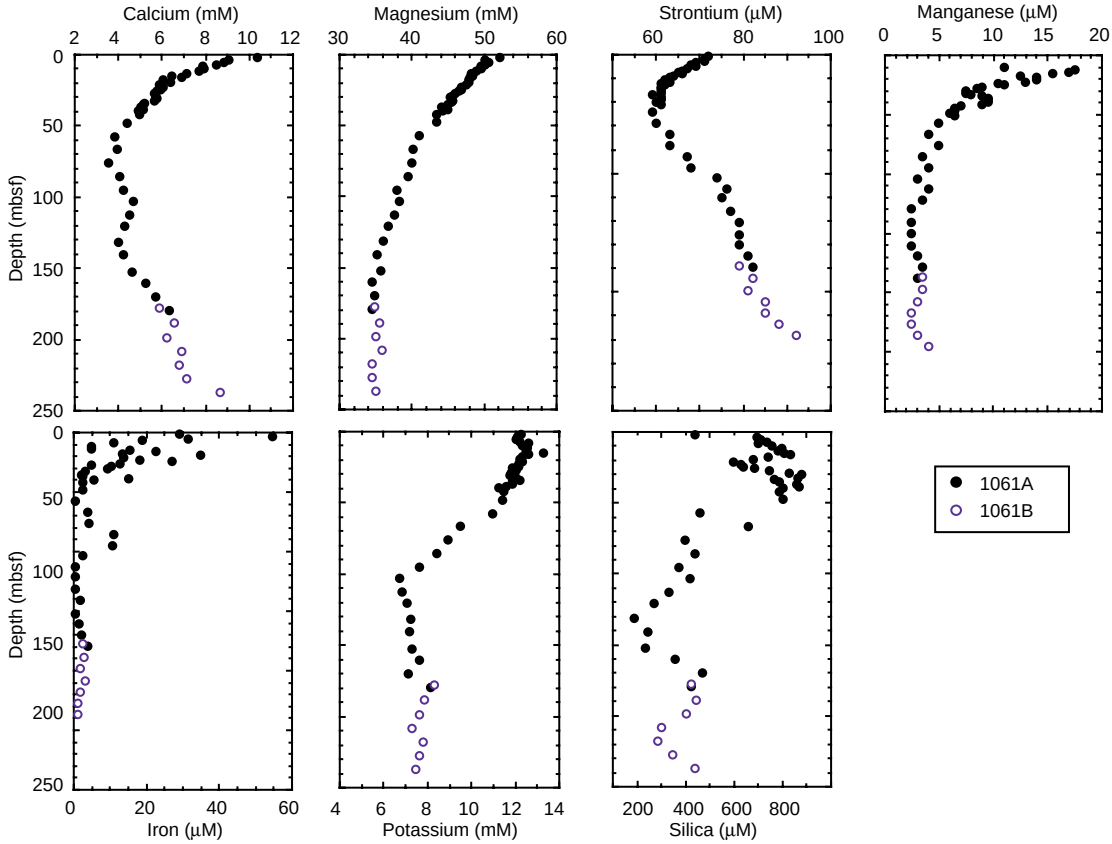

Figure 83. Concentration vs. depth profiles for interstitial waters at Site 1062.

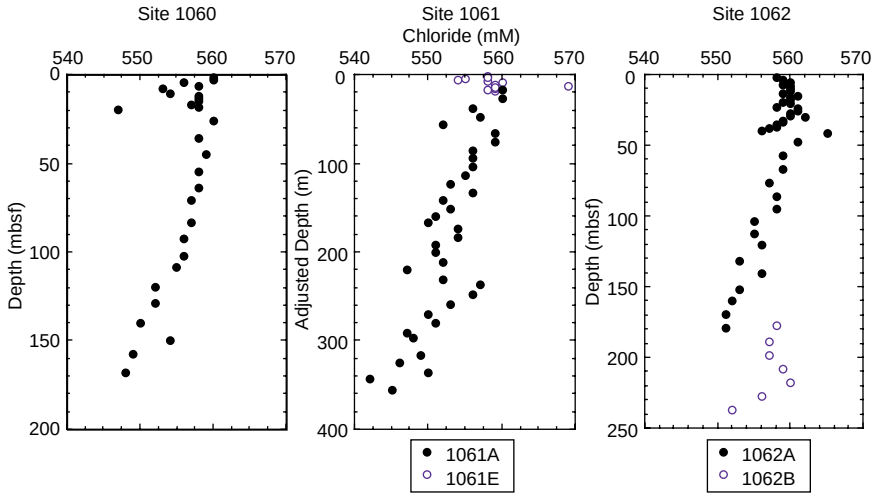

Figure 84. Downhole chloride profiles at Sites 1060, 1061, and 1062. In the case of Hole 1061A, note that the depth scale is labeled Adjusted Depth because 11 m was added to mbsf depths to correct for overpenetration of the APC.

linity decreases downhole so that silica remains in the solid phase. In the methanogenesis zone, potassium and silica appear to be related to the lithologic changes within the sediments rather than to the ion-exchange processes and alkalinity. Concentrations of these elements are higher throughout the sediment column at Site 1060 and in the upper part of the sediment column at Sites 1061 and 1062, where the sedimentation rates are high and the sediments are relatively rich in aluminosilicates (see "Biostratigraphy" and "Lithostratigraphy" sections, this chapter). However, potassium and silica decrease with depth at Sites 1061 and 1062, where sedimentation rates are low and relatively carbonate-rich layers predominate. Similar downhole-decreasing potassium concentration profiles have been observed on the southern and western Bermuda Rise (Sites 386 and 387), where black shales underlying the sites were inferred to be a sink for potassium (Miller et al., 1979). Perhaps a similar sink occurs below the lower portions of the Blake-Bahama Outer Ridge.

Gas Hydrate

Although gas hydrate was not directly observed, interstitial chloride data suggest that hydrate underlies all of these sites (Fig. 84). As gas hydrate dissociates during core recovery, it releases freshwater

into the pore space, diluting interstitial chloride concentrations and salinity (Hesse and Harrison, 1981; Hesse et al., 1985; Kvenvolden and Kastner, 1990; Kastner et al., 1990). Thus, the presence of gas hydrate is recognized by the freshening of interstitial waters as indicated by relatively low interstitial chloride concentrations.

All three deep Blake-Bahama Outer Ridge sites display downward freshening chloride profiles (Fig. 84). Chloride concentrations decrease from seawater values by 2%, 3%, and 2% at Sites 1060, 1061, and 1062, respectively. The chloride concentration profile at Site 1062 shows a ~1% offset in chloride values at ~160 mbsf, probably reflecting slight seawater contamination during XCB coring. Chloride excursions from baseline values, like those observed at Site 1056 (see "Inorganic Geochemistry" section, "Intermediate Depth Blake Outer Ridge" chapter, this volume), are absent at these deep-water sites.

Discussion

Interstitial chloride and geophysical data suggest that gas hydrate occurs at depth at Sites 1060, 1061, and 1062. Most DSDP and ODP sites on the Blake Ridge display strong, downhole freshening profiles indicative of gas hydrate below (Leg 11, Sites 102–104, Sayles et al., 1972; Leg 76, Site 533, Jenden and Gieskes, 1983; Leg 164, Sites 994, 995, and 997, Paull, Matsumoto, Wallace, et al., 1996), and Sites 1060, 1061, and 1062 are no exception. In addition, a distinct BSR appears at depth at Sites 1060 and 1061 (see "Site Geophysics" chapter, this volume), which indicates the presence of methane gas bubbles associated with the base of gas hydrate stability (Singh et al., 1993; Bangs et al., 1993; Holbrook et al., 1996). The lack of recognizable chloride excursions from baseline values suggests that gas hydrate was not cored at any of these sites.

Linear sulfate profiles at Sites 1060 and 1061 suggest that a substantial portion of the sulfate depletion is the result of anaerobic methane oxidation and that significant amounts of methane are diffusing-upward to be consumed at the sulfate/methane boundary. This apparent indicator of upward methane flux is consistent with significant amounts of methane below as implied by the presence of gas hydrate.

The concave-down sulfate profile observed at Site 1062 suggests that upward methane flux is much lower and that a predominant amount of the sulfate is consumed by microbially mediated reactions with sedimentary organic matter (see the discussion above). The presence of gas hydrate at depth, together with reflectors below the BSR suggestive of gassy sediments, however, implies substantial subsurface inventories of methane, which seems inconsistent with a sulfate profile suggestive of low methane flux.

PHYSICAL PROPERTIES

Introduction

Climate change plays a major role in controlling sedimentation rate, sediment content, and depositional processes in the deep ocean. Sites 1060 and 1061 are located on the Blake Outer Ridge at water depths of 3481 and 4047 m, respectively. The high sedimentation rates at these sites (from 10 to 40 cm/k.y.) offer an opportunity to measure high-frequency (millennial scale) changes in physical properties records in an environment where downslope reworking of sediment is reduced compared to shallower water sites. On long time scales, physical property records are dominated by orbitally forced glacial to interglacial changes in lithology (~100-k.y. cycles), with weaker 40- and 20-k.y. cyclic influences recorded in the GRAPE record. Determining the period of higher frequency cycles will require more age control than is currently available.

MST Measurements

The MST data for Holes 1060A, 1061A, 1062A, and 1062E are on CD-ROM (back pocket, this volume) and presented in Figures 85 through 88. Magnetic susceptibility data were generally collected at 4-cm intervals for the whole depth of each hole. Natural gamma ray (NGR) was measured every 50 cm for the entire depth of each "A" hole at every site. A 2-cm interval was used for the *P*-Wave Logger (PWL) and GRAPE in the uppermost part of each hole until the PWL no longer collected data. The GRAPE interval was increased to 4 cm afterwards. The PWL data collection depths for Sites 1060 and 1061

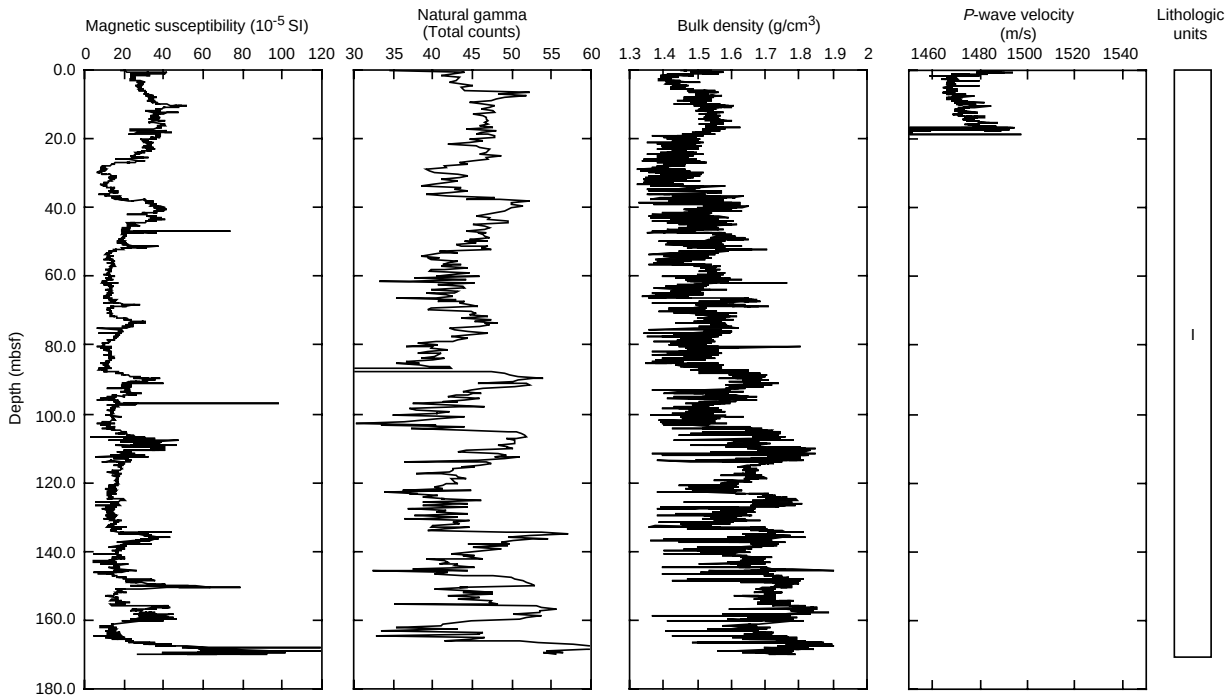

Figure 85. Vertical profiles of MST data from Hole 1060A. GRAPE data values <1.1 g/cm^3 were edited out before plotting.

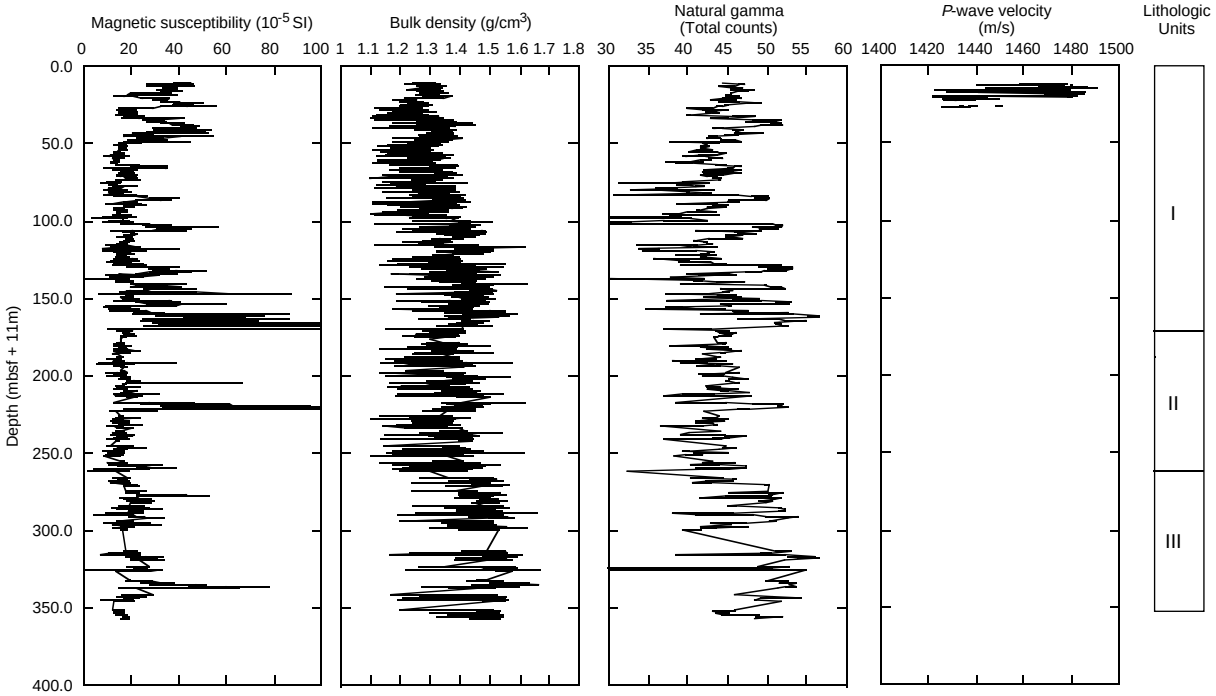

Figure 86. Vertical profiles of MST data from Hole 1061A. GRAPE data values <1.1 g/cm^3 were edited out before plotting. All data for Hole 1061A are plotted at mbsf +11 m to account for an apparent offset in depths relative to the mudline.

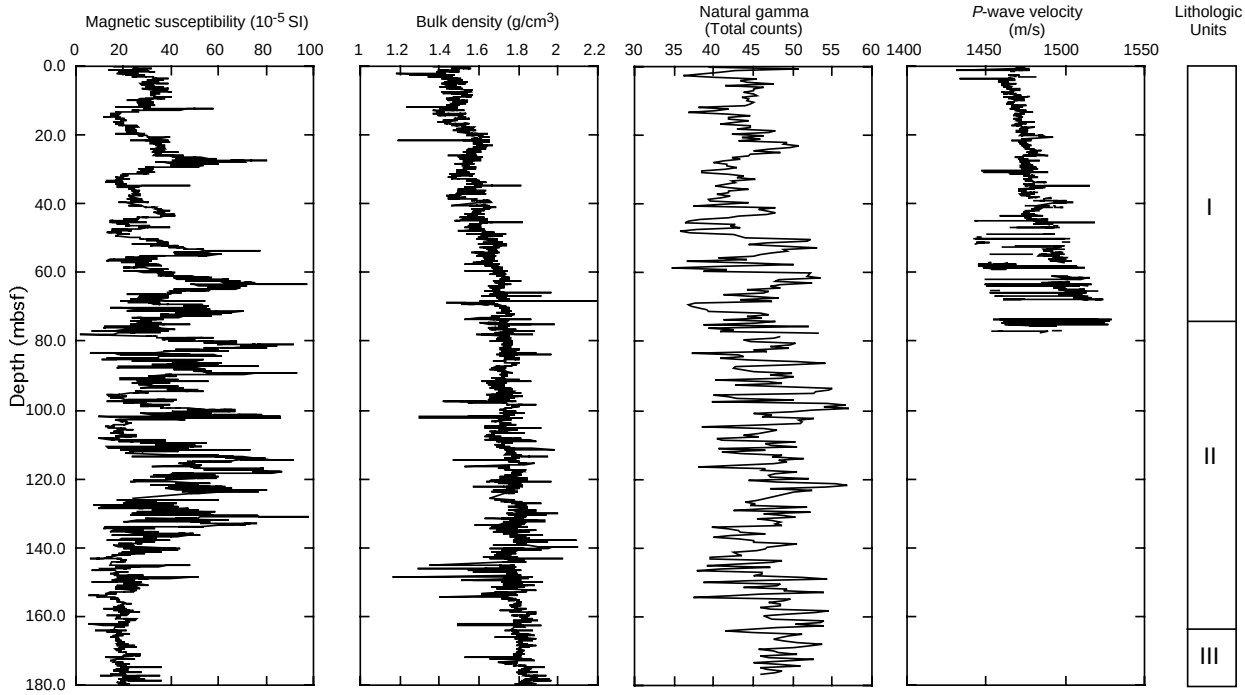

Figure 87. Vertical profiles of MST data from Hole 1062A. GRAPE data values <1.1 g/cm^3 were edited out before plotting.

(between 25 and 30 mbsf) were influenced by the presence of gas and gas-induced core fragmentation and cracking. Reduced interstitial gas at Site 1062 (see "Organic Geochemistry" section, this chapter) allowed for an extension of PWL data collection to a depth of 50–70 mbsf.

Sites 1060 and 1061 exhibit characteristics similar to the previous Sites (1056 through 1059) in terms of magnetic susceptibility, NGR, and GRAPE. All parameters show higher values during glacial periods. This is attributed to higher clay and heavy-mineral components during these periods, with reduced biogenic carbonate production. NGR and GRAPE measurements proved to be valuable for lithologic correlation with downhole log data at Site 1061 (also see "Downhole Logging" section, this chapter) where the amplitude and wavelength of the core and log cycles closely correspond. At this site, changes in NGR variability at 160 and 250 mbsf also coincide with transitions from lithologic Unit I to Unit II and from Unit II to Unit III, respec-

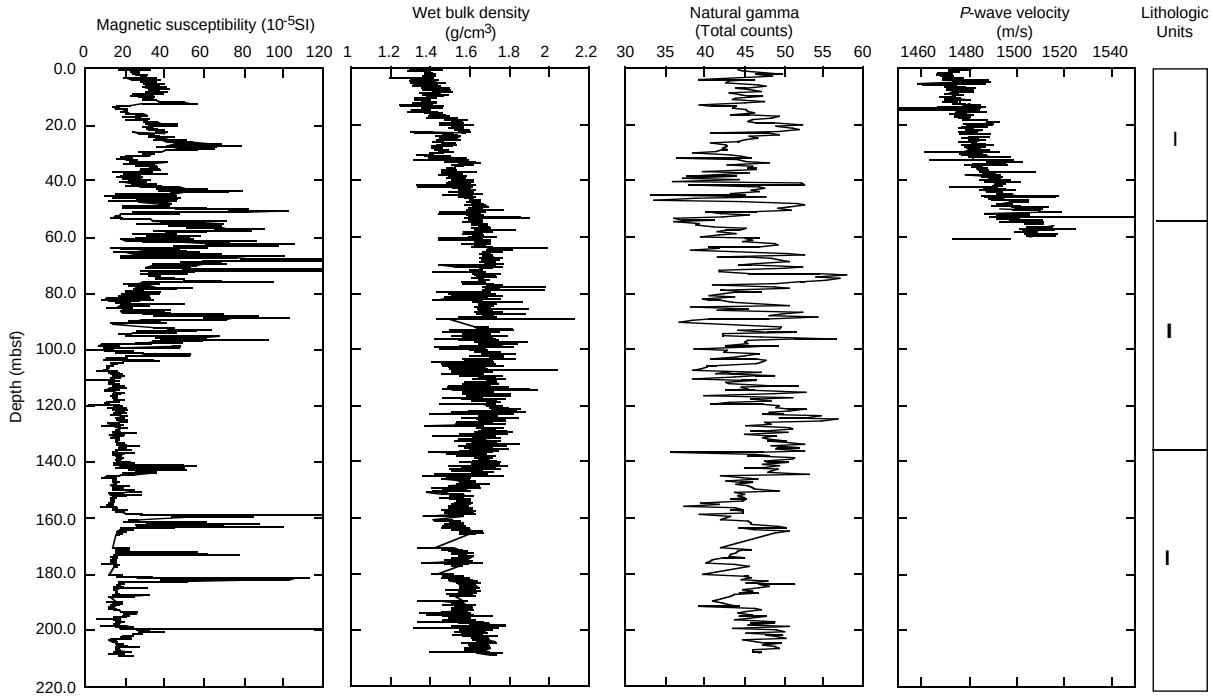

Figure 88. Vertical profiles of MST data from Hole 1062E. GRAPE data values <1.1 g/cm^3 were edited out before plotting.

tively. GRAPE data record the same lithologic structure as a decrease in bulk density, corresponding to Unit II (see "Lithostratigraphy" section, this chapter). A similar correspondence between lithology and NGR and GRAPE data is valid for Site 1062 also. The amplitude of GRAPE bulk density cycles is much diminished at Site 1062, related to "in phase" variation between grain density and porosity (see below).

A comparison of GRAPE and PWL measurements on a decimeter to meter scale in the upper 30 m in Hole 1062A shows "in phase" and "out of phase" relationships, where high *P*-wave velocities are associated with both high and low GRAPE densities. This relationship is also apparent at Site 1063, where the presence of abundant sand-sized biogenic silica is thought to depress bulk density and increase *P*-wave velocity (Silva et al., 1976). It is uncertain whether this explanation applies to Site 1062, where only trace amounts of biogenic silica were noted (see "Lithostratigraphy" section, this chapter). It is possible that biogenic silica-rich layers do occur and were not specifically identified and sampled at Site 1062, or that low density zones are associated with high water content and coarser grained sediments of another origin, resulting in a similar mechanical response to that seen at Site 1063.

Index Properties

Index property samples were taken at a frequency of approximately two per section for Holes 1060A, 1061A, 1061D (first three cores), 1062A, 1062B (147–238 mbsf), and 1062E. Values for bulk density, grain density, dry density, water content, and porosity at these sites are listed in Tables 44–46. Summary statistics are presented in Table 47. Bulk density, porosity, and water content at Sites 1060 and 1061 show a very similar trend with depth to that observed at Sites 1056–1059 (Figs. 89, 90; also see Figs. 88–91, "Intermediate Depth Blake Outer Ridge" chapter, this volume).

At Sites 1060 and 1061, bulk density increases from 1.35–1.5 g/cm^3 at the surface to around 1.8 g/cm^3 at 160 mbsf, corresponding to lithologic Unit I at both sites. At Site 1061, bulk density then decreases to 1.7 g/cm^3 in lithologic Unit II (160–250 mbsf) before increasing again to 1.8–1.9 g/cm^3 at the base of the hole (Unit III; 250–350 mbsf). Bulk density variability at these sites is driven by glacial to interglacial variations in both grain density and water content. Low grain-density values, typically around 2.7 g/cm^3, occur during interglacial periods and are associated with higher water and carbonate content. Higher grain densities, typically around 2.8 g/cm^3, occur during glacial periods and are associated with zones of low water and carbonate content (Figs. 89–92). The frequency and amplitude of these cycles suggest that they are controlled by 100- and 40-k.y. orbitally-forced climate changes, with the 100-k.y. forcing being dominant above ~160 mbsf (corresponding to lithologic Unit I at Site 1060) and the 40-k.y. forcing dominant below this depth (Units II and III at Site 1061).

Bulk density at Site 1062 also increases from 1.35–1.5 g/cm^3 at the surface to 1.8 g/cm^3 at 170 mbsf in 1062A, and to 1.75 g/cm^3 at 120 mbsf in Hole 1062E, corresponding to lithologic Units I and II in both holes. In Hole 1062A this is followed by a decrease to 1.72 g/cm^3 at 200 mbsf before increasing again to 1.85 g/cm^3 at the bottom of the hole. In Hole 1062E bulk density decreases to 1.65 g/cm^3 at 155 mbsf and increases to 1.75 g/cm^3 at the base of the hole.

As noted in the GRAPE data, the amplitude of the bulk density cycles is much smaller than at all previous sites (with the exception of Site 1054). An examination of grain density and water content values for this site shows that they vary "in phase"; that is, periods of high grain density correspond to periods of high water content and vice versa, thus suppressing the amplitude of bulk density cycles. This is in contrast to the pattern seen at previous sites. Additionally, longer term trends in grain density are also apparent at Site 1062. Grain density in Holes 1062A and 1062E decreases from the surface to 40 mbsf and 20 mbsf, respectively. An abrupt increase (over an interval of 2–5 m) in grain density then occurs at these depths, followed by a slow overall decrease to the bottom of the holes. Two zones of high-amplitude fluctuations in grain density (from 45 to 130 mbsf and 170 to 240 mbsf in Holes 1062A and 1062B, respectively, and from 20 to 80 mbsf and 150 to 210 mbsf in Hole 1062E; see Figs. 91, 92) are superposed on this long term trend. The occurrence of these zones can possibly be attributed to greater variability in the supply of detrital carbonate (grain density up to 2.94 g/cm^3) and quartz (density 2.65 g/cm^3) caused by increased shedding of material from the Bahama

Table 44. Index properties of samples from Site 1060.

Leg	Site	Hole	Core	Type	Section	Top	Bottom	Depth (mbsf)	Water content wet (%)	Water content dry (%)	Wet bulk density (g/cm^3)	Grain density (g/cm^3)	Dry density (g/cm^3)	Porosity (%)	Void ratio
172	1060	A	1	H	1	22	24	0.22	49.31	97.27	1.52	2.84	0.77	72.96	2.70
172	1060	A	1	H	1	93	95	0.93	50.77	103.13	1.47	2.72	0.72	73.30	2.74
172	1060	A	1	H	2	28	30	1.78	59.75	148.47	1.37	2.77	0.55	80.07	4.01
172	1060	A	1	H	2	121	123	2.71	60.10	150.64	1.37	2.82	0.54	80.58	4.15
172	1060	A	1	H	3	38	40	3.38	57.88	137.40	1.38	2.72	0.58	78.51	3.65
172	1060	A	1	H	3	107	109	4.07	57.36	134.49	1.39	2.71	0.59	78.10	3.56
172	1060	A	1	H	4	39	41	4.89	56.68	130.83	1.41	2.77	0.61	78.02	3.55
172	1060	A	1	H	4	117	119	5.67	53.35	114.36	1.44	2.71	0.67	75.21	3.03
172	1060	A	1	H	5	44	46	6.44	52.10	108.76	1.49	2.98	0.71	76.01	3.16
172	1060	A	1	H	5	118	120	7.18	50.17	100.66	1.48	2.73	0.74	72.88	2.68

This is a sample of the table that appears on the volume CD-ROM.

Table 45. Index properties of samples from Site 1061.

Leg	Site	Hole	Core	Type	Section	Top	Bottom	Depth (mbsf)	Water content wet (%)	Water content dry (%)	Wet bulk density (g/cm^3)	Grain density (g/cm^3)	Dry density (g/cm^3)	Porosity (%)	Void ratio
172	1061	A	1	H	1	44	46	0.46	48.33	93.53	1.52	2.76	0.78	71.57	2.52
172	1061	A	1	H	1	112	114	1.14	51.64	106.79	1.46	2.73	0.71	74.07	2.85
172	1061	A	1	H	2	34	36	1.86	51.89	107.87	1.45	2.68	0.70	73.89	2.83
172	1061	A	1	H	2	119	121	2.71	52.50	110.52	1.45	2.71	0.69	74.56	2.93
172	1061	A	1	H	3	48	50	3.5	51.34	105.51	1.46	2.71	0.71	73.66	2.79
172	1061	A	1	H	3	117	119	4.19	50.97	103.97	1.46	2.67	0.72	73.06	2.71
172	1061	A	1	H	4	36	38	4.88	49.66	98.63	1.50	2.78	0.76	72.80	2.68
172	1061	A	1	H	4	109	111	5.61	51.86	107.72	1.46	2.71	0.70	74.09	2.86
172	1061	A	1	H	5	34	36	6.36	49.46	97.86	1.49	2.71	0.76	72.11	2.59
172	1061	A	1	H	5	88	90	6.9	48.88	95.60	1.50	2.72	0.77	71.75	2.54

This is a sample of the table that appears on the volume CD-ROM.

Table 46. Index properties of samples from Site 1062.

Leg	Site	Hole	Core	Type	Section	Top	Bottom	Depth (mbsf)	Water content wet (%)	Water content dry (%)	Wet bulk density (g/cm^3)	Grain density (g/cm^3)	Dry density (g/cm^3)	Porosity (%)	Void ratio
172	1062	A	1	H	1	33	35	0.33	49.964	99.855	1.489	2.726	0.745	72.665	2.658
172	1062	A	1	H	1	101	103	1.01	60.471	152.97	1.36	2.79	0.54	80.7	4.18
172	1062	A	2	H	1	93	95	3.13	56.04	127.47	1.41	2.75	0.62	77.41	3.42
172	1062	A	2	H	2	30	32	4	52.881	112.22	1.45	2.74	0.68	75.05	3
172	1062	A	2	H	2	113	115	4.83	51.55	106.39	1.46	2.7	0.71	73.73	2.8
172	1062	A	2	H	3	25	27	5.45	55.294	123.68	1.43	2.88	0.64	77.72	3.48
172	1062	A	2	H	3	112	114	6.32	58.525	141.1	1.38	2.73	0.57	79.05	3.77
172	1062	A	2	H	4	39	41	7.09	50.981	104	1.48	2.77	0.72	73.8	2.81
172	1062	A	2	H	4	117	119	7.87	50.071	100.28	1.49	2.76	0.74	73.04	2.7
172	1062	A	2	H	5	27	29	8.47	52.121	108.86	1.46	2.74	0.7	74.44	2.91

Note: Zones of high carbonate variability are marked.

This is a sample of the table that appears on the volume CD-ROM.

Table 47. Average values and standard deviation of index properties measured at Sites 1060–1062.

Hole		Wet mass (g)	Dry volume (g/cm^3)	Dry mass (g)	Water content (% wet mass)	Water content (% dry mass)	Bulk density (g/cm^3)	Grain density (g/cm^3)	Dry density (g/cm^3)	Porosity (%)	Void ratio
1062A/B	Mean	10.691	2.499	6.806	37.237	61.737	1.695	2.739	1.072	60.851	1.652
	SD	2.751	0.655	1.771	7.069	21.678	0.119	0.077	0.187	6.754	0.581
1062E	Mean	10.216	2.367	6.390	38.966	65.984	1.656	2.708	1.017	62.434	1.744
	SD	3.407	0.843	2.303	6.363	20.839	0.100	0.066	0.159	5.818	0.543
1061A/D	Mean	10.605	2.390	6.505	39.535	67.064	1.652	2.737	1.004	63.283	1.792
	SD	2.706	0.581	1.571	5.780	17.811	0.098	0.094	0.151	5.437	0.474
1060A	Mean	10.8748	2.398	6.525	41.930	74.418	1.614	2.738	0.943	65.496	1.989
	SD	2.355	0.637	1.735	6.340	20.583	0.104	0.126	0.161	5.758	0.562

Note: SD = standard deviation.

Banks during these periods (see “Lithostratigraphy” section, this chapter).

A comparison of the reflectance parameter a* (where “reddish” colored sediment is often signified by an a* value greater than 0) with grain density is shown for Site 1060 in Figure 93. The generally close correlation between the two variables suggests that minerals heavier than calcite (density 2.7 g/cm^3) are more abundant in glacial periods, influencing overall grain density. Although the red coloration appears to be associated with hematite (density 5.275 g/cm^3), this mineral occurs in trace amounts only (see XRD results in “Lithostratigraphy” section, this chapter) and therefore cannot be the sole cause of high glacial grain densities.

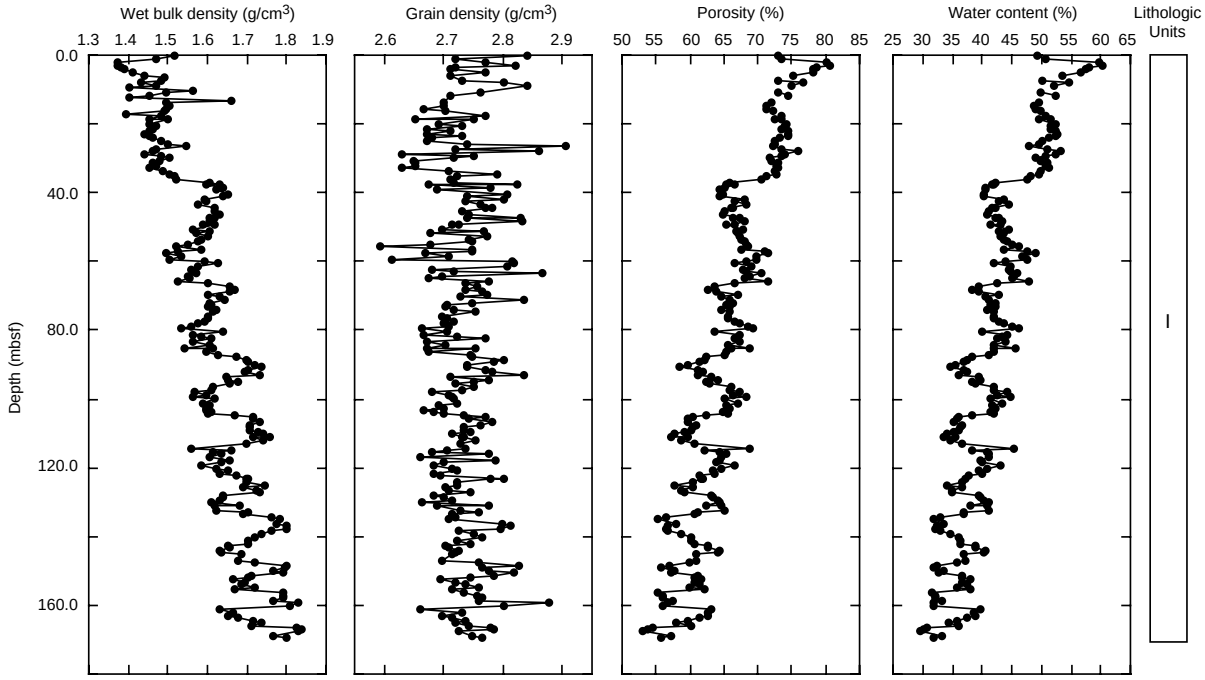

Figure 89. Index properties measurements of wet bulk density, grain density, porosity, and water content vs. depth for Hole 1060A.

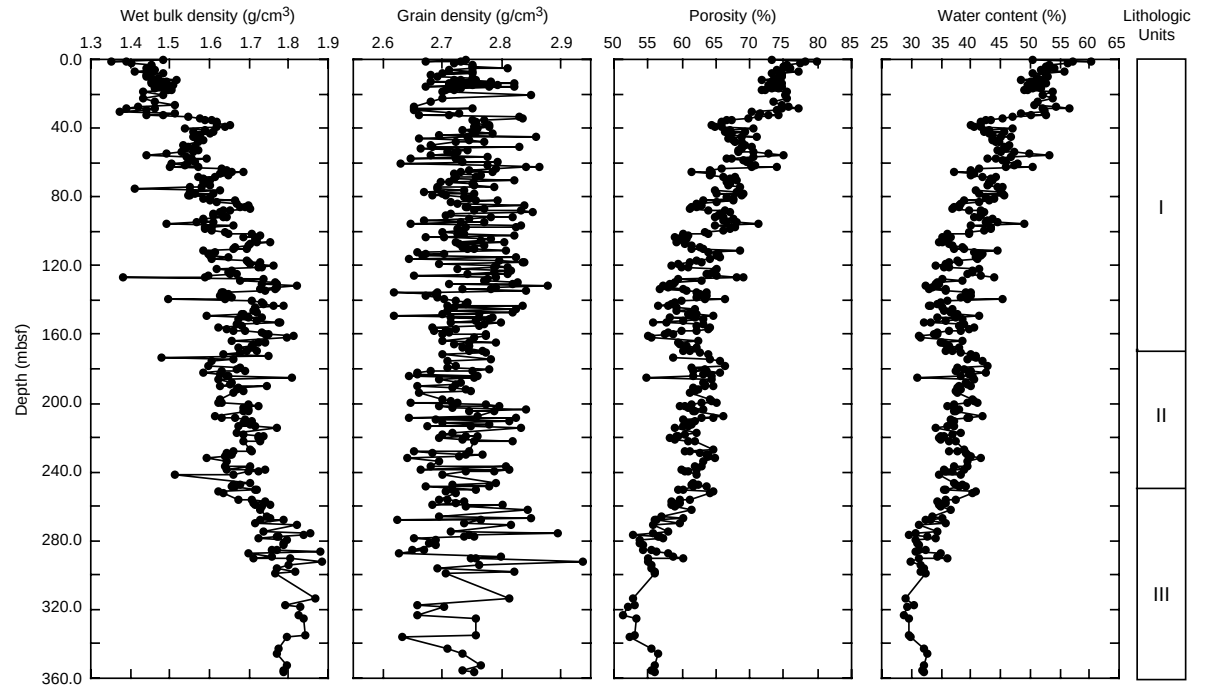

Figure 90. Index properties measurements of wet bulk density, grain density, porosity, and water content vs. depth for Holes 1061A and 1061D (combined data). Measurements made in Hole 1061A are plotted at mbsf + 11 m to account for an apparent offset in depths relative to the mudline.

Acoustic Velocity

At Sites 1060, 1061, and 1062, acoustic velocities were recorded on whole cores using the PWL from the MST, and on half-split sections using the Digital Sound Velocimeter (DSV; see "Physical Properties" section, "Explanatory Notes" chapter, this volume). The acoustic profiles (from 2-cm sampling intervals) obtained with the PWL are presented in the MST measurements paragraph (this section). For some PWL records, significantly lower (10–20 m/s) velocities compared to the discrete velocity measurements most likely indicate calibration problems of the PWL. However, as the offset is usually constant, postcruise processing can improve the quality of the PWL data.

Longitudinal velocities (perpendicular to bedding, z-direction) and transverse velocities (parallel to bedding, y-direction) have been obtained with the DSV at a resolution of two measurements per section at Holes 1060A, 1061A, 1061C, 1061D, 1062A, 1062B, and 1062E (Tables 48–50). Figure 94 shows differences in the general

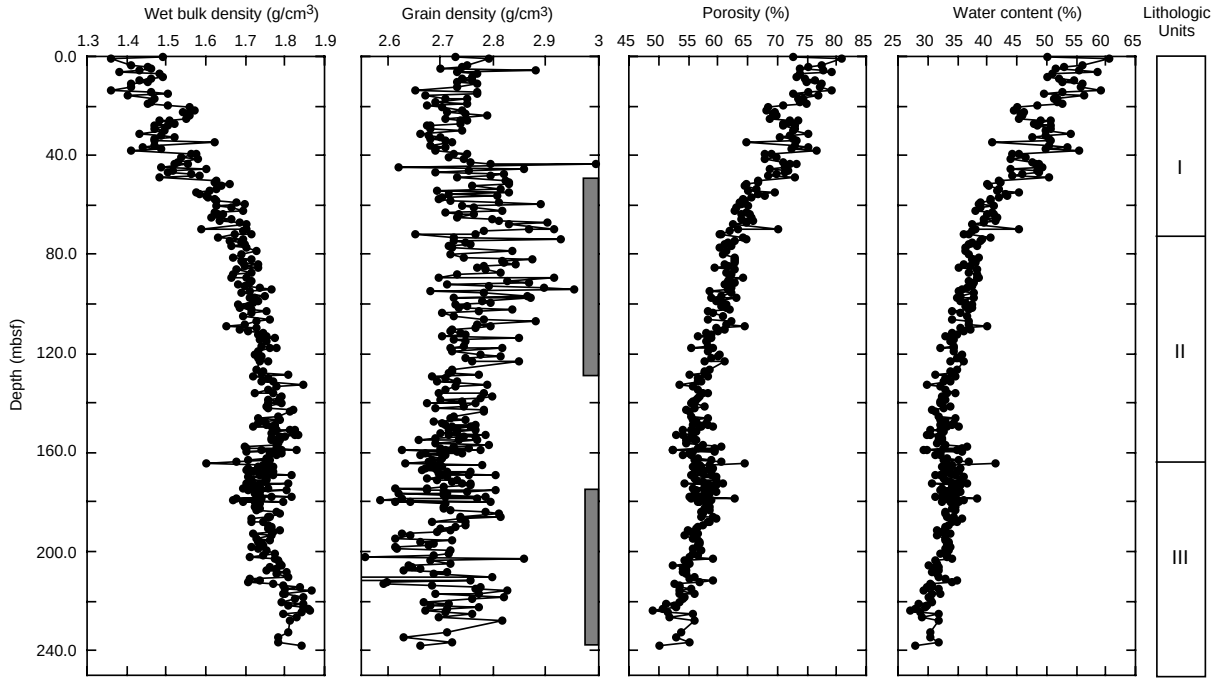

Figure 91. Index properties measurements of wet bulk density, grain density, porosity, and water content vs. depth for Hole 1062A and 1062B (combined data). Zones of high-amplitude variation in grain density, possibly related to influxes of detrital carbonate from the Bahama Banks, are denoted by hatching.

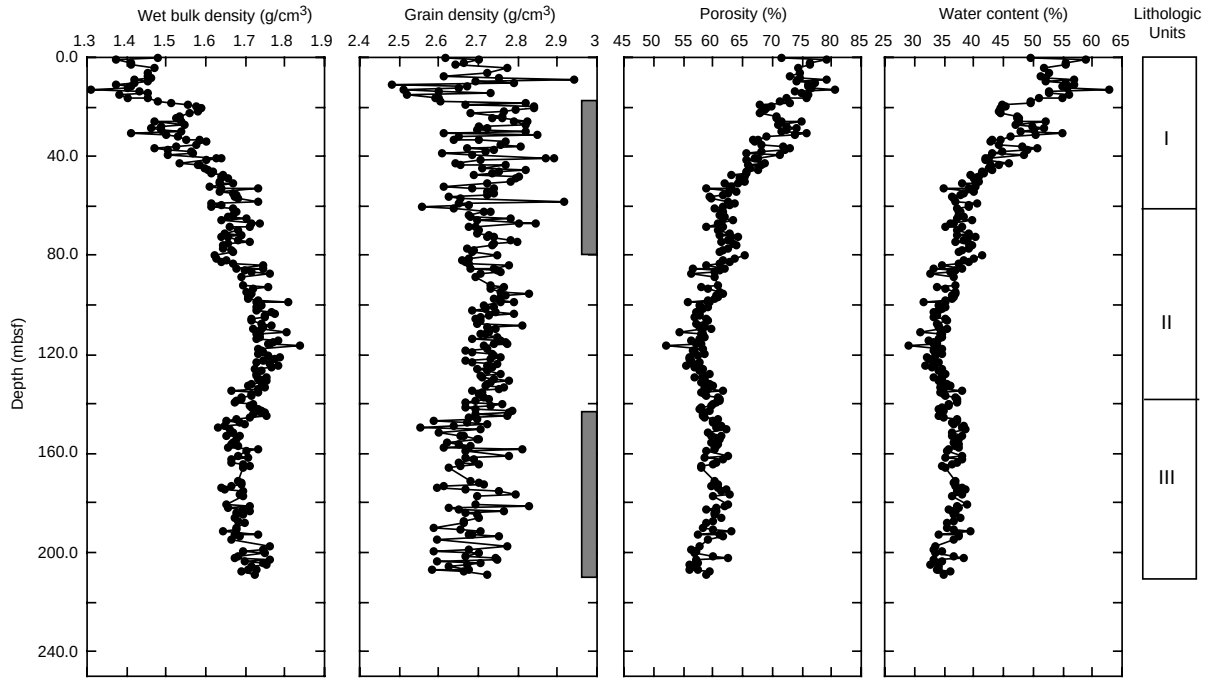

Figure 92. Index properties measurements of wet bulk density, grain density, porosity, and water content vs. depth for Hole 1062E. Zones of high amplitude variation in grain density, possibly related to influxes of detrital carbonate from the Bahama Banks, are denoted by hatching.

depth trends in velocity between the sites. Although velocities at Sites 1060 and 1061 are decreasing (gradients of –1/s and –0.4/s, respectively), a positive gradient of 0.2/s is observed at Site 1062. Superimposed on the general trend are changes in velocity related to variations in sediment composition. Comparison of the velocity records with measurements of carbonate content and lightness reveals that most velocity maxima correlate with lighter colored, carbonate-rich sediment.

For all sites, the sediments exhibit a slightly (<0.5%) positive average velocity anisotropy (transverse velocities higher than longitudinal velocities), indicating that a considerable part of the sediment fabric is oriented in the horizontal plane. However, changes in anisot-

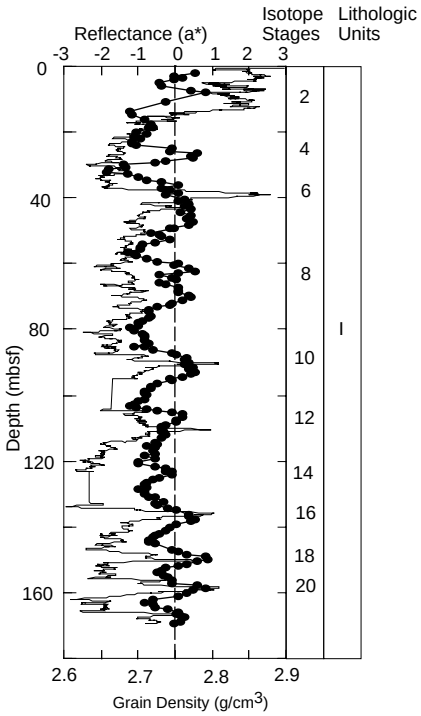

Figure 93. Grain density (smoothed with a 5-point running mean; thick line with circles) and reflectance parameter a* (smoothed with a 10-point running mean; thin line). Glacial periods often have higher grain densities and contain distinctive reddish layers (in general denoted by an a* value >0).

ropy are too small to allow for detailed correlation with changes in sediment color.

A comparison between longitudinal velocities obtained at the western (Hole 1062A) and eastern flank (Hole 1062E) of a mud wave shows that the velocity structure is similar at both locations for the upper 50 m of the sediment column (Fig. 95).

Shear Strength

At Sites 1060, 1061, and 1062 measurements of undrained shear strength (Tables 51–53) were taken at approximately two per section using the vane-shear device and the pocket penetrometer (see "Explanatory Notes" chapter, this volume) in intervals cored with the APC. Brittle failure along parting cleavages of the XCB "biscuits" made measurement of shear strength in these sections unreliable. Shear strength increases from about 2 kPa at the seafloor to 120–160 kPa at 160 mbsf (Fig. 96). Site 1061 shows the lowest gradient with a slope of 0.5 kPa/m. Holes 1060A and 1062E show slightly elevated gradients (0.57 kPa/m), whereas Hole 1062A has a gradient of 0.74 kPa/m.

Thermal Conductivity and Heat Flow

At Sites 1060 (Holes 1060A, 1060C, 1060D, and 1060E), 1061 (Holes 1061A and 1061B), and 1062 (Holes 1062A and 1062E) thermal conductivity was measured at a resolution of one to three measurements per core (Tables 54–56; Fig. 97). Thermal conductivity increases with depth at Sites 1061 and 1062. A higher gradient is observed at Site 1062. Linear least-squares approximations to the increase in conductivity with depth result in: $k = 0.9 + 0.0003z$ for Site 1061 and $k = 0.9 + 0.0011z$ for Site 1062, where k is thermal conductivity (W/[m·K]) and z is depth in mbsf. In contrast, thermal conductivity at Site 1060 exhibits higher variability and decreasing values with depth.

To calculate heat flow at Site 1062, in situ temperature was measured at Hole 1062A using the Adara temperature shoe on five of the APC cores (172-1062A-4H, 7H, 10H, 13H, and 16H). whereas the results of the two shallowest measurements were discarded because of unstable measurement conditions, deeper measurements show excellent results and were used to calculate equilibrium temperatures extrapolated from transient temperature data. Temperatures recorded were 7.66°C at 87.7 mbsf, 8.40°C at 116.2 mbsf, and 9.55°C at 144.7 mbsf. Additionally, the mudline temperature of 2.49°C was obtained from the initial Adara tool measurement taken at the mudline in Hole 1062A before the measurement taken at Core 172-1062A-10H. This was used as the reference bottom seawater temperature. The linear temperature gradient calculated from in situ temperatures derived from the three deep measurements is 0.033°C/m (Fig. 98).

Combining the average thermal conductivity of 1.024 W/(m·K) at Site 1062 with the temperature gradient results in a heat flow of 34.0 mW/m^2. This value agrees with heat-flow measurements taken during ODP Leg 164 at Blake Ridge Sites 994 (33.4 mW/m^2), 995 (34.2 mW/m^2), and 997 (35.9 mW/m^2) (Paull, Matsumoto, Wallace, et al., 1996).

Resistivity

Resistivity at Sites 1060, 1061, and 1062 (Fig. 99) was measured using the Wayne-Kerr Precision Component Analyzer with a four-electrode probe (see "Physical Properties" section, "Explanatory Notes" chapter, this volume). Generally, two measurements per section were made (Tables 57–59). A comparison of resistivity measurements at Hole 1061A with downhole logging measurements shows a close relationship between the two data sets in terms of wavelength, although the amplitude of the cycles is greater in the core measurements. In general, resistivity varies as a function of porosity and the cyclicity shown matches that of index property measurements of porosity discussed above. Similar trends are observed at Sites 1060 and 1062.

DOWNHOLE LOGGING

Logging Operations

Hole 1061A was logged with the triple combination and FMS-Sonic tool strings (see "Downhole Logging" section, "Explanatory Notes" chapter, this volume), after the hole had been reamed and flushed of debris. Logging operations started at 2200 hr on 10 March and finished at 1300 the next day (see "Operations" section, this chapter). We ran one main triple combination pass, with a repeat of the bottom section, and two full passes of the FMS-Sonic (Fig. 100). The wireline heave compensator was used for all passes except the first FMS-Sonic, when it failed to start.

The depth to the logged measurements is calculated from the length of cable played out, minus the cable length to the seafloor (taken to be the step reduction in gamma-ray log at the sediment/water boundary); it is calculated differently from the core depth, based on drill-pipe advance beyond a recovered mudline. Different errors are associated with the two depths: core expansion and incomplete recovery in the case of the cores, and cable stretch (~1 m/km) in the case of the logs. Hence, there can be small but significant offsets between the two, and this should be taken into account when looking at the figures. Confusion should not arise, because log measurements are always on the log-depth scale, and core measurements always on the core-depth scale.

In the case of Hole 1061A, the situation was complicated by the non-recovery of the mudline and the subsequent adoption of an "mbsf + 11 m" depth scale for core recovery, best described diagrammatically (Fig. 100). A large-scale plot of logs at Holes 1061A and 1063A, along with lithologic and age data, are shown in Figure 101 (on back-pocket foldout, this volume). The mbsf + 11 scale matches

Table 48. Compressional wave velocity measurements from Site 1060.

Leg	Site	Hole	Core	Type	Section	Interval (cm)	Depth (mbsf)	Temp. (°C)	Velocity 1 Z-direction (m/s)	Velocity 2 Y-direction (m/s)	Velocity 3 X-direction (m/s)
172	1060	A	1	H	1	22	0.22	21.9	1514	1520	
172	1060	A	1	H	1	94	0.94	21.8	1492	1495	
172	1060	A	1	H	2	30	1.8	22.3	1494	1497	
172	1060	A	1	H	2	124	2.74	22.3	1482	1489	
172	1060	A	1	H	3	40	3.4	22.9	1491	1491	
172	1060	A	1	H	3	108	4.08	22.9	1492	1494	
172	1060	A	1	H	4	41	4.91	23.1	1491	1495	
172	1060	A	1	H	4	119	5.69	23.1	1488	1491	
172	1060	A	1	H	5	44	6.44	23.3	1487	1494	
172	1060	A	1	H	5	118	7.18	23.3	1487	1488	
172	1060	A	1	H	6	54	8.04	23.6	1488	1490	
172	1060	A	1	H	6	116	8.66	23.7	1483	1489	
172	1060	A	2	H	1	120	10.2	22.5	1483	1490	
172	1060	A	2	H	1	50	9.5	22.5	1481	1485	
172	1060	A	2	H	2	104	11.54	21.8	1475	1476	
172	1060	A	2	H	2	20	10.7	21.8	1490	1494	
172	1060	A	2	H	3	118	13.18	21.9	1487	1485	
172	1060	A	2	H	3	12	12.12	21.9	1487	1488	
172	1060	A	2	H	4	120	14.7	22.3	1482	1485	
172	1060	A	2	H	4	26	13.76	22.3	1494.1	1495	
172	1060	A	2	H	5	110	16.1	22.9	1487.8	1484	
172	1060	A	2	H	5	38	15.38	22.9	1483.3	1485	
172	1060	A	2	H	6	120	17.7	23.2		1493	
172	1060	A	2	H	6	60	17.1	23.2		1488	
172	1060	A	2	H	7	34	18.34	23.4		1480	
172	1060	A	3	H	1	116	19.66	22.6		1480	
172	1060	A	3	H	1	14	18.64	22.6		1470	
172	1060	A	3	H	2	135	21.35	22.6		1412	
172	1060	A	3	H	2	25	20.25	22.6		1412	
172	1060	A	3	H	3	124	22.74	22.8		1410	
172	1060	A	3	H	3	30	21.8	22.8		1428	
172	1060	A	3	H	4	89	23.89	22.2		1485	
172	1060	A	3	H	4	18	23.18	22.2		1379	
172	1060	A	3	H	5	128	25.78	22.2		1297	

This table also appears on the volume CD-ROM.

Table 49. Compressional wave velocity measurements from Site 1061.

Leg	Site	Hole	Core	Type	Section	Interval (cm)	Depth (mbsf)	Depth (mbsf +11 m)	Temp. (°C)	Velocity 1 Z-direction (m/s)	Velocity 2 Y-direction (m/s)	Velocity 3 X-direction (m/s)
172	1061	A	1	H	1	45	0.45	11.45	19.7	1485	1486	
172	1061	A	1	H	1	114	1.14	12.14	19.7	1487	1489	
172	1061	A	1	H	2	34	1.84	12.84	20.3	1486	1486	
172	1061	A	1	H	2	121	2.71	13.71	20.3	1484	1490	
172	1061	A	1	H	3	47	3.47	14.47	21.2	1485	1486	
172	1061	A	1	H	3	118	4.18	15.18	21.2	1491	1500	
172	1061	A	1	H	4	36	4.86	15.86	21.3	1488	1488	
172	1061	A	1	H	4	109	5.59	16.59	21.3	1488	1494	
172	1061	A	1	H	5	34	6.34	17.34	21.2	1492	1502	
172	1061	A	1	H	5	87	6.87	17.87	21.2	1500	1503	

This is a sample of the table that appears on the volume CD-ROM.

Table 50. Compressional wave velocity measurements from Site 1062.

Leg	Site	Hole	Core	Type	Section	Interval (cm)	Depth (mbsf)	Temp. (°C)	Velocity 1 Z-direction (m/s)	Velocity 2 Y-direction (m/s)	Velocity 3 X-direction (m/s)
172	1062	A	1	H	1	36	0.36	19.1	1491	1495	
172	1062	A	1	H	1	102	1.02	19.7	1488	1482	
172	1062	A	2	H	1	95	3.15	18.7	1473	1482	
172	1062	A	2	H	2	32	4.02	19.6	1483	1489	
172	1062	A	2	H	2	113	4.83	19.2	1481	1480	
172	1062	A	2	H	3	27	5.47	20	1477	1480	
172	1062	A	2	H	3	113	6.33	20.3	1483	1487	
172	1062	A	2	H	4	40	7.1	20.3	1486	1493	
172	1062	A	2	H	4	118	7.88	20.5	1483	1491	
172	1062	A	2	H	5	29	8.49	20.6	1488	1484	

This is a sample of the table that appears on the volume CD-ROM.

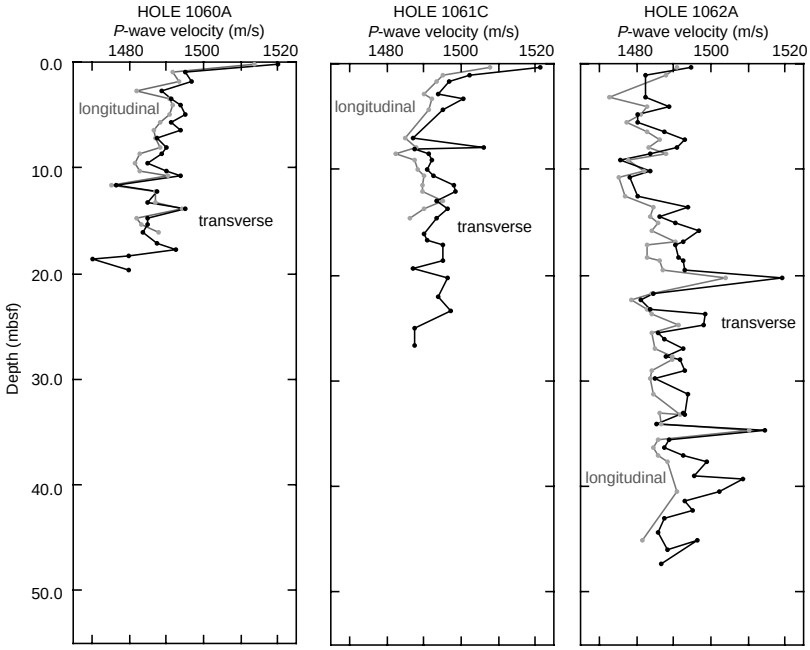

Figure 94. Measurements of longitudinal and transverse velocity vs. depth for Holes 1060A, 1061C, and 1062A.

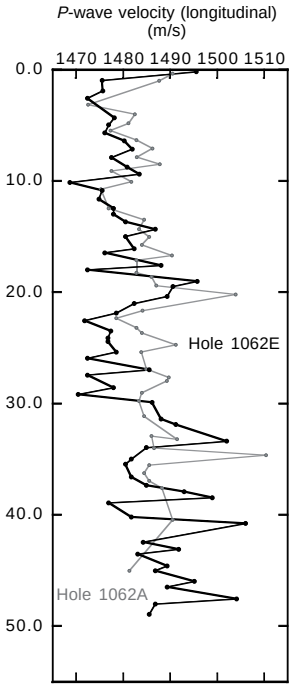

Figure 95. Comparison of longitudinal velocity profiles obtained at the western (Hole 1062A) and eastern flank (Hole 1062E) of a mud wave.

the log mbsf to within 2 m on the basis of depth offsets between log and physical properties data (Fig. 102).

Log Quality

Borehole caliper measurements showed that the hole had an average diameter of about 12 in, with narrow but frequent washouts, and thicker intervals of washout to 16 in toward the top of the logged section. The narrow washouts caused bad contact with the borehole wall and hence spikes in some of the logs; for example, the APLC porosity reads 100% (i.e., borehole fluid) in places. Bulk density, shallow resistivity (SFLU), and natural gamma display similar spikes. Although some of the washouts are likely caused by the drill bit rotating at the same depth for a period of time (e.g., in between taking cores), they are probably also lithologically controlled; for example, the carbonate-rich layers in the upper unit seem to be more easily washed out than the clay-rich sediment. Thus, much of the negative spikes of the natural gamma log are probably caused by real lithological variability. The deeper penetrating logs, such as medium resistivity, are much less affected by borehole roughness, but show a similar pattern, again suggesting lithologic variability.

The absolute values of the density and density-derived porosity match very well with the index physical properties of the cores, apart from the anomalous density lows at washouts (Fig. 102). The core natural gamma profile tracks the downhole natural gamma very well.

The initial sonic velocities derived from each of the interval transit times (Δt) gave logs which were offset from each other. In fact the Δt for the two 3-m transits (lower transmitter to lower receiver and upper transmitter to upper receiver), which should be the same, were offset from each other by a time equivalent to an extra separation of 15 cm (the distance to the next highest receiver on the tool). Recalculating the velocities taking into account this 15-cm offset yielded logs that overlay each other much better, and examples of these velocities are shown in Figure 102. The origin of this problem remains unclear. The Schlumberger engineer could find no physical or electrical problem with the tool. On previous legs, the tool performed well in lithified rock and poorly in soft sediment. Anomalous spikes in the log are caused by cycle skipping (misreading the first arrival at the receiver) and these are removed during the onshore processing. The deep penetration resistivity log (IDPH) did not record during logging, so the plain induction measurement (ILD) was used as a substitute. The triple combo reached to within 2 m of the bottom of the hole, and the FMS-Sonic to within 12 m, because of increasing debris in-fill with time.

Logging Units

The sedimentary sequence could be divided into four distinct units on the basis of changes in the character of the downhole logs (Figs. 102, 103).

Table 51. Undrained shear-strength measurements from Site 1060.

Leg	Site	Hole	Core	Type	Section	Interval (cm)	Depth (mbsf)	Method	Spring no.	Undrained shear strength (kPa)	Residual strength (kPa)
172	1060	A	1	H	1	108	1.08	Vane	B-1	2.4	1.4
172	1060	A	1	H	2	134	2.84	Vane	B-1	2.1	1.0
172	1060	A	1	H	3	125	4.25	Vane	B-1	1.9	1.6
172	1060	A	1	H	4	109	5.59	Vane	B-1	4.1	2.3
172	1060	A	1	H	5	134	7.34	Vane	B-1	4.0	
172	1060	A	2	H	1	99	9.99	Vane	B-1	8.6	4.3
172	1060	A	2	H	2	76	11.26	Vane	B-1	8.6	5.2
172	1060	A	2	H	3	90	12.9	Vane	B-1	7.3	
172	1060	A	2	H	4	92	14.42	Vane	B-1	10.2	5.1
172	1060	A	2	H	5	79	15.79	Vane	B-1	10.0	6.1

This is a sample of the table that appears on the volume CD-ROM.

Table 52. Undrained shear-strength measurements from Site 1061.

Leg	Site	Hole	Core	Type	Section	Interval (cm)	Depth (mbsf)	Method	Spring no.	Undrained shear strength (kPa)	Residual strength (kPa)
172	1061	A	1	H	1	129	1.29	Vane	B-1	8.95	4.15
172	1061	A	1	H	2	133	2.83	Vane	B-1	10.61	4.53
172	1061	A	1	H	2	15	1.65	Vane	B-1	9.24	4.09
172	1061	A	1	H	3	14	3.14	Vane	B-1	9.01	4.05
172	1061	A	1	H	3	133	4.33	Vane	B-1	10.63	4.89
172	1061	A	1	H	4	55	5.05	Vane	B-1	10.14	5.24
172	1061	A	1	H	4	124	5.74	Vane	B-1	10.99	4.8
172	1061	A	1	H	5	16	6.16	Vane	B-1	8.95	3.88
172	1061	A	1	H	5	127	7.27	Vane	B-1	12.16	5.88
172	1061	A	1	H	6	12	7.62	Vane	B-1	13.63	6.95

This is a sample of the table that appears on the volume CD-ROM.

Table 53. Undrained shear-strength measurements from Site 1062.

Leg	Site	Hole	Core	Type	Section	Interval (cm)	Depth (mbsf)	Method	Spring no.	Undrained shear strength (kPa)	Residual strength (kPa)
172	1062	A	1	H	1	49	0.49	Vane	B-1	3.13	1.45
172	1062	A	1	H	1	113	1.13	Vane	B-1	1.83	0.847
172	1062	A	2	H	1	103	3.23	Vane	B-1	4.45	2.091
172	1062	A	2	H	2	44	4.14	Vane	B-1	6.31	3.368
172	1062	A	2	H	2	124	4.94	Vane	B-1	3.69	1.699
172	1062	A	2	H	3	37	5.57	Vane	B-1	4.67	2.306
172	1062	A	2	H	3	125	6.45	Vane	B-1	5.96	3.34
172	1062	A	2	H	4	52	7.22	Vane	B-1	7.18	3.519
172	1062	A	2	H	4	109	7.79	Vane	B-1	5.98	3.047
172	1062	A	2	H	5	40	8.6	Vane	B-1	8.43	4.438

This is a sample of the table that appears on the volume CD-ROM.

Unit 1 (0–171 mbsf)

The uppermost unit is characterized by a strong, long-wavelength cyclicity of the natural gamma, bulk density, porosity, and resistivity logs. In this unit, most gamma peaks correspond to magnetic susceptibility peaks (see "Physical Properties" section, this chapter), which have been shown to correlate with glacial stages (see "Sedimentation Rates" section, this chapter). Thus, the logged peaks in Unit 1 show that the glacial sediments have higher clay contents, are denser and less porous, and have a higher resistivity (because of the decreased porosity) than the corresponding interglacial sediments. The cycles are seen most clearly in the medium resistivity record. The lowest resistivity values of the whole log are recorded close to the boundary between Units 1 and 2, at 168 mbsf, together with a thin, high-density spike.

Unit 2 (171–270 mbsf)

The top of Unit 2 is marked by a downhole step decrease in bulk density and resistivity values, in contrast to the expected general downhole compaction trend. The long-wavelength cycles of Unit 1 are replaced by shorter and less distinct cycles, and most of the logs show a more limited range of variability. There is one broad resistivity and density high between 218 and 228 mbsf; this may correspond in part to a lithified layer recovered at about 215 mbsf (see "Lithostratigraphy" section, this chapter).

The uranium log and Th/K ratio are of particular interest in Unit 2. Uranium displays a large (factor of two) variability, with a regular cyclicity (see below). Th/K also shows a wide range, and for the most part tends to be high when uranium is low (see below).

Unit 3 (270–327 mbsf)

Unit 3 is picked on the basis of a downhole increase in density, resistivity, and velocity over an interval of about 10 m. There is also a step increase in the Th/K ratio, a little below the unit boundary at 278 mbsf. Compaction and lithification may play a role here, but the steepness of the change in properties at the boundary and chemical change indicated by the Th/K ratio indicates there is also a compositional change.

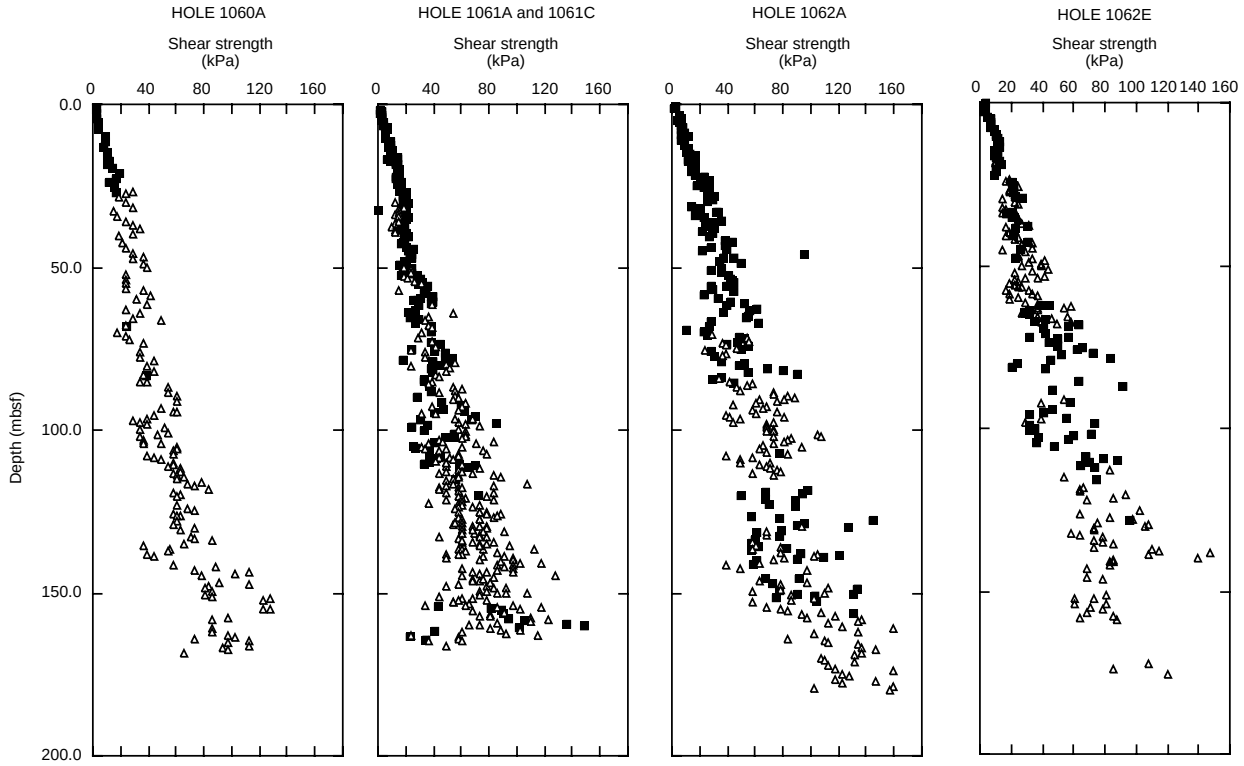

Figure 96. Comparison of vertical profiles of undrained shear strength for Sites 1060, 1061, and 1062. Data from Hole 1061A are plotted at mbsf + 11 m to account for an apparent offset in depths relative to the mudline.

Table 54. Thermal conductivity measurements from Site 1060.

Leg	Site	Hole	Core	Type	Section	Interval (cm)	Depth (mbsf)	Thermal conductivity (W/[m·K])
172	1060	A	1	H	1	50	0.5	0.951
172	1060	A	1	H	2	50	2	0.872
172	1060	A	1	H	3	50	3.5	0.883
172	1060	A	12	H	3	47	107.47	0.880
172	1060	A	13	H	3	60	117.1	0.936
172	1060	A	14	H	3	70	126.7	1.044
172	1060	A	15	H	3	67	136.17	0.927
172	1060	A	16	H	3	50	145.5	1.199
172	1060	A	17	H	3	50	155	1.124
172	1060	A	18	H	3	50	164.5	1.030
172	1060	B	1	H	1	50	0.5	0.944
172	1060	B	2	H	1	50	6.9	0.894
172	1060	B	2	H	3	50	9.9	0.924
172	1060	B	2	H	5	50	12.9	0.988
172	1060	B	3	H	1	50	16.4	0.928
172	1060	B	3	H	3	50	19.4	0.917
172	1060	B	3	H	5	50	22.4	0.874
172	1060	B	4	H	1	66	26.06	0.854
172	1060	B	4	H	3	50	28.9	0.814
172	1060	B	4	H	5	50	31.9	0.854
172	1060	B	5	H	1	50	35.4	0.798
172	1060	B	5	H	3	50	38.4	0.815
172	1060	B	5	H	5	50	41.4	0.891
172	1060	B	6	H	1	50	44.9	0.849
172	1060	B	6	H	3	50	47.9	0.965
172	1060	B	6	H	5	50	50.9	0.810
172	1060	B	7	H	1	50	54.4	0.911
172	1060	B	7	H	3	50	57.4	0.864
172	1060	B	8	H	3	50	66.9	0.853
172	1060	B	9	H	3	50	76.4	0.905
172	1060	B	10	H	3	50	85.9	0.976
172	1060	B	11	H	3	50	95.4	0.843
172	1060	B	12	H	3	30	103.07	0.960
172	1060	B	13	H	3	60	114.5	0.897
172	1060	B	14	H	3	60	124	1.074

This table also appears on the volume CD-ROM.

Table 55. Thermal conductivity measurements from Site 1061.

Leg	Site	Hole	Core	Type	Section	Interval (cm)	Depth (mbsf)	Depth (mbsf +11 m)	Thermal conductivity (W/[m˙K])
172	1061	A	1	H	3	50	3.5	14.5	0.934
172	1061	A	2	H	3	50	13	24	0.857
172	1061	A	3	H	3	50	22.5	33.5	0.867
172	1061	A	3	H	5	50	25.5	36.5	0.897
172	1061	A	4	H	3	50	32	43	0.936
172	1061	A	5	H	3	60	41.6	52.6	0.878
172	1061	A	6	H	3	50	51	62	0.854
172	1061	A	7	H	3	50	60.5	71.5	0.876
172	1061	A	8	H	3	50	69.86	80.86	0.949
172	1061	A	9	H	3	50	79.5	90.5	0.835

This is a sample of the table that appears on the volume CD-ROM.

Table 56. Thermal conductivity measurements from Site 1062.

Leg	Site	Hole	Core	Type	Section	Interval (cm)	Depth (mbsf)	Thermal conductivity (W/[m˙K])
172	1062	A	1	H	1	50	0.5	0.897
172	1062	A	2	H	1	50	2.7	0.560
172	1062	A	2	H	3	50	5.7	0.903
172	1062	A	2	H	5	50	8.7	0.961
172	1062	A	3	H	1	50	12.2	0.872
172	1062	A	3	H	3	50	15.2	0.903
172	1062	A	3	H	5	50	18.2	0.934
172	1062	A	4	H	1	50	21.7	0.957
172	1062	A	4	H	3	50	24.7	0.976
172	1062	A	4	H	5	50	27.7	0.932

This is a sample of the table that appears on the volume CD-ROM.

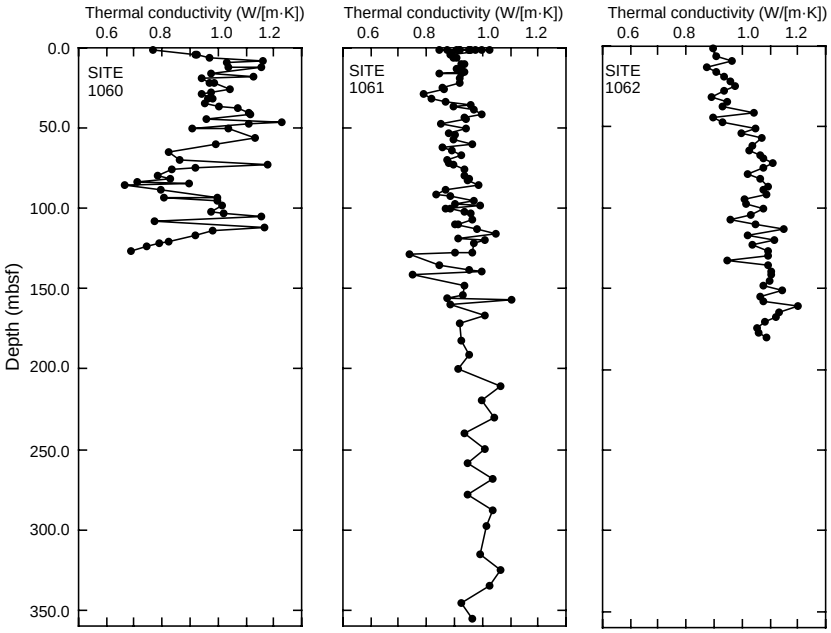

Figure 97. Thermal conductivity vs. depth at Sites 1060, 1061, and 1062. Data from Hole 1061A are plotted at mbsf plus + 11 m to account for an apparent offset in depths relative to the mudline (see "Stratigraphic Correlation" section, this chapter).

Unit 4 (327 mbsf to the Bottom of Hole)

This lowermost unit is picked on the basis of a sharp drop in resistivity at 327 mbsf, although the other logs do not show such a dramatic feature at this boundary. Because of the position of the natural gamma tools at the top of the tool strings, only 8 m of Unit 4 has natural gamma logged, but no large change in natural gamma is seen in core or log data. The resistivity decreases further below 344 mbsf.

Porosity Measurements

The APS tool derives its porosity measurement from the slowing of fast neutrons by hydrogen in the formation. It assumes all the formation's hydrogen is in pore water (and that the matrix is limestone in the case of APLC, the main porosity measurement given by the APS), and takes no account of the hydrogen in the bound water of clays. This results in an overestimate of porosity for the clay-rich sediments of Hole 1061A.

An improved estimate of porosity (Φ) was derived from the bulk density log (RHOB) using the following equation:

$$\Phi = (\rho_{gr} - \rho_b)/(\rho_{gr} - \rho_w),$$

where the mean grain density of the index physical properties measurements (2.734 ± 0.099 g/cm^3) was used for the grain density (ρ_{gr}), 1.03 g/cm^3 for pore-water density (ρ_w), and RHOB for the bulk density (ρ_b). The density-derived porosity estimates are very close to the core index property porosities, except in the thin, washed-out layers where tool contact with the borehole wall was poor.

Uranium

Uranium is present in seawater as the UO_2^{2+} ion, and the principal way that it is incorporated into sediment is by adsorption onto organic matter (Serra, 1984). So the simplest interpretation of uranium peaks is that they correspond to peaks in organic matter and TOC. It is difficult to say whether there is a good correspondence of TOC% (see "Geochemistry" section, this chapter) with uranium, because the precision of the shipboard TOC measurements is low, there are relatively few of them, and the log depth differs from the core depth by up to 2 m. However, initial comparison suggests that relating uranium only to TOC is too simplistic. As a first interpretation, uranium peaks represent high production, influx, and preservation of organic matter.

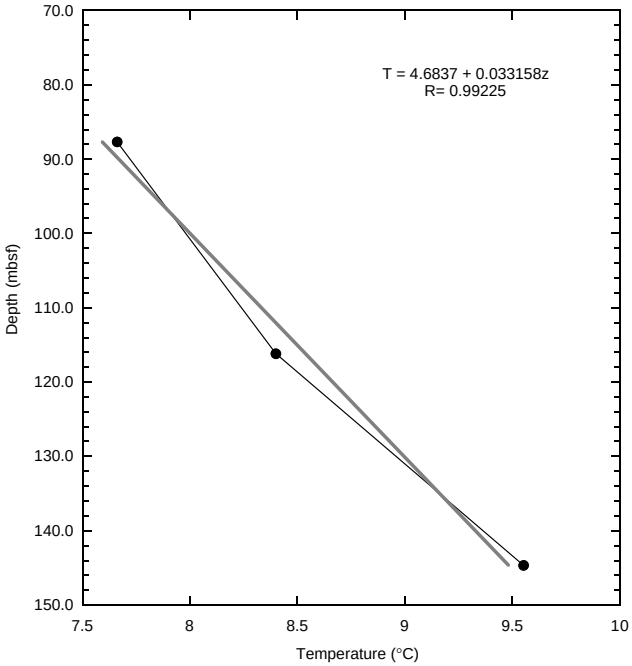

Figure 98. Equilibrium temperature (T) as a function of depth (z) for Hole 1062A.

In Unit 1, maxima in uranium appear broadly correlated with maxima in natural gamma, although there are many more short, high uranium intervals than there are longer natural gamma intervals. At the Unit 1/Unit 2 boundary, there is a step decrease downhole in uranium.

In Unit 2, the uranium record's apparent periodicity of about 35 k.y. (by FFT) suggests that uranium is, in fact, tracking the climatic changes, known to cycle at 40 k.y. during this interval.

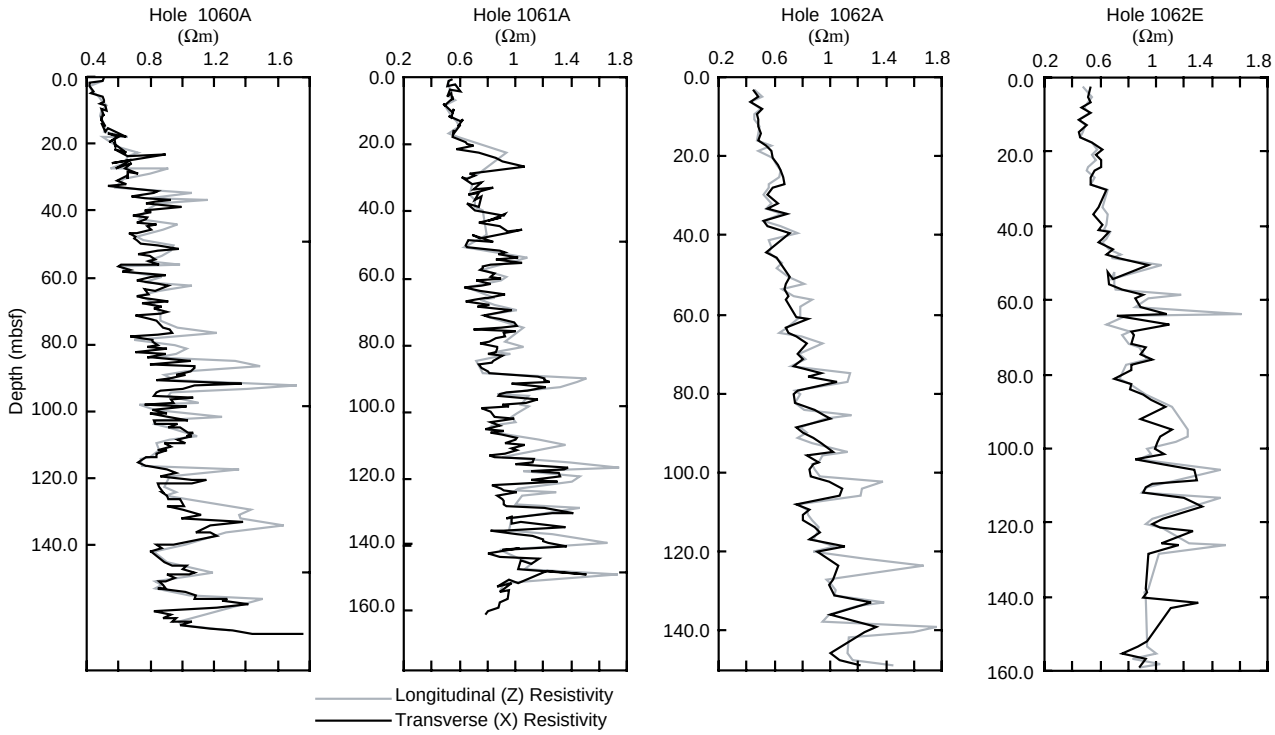

Figure 99. Resistivity at Sites 1060, 1061, and 1062.

Table 57. Resistivity measurements from Site 1060.

Leg	Site	Hole	Core	Type	Section	Interval (cm)	Depth (mbsf)	Temp. (°C)	Resistivity Z-direction (Ωm)	Resistivity Y-direction (Ωm)
172	1060	A	1	H	1	24	0.24	22		0.509
172	1060	A	1	H	1	96	0.96	22.8	0.502	0.497
172	1060	A	1	H	2	31	1.81	21.8		0.414
172	1060	A	1	H	2	126	2.76	22.3	0.420	0.415
172	1060	A	1	H	3	33	3.33	22.5		0.422
172	1060	A	1	H	3	110	4.1	22.8	0.431	0.439
172	1060	A	1	H	4	33	4.83	22.4		0.423
172	1060	A	1	H	4	125	5.75	22.7	0.478	0.497
172	1060	A	1	H	5	70	6.7	23.1		0.503
172	1060	A	1	H	5	125	7.25	22.8	0.496	0.503

This is a sample of the table that appears on the volume CD-ROM.

Table 58. Resistivity measurements from Site 1061.

Leg	Site	Hole	Core	Type	Section	Interval (cm)	Depth (mbsf)	Temp. (°C)	Resistivity Z-direction (Ωm)	Resistivity Y-direction (Ωm)
172	1061	A	1	H	1	47	0.47	19.9		0.544
172	1061	A	1	H	1	116	1.16	20.2	0.518	0.520
172	1061	A	1	H	2	122	2.72	20.6	0.523	0.510
172	1061	A	1	H	2	37	1.87	20		0.565
172	1061	A	1	H	3	120	4.2	21.1	0.540	0.604
172	1061	A	1	H	3	50	3.5	20.6		0.531
172	1061	A	1	H	4	112	5.62	21.2	0.531	0.514
172	1061	A	1	H	4	39	4.89	21.1		0.538
172	1061	A	1	H	5	90	6.9	21	0.570	0.548
172	1061	A	1	H	5	36	6.36	21		0.544

This is a sample of the table that appears on the volume CD-ROM.

Table 59. Resistivity measurements from Site 1062.

Leg	Site	Hole	Core	Type	Section	Interval (cm)	Depth (mbsf)	Temp. (°C)	Resistivity Z-direction (Ωm)	Resistivity Y-direction (Ωm)
172	1062	A	2	H	1	101	3.21	19.4	0.455	0.448
172	1062	A	2	H	2	116	4.86	19.9	0.509	0.484
172	1062	A	2	H	3	114	6.34	19.8	0.430	0.423
172	1062	A	2	H	4	120	7.9	20.4	0.497	0.507
172	1062	A	2	H	5	95	9.15	20.4	0.453	0.476
172	1062	A	2	H	6	104	10.74	20.4	0.456	0.487
172	1062	A	3	H	1	84	12.54	19.9	0.488	0.487
172	1062	A	3	H	2	112	14.32	19.9	0.486	0.498
172	1062	A	3	H	3	107	15.77	19.9	0.471	0.487
172	1062	A	3	H	4	96	17.16	20.1	0.581	0.536

This is a sample of the table that appears on the volume CD-ROM.

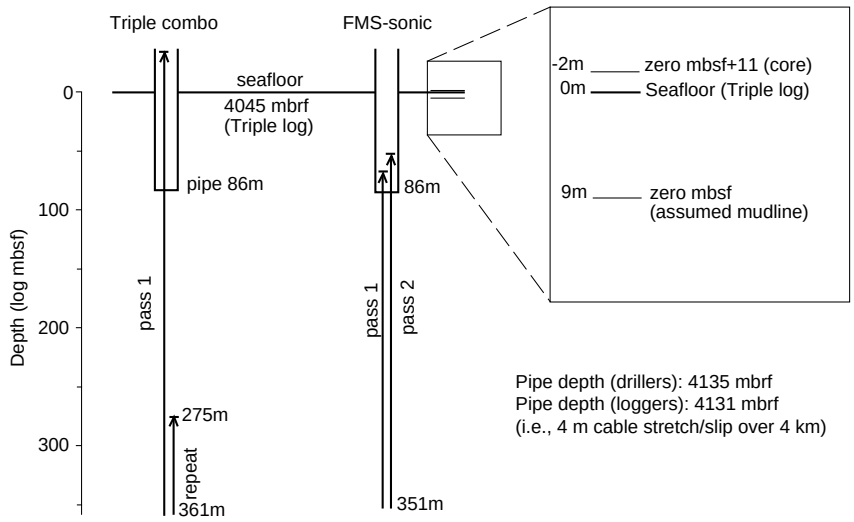

Figure 100. Graphic summary of downhole logging operations at Hole 1061A. Seafloor was picked on the basis of the step in the natural gamma logs at the sediment/water boundary.

Clay Lithology

Clays contain radioactive isotopes of potassium and thorium, whose radiation is measured by the HNGS tool on the triple combination and NGT on the FMS-Sonic tool strings. Moreover, different clays contain different proportions of potassium and thorium, which enable them to be distinguished by logging (Rider, 1996; Serra, 1984; see Table 60).

Because illite contains much more potassium than either kaolinite or chlorite, and all three contain thorium, the ratio Th/K (Fig. 103) increases when kaolinite and chlorite concentrations increase. In Unit 1, high Th/K corresponds to low overall clay (from CGR, and therefore interglacials), which could mean that the illite clay fraction is reduced at these times. In Unit 3, the Th/K ratio is high while CGR remains high, indicating an increased chlorite/kaolinite input. Since kaolinite (and chlorite) are derived from continental rocks, a high Th/K ratio may be indicative of higher levels of continental (glacial) erosion.

The potassium log may be scaled directly in terms of illite content, if it is assumed that all the potassium is in the illite, and 100% illite contains 5.2% potassium (Table 60). The potassium scale of 0% to 3% on Figure 103 then runs from 0% to 57.7% illite. This is a percentage of the bulk sediment, including pore space. Assuming average porosities of 55% at Hole 1061A, this calculation yields illite contents ranging from 44% to 89%, with an average of around 66%. Even if the above assumptions lead to an overestimate, illite clay is still likely to be the major component of the sediment.

The crossplot of photoelectric factor (PEF) vs. potassium (Fig. 104) indicates that illite is the dominant clay throughout Hole 1061A, and of the other clays, kaolinite and/or montmorillonite are more abundant than chlorite. All four logging units overlap on Figure 104, but some differences can be picked out: Unit 1 has a wide spread with a bias toward illite; Unit 2 has the widest spread of the four units; Unit 3 has the highest PEF values, indicating more chlorite than the other units; and Unit 4 is tightly grouped at the top right, towards illite and chlorite.

Shipboard XRD analyses of core samples indicate illite and probably chlorite dominate the clays in Hole 1061A (see "Lithostratigraphy" section, this chapter).

The clay interpretation of the natural gamma logs also differs from the type of clays expected from glacial erosion. An illite/chlorite mix is expected during most of the Pleistocene, a kaolinite/illite/chlorite mix is expected at the beginning of glaciation, and high levels of kaolinite are expected before glaciation.

The offset between APS porosity and porosity derived from density may be attributed to the presence of bound water in the clays. Indeed, if the HI of the clays is known (Table 60), the percentage of kaolinite/chlorite-dominated clay can be calculated. However, the results of this calculation can be difficult to interpret. Also, the bad pad contact caused by hole roughness affects both APS and density logs, introducing additional uncertainty.

FMS

The two FMS runs produced very similar images, with the second run tracking in the grooves in the borehole wall made by the first. There was some tool sticking, which was corrected for in the shipboard processing, using tool acceleration data recorded by the GPIT in the tool string.

The small range of variability in resistivity and rugose borehole wall meant that the FMS images contain many artifacts from poor pad contact with the borehole wall. However, some features can be

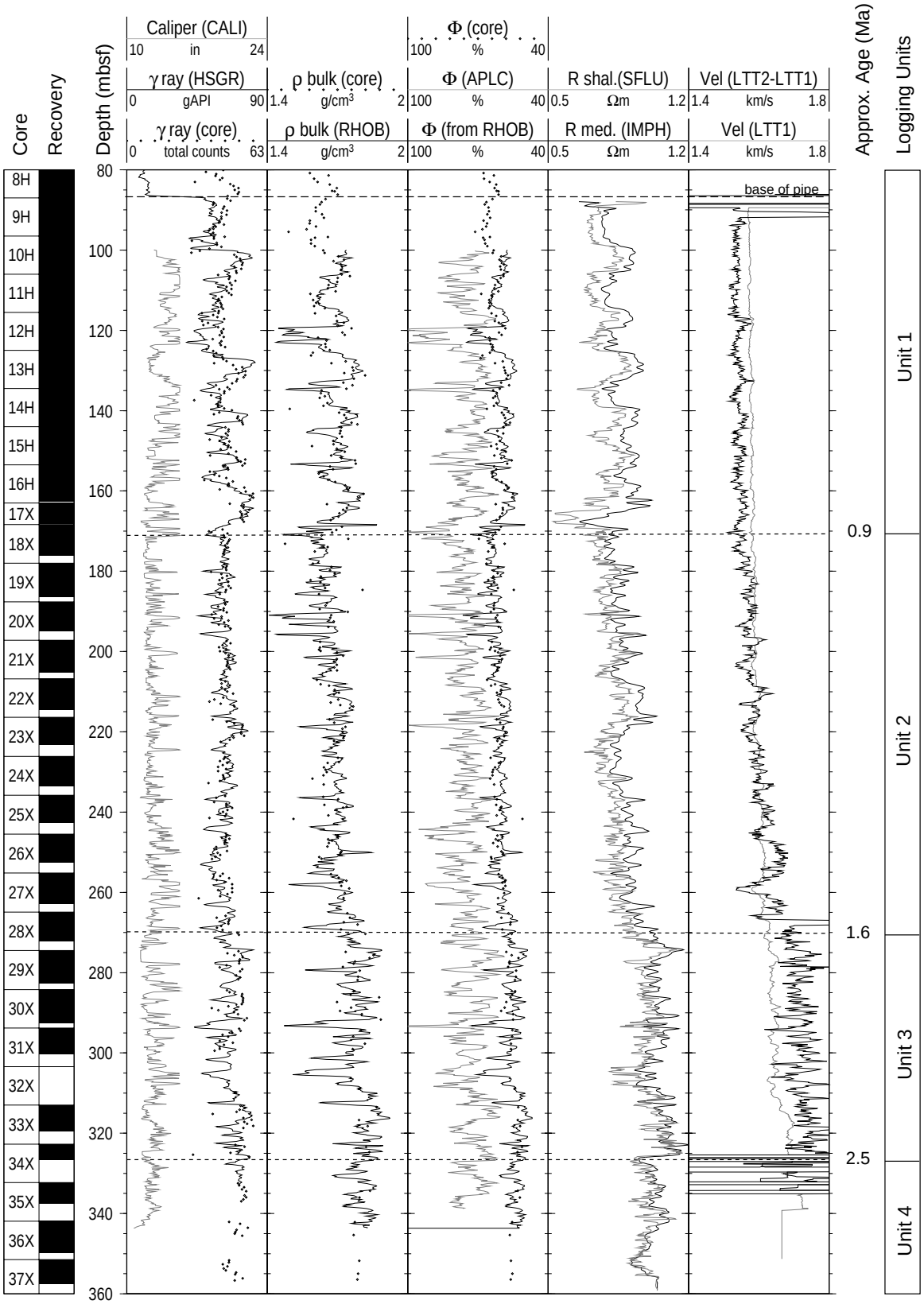

Figure 102. Downhole logs of caliper, total natural gamma, bulk density (ρ), porosity (Φ), resistivity, and velocity from Hole 1061A, with core measurements of bulk density and porosity (index properties) and natural gamma (MST track). Logging units were chosen purely on the basis of the logs; their approximate ages were taken from biostratigraphy ("Biostratigraphy" section, this chapter). Depths of the logged measurements are in depth below logged seafloor, and the core measurements and recovery column are in mbsf + 11 m.

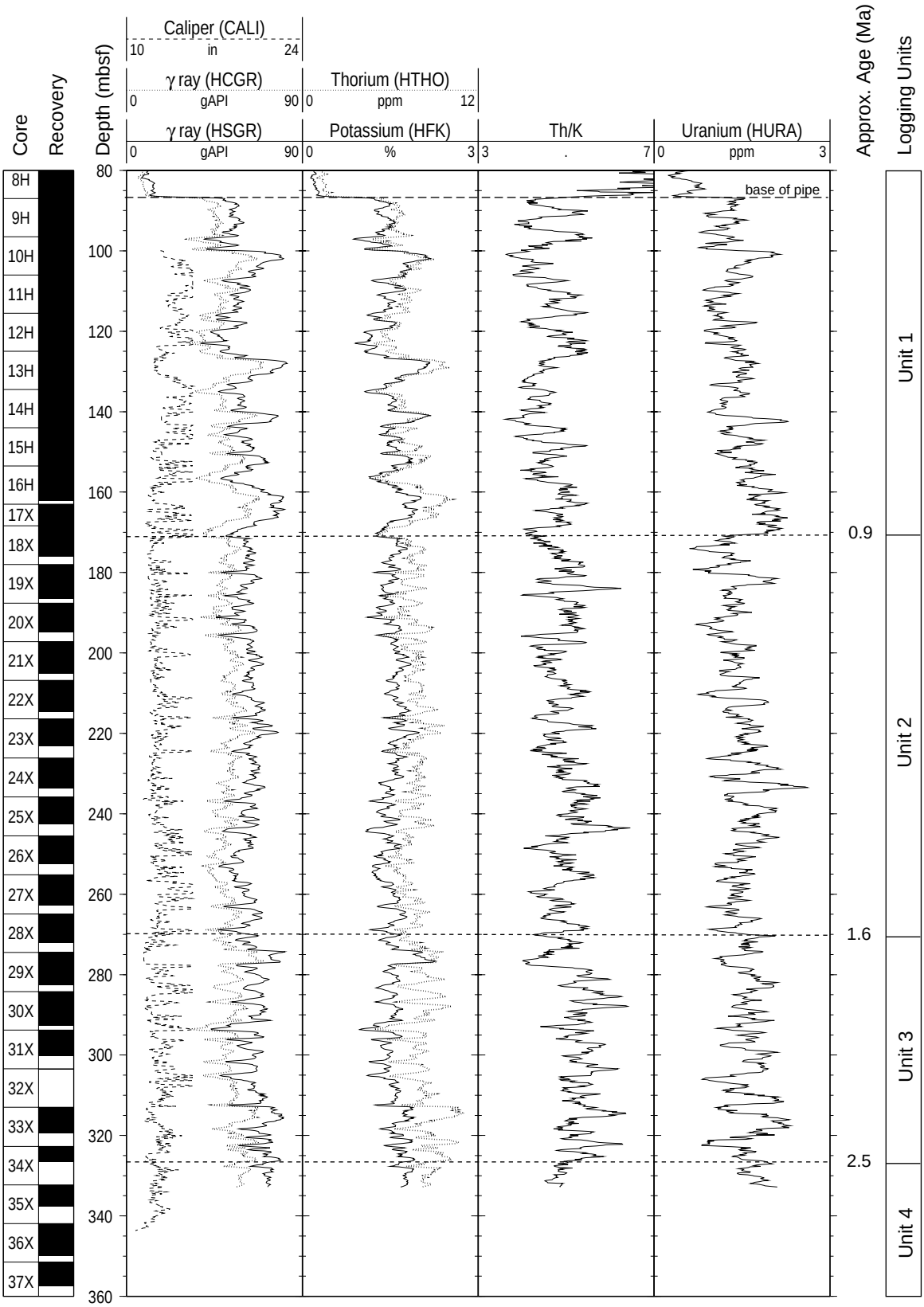

Figure 103. Downhole logs from Hole 1061A obtained with the HNGS natural gamma tool. Depths are in depth below logged seafloor. Logging units were chosen on the basis of the logs; their approximate ages were taken from biostratigraphy (“Biostratigraphy” section, this chapter).

Table 60. Chemical and nuclear parameters for some common clay minerals (Rider, 1996).

	K (av. %)	Th (ppm) approx.	PEF (barns/e)	Σ_f (c.u.)	H_2O (av. %)	HI	CNL porosity (%)
Illite	5.2	6-12	3.03	16.74	8	0.09	30
Kaolinite	0.63	18-26	1.49	13.04	13	0.37	37
Chlorite	0		6.2	~30	14	0.32	52
Glauconite	4.5	2-8	4.79	20.89			
Montmorillonite	0.22	10-24	1.63	8.10	18-22	0.17	44

Note: av. = average, HI = hydrogen index, CNL = compensated neutron log; PEF Fe-Chlorite 12.36, Mg-Chlorite 1.39; Σ_f Fe-Chlorite 47.44, Mg-Chlorite 11.34.

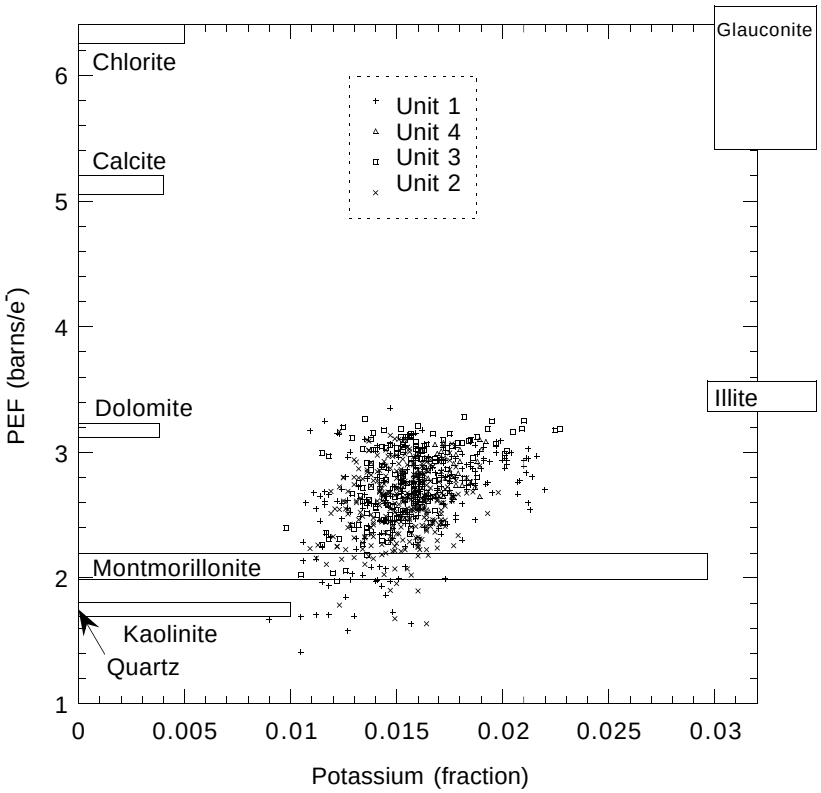

Figure 104. Crossplot of PEF (photoelectric factor) vs. potassium. Fields are given for various clays and other minerals.

observed, including a resistive feature with a flat underside and graded top at 117 mbsf (Fig. 105) and further thin resistive features at 141 and 197.2 mbsf. Such resistive features often indicate beds of sediment with a coarser grain size than adjacent units (Serra, 1989).

Temperature Logs

The Lamont temperature tool was lowermost in the triple combination tool string. It measures borehole fluid temperatures (Fig. 106). The measurement itself is very accurate, but because the fluid temperature depends on the length of time it was circulated (roughly 6 hr before drilling), it is not normally in equilibrium with the formation temperature. The upward pass of the first log has a temperature gradient of about 10°C/km. At this site the temperature log might, in principle, have been used to detect the heat produced by the exothermic dissociation of methane hydrate, but for the above reason and the absence of hydrate.

SITE GEOPHYSICS

Surveys

Three surveys were conducted before dropping the beacon at Sites 1060, 1061, and 1062 (Figs. 107–109). At Sites 1060 (Line 4) and 1061 (Line 5), the survey pattern consisted of a simple cross designed to determine the consistency of layering at the sites, whereas at Site 1062 (Line 6), a slightly more complex survey was run to provide information about changing wave orientation with time. Information collected during the survey at Site 1060 resulted in moving the site slightly to avoid an acoustic anomaly on the seismic profile. Sites 1061 and 1062 were drilled at the planned positions. The surveys were undertaken using a generator injector (GI) gun and 3.5-kHz subbottom profiler (Figs. 110–113). An 80-in^3 water gun was used during part of the survey at Site 1060 to provide a comparison between the two sources. The 3.5-kHz profile shown here for Site 1062 (Fig. 113) was collected during *Knorr* Cruise 140, Leg 2, along the same survey track followed for the seismic profile.

Site 1060

The 3.5-kHz profiles show a uniform layering pattern. The seismic record shows similar reflections in all parts of the survey (Fig. 110), but there are some lateral changes in the depths and intensities of individual reflections (e.g., near shotpoint 330; Fig. 110). This is most likely the result of sound-velocity anomalies caused by the nonuniform distribution of gas hydrate in the sediment column. The proposed location of Site 1060 was near one of these acoustic anomalies, so an alternate site was chosen where the reflection pattern showed

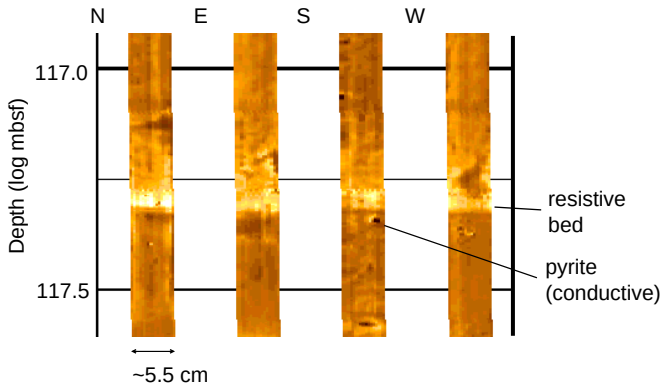

Figure 105. FMS microresistivity image of a lithological feature at 117.3 mbsf. Pyrite concretions are relatively conductive and appear as dark spots throughout the sequence.

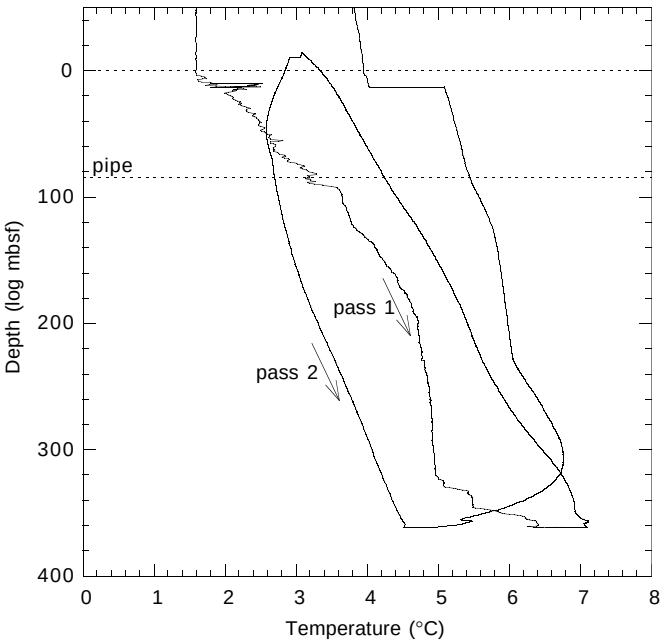

Figure 106. Temperature log from the Lamont temperature tool, at the base of the triple combination tool string (see text).

less variability. The reflections were also somewhat farther apart at the alternate site, suggesting an overall higher sedimentation rate. The seismic profile at Site 1060 shows numerous parallel reflections in the uppermost 0.3 s TWT (236 m). Parallel reflections are also present deeper than 0.3 s TWT, but they are less distinct, perhaps because of sound attenuation. There is a series of prominent longer wavelength reflections from 0.18 to 0.21 s TWT (139–163 m) that may correspond to lithologic variations in MISs 16–21 near the base of the hole. The seismic record shows the presence of a weak BSR at 0.60–0.65 s TWT, suggesting the presence of gas hydrate.

Site 1061

The 3.5-kHz and seismic profiles at this site show a uniform layering pattern, and the site was drilled, as proposed, immediately to the west of the Blake Outer Ridge crest. The seismic profile at Site 1061 shows numerous parallel reflections to 0.32 s TWT (253 m). Parallel reflections are also present deeper than 0.32 s TWT, but they are less distinct, perhaps because of sound attenuation. There are series of

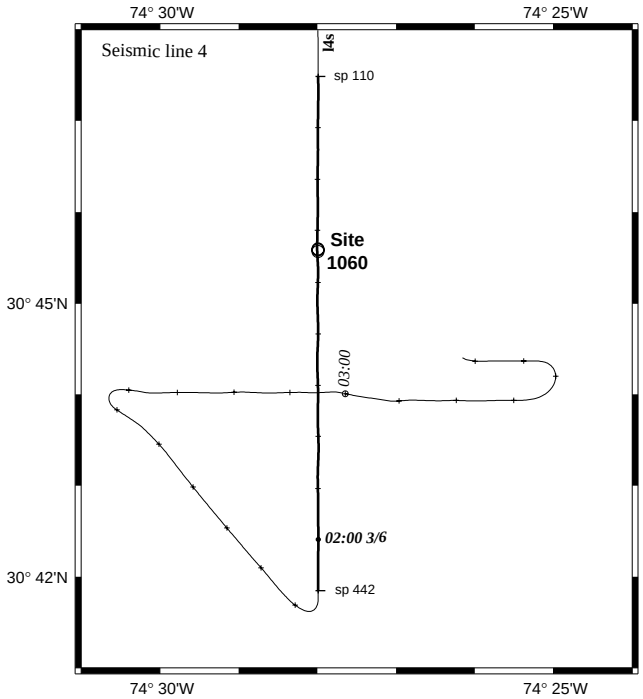

Figure 107. Survey track over Site 1060, with dates, times (UTC), and selected shotpoints (SP) given along the survey line. The track of the seismic profile in Figure 110 is thicker.

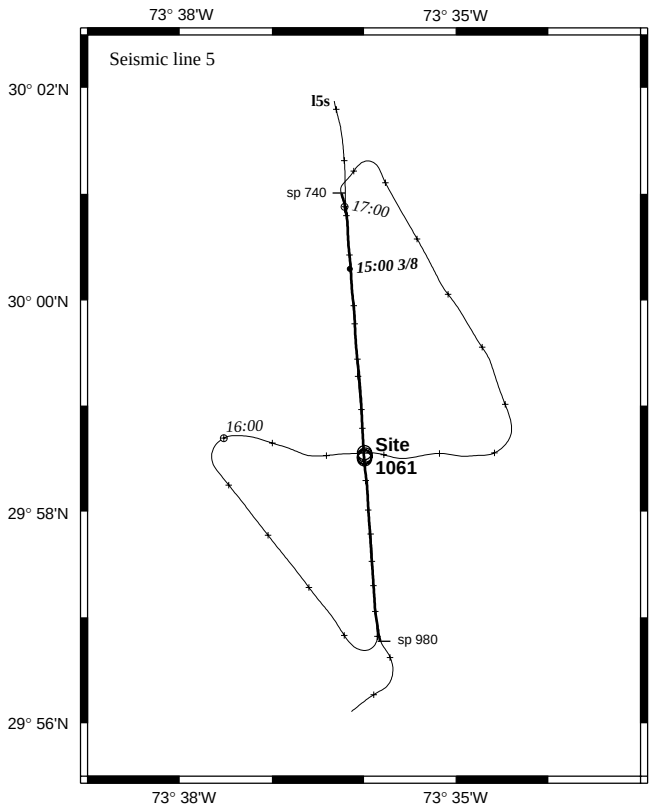

Figure 108. Survey track over Site 1061, with dates, times (UTC), and selected shotpoints (SP) given by the numbers along the survey line. The track of the seismic profile in Figure 111 is thicker.

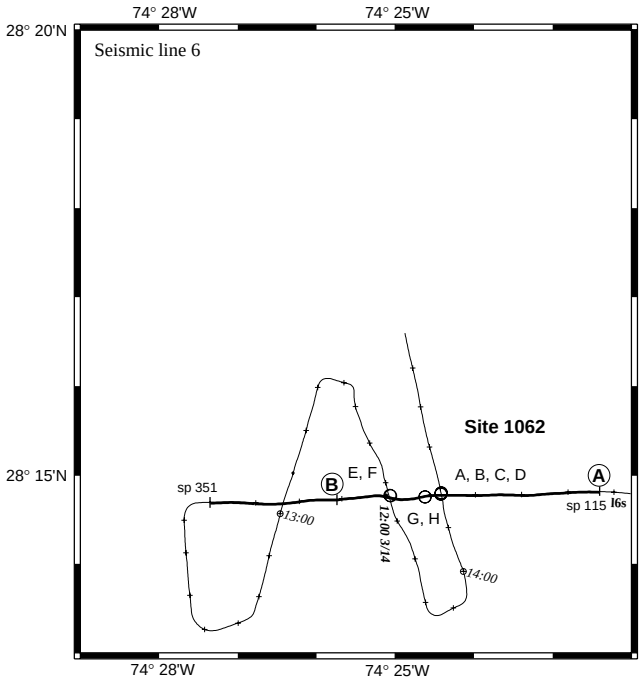

Figure 109. Survey track over Site 1062, with dates, times (UTC), and selected shotpoints (SP) given by the numbers along the survey line. The track of the seismic profile in Figure 112 is thicker. A–B marks the *Knorr* 3.5-kHz profile in Figure 113.

three prominent, longer wavelength reflections from 0.15 to 0.18 s TWT (115–139 m) that may correspond to lithologic variations in MISs 16–22 (see "Sedimentation and Mass Accumulation Rates" section, this chapter). The boundary between lithologic Units I and II at Site 1061 is at ~160 mbsf. This correlates to a time of 0.205 s TWT on the seismic profile, just beneath the depth of the prominent, longer wavelength reflections. The top of lithologic Unit III is at ~260 mbsf (0.33 s TWT), at about the depth where the seismic reflections become less distinct. The seismic record shows the presence of a weak BSR at 0.65 s TWT, suggesting the presence of gas hydrate (Fig. 111).

Site 1062

A mud-wave field near 28°17′N, 74°24′W was surveyed in advance of drilling at Site 1062 to confirm the site location and to collect high-resolution seismic and 3.5-kHz records to image mud-wave structure. Previous studies have shown that mud-wave crests in this area are oriented N10°E, wave heights range from 20 to 60 m, and wavelengths from 2 to 2.5 km. Regional contours in the area trend N25°W; thus, the wave crests are at an angle of about 35° to the regional contours (Hollister et al., 1974; Flood and Hollister, 1974). Short-term current meter measurements and bottom photographs show that bottom currents in this area flow along the regional contours to the northwest at speeds up to about 10 cm/s. The wave selected for detailed study (crestal location 28°14.75′N, 74°24.6′W; crestal depth 4723 m) has a height of 37 m.

Many of the individual near-surface reflections recorded by the 3.5-kHz profiler (Fig. 113) can be traced across the mud-wave profile, and the reflections are more closely spaced on the western wave flank than on the eastern wave flank, suggesting that the mud wave has migrated with time. Because of the oblique wave orientation, this migration has both upslope (to the east) and upcurrent (to the south) components. The wave migration pattern is consistent with the depth of 3.5-kHz penetration (75 m). The seismic record images wave structure to about 0.45 s TWT and regional reflectors to >1 s TWT sub-bottom, and shows at least two distinct changes in wave migration patterns that may be related to climatic or circulation events. The migration pattern observed on the 3.5-kHz record extends to 0.08–0.10 s TWT sub-bottom, and the wave has migrated less than 1/4 wavelength in this interval. The seismic profile (Fig. 112) shows that between ~0.19 and ~0.30 s TWT, wave migration is more pronounced, and waves migrate over 1/2 a wavelength. The waves appear to have undergone a reorganization at ~0.30 s TWT sub-bottom because, below a distinct seismic horizon, waves are more irregular even though they still show a migration pattern, and there are intervals where wave troughs appear to fill. Mud waves can be followed to ~0.45 s TWT sub-bottom on the seismic profile.

Holes were located on the eastern wave flank (Holes 1062A–1062D), the western wave flank (Holes 1062D and 1062F), and the wave crest (Holes 1062G and 1062H). Because of wave migration patterns, the crests of deeper waves can underlie the troughs of shallower waves. Sites that start on the eastern flank of a near-surface wave sample the trough of a buried wave at depth, and then sample the western flank of a more deeply buried wave. Similarly, sites that start on the western wave flank sample the crest of a buried wave at depth, and then sample the eastern flank of a more deeply buried wave. These changes in the relative position of a hole with respect to the wave crest with depth, as well as the lateral distribution of holes across the mud-wave profile in general, will need to be considered when summarizing drilling results from this site.

The change in mud-wave growth patterns at 0.10 s TWT (76 m) at Holes 1062A through 1062D appears also to correspond to change from longer wavelength reflections above to shorter wavelength reflections below. The contact between lithologic Unit I and lithologic Unit II at these holes is at 78 mbsf (see "Lithostratigraphy" section, this chapter). The Unit I/Unit II boundary corresponds to ~MIS 16, slightly younger than the change from longer wavelength reflections to shorter wavelength reflections at Site 1061. Thin turbidites are common in Unit II at Site 1062, but rare in Unit I, suggesting that the change from shorter to longer wavelength reflections results from the reduction in the number of turbidites in the sediments. The deepest core at Site 1062 does not appear to have collected samples of the sediments associated with the wave reorganization at 0.35 s TWT (278 m) at this site. However, the deepest core recovered at Hole 1062B, which was drilled to 239 mbsf (corresponding to 0.305 s TWT) may have collected samples of wave crest just above the reorganization event. The age at the bottom of the hole is 4.27 Ma, and linear extrapolation of sedimentation rates suggests an age of 4.88 Ma for the reorganization in wave structure.

Prominent reflections are also observed deeper in the seismic record, and some of these are related to changes in sedimentation patterns that occurred as the North Atlantic basin evolved. One of the reflections (at ~0.8 s TWT), however, is diffuse and discontinuous, and may be a BSR, suggesting the presence of gas hydrate at depth.

REFERENCES

Baldauf, J.G., 1984. Cenozoic diatom biostratigraphy and paleoceanography of the Rockall Plateau region, North Atlantic, Deep Sea Drilling Project Leg 81. *In* Roberts, D.G., Schnitker, D., et al., *Init. Repts. DSDP,* 81: Washington (U.S. Govt. Printing Office), 439–478.

————, 1987. Diatom biostratigraphy of the middle- and high-latitude North Atlantic Ocean, Deep Sea Drilling Project Leg 94. *In* Ruddiman, W.F., Kidd, R.B., Thomas, E., et al., *Init. Repts. DSDP,* 94 (Pt. 2): Washington (U.S. Govt. Printing Office), 729–762.

Bangs, N.L.B., Sawyer, D.S., and Golovchenko, X., 1993. Free gas at the base of the gas hydrate zone in the vicinity of the Chile triple junction. *Geology,* 21:905–908.

Barron, J.A., 1985. Late Eocene to Holocene diatom biostratigraphy of the equatorial Pacific Ocean, Deep Sea Drilling Project Leg 85. *In* Mayer, L., Theyer, F., Thomas, E., et al., *Init. Repts. DSDP,* 85: Washington (U.S. Govt. Printing Office), 413–456.

Berner, R.A., 1980. *Early Diagenesis: A Theoretical Approach:* Princeton, NJ (Princeton Univ. Press).

Bonhommet, N., and Babkine, J., 1967. Sur la presence d'aimentations inverses dans la Chaine des Pus, in *C. R. Acad. Sci. Ser. 2,* 264:92.

Borowski, W.S., Paull, C.K., and Ussler, W., III, 1996. Marine pore-water sulfate profiles indicate in situ methane flux from underlying gas hydrate. *Geology,* 24:655–658.

Claypool, G.E., and Kaplan, I.R., 1974. The origin and distribution of methane in marine sediments. *In* Kaplan, I.R. (Ed.), *Natural Gases in Marine Sediments:* New York (Plenum), 99–139.

Dickens, G.R., Paull, C.K., Wallace, P., and the ODP Leg 164 Scientific Party, 1996. Direct measurement of in situ methane quantities in a large gas-hydrate reservoir. *Nature,* 385:426–428.

Droxler, A.W., Bruce, C.H., Sager, W.W., and Watkins, D.H., 1988. Pliocene-Pleistocene variations in aragonite content and planktonic oxygen-isotope record in Bahamian periplatform ooze, Hole 633A. *In* Austin, J.A., Jr., Schlager, W., et al., *Proc. ODP, Sci. Results,* 101: College Station, TX (Ocean Drilling Program), 221–244.

Emerson, S., and Hedges, J.I., 1988. Processes controlling the organic carbon content of open ocean sediments. *Paleoceanography,* 3:621–634.

Emerson, S.R., and Bender, M.L., 1981. Carbon fluxes at the sediment-water interface of the deep-sea: calcium carbonate preservation. *J. Mar. Res.,* 39:139–162.

Espitalié, J., Deroo, G., and Marquis, F., 1986. La pyrolyse Rock-Eval et ses applications, Partie III. *Rev. Inst. Fr. Pet.,* 41:73–89.

Flood, R.D., 1978. Studies of deep-sea sedimentary microtopology in the North Atlantic Ocean [Ph.D. dissert.]. Woods Hole Oceanographic Inst./ Massachusetts Inst. of Technology.

————, 1988. A lee wave model for deep-sea mud wave activity. *Deep-Sea Res. Part A,* 35:973–983.

————, 1994. Abyssal bedforms as indicators of changing bottom current flow: examples from the U.S. East Coast continental rise. *Paleoceanography,* 9:1049–1060.

Flood, R.D., and Hollister, C.D., 1974. Current-controlled topography on the continental margin off the eastern United States. *In* Burk, C.A., and Drake, C.L. (Eds.), *The Geology of Continental Margins:* New York (Springer-Verlag), 197–205.

Gieskes, J.M., 1981. Deep-sea drilling interstitial water studies: implications for chemical alteration of the oceanic crust, layers I and II. *In* Warme, J.E., Douglas, R.G., and Winterer, E.L. (Eds.), *The Deep Sea Drilling Project: A Decade of Progress.* Spec. Publ.—Soc. Econ. Paleontol. Mineral., 32:149–167.

Hesse, R., and Harrison, W.E., 1981. Gas hydrates (clathrates) causing pore-water freshening and oxygen isotope fractionation in deep-water sedimentary sections of terrigenous continental margins. *Earth Planet. Sci. Lett.,* 55:453–462.

Hesse, R., Lebel, J., and Gieskes, J.M., 1985. Interstitial water chemistry of gas-hydrate-bearing sections on the Middle America Trench slope, Deep-Sea Drilling Project Leg 84. *In* von Huene, R., Aubouin, J., et al., *Init. Repts. DSDP,* 84: Washington (U.S. Govt. Printing Office), 727–737.

Hoehler, T.M., Alperin, M.J., Albert, D.B., and Martens, C.S., 1994. Field and laboratory studies of methane oxidation in anoxic marine sediment: Evidence for a methanogen-sulfate reducer consortium. *Global Biogeochem. Cycles,* 8:451–463.

Holbrook, W.S., Hoskins, H., Wood, W.T., Stephen, R.A., Lizzarralde, D., and the Leg 164 Science Party, 1996. Methane gas-hydrate and free gas on the Blake Ridge from vertical seismic profiling. *Science,* 273:1840–1843.

Hollister, C.D., Flood, R.D, et al., 1974. Abyssal furrows and hyperbolic echo traces on the Bahama Outer Ridge. *Geology,* 2:395–400.

Jenden, P.D., and Gieskes, J.M., 1983. Chemical and isotopic composition of interstitial water from Deep Sea Drilling Project Sites 533 and 534. *In* Sheridan, R.E., Gradstein, F.M., et al., *Init. Repts. DSDP,* 76: Washington (U.S. Govt. Printing Office), 453–461.

Kastner, M., Elderfield, H., Martin, J.B., Suess, E., Kvenvolden, K.A., and Garrison, R.E., 1990. Diagenesis and interstitial-water chemistry at the Peruvian continental margin—major constituents and strontium isotopes. *In* Suess, E., von Huene, R., et al., *Proc. ODP, Sci. Results,* 112: College Station, TX (Ocean Drilling Program), 413–440.

Keigwin, L.D., and Jones, G.A., 1994. Western North Atlantic evidence for millennial-scale changes in ocean circulation and climate. *J. Geophys. Res.,* 99:12397–12410.

Kvenvolden, K.A., and Kastner, M., 1990. Gas hydrates of the Peruvian outer continental margin. *In* Suess, E., von Huene, R., et al., *Proc. ODP, Sci. Results,* 112: College Station, TX (Ocean Drilling Program), 517–526.

Lund, S.P., 1993. Paleomagnetic secular variation. *Trends in Geophys. Res., Counc. Sci. Res. Integr.,* Trivanbum, India, 143–155.

Mackin, J.E., and Aller, R.C., 1984. Ammonium adsorption in marine sediments. *Limnol. Oceanogr.,* 29:250–257.

Martens, C.S., and Berner, R.A., 1974. Methane production in the interstitial waters of sulfate-depleted marine sediments. *Science,* 185:1167–1169.

McIver, R.D., 1975. Hydrocarbon occurrences from JOIDES Deep Sea Drilling Project. *Proc. Ninth Petrol. Congr.,* 269–280.

Meyers, P.A., 1994. Preservation of elemental and isotopic source identification of sedimentary organic matter. *Chem. Geol.,* 144:289–302.

Miller, R.S., Lawrence, J.R., and Gieskes, J.M., 1979. Interstitial water studies, Sites 386 and 387, Leg 43. *In* Tucholke, B.E., Vogt, P.R., et al., *Init. Repts. DSDP,* 43: Washington (U.S. Govt. Printing Office), 669–674.

Morse, J.W., and Mackenzie, F.T., 1990. *Geochemistry of Sedimentary Carbonates.* Dev. in Sedimentology, 48: Amsterdam (Elsevier).

Müller, P.J., 1977. C/N ratios in Pacific deep sea sediments: effect of inorganic ammonium and organic nitrogen compounds sorbed by clays. *Geochim. Cosmochim. Acta,* 41:765–776.

Needham, H.D., Habib, D., and Heezen, B.C., 1969. Upper Carboniferous palynomorphs as a tracer of red sediment dispersal patterns in the Northwest Atlantic. *J. Geol.,* 77:113–120.

Paull, C.K., Matsumoto, R., Wallace, P.J., et al., 1996. *Proc. ODP, Init. Repts.,* 164: College Station, TX (Ocean Drilling Program).

Pedersen, T.F., and Shimmield, G.B., 1991. Interstitial water chemistry, Leg 117: contrasts with the Peru Margin. *In* Prell, W.L., Niitsuma, N., et al., *Proc. ODP, Sci. Results,* 117: College Station, TX (Ocean Drilling Program), 499–513.

Reeburgh, W.S., 1976. Methane consumption in Cariaco Trench waters and sediments. *Earth Planet. Sci. Lett.,* 28:337–344.

Rider, M., 1996. *The Geological Interpretation of Well Logs:* Caithness (Whittles Publishing).

Rosenfeld, J.K., 1979. Ammonium absorption in nearshore anoxic sediments. *Limnol. Oceanogr.,* 24:356–364.

Sayles, F.L., Manheim, F.T., and Waterman, L.S., 1972. Interstitial water studies on small core samples, Leg 11. *In* Hollister, C.D., Ewing, J.I., et al., *Init. Repts. DSDP,* 11: Washington (U.S. Govt. Printing Office), 1197–1008.

Schoell, M., 1980. The hydrogen and carbon isotopic composition of methane from natural gases of various origins. *Geochim. Cosmochim. Acta,* 44:649–661.

Serra, O., 1984. *Fundamentals of Well-Log Interpretation* (Vol. 1): *The Acquisition of Logging Data:* Dev. Pet. Sci., 15A: Amsterdam (Elsevier).

————, 1989. *Formation MicroScanner Image Interpretation:* Houston (Schlumberger Educ. Services), SMP-7028.

Shipboard Scientific Party, 1988. Leg 101—an overview. *In* Austin, J.A., Jr., Schlager, W., et al., *Proc. ODP, Sci. Results,* 101: College Station, TX (Ocean Drilling Program), 455–472.

————, 1996. Explanatory notes. *In* Paull, C.K., Matsumoto, R., Wallace, P.J., et al., *Proc. ODP, Init. Repts.,* 164: College Station, TX (Ocean Drilling Program), 13–41.

Silva, A.J., Hollister, C.D., Laine, E.P., and Beverly, B., 1976. Geotechnical properties of the Northern Bermuda Rise. *Mar. Geotechnol.,* 1:195–232.

Singh, S.C., Minshull, T.A., and Spence, G.D., 1993. Velocity structure of a gas hydrate reflector. *Science,* 260:204–207.

Smith, J.D., and Foster, J.H., 1969. Geomagnetic reversal in Brunhes normal polarity epoch. *Science,* 163:565–567.

Stein, R., Brass, G., Graham, D., Pimmel, A., and the Shipboard Scientific Party, 1995. Hydrocarbon measurements at Arctic Gateways sites (ODP Leg 151). *In* Myhre, A.M., Thiede, J., Firth, J.V., et al., *Proc. ODP, Init. Repts.,* 151: College Station, TX (Ocean Drilling Program), 385–395.

Whelan, J.K., and Sato, S., 1980. C_1–C_5 hydrocarbons from core gas pockets, Deep Sea Drilling Project Legs 56 and 57, Japan Trench Transect. *In* Langseth, M., Okada, H., et al., *Init. Repts. DSDP,* 56/57 (Pt. 2): Washington (U.S. Govt. Printing Office), 1335–1347.

Ms 172IR-105

NOTE: Core-description forms ("barrel sheets") and core photographs can be found in Section 4, beginning on page 325. Forms containing smear-slide data can be found on CD-ROM. See Table of Contents for material contained on CD-ROM.

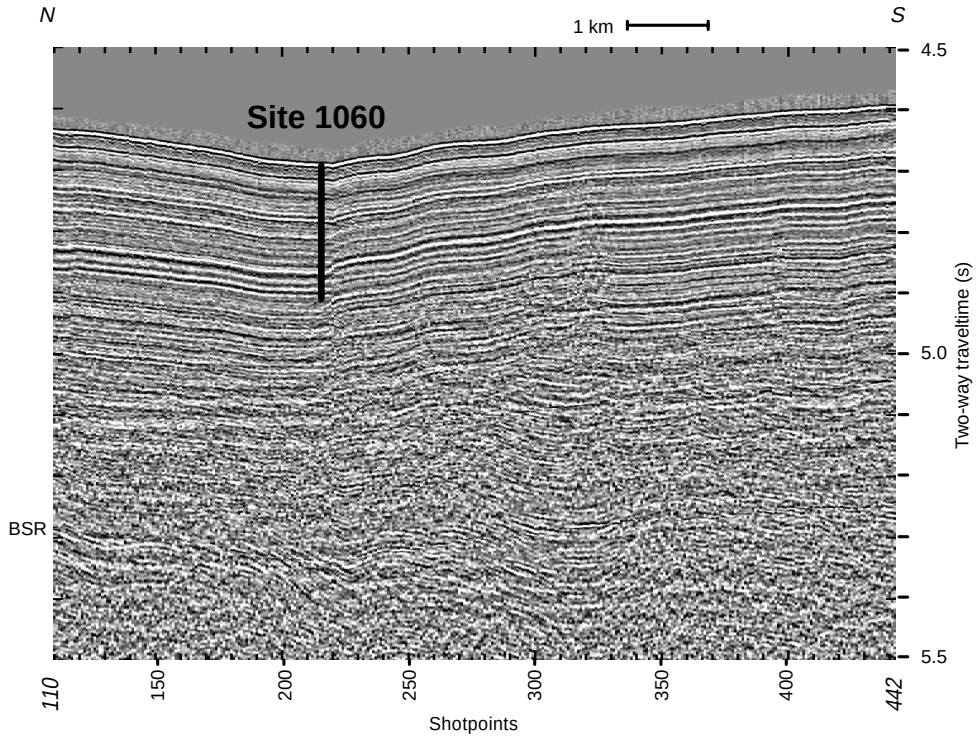

Figure 110. Seismic profile along the track shown in Figure 107 showing the location of Site 1060 on the Blake Outer Ridge crest at 3430 m.

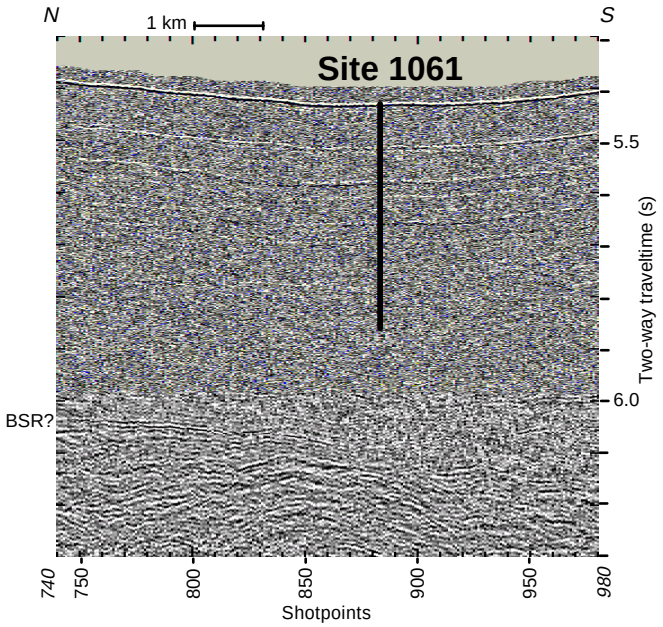

Figure 111. Seismic profile along the track shown in Figure 108 showing the location of Site 1061 on the Blake Outer Ridge crest at 3975 m.

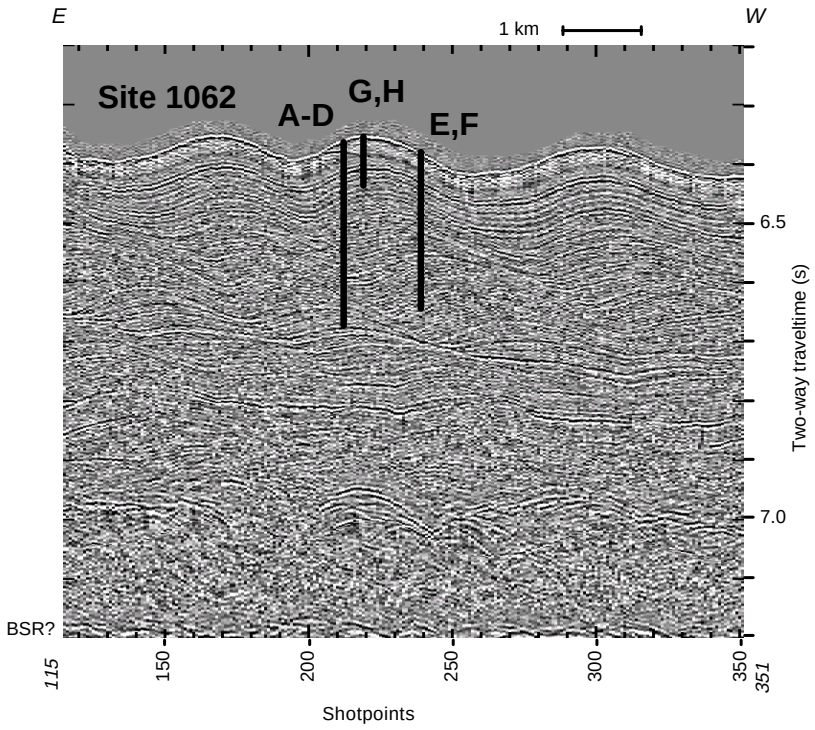

Figure 112. Seismic profile along the east-west portion of the track shown in Figure 109 showing the location of the different holes at Site 1062 on the Bahama Outer Ridge at 4725 m. The mud wave near the center of the profile was studied.

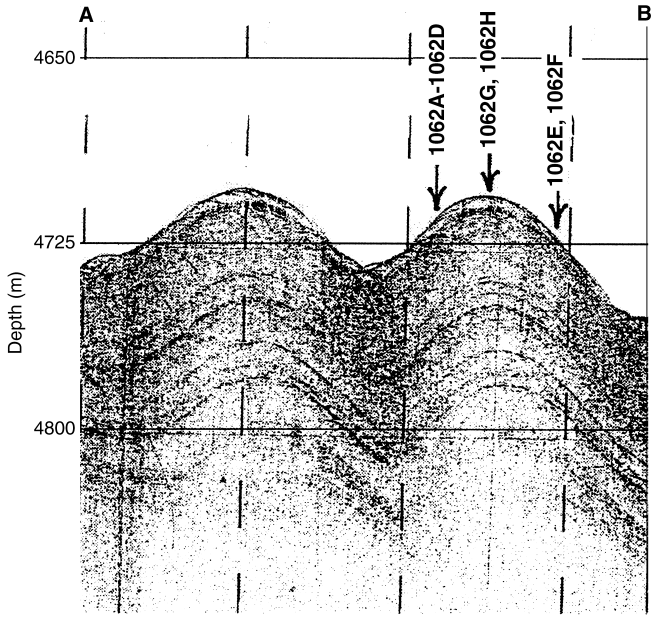

Figure 113. 3.5-kHz profile collected at Site 1062 during *Knorr* Cruise 140, Leg 2. The location of this profile is shown on Figure 109. The reflection pattern suggests mud-wave migration to the east.

Prior Chapter Contents Next Chapter